Fabrication and properties of novel open porous calcium phosphate bioceramics

Gittings, Jonathan Paul

Award date:
2005

Awarding institution:
University of Bath

Fabrication and Properties of Novel Open Porous Calcium Phosphate Bioceramics

Submitted by Jonathan Paul Gittings
for the degree of Ph.D.
from the University of Bath
2005

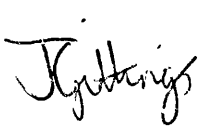

Jonathan Paul Gittings

ProQuest LLC
789 East Eisenhower Parkway
P.O. Box 1346
Ann Arbor, MI 48106-1346

ABSTRACT

Calcium phosphate (CaP) ceramics having an interconnecting porosity network with pores in the appropriate size range for bone ingrowth and re-vascularisation, offer the possibility of a structural-biological matrix for diseased or damaged bone. In order to be integrated by the host bone, the bioceramic must have adequate mechanical strength to avoid failure whilst offering a bioactive surface for possible bone ingrowth. The aim of the current research was to address this need and to develop novel fabrication procedures, in order to manufacture CaP bioceramics consisting of hydroxyapatite (HA), α-tricalcium phosphate (α-TCP) and β-tricalcium phosphate (β-TCP), with pores in the correct size range for bone formation and ingrowth, combined with sufficient mechanical properties to potentially be used for load-bearing applications.

CaP Open Porous Scaffolds (OPS) and CaP Spinal Fusion (SF) bioceramics have been successfully developed with open interconnected porosity ranging from 72-95% by volume. CaP bioceramic phases have been prepared with pore sizes from 50-1000μm, thereby offering a structural template for bone ingrowth. Surface defects were found to be the cause for the low strengths reported within the OPS bioceramics. Sol-gel solutions that can be applied as low viscosity coatings, and which then on sintering form chemical bonds to the CaP surface, were used to address the issue of surface defects, without compromising the structure of the interconnected porosity network. The subsequent densification of the sol-gel ceramic was found to increase the strength of the materials. This process resulted in strength increases of up to 163%, with strengths over 6MPa. The novel fabrication procedures developed can be used to produce a range of diverse CaP bioceramics for specific clinical applications in a range of sizes, shapes and chemical compositions. These include novel CaP bioceramics for aiding bone ingrowth and re-vascularisation in such applications as spinal fusion, chondylar repair, maxillofacial surgery (jaw reconstruction) and impaction grafting. HA/TCP granular materials have been developed with improved mechanical resistance and structural characteristics compared to a commercially available product, for use as a bone graft substitute material.

This study confirms the potential of the fabricated CaP bioceramics for use as bone substitute materials. The research was driven by both the need to improve the materials' structure-property relationship and also to meet clinical needs.

Acknowledgements

This research was made possible with the financial and materials assistance of Stryker Orthopaedics. I would like to take this opportunity to thank the company for their support. In particular I would like to thank Dr. Gerard Insley for his continual assistance, help and dedication to bioceramic research.

I would like to thank the staff and technicians within the Sports, Medical and Materials Group and Centre for Orthopaedic Biomechanics within the Department of Mechanical Engineering at the University of Bath, all of whom shared consistently their considerable knowledge and experience. A special thanks goes to Mr. Barry Chapman for grateful assistance with X-Ray Diffraction, and Mr. Frank Hammett and Mr. Peter Taylor for their help with polishing and optical photography. Thanks also go to Mr. Chris Arnold, Mr. Ian Trussler, Mr. Chris Carey and Mr. Nick Gathercole for their aid and assistance with mechanical testing and sintering.

Acknowledgment should also be given to the Science and Engineering Research Council for funding with the Scanning Electron Microscope and thanks must be given to the Centre of Electron Optics at the University of Bath, in particular Mr. Hugh Perrott and Mrs. Ursula Potter, who have been a source of invaluable information and assistance.

For their endless guidance, patience and expertise, I would like to offer my immeasurable gratitude to my supervisors, Dr. Irene Turner and Prof. Tony Miles, for the supervision provided throughout the duration of this research. Thank you Irene, thank you Tony.

A grateful thanks also goes to Dr. Chris Bowen for his support. Thanks go to Dr. Brian Casey for his guidance and support for working in conjunction with the author on the development of the Impact-Impregnated bioceramics. I would also like to offer my appreciation for his invaluable knowledge and insight into ceramic technology, fabrication and properties to Prof. Ron Stevens.

A massive thank you is extended to my mother, Margaret, and to my brothers Nicholas and Matthew (and their families), who have all supported me throughout the course of this research.

FABRICATION AND PROPERTIES OF NOVEL OPEN POROUS CALCIUM PHOSPHATE BIOCERAMICS

Glossary of Terms

Allograft - harvested bone graft in bone banks, taken from donor patients

Autograft - bone graft taken from patient at time of surgery

Hydroxyapatite (HA) - calcium phosphate based mineral component found in natural bone – $Ca_{10}(PO_4)_6(OH)_2$

In-Vitro - physical model simulating a biological environment appropriate for biomaterial evaluation

In-Vivo - biological evaluation study of a biomaterial in a living organism, animal or human

Osteoblast - bone forming cell

Osteoclast - bone resorbing cell

Osteoconduction - bone growth along surface of implant material, due to formation of hydroxycarbonate apatite mineral

Osteocyte - bone cells found in newly formed osteoid growth

Osteogenesis - bone remodelling i.e. continued bone growth

Osteoinduction - bone ingrowth into graft material and throughout interconnected structure of graft

α-Tricalcium Phosphate (α-TCP) - calcium phosphate based mineral – α-$Ca_3(PO_4)_2$

β-Tricalcium Phosphate (β-TCP) - calcium phosphate based mineral – β-$Ca_3(PO_4)_2$

Chapter 1 An Introduction to Calcium Phosphate Bioceramics

The concept of surgical replacement of diseased or damaged bone with a synthetic substance, into which bone can grow and regenerate, in order to affect a permanent repair, is extremely attractive in orthopaedics.

Currently, bone can be replaced by using autograft and allograft material. However, these methods have significant consequences for the patient. Autograft is bone supplied by the patient at the time of surgery. A second incision site is created introducing an increased possibility of persistent pain or even more serious problems such as infection. Allograft procedures use donated bone graft material in order to alleviate diseased or damaged bone. The recipients of allogenic bone grafts have a greater possibility of succumbing to infections. In addition, the amount of allogenic graft material is severely limited and of poor quality. Another reason for the development of bone substitute materials is the ever demanding operating procedures that are stretching allograft bone stocks to their limits. It is not uncommon for revision joint replacement procedures to use allograft material as a structural and biological matrix for graft incorporation. Hence, there is a need for a synthetic material that can provide a scaffold for the restoration and repair of natural bone in the body without risking infection. The main requirement for such a material would be to maintain structural integrity whilst acting as a support structure for re-vascularisation.

Over the past thirty years different groups of bone replacement material have been developed and their effectiveness as synthetic graft materials assessed. These materials are termed bioceramics and include ceramics, glasses and glass-ceramics. Generally, synthetic materials become encapsulated by fibrous tissue and become isolated from the surrounding bone when placed in an *in-vivo* environment. Since the early 1970's, this issue has been overcome by the finding that synthetically derived hydroxyapatite (HA) is bioactive in the body. HA is a member of the calcium phosphate (CaP) family and is the main mineral component of bone. It interacts with the host bone by exchanging calcium (Ca^{2+}) and phosphate (PO_4^{3-}) ions to form apatite precipitations on the ceramic substrate. This stimulates bone growth and enhances the biointegration of the implant material with the host bone.

The macroporosity is an important criterion in bone ingrowth and plays a key role in a process known as osteoconduction, which facilitates possible bone growth. A large interconnected

macroporosity network with pore sizes ranging from 150 - 300μm, aids the infiltration of bone and re-vascularisation, allowing bone remodelling. Osteoconductive bioceramics provide a scaffold for the ingrowth of bone and are affected by the total porous volume of the material. Porous materials have the advantage of allowing the circulation of bodily fluids and of increasing the possibility of firm attachment of regenerative bone cells such as osteoblasts (bone forming cells) to their surface, hence promoting bone growth at the defect site. However, it is inherent that an increase in the total porous volume of an implant decreases its mechanical strength. Therefore, there is a trade off between the incorporation of bony tissue and the structural integrity of the ceramic.

The brittle nature of bioactive ceramics such as the calcium phosphates, has limited their scope for clinical applications and hence research needs to be conducted in order to improve their properties. It is necessary to develop bioactive ceramic CaP materials, which more closely approximate the mechanical properties of bone, in addition to having a porous, interconnected structure that can be used to facilitate bone growth.

The goal of the research was to improve on the structure-property relationship of existing bioceramics to enable use in load-bearing applications. The bone substitute material should also have an interconnected porosity network in the correct size range for bone ingrowth.

1.1 Aims of Research

- To develop and fabricate calcium phosphate (CaP) bioceramics, consisting hydroxyapatite (HA), α-tricalcium phosphate (α-TCP) and β-tricalcium phosphate (β-TCP), with pores in the correct size range for bone formation and bone ingrowth. This necessitates the fabrication of materials with an interconnected hierarchial macroporosity network, having pores in the 150 - 300μm size range, for continued bone ingrowth within the synthetic bone graft material.

- To improve the structural integrity and mechanical properties of the materials, whilst retaining the interconnected macroporosity network required for bone remodelling.

- To produce materials that can be tailored in size and shape, and also in chemical composition.

- To develop novel fabrication techniques to show the diversity of applications possible with the materials developed, and the versatility in the range of samples that is possible to produce.

- To develop bioceramics for specific clinical applications that includes spinal fusion interbody applications, chondylar repairs (knee defects), block material for potential use in maxillofacial surgery (mandible/jaw reconstruction) and a granular material for use in impaction grafting in revision hip procedures.

1.2 Thesis Layout

The research presented here is organised into four main chapters, these being; *Literature Review*, *Materials and Experimental Methods*, *Results and Discussion and General Discussion* and *Conclusions*. The *Literature Review* chapter gives a detailed review of current bone substitute materials and their applications, the need for synthetic alternatives and details of some general fabrication techniques for the production of synthetic bone substitute materials. The *Materials and Experimental Methods* chapter outlines the novel fabrication techniques developed, and the methods and apparatus used to characterise the materials that were produced. The results obtained, along with an analysis of these findings, are presented in the *Results and Discussion* chapter. In the *General Discussion and Conclusions* chapter, the major findings of the research are brought together and analysed in terms of the broader context of the subject. The overall conclusions from the research are highlighted along with the opportunities for further investigation in the future work section of the chapter.

Chapter 2 Literature Review –

2.1 Bone

In order to understand the requirements of a bone replacement material, one must understand bone histology, structure and biology, in addition to the factors that govern and affect the remodelling and development of bone. This section reviews these properties from the point of view of a materials scientist. Factors that are relevant to the incorporation of bone into a bioceramic graft material are of primary importance from this perspective and therefore this is where the focus lies.

2.1.1 Structure of Bone

2.1.1.1 Cortical Bone

The total adult skeletal mass of bone comprises 80% cortical bone. It forms the outer layer of bone walls and offers support and protection; it can be classed as a biomechanical material [1]. The turnover (i.e. remodelling rate) of cortical bone is slow in comparison to the rapid turnover in cancellous bone (spongy or trabecular bone). However, cortical bone has an important role in bone remodelling (section 2.1.4). It supplies the only source for new bone forming cells that originate in bone marrow via the cortical capillary [2]. Figure 2.1 shows the structure of cortical bone.

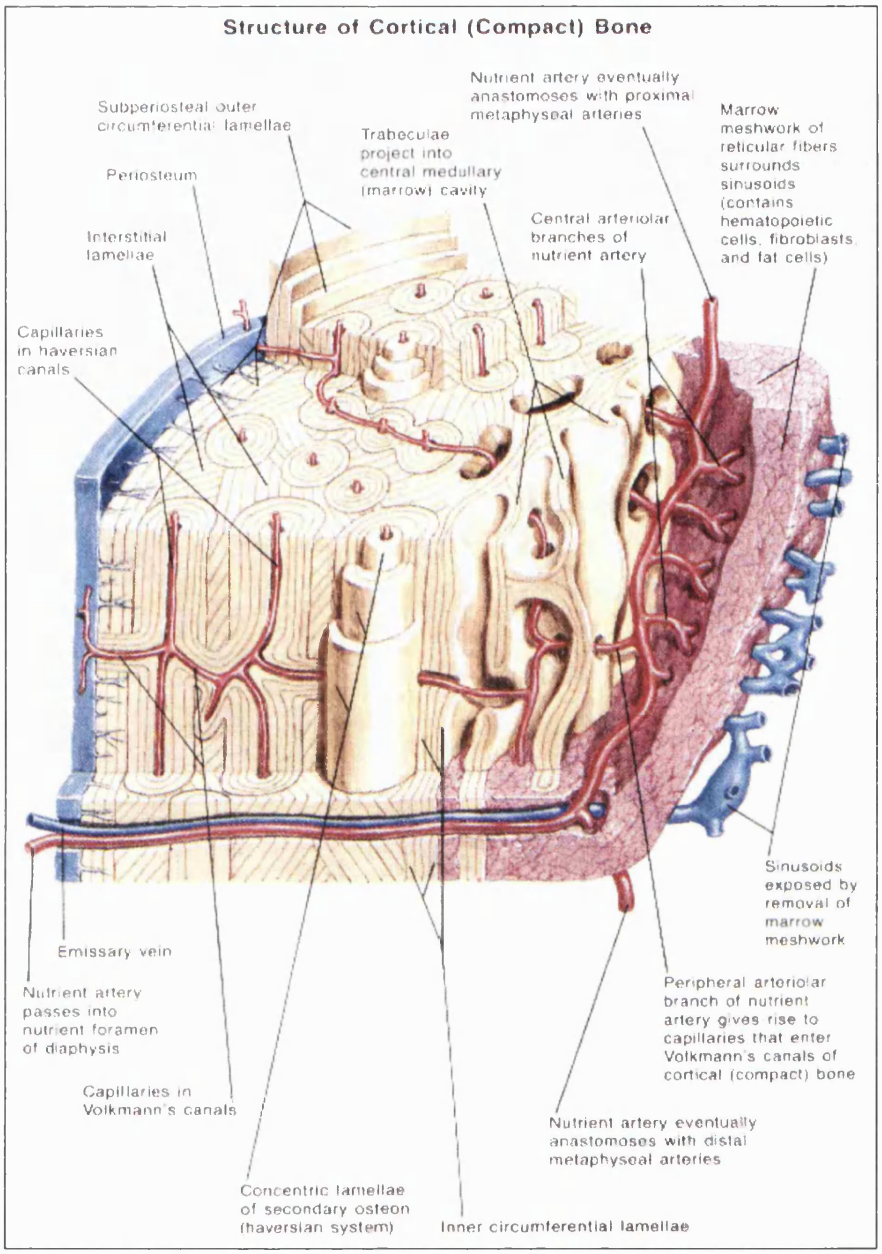

Figure 2.1: Structure of cortical bone [3]

Figure 2.1 above, indicates how cortical bone consists of long, cylindrical concentric layers of bone surrounding a capillary. It is these osteons (or Haversian systems) that are the fundamental functional unit of cortical bone [4]. The importance of these osteons as far as producing a regenerative synthetic material, from a point of view of porosity requirements, will be discussed in section 2.1.2.

2.1.1.2 Cancellous bone

Cancellous bone comprises 20% of adult skeletal bone mass. It is metabolically active and consists of a lattice of large plates and rods known as the trabeculae. Figure 2.2 shows the structure of cancellous bone.

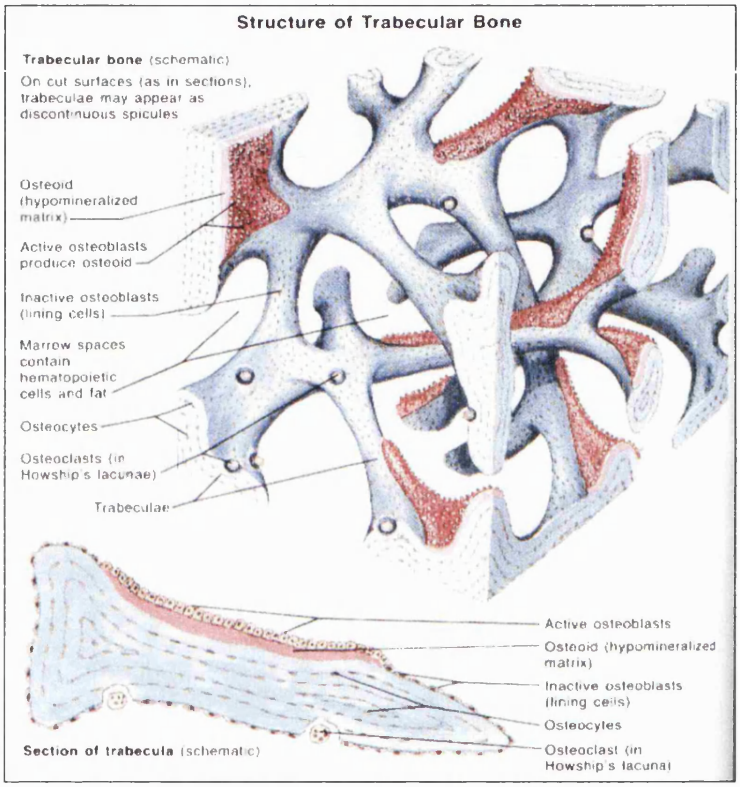

Figure 2.2: Structure of cancellous (trabecular) bone [3]

Bone marrow occupies the intertrabecular spaces in living bone [5]. The main differences in the function of the two varieties of bone are that cancellous bone is far more metabolically active and thus controls mineral homeostasis [6]. To a lesser extent it offers structural support, but not the biomechanical properties offered by cortical bone [7].

Cancellous bone surfaces contribute to more than 61% of the total bone surface. This is due to the fact that the trabecular surface to volume ratio is eight times greater than in cortical bone. This explains the large porosity in cancellous bone and why it is the main site for bone remodelling activity and bone turnover regulation [1].

Figure 2.3 illustrates the structural differences between cortical and cancellous bone.

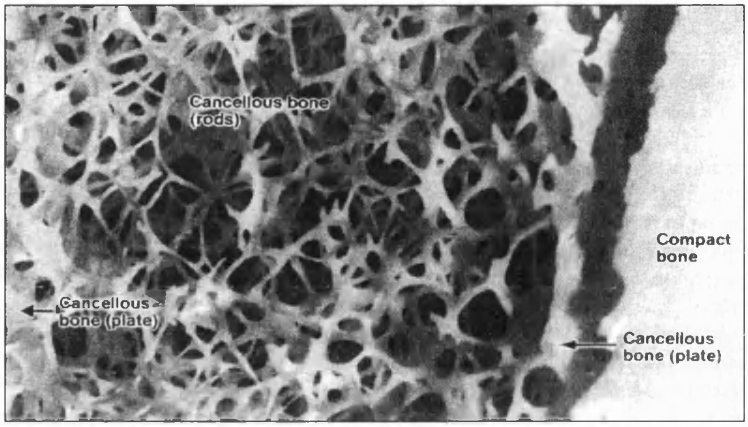

Figure 2.3: Structural differences between cortical (compact) and cancellous (trabecular) bone [8]

2.1.2 Composition and Hierarchial Structure of Bone

The skeleton is an adaptable and well architectured frame but also is a dynamic mineral reserve bank in which the body stores its calcium and phosphate ions [3]. Bone cells account for only a small portion (~ 2%) of the entire organic component of bone, most of which is osteoid (mineralised bone tissue) produced by bone forming cells [8, 9]. The composition of dried bone by weight is 70% mineral and 30% organic. The mineral component consists of 95% hydroxyapatite – $Ca_{10}(PO_4)_6(OH)_2$, the remaining 5% includes bone apatite impurities such as carbonate ions and small amounts of magnesium, sodium, potassium and fluoride and chloride ions [10, 11]. The main mineral component of bone is hydroxyapatite, which is a member of the calcium phosphate family [12]. The organic component of bone consists of 98% matrix and 2% bone cells. The matrix mainly consists of 95% collagen and 5% noncollagenous proteins [5]. Typical bone cells (section 2.1.3) include bone forming cells (osteoblasts), bone resorbing cells (osteoclasts) and cells that originate from osteoblastic formation when surrounded by newly formed matrix (osteocytes) [13].

It is important to understand the structural relationships present in bone in order to understand the mechanical properties of bone material. There is a hierarchial structural organisation to bone, making the material heterogeneous and anisotropic as well as endowing viscoelasticity [14]. Figure 2.4 illustrates this hierarchy.

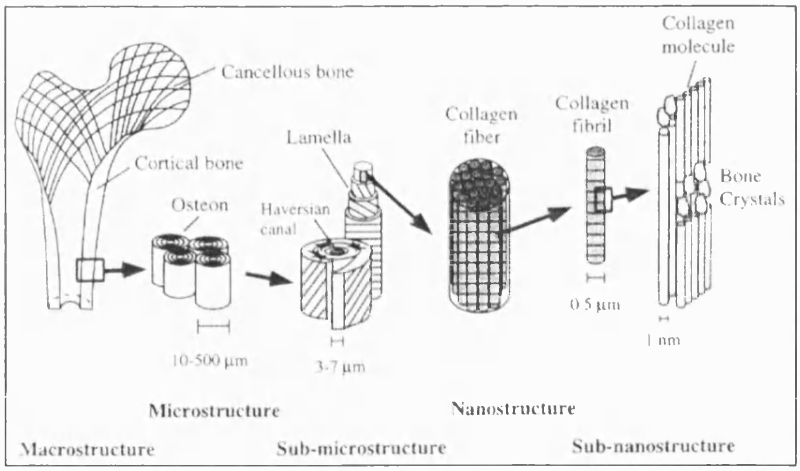

Figure 2.4: The hierarchial structure of bone [15]

It can be seen that the structural organisation of bone is as follows:

(1) Cancellous and Cortical Bone.

(2) The Macrostructure: 10 – 500µm, including Haversian systems, osteoid growth and single trabeculae.

(3) The Microstructure: 1 – 10µm, including lamellae and collagen fibrils.

(4) The Nanostructure: this includes collagen molecules and bone crystals, mainly hydroxyapatite.

2.1.2.1 Cancellous and Cortical Bone

Both types of bone (cancellous and cortical) can be distinguished by their porosity or density [16]. Due to the broader range of densities present in cancellous bone than in cortical bone, there is also a wider range of mechanical properties for cancellous bone depending on density, location and microstress analysis [15]. The preferred direction of growth for the trabecular struts is down the main stress trajectories of the bone – this is known as Wolff's law [16, 17]. Cortical bone is inherently denser and therefore mechanically a more robust material, but it is also affected by microstructural changes due to porosity, the mineralisation level and the organisation of the solid matrix.

2.1.2.2 Macrostructure

The osteons present in the hierarchial structure consist of lamellar sheets (mineralised collagen fibrils) wrapped in concentric layers around a central canal to form what is known as an osteon or Haversian system. Single osteons are usually 150 – 250μm in diameter running roughly parallel to the long axis of the bone. For bone ingrowth to occur, a minimum porosity size for osteoid growth is required [15], this relates to the diameter of the single osteon. The concentric lamellar layers of an osteon surround a supply route for bone cells known as the Haversian canal. It is an important structural parameter when considering porosity requirements for replacement bone graft material [18].

2.1.2.3 Microstructure

The lamellae found in the osteons are 3 – 7μm in thickness. The most common model proposed is that the lamellae lie parallel to each other down the long axis of the osteon [15]. Bone is anisotropic in both its structure and properties. The lamellae, which consist of bundles of collagen fibres, are orientated at different degrees within the osteon. Nanoindentation methods can now resolve that the orientation and properties of the lamellae are anisotropic [19].

2.1.2.4 Nanostructure

The nanostructure and sub-nanostructure of bone is made up of collagen fibres, surrounded and infiltrated by mainly hydroxyapatite bone crystals. The dimensions of bone mineral crystals are 50 x 25 x 3 nm [16]. Collagen fibres constitute the shape-forming structural framework of bone in which the hydroxyapatite crystals are situated. The hydroxyapatite confers rigidity to the collagen framework [1].

It is at this level that bone can be described best as a complex engineering composite material. Mineral crystals reinforce the collagen fibres and typical fracture and viscoelastic properties cannot be explained by typical molecular mechanisms. Figure 2.5 illustrates a typical stress-strain curve for cancellous bone, indicating the unusually high strains that can be sustained by the material.

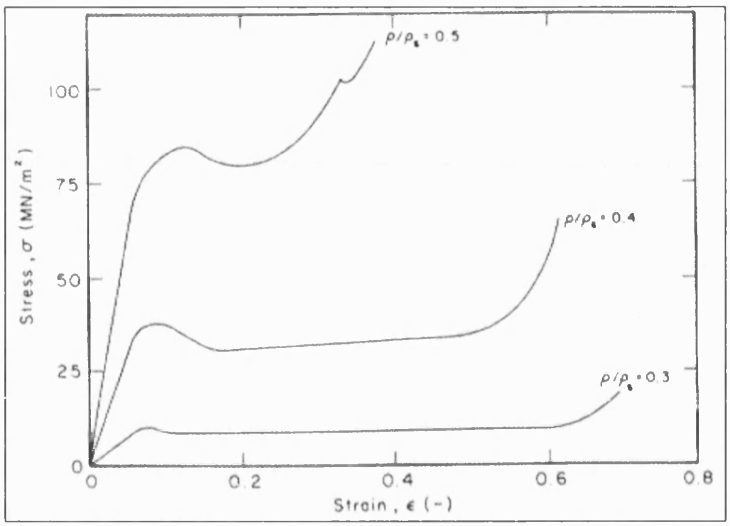

Figure 2.5: Stress-strain compression curves for cancellous bone. As relative density increases, Young's modulus also increases [16]

It can be seen that bone is a unique material with several distinct levels of structural organisation. Knowledge of this hierarchial organisation is needed in order to have complete understanding of its mechanical properties [11].

2.1.3 Bone Cells

Bone is a specialised connective tissue composed of intercellular calcified material, the bone matrix and three cell types. Osteoclasts are multinucleated giant cells involved in the resorption and remodelling of bone tissue. Osteoblasts are bone forming cells, these synthesize the organic components of the matrix. Osteocytes are bone cells that are found in cavities within the matrix [8].

2.1.3.1 Osteoclasts (*osteon*, bone + *klastos*, broken)

Osteoclasts resorb mineralised bone matrix. An osteoclast is a multinucleated giant cell that ranges in diameter from 20 – 100μm (containing as many as 100 nuclei per cell) [3]. Actively resorbing osteoclasts are usually found in cavities on bone surfaces, known as Howship's lacunae. Osteoclasts are derived from the fusion of bone marrow-derived cells. Bone growth occurs on the trabeculae of cancellous bone as its mean surface to volume ratio is eight times greater than that for cortical bone [1]. Osteoclasts adhere to the bone surface, which acts as a

permeable seal to maintain the microenvironment for bone resorption to occur [13]. This is made possible due to the formation of a ruffled border which is bone surface facing to ensure the integrity of the microenvironment. Figure 2.6 shows the formation of this microenvironment and how osteoclasts help to resorb mineralised bone matrix.

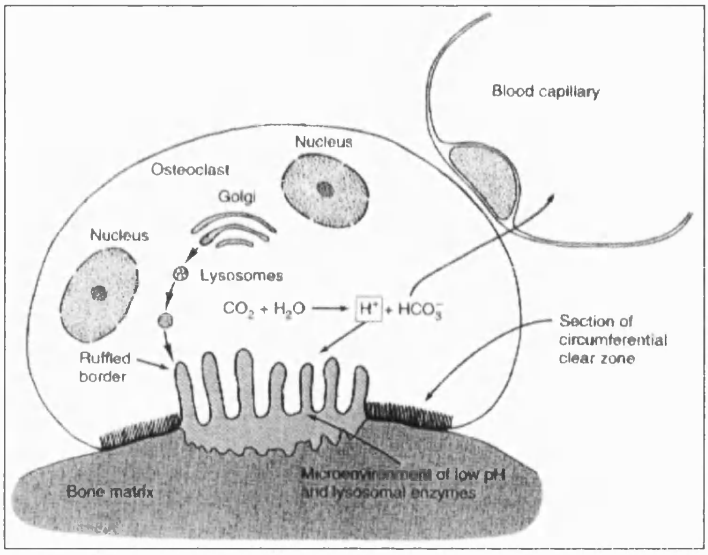

Figure 2.6: The process of bone resorption. Bone matrix is removed and the products of bone resorption are taken up by the osteoclasts' cytoplasm and eventually transferred to blood capillaries [8]

The osteoclast secretes collagen and other enzymes and pumps protons into sub cellular pockets (the microenvironment mentioned above), promoting the localised digestion of collagen and dissolving calcium salt crystals [8]. As a consequence of this, osteoclasts are polarised when active [15]. The life span of an osteoclast *in vivo* appears to be up to 7 weeks with a half-life of 6 – 10 days. To summarise, the osteoclasts solubilise both the mineral and organic component of the matrix ready for remineralisation [10].

2.1.3.2 Osteoblasts (*osteon*, bone + *blastos,* formation)

Osteoblasts are bone-forming cells. These synthesize and secrete unmineralised bone matrix (the osteoid) [3]. The osteoid (~ 10μm in width) is key to the development of new bone matrix and remodelling, be it from growth, healing or disease. Osteoblasts also participate in the calcification of bone and help regulate the flux of calcium and phosphate ions in and out of bone.

Osteoblast cells are essential to bone remodelling. The schematic in figure 2.7 illustrates the beginnings of osteoid growth.

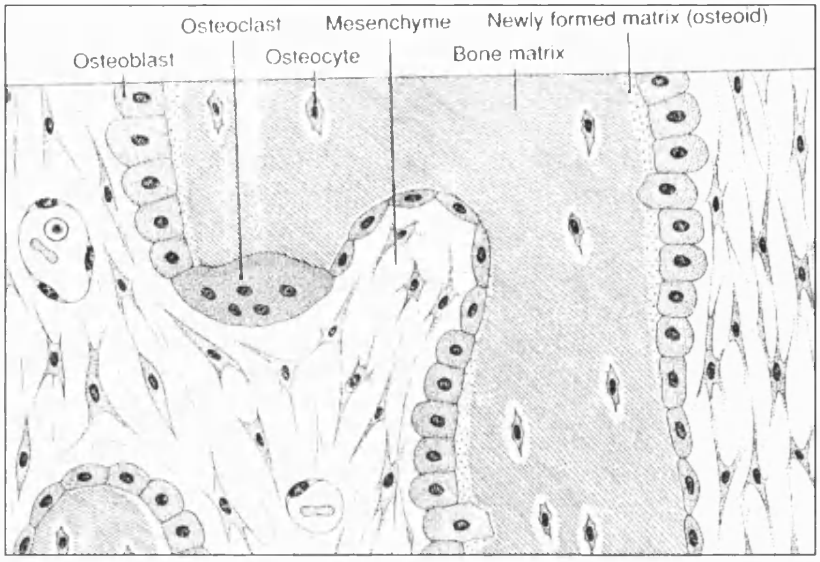

Figure 2.7: Intramembranous ossification [8]

The bone remodelling that is shown in figure 2.7 above is described in greater detail in section 2.1.4.1 – Formation of Bone Growth - Osteogenesis. Osteoblasts synthesise collagen and form a matrix that traps cells. Meanwhile, the osteoblasts differentiate to become osteocytes. The lower part of the illustration (figure 2.7) shows osteoblasts being trapped in newly formed bone matrix, which is the beginning of osteocyte growth [8]. Osteoid is the secretion of unmineralised bone matrix (from the osteoblastic cells) that leads to the synthesis of the organic bone matrix. Osteoblasts require a scaffold (e.g. trabecular or Haversian system) on which to synthesise the osteoid [20].

2.1.3.3 Osteocytes (*osteon*, bone + *kytos*, cell)

Osteocytes, which derive from osteoblasts, lie in the Howship's lacunae situated between lamellae of the matrix [19]. These cells are formed after the bone forming osteoid stage and are 20 – 60μm in size. This allows fluid flow to transfer information to surface cells. Osteocytes may (1) stabilise bone mineral by maintaining the ionic concentration that controls the efflux of calcium ions, (2) detect microdamage and (3) respond to strain in order to influence and adapt modelling behaviour through cell-cell interaction [1]. They play a key role in the restructuring process that constitutes the regulation of mineral activity and the sensing of strains [8].

2.1.4 Bone Remodelling and Osteogenesis

Bone remodelling produces and maintains bone that is both biomechanically robust and metabolically active. Mature bone is superior to immature (woven) bone from a structural point of view, however the quality of mature bone deteriorates with time. Thus bone must renew or replace itself continuously [9]. The remodelling process has many different influential effects on bone quality at the tissue level. It helps to respond to local stresses by changing its microarchitecture and replacing dead or hypermineralised bone [14]. Bone forming surfaces are characterised by a covering of osteoblasts. Resorbing bone surfaces have cavities that contain osteoclasts [6]. The concept of bone remodelling is that every bone-remodelling unit (BRU) is initiated by the activation of osteoclastic cells [17]. An activation-resorption sequence occurs called coupling. The process is followed by new bone formation by autoinduction [20]. In which both the inductor cells and the induced cells are derived from ingrowing cells of the host bed. During remodelling, bone surfaces may be in one of three functional states: forming, resorbing or quiescent [21]. The system is more complex than a simple chemical stimulus and direct cell response. The remodelling process demands tight regulation and fine-tuning of osteoclast and osteoblast activity [10].

2.1.4.1 Formation of Bone Growth - Osteogenesis

Figure 2.7 illustrates the processes that occur during bone remodelling and these are explained in detail here. For the removal and replacement of pre-existing bone to take place, the bone surface must be activated and mineralised in six consecutive steps. Once concluded (be it a new osteon or trabecular surface area) the new ossified tissues and bone structure can be said to have undergone osteogenesis. These stages are as follows:

(1) Resting: Inactive surfaces are termed in the resting stage. This consists of about 80% cancellous and cortical bone at any one time [7].

(2) Activation: The conversion of quiescent bone surface to a level whereby resorption activity takes place is referred to as activation. The recruitment of osteoclasts is required in order to resorb mineralised bone tissue [1, 6].

(3) Resorption: Erosion of bone takes place due to the intimate contact of osteoclasts with the exposed surface bone. This creates cavities known as Howship's lacunae. The mean depth of erosion is around 60μm [1].

(4) Reversal: The coupling of osteoclasts and osteoblasts occurs at this stage due to the lack of osteoclasts and the presence of mononuclear cells within the cavities. Osteoblast stimulating factors are released from the bone matrix in order to polarise the osteoblasts [12].

(5) Formation: Matrix syntheses followed by extracellular mineralisation are the two stages of bone formation. The new osteoblasts begin to deposit a layer of bone matrix referred to as the osteoid seam.

(6) Mineralisation: There is a negative bone balance as a result of bone remodelling. Creating a negative bone balance conserves trabecular bone next to the marrow. Remodelling increases as a result of disease [20]. Mineralisation by osteoblast activity occurs automatically as a result of forming an osteoid seam.

Matrix formation occurs at the interface between osteoblasts and osteoid growth and is the basis for bone remodelling. Full regeneration of bone only occurs once complete mineralisation has taken place [3]. This is known as osteogenesis and complete mineralisation can take between 3 – 6 months [5]. It is this development of osteoid growth and replacement of immature bone and old bone via resorption and remodelling that is known as bone regeneration and osseous growth [1].

Remodelling continues throughout life, secondary bone is continuously resorbed and replaced by new generations of bone e.g. cortical bone has a mean age of twenty years and cancellous bone one to four years [12]. The process helps to maintain the strength of bones for load bearing and to keep the strains experienced from exceeding the modelling threshold, thus reducing microdamage. In addition, calcium homeostasis is maintained in order to help repair any structural damage [17, 18].

2.2 Bone Grafts

Bone grafts have been employed for bone repair for more than a hundred years [17]. The following section will assess the demands placed on a bone graft, the different bone grafts available, the advantages and disadvantages of these grafts and ultimately the need to develop a synthetic alternative for use when bone grafting.

2.2.i Osteoconduction and Grafting

Bone graft tissues are osteoconductive [12, 20, 22]. This is the ability of a material to encourage bone growth along its surface when placed in the vicinity of viable bone or differentiated bone-forming cells. Figure 2.8 represents a structural allograft from the iliac crest, which is located in the pelvis. Note the highly porous cancellous bone area that is necessary for full osteogenesis and marrow formation due to its high surface to volume ratio, thus termed a metabolically active material.

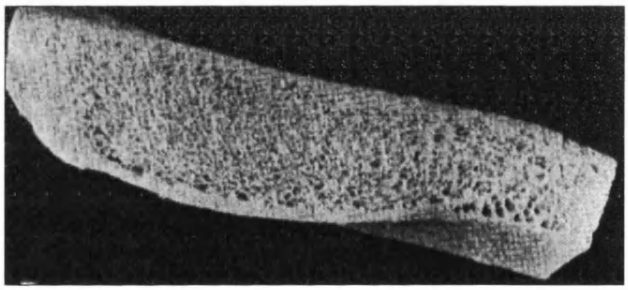

Figure 2.8: Bone graft material from iliac crest in the hip (whole picture ~ 25mm) [23]

Bone grafting is a dynamic procedure. A successful bone graft must interact and exchange calcium and phosphate ions with the host in order to provide functions for and allow osteogenesis whilst maintaining mechanical support [22, 24]. Therefore, over time the structure is completely encased in remodelled bone deposits from the host [25]. Figure 2.9 below illustrates the three-dimensional relationship and time sequence for the incorporation of a bone graft by bone cells and osteoid growth.

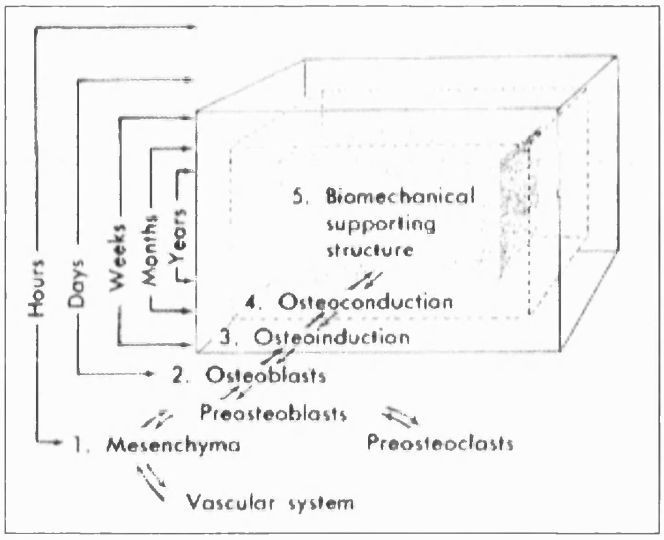

Figure 2.9: Ideal bone graft material for incorporation of osteoid growth [24]

Initial migration of fluid and osteoprogenitor cells into the porous structure allows an excellent surface area on which bone cells can operate [12]. The porosity is key in order to allow bone cells such as osteoclasts (20-100μm), osteoblasts (15-30μm) and osteocytes (20-60μm) to provide fibrovascular tissue growth which is followed by further cemented bone layers on top leading to lamellar bone and osteoinduction (osteons ~ 150-250μm) [12].

Bone grafts can be classified as either bulk or particulate (granular) or structural and non-structural, depending on their purpose [26]. Particulate grafts are used for non-structural functions (e.g. space fillers) where as structural grafts must be able to withstand the forces applied to the host area. This occurs in bulk bone grafts such as for large bone segmental defects.

There are two main bone grafts used: autografts and allografts. It is necessary to assess and evaluate these bone grafts before understanding why there is a growing demand for a synthetic bone graft material.

2.2.1.1 Autografts

Autograft material is bone stock taken from the patient at the time of surgery. Due to the difficulty in finding a suitable donor site coupled with the high rate of donor site morbidity, it is a procedure rarely used [22].

Autografts are described biologically as "the golden standard". They facilitate osteogenesis. Cancellous autografts with their high surface area, high porosity and pore interconnectivity, permit fluid flow and capillary growth, and allow bone cells to dominate bone resorption [27]. Remodelling and the incorporation of bony tissue throughout the graft is usually complete within a year [12]. However, early stabilisation due to the bioactivity offered by the graft is the reason for good early fixation [22].

2.2.1.2 Allografts

Allograft material is harvested and placed in bone banks that must adhere to the standards of such institutes as the American Association of Tissue Banks [22]. It is harvested from joints and bones of patients who are severely affected by such diseases as osteoarthritis and osteoporosis. There is also a limited supply of allograft. Due to disease and infection, it can take up to three hip joints to provide enough cortico-cancellous allograft material for one revision hip replacement. Thus, there is always a negative growth rate in the bone banks. The material is preserved by freeze-drying methods, however this significantly reduces the immune response [22]. There is always some doubt in the patients' minds about the risk of transmission of infections, even though every bone sample accepted as allograft is treated and analysed [28].

The main difference in the two grafts biologically is that necrotic (dead) graft bone remains in the allograft significantly longer than autografts [29]. Vascular ingrowth is slower and less extensive than with autografts. Depending on the degree of generic disparity between the host and graft there may be adverse histological responses such as inflammation [30].

Allograft is used in greater quantities than autograft mainly to avoid a second morbidity site and due to the difficulty in harvesting a sufficient amount of bone material from the patient's own skeleton [26]. Allograft material can be cortical, cancellous or a combination of both. Therefore, it can offer an excellent combination of properties from structural support to bioactivity and osteogenesis. Bone grafting is a necessity in such procedures as revision Total Hip Replacement (THR) and revision Total Knee Replacement (TKR) [31-33].

2.2.2 Applications of Bone Grafts

A brief introduction to some of the procedures in which bone grafting is used is now presented. It demonstrates the diversity and wide range of their application. It also indicates how many different forms of bone graft are required from bulk material through to particulate and powder forms of bone graft.

2.2.2.1 Total Hip Replacement (THR)

In the UK each year 50,000 hip replacement operations are performed with a 1% failure rate and of those 15% are hip revisions [28]. It is quite common for people to outlive their first hip and have two, three or more hip revisions.

The goal of THR has remained the same since the procedure began in the 1960's, that is, to achieve a durable, painless and functional hip in those people affected by severely limiting arthritic conditions [31-33]. In THR both parts of the joint, the femoral head and the acetabular socket, are replaced. During hip replacement surgery, on the femoral side, the head is removed and a surgical grade chrome cobalt steel or titanium stem with a metal or ceramic ball is inserted into the medullary canal of the femur. The stem is usually fixed using polymethylmethacrylate (PMMA) cement. On the pelvic side, an area of the acetabulum is removed and a hemispherically shaped hole is forged out. A polymer or ceramic cup is inserted and fixed usually with PMMA cement [34-36]. Figure 2.10 shows an illustration of a hip prosthesis.

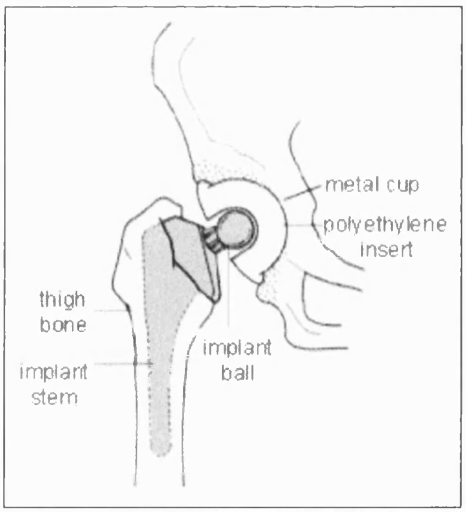

Figure 2.10: Hip prosthesis [34]

The materials selected for their application in THR (figure 2.10) have been chosen due to their low weight and high strength (stainless steel or titanium for implant stem and implant ball), and their low coefficient of friction (polymer or ceramic insert). The integration of the cup into the acetabular bone, by cementing, is done to achieve an intimate contact between fixation and host bone.

THR expanded in the 1960's and 1970's due to the pioneering work of Sir John Charnley (1910 – 1983). He devised the first low friction arthroplasty whereby both ball and socket were replaced with the acetabular and femoral components usually fixed in place with bone cement. The innovative feature was the use of very small femoral heads with a diameter of 22.5mm. These were fixed in place using acrylic cement and articulated on a polyethylene socket - hence the term metal on plastic joint. This particular design dramatically improved the quality of life for patients. The procedure is quicker with shorter hospital stays and more consistent pain relief than previously experienced with existing procedures [34]. Many variations have been developed including McKee's metal on metal joint and ceramic-ceramic ball and socket prostheses [35].

The stability of the implant depends on the mechanical fixation and interlocking of the implant. If cyclic movement under loading is less than 75μm, then living bone forms up to the surface of the implant [34]. Hip replacements are subjected to two kinds of micromovement post-surgery. One is cyclic, which is recoverable, the second is migration, which is non-recoverable displacement. If this subsidence occurs early on then there is a high probability of failure and hence the need for revision operations.

2.2.2.2 Impaction Grafting

Impaction grafting fundamentally addresses the problem of bone stock loss, instead of the compensation of bone. The large femoral cavity in hip revision operations affected by bone loss (due to subsidence) is filled with morsellised cancellous bone harvested from donor femoral heads [37]. The ideal graft should be mechanically stable, have at least osteoconductive properties, be free from infection, readily available and easy to store. The problems with allograft material associated with impaction grafting are its availability, quality, antigenicity, risk of infection and storage problems. However, if the allograft does not offer a site for the development of vascularisation (i.e. osteoclastic and osteoblastic activity) migration and subsidence of the femoral stem can occur [31, 37, 38].

One procedure for impaction grafting is in hip revision, whereby stem loosening occurs due to both cyclic and migration movement of the stem. The impaction grafting procedure is described and shown in figures 2.11 and 2.12.

A flexible stainless steel mesh is fixed peripherally to the femoral head and acetabular region in order to secure rigidity. Frozen morsellised allograft bone chips are then impacted into the mesh and femoral head by metal impactors and the use of a hammer. The allograft is compressed tightly with the hammer to ensure good fixation (figure 2.11). Usually a second layer of allograft is then layered on top of the first in order to optimise the packing properties of the allograft (i.e. good fixation). Finally a polyethylene cup is cemented in place with bone cement in order for the implant ball to articulate against the femoral head (figure 2.12).

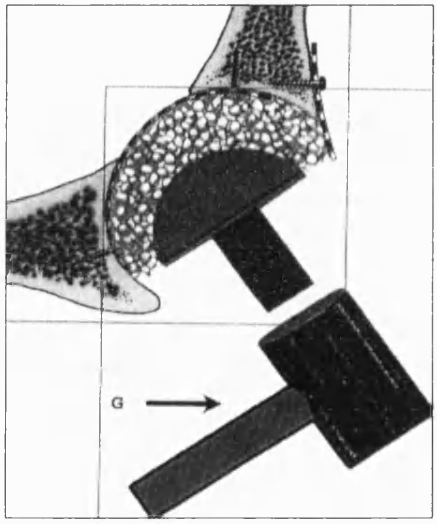

Figure 2.11: Allograft is compressed tightly with a hammer [31]

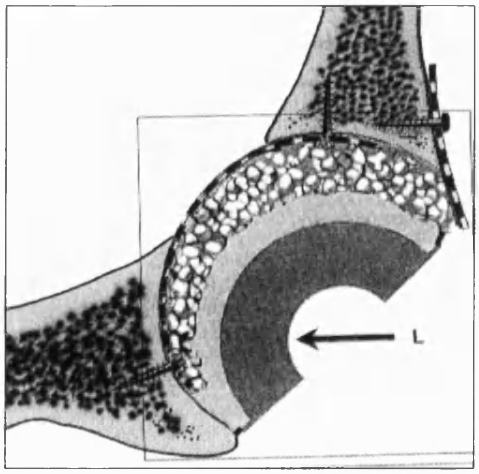

Figure 2.12: A polyethylene cup (L) is cemented in place with bone cement [31]

Allograft material is not consistent in its properties both biologically and structurally; this is the main reason why there is a need for a bone replacement material.

2.2.2.3 Bone Grafting in Total Knee Replacement (TKR)

The use of bone graft for femoral component revision can be subdivided into two broad categories. Particulate graft usually fills small defects less than $1cm^3$. Structural allograft is often used for defects greater than $1cm^3$ [29, 32, 33, 39]. Structural bone grafting in knee revision operations generally has good results at short-to-medium follow-ups compared with THR [32]. Impacted morsellised allograft is used in revision TKR [29, 33]. The goal for revision TKR is the same as for revision THR. Figure 2.13 shows significant bone loss in the knee joint of a patient ($>1cm^3$), needing bulk allograft to offer structural support.

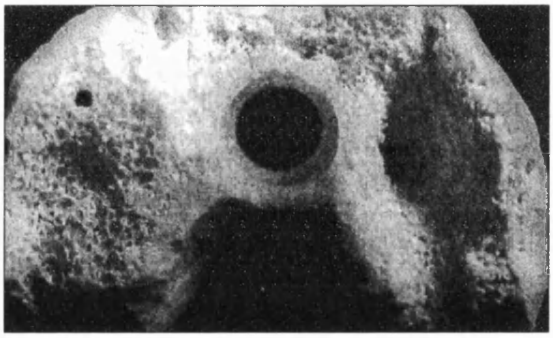

Figure 2.13: View of the major defect component looking down on the knee joint [32]

In a situation where particulate (granular) allograft material is used it is important that the chips are not made too small because a slurry will be formed that cannot support the implant [33].

Histological evaluation provides the only absolute evidence for graft viability – stability and bony tissue incorporation. To achieve this goal, integrity of the implant-interface, graft-host bone interface and a securely supported stem are imperative in the tibia and femur [33, 40]. In the best case scenario, due to the poor biocompatibility of allograft compared to autograft, the allograft may show healing at the graft-host junction. This is followed by vascular invasion and osteoclastic resorption of the existing dead bone followed by osteoblastic deposition of viable bone over a time period of a few days [29].

Allograft material is in much greater supply than autograft, even though it is biologically inferior to autograft. However, as previously discussed, allograft reserves are rapidly becoming depleted and there is a demand for a synthetic alternative to combine the biological properties of autografts and the structural support of allograft without the risk of infection or antigenicity.

2.2.2.4 Interbody Spinal Fusion Applications

Over 200,000 surgical spine procedures are performed in the United States each year. This compares with 50,000 in the United Kingdom and Europe. This relatively new procedure is an attempt to fuse two interbody vertebrae by creating a bone regenerative bridge. This bridge must have osteoconductive and osteoinductive properties combined with a stiff, strong durable structure that allows further remodelling and complete osteogenesis (i.e. the implant is completely overtaken by the host capillaries, cells and tissue) [41].

Lumbar interbody fusions use cage devices made of titanium (due to its low weight and high strength) to improve the overall stiffness of the graft. The structural allograft sits inside the cage and allows osteoconduction through the transfer of lattice ions to and from the graft and host. Spinal fusion rate (ingrowth of bone into the graft) increases with mechanical loading [13, 19], therefore, it is necessary to provide stress shielding for the main regenerative graft [14, 42]. Stress shielding is a phenomenon undertaken by cortical bone in certain parts of the body in order to relieve the cancellous bone region of the high stresses that could cause failure. A titanium cage is used as an attempt to create an optimal structural environment for fusion due to the high compressive forces subjected to the vertebrae in the spine [43]. The graft material is either in bulk or particulate form and is fixed inside the titanium cage in contact with the two vertebrae.

2.2.2.5 Maxillofacial and Long Bone Segmental Defects

Maxillofacial operations require very little structural support compared with the high mechanical loading of the hip, knee and spine. Therefore, usually it is possible to for the surgeon to remodel the whole (or part) of the mandible without having to undertake an autograft procedure.

Long bone segmental defects such as caused by fracture of the tibia, fibia or femur are extremely difficult to graft as there is often a need for a structural cortico-cancellous graft that enables good

vascularisation properties and offers structural support [44]. The quality of graft needed is very high and these applications can be termed "specialised".

To summarise, there is a need to produce in large supply a synthetic alternative to natural bone graft material in both bulk and particulate form. The material must be able to influence the activity of osteoclastic cells which in turn stimulate osteoblastic development and enhance bonding of the implants to host bone. This biological requirement must be conjoined with a structurally long lasting framework for complete incorporation of bony tissues. The examples of procedures required to restore bone stock loss or to increase the quality of the bone at the defect site is ever increasing, as is the need for both bulk and particulate forms of synthetic graft materials for more advanced, specialised techniques.

2.3 Requirements of a Bone Replacement Material - Calcium Phosphate

Due to the immunological restrictions and limited availability associated with both autografts and allografts, there is a need to find a synthetic alternative that is able to offer both potential for osteogenesis and structural support in both bulk and particulate form.

The following section details the requirements of a synthetic bone graft as well as the potential of a replacement material to fulfil this obligation i.e. to be a successful biomineralised regenerative bone replacement. The synthetic material should offer the same properties as a bone graft, which is a full structural and biological matrix for complete revascularisation of the implant area.

The minimum requirement for a graft material is to interact with the host's mechanical and biologic environment in order to induce osteogenesis (complete bone remodelling over time) [22]. It is this criterion that finally governs the potential of a graft material for bone replacement applications. The main requirements of a bone replacement material are:

1) Bioactivity – chemical interaction with bone required for bone formation.
2) Mechanical Properties – need to ensure structural integrity of implant.
3) Porosity – to allow remodelling of osseous tissues (osteogenesis).

It has been found since the 1970's that certain ceramic materials exhibit unique biological properties when placed in an osseous environment [45-48]. Table 2.1 shows a list of synthetic calcium phosphate (CaP) bioceramics and other materials developed commercially that exhibit this property.

Calcium phosphate's are a class of ceramics that can be termed bioactive. CaP ceramics exhibit osteoconductivity and have been shown to possess a strong CaP-bone interface [49-53]. The materials properties required of a bone replacement material (detailed above), along with details of chemical activity are detailed in this section.

The motivation for using CaP ceramics was initially due to the finding that calcium phosphates were biocompatible with bone mineral [54, 55]. It must be remembered that bone mineral is in the form of hydroxyapatite (HA – Ca_{10} $(PO_4)_6$ $(OH)_2$), which is a member of the calcium

phosphate family. A layer of biologically active hydroxycarbonate apatite must form for a bond with tissue to occur. It is the rate of hydroxycarbonate apatite formation that varies greatly from the pure stoichiometric form of hydroxyapatite to the calcium deficient tricalcium phosphate – $Ca_3 (PO_4)_2$ (TCP) [55]. Due to the ever-increasing joint replacement and revision procedures that now occur, there is a growing demand for a biocompatible synthetic bone replacement material.

CaP ceramics have outstanding properties. These include a similarity in chemical composition to bone mineral, bioactivity and the ability to promote cellular function leading to formation of a strong bond between bone and the implant interface [49-56]. In addition, they have the unique property known as osteoconduction and with the correct pore size distribution even osteoinduction [55-57]. Osteoconduction is the ability to invite cell growth to supply bone formation, and osteoinduction is the capability to provide osteogenesis i.e. bone remodelling as would occur in natural bone.

Name	**Manufacturer**	**Material**
Endobon	Merck, CH	Biological hydroxyapatite (HA)
BoneSource	Orthofix Inc., USA	Tricalcium phosphate (TCP)
Vitoss	Orthovita, USA	Tricalcium phosphate (TCP)
Triosite	Zimmer, USA	Biphasic HA/TCP
BoneSave	Stryker Orthopaedics, USA	HA/TCP granules
OP-1	Stryker Biotech, USA	Recombinant human BMP-7 with type I collagen
Bioglass	US Biomat. Corp., USA	Bioactive glass

Table 2.1: List of some well known commercial synthetic calcium phosphates and other materials developed commercially.

CaP ceramic graft material offers the possibility of being completely remodelled by the host surrounding host bone so that in this respect is like a scaffold material offering initial support and integrity to a defect area (e.g. bone loss due to osteoporosis) [50].

Therefore, the possibility of calcified tissue replacement following the implantation of a CaP based substrate is a concept that deserves extensive study. It is essential that the replacement material does not suffer deterioration once implanted. CaP implant materials are composed of the same ions that make up the bulk of natural bone mineral [54, 58]. As a consequence, when these

materials are implanted in bone they are capable of participating in CaP solid solution reactions at their surfaces.

The one property that bioceramics must have is survivability (i.e. a life span of > 20 years). The unique set of requirements set out at the beginning of this section, have made specially designed bioceramics one of the most remarkable accomplishments of ceramic research. The development of CaP ceramics has in the past concentrated upon enhancing the biological response of apatitic implants [59, 60]. The future research trends appear to focus on improving the strength of CaP bioceramics without compromising an interconnected porosity distribution suitable for possible osteogenesis [50].

2.3.1 Biocompatibility of the Calcium Phosphates and Natural Bone Mineral

The biocompatibility of CaP ceramics correlates with statements such as that made by Hench in 1975 that "an ideal implant material must have a dynamic surface chemistry that induces histological changes at the implant interface which would normally occur if the implant were not present" [51]. The success of CaP compositions can be attributed to the essential roles of calcium (Ca^{2+}) and phosphate (PO_3^{4-}) ions in the natural process of bone regeneration. CaP based compounds are osteoconductive and can establish a physico-chemical bond to bone during the bone regenerative process. Their degree of reactivity with living tissues, which relates to the healing ability, depends on the chemistry as well as on the physical structural features such as mineralogical composition, crystalline state, porosity, pore size, interconnectivity of pores and sintering temperature.

Hydroxyapatite ceramics have proved to be biocompatible and bioactive materials that can chemically bond with bone; de Groot [61] reports of trials that have been successfully completed for repair of bone defects and augmentation of osseous tissues. The work of de Groot, Best, Bonfield et. al [62, 63] on dense sintered synthetic hydroxyapatite, has shown this ceramic to be totally biocompatible and to form a direct bond with the neighbouring bone [64-72].

The biocompatibility of the CaP family is not only suggested by its composition, but also by results of *in vivo* implantation, which according to published information show no inflammation and no foreign body response [73, 74]. New bone formation has been found to develop at both

the edge of a defect and on the ceramic surface; according to many authors it is conducted along the hydroxyapatite, forming a bridge between the host bone and the hydroxyapatite [61, 75-77].

Figures 2.14 and 2.15 demonstrate the osseoconduction properties over time of a synthetic CaP implant, indicating excellent biocompatibility. In this experiment a material known as "Synthos" is used to induce regeneration of bony defects in rabbits. Note the increase in size of blood vessels in figure 2.15 that is taken 58 days postoperatively [78].

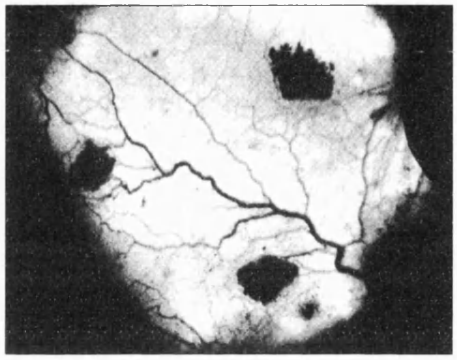

Figure 2.14: Photomicrograph taken at 8 days postoperative showing increased vascularisation through implant material. Scale 1cm ~ 100μm. [78]

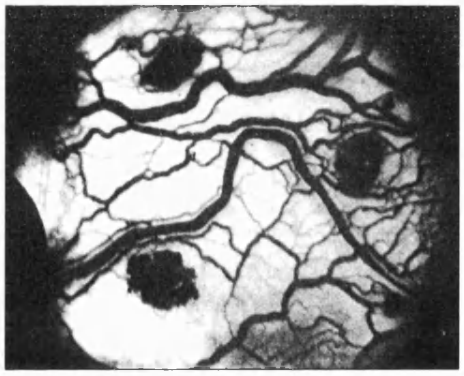

Figure 2.15: Photomicrograph showing the tremendous increase in size of blood vessels in implant material, associated with osseoconduction and excellent biocompatibility after 58 days post-operative. Scale 1cm ~ 100μm. [78]

The resorption of CaP ceramics has been the subject of many studies [74, 79-81]. It has been suggested that the resorption rate of CaP implants is related to their form, chemical composition and structure, including macroporosity and microporosity. Both chemical dissolution and cell-mediated resorption are involved in the resorption process, which accounts for the bioactivity of these materials and also for the osseoconductive properties [52, 53, 57, 74, 79, 80].

In order to promote remodelling and osteogenic growth, Urist proposed a novel factor to help induce bone growth [20]. The factor, Bone Morphogenetic Protein or BMP, is responsible for a variety of events in cellular embryogenesis [62]. An example of a BMP is recombinant human BMP (rhBMP), which induces bone formation in a process that mimics ossification. BMPs are used in conjunction with drug delivery systems. These range from collagen composites to varying polymeric scaffolds to bioceramics. An ideal delivery system that would allow a slow release of the BMPs should be biologically and immunologically active, quickly absorbed and supportive of osteogenesis [62]. Large microporosities are formed in CaP bone replacement materials, and it is through this medium that BMPs can be released as a drug release mechanism in order to promote remodelling.

CaP ceramics have been shown histologically to be mineralised by active osteoblasts, as figure 2.16 indicates [8].

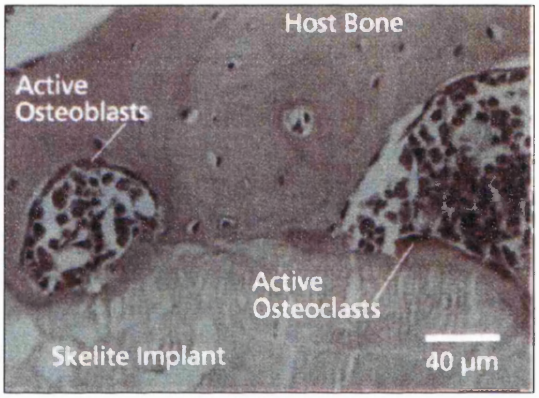

Figure 2.16: The presence of bone cells encourages bone remodelling [8]

It appears from the studies previously referred to, that the resorption of CaP biomaterials is beneficial to bone formation and that free Ca^{2+} ions could be considered as the origin of bioactivity. However, too much dissolved Ca^{2+} and PO_4^{3-} ions, leads to a sharp change in the microenvironment that may disturb the activity of the host cells, and create adverse effects on tissues [77, 80, 82].

However, the crucial bioactivity demands of these implant materials must be combined with initial mechanical properties comparable to that of natural bone so that the materials structural integrity is upheld [83-85].

2.3.2 Dependence of Bone Ingrowth on the Pore Size and Pore Distribution – Tissue Reaction and the Effect on Strength

In the development of CaP ceramics, attention is particularly placed on the influence of pore size on the bone ingrowth behaviour. Macropores of at least 50 - 100μm are required to host the cellular and extracellular components of both bone and blood vessels, and those greater than 150μm are expected to be effective for osseoconduction to be successful [64, 65, 86, 87, 88]. Therefore, the control of porosity within CaP ceramics is an important subject for investigation.

The characteristics of porosity strongly affect the mechanical behaviour of ceramic foams (with interconnecting networks of pores making osseoconduction possible) with compressive modulus and compressive strength being highly sensitive to both density and pore isotropy [89, 90, 91]. Therefore, implants with larger pore sizes will inherently be weaker as a result of an associated reduction in density, however they may be more successful in promoting osseoconduction [54, 72].

Numerous authors [65, 70, 73, 80] suggest a minimum pore size of 150 – 300μm is required for sustained healthy bone ingrowth in ceramic structures. There is a general agreement that an increase in the volume of bone ingrowth is directly related to an increase in pore size. However, some authors [84, 92] have challenged this, suggesting that it is an increase in the connectivity of the pores and the frequency of the pore interconnections, that results in greater penetration of bone ingrowth [76].

Since bone differs structurally depending on its function and location in the body, the same pore shape and size may not be ideal for all potential uses [20]. Pore size and topography can be carefully modulated to control the interconnectivity of the porous network (by changing the porosifier size), which has been found to be an important factor in CaP bioceramics [49, 93, 94]. Osseous proliferation is sensitive to surface topography, strain and other mechanical stimuli. Cells can discriminate against even subtle changes in topography, and they are most obviously sensitive to chemistry, topography and surface energy [95].

Previous studies have shown how porous devices are prepared by impregnation: cellulose sponges with controlled pore morphology are treated in a hydroxyapatite slurry to obtain the

bimodal porous structure [86]. Figures 2.17 and 2.18 show the morphology of the porous structures, and in particular the macro-and microporosity.

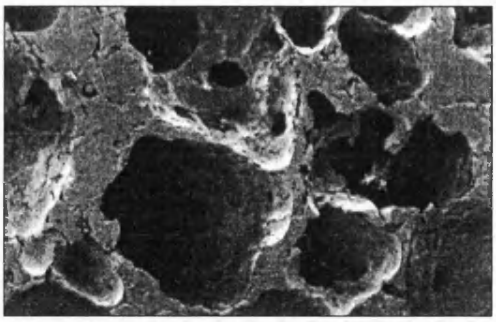

Figure 2.17: Morphology of porous hydroxyapatite at low magnification, indicating macroporosity distribution (25mm=500μm) [86]

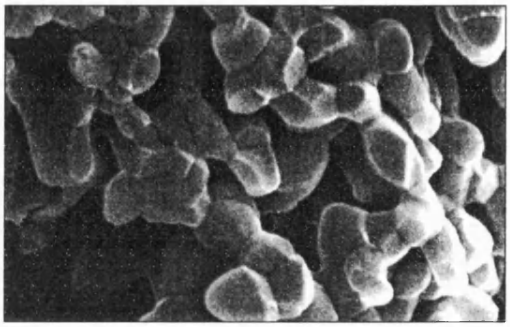

Figure 2.18: Morphology of porous hydroxyapatite at high magnification, indicating microporosity distribution (27mm=5μm) [86]

Macrostructural analysis has demonstrated from previous studies the complex inter-relationship between the structural features of an open pore structure, pore size and density [57, 63, 96, 97]. Compression testing has also demonstrated the effect of density and macro/microstructural anisotropy on the mechanical properties of the ceramic devices. Figure 2.19 shows the results of a study carried out by Hing, Best and Bonfield [63] on the variation of compressive stress with apparent density (given as the dry weight of the body divided by the volume) of a commercially available product Endobon®, which is a biological hydroxyaptite (Ca/P ratio of 1.67). NB. This is not the real density of the specimen, which is measured by submerging the specimen in deionised water.

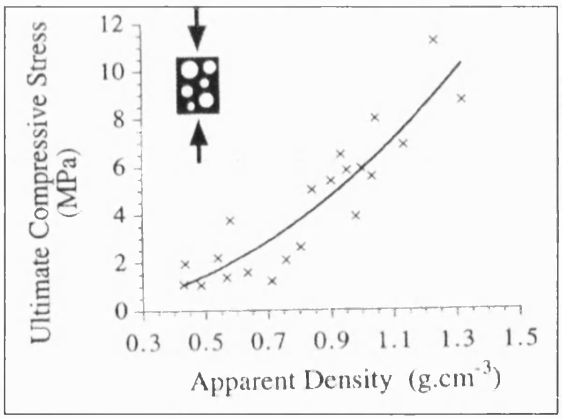

Figure 2.19: Effect of variation of the apparent density on the ultimate compressive strength of porous HA samples [63]

The results obtained from previous studies on porous HA [63, 86, 89] in particular by Hing, Best and Bonfield, underline the importance of a full structural and mechanical characterisation of porous ceramic implant materials, and the extensive study still required to further develop this technology.

The strength-porosity correlation may in form the design of porous CaP ceramics with optimised mechanical strengths. Figure 2.20 shows how porosity affects the compressive strength of dense CaP bioceramics as a result of the different types of pore geometry (created by using different shaped particles as a porosifier).

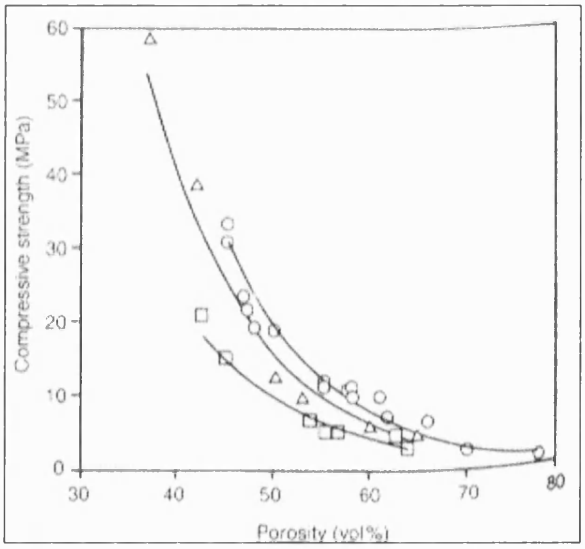

Figure 2.20: The compressive strength-porosity behaviour of porous HA ceramics with different types of pore geometry; circle: spherical, triangle: ellipsoid, rectangular: oblate [80]

Hing and Bonfield et. al [89] also stated how the bone ingrowth has a strong reinforcing effect on porous CaP ceramic implants. An increase in ultimate compressive stress from 2MPa to 20MPa has been reported for coralline porous HA after 100 days implantation (figure 2.21) [79].

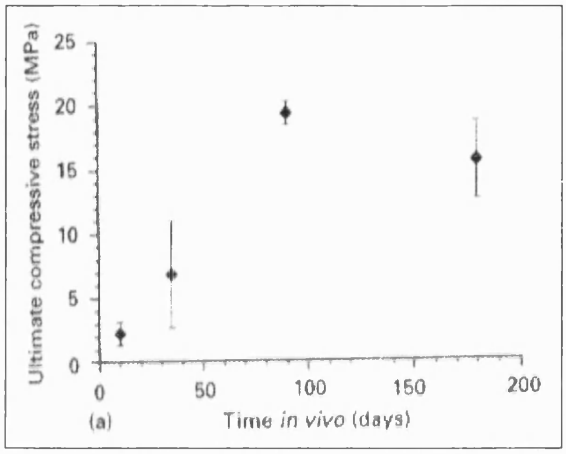

Figure 2.21: The variation of compressive stress as a function of implantation time [79]

Porous, interconnected structures that possess a bioactive element, invite ingrowth of bone into the implant leading to a more securely fixed and integrated repair. Ideally, porous implants should induce a response similar to that of fracture healing when placed in an osseous environment [42, 52, 89].

The porosity distributions that result from the use of cellulose sponges as a porosifier, give rise to both macro-and microporosity (figures 2.17 and 2.18), and also give rise to an interconnected network of porosity. All these parameters are important when considering the development of CaP ceramics, as through the interconnecting porosity the nutrients are exchanged between pores, enhancing bone ingrowth into the scaffold [86, 98]. Thus, the pore size has to be considered in order to optimise the mechanical strength of CaP ceramic bone substitutes for clinical load-bearing applications [27, 99-102].

The structural and mechanical properties of some current bone replacement materials are reviewed in table 2.2. The structural and mechanical properties of cancellous and cortical bone are also included for comparison purposes.

Material	Cortical bone	Cancellous bone	Porites (coral)	Bioglass 45S5	Endobon ®	HA (pure)	HA/ TCP	HA	HA
Content	Apatite (+ mineral impurities) *	Apatite (+mineral impurities) *	Coral HA	45% SiO_2, 24.5% Na_2O, 24.5% CaO, 6% P_2O_5	HA	HA Ca/P ratio = 1.67 (>99.2 %)	HA/ TCP (60/40)	HA	HA
Density (g/cm^3)	1.6 - 2.1	0.05 – 1.0	1.6	2.66	0.4 – 1.2	3.16	0.6 – 0.9	0.3 – 0.8	0.03 – 0.06
Compressive Strength (MPa)	100 – 230	2 – 12	193	126	1.11	500 – 1000	5 – 7	1.6 – 3.3	0.05
Youngs Modulus (GPa)	7 – 30	0.05 – 0.1	76 – 83	35	0.2 – 3.1	80 – 110	-	3.6 – 15.0	-
Volume porosity (%)	5 – 10	40 - 95	47 – 51	< 5	10 – 40	Dense	40 – 60	72 - 90	> 95
Interconnected or isolated porosity?	Int.	Int.	Int.	Isol.	Int.	Isol.	Isol.	Int.	Int.
Pore size range (μm)	10 – 200	10 – 1000 **	~ 150	30 – 60	100 – 400	< 10	100 - 400	15 - 120	50 - 500
Reference	Rho et. al. [15]	Rho et. al. [15]	Ravagli oli et. al. [48]	Hench [47]	Hing et. al. [63]	Simske et. al. [21]	Liu [123]	Sepul veda [121]	Binner [110]

* The content of bone varies due to its location in the body.
** Porosity size range in bone can be greater than this.

Table 2.2: Review of structural and mechanical properties of some current bone replacement materials.

It can be seen from table 2.2 that it is difficult to combine both an interconnected, high volume porosity network, with sufficient mechanical properties for load-bearing applications. Work done by Sepulveda and Binner on HA foams illustrates this point. On the other hand, those materials with a low volume porosity and isolated porosity have sufficient mechanical properties for possible load-bearing applications.

Therefore, the relevance for extensive study into the nature of the porosity and its distribution within CaP ceramics is obvious. Special attention must be given to achieve a full characterisation of the micro-macroporosity distribution, its morphology and hence resulting effect on mechanical properties, in particular compressive strength. It is therefore a challenge to attempt to reproduce those structures as found in cortical and cancellous bone [90].

2.3.3 Chemistry and Phase Transitions of Calcium Phosphates

The calcium phosphates belong to a family of minerals crystallising with a hexagonal symmetry, which are found extensively in nature [67, 103]. The chemistry of calcium phosphates is extremely complex with a series of related inter-substitions possible, giving rise to various "impure" and/or calcium deficient apatites e.g. natural bone can have up to 8% carbonate [104], resulting in numerous biphasic calcium phosphates being formed.

The general chemical formula of the apatites is $M_5(YO_4)_3X$

where M = divalent cation (such as Ca^{2+})
X = univalent anion (such as OH^-)
Y = trivalent species usually phosphorous, which forms an oxyanion.

As the name hydroxyapatite (HA) is used for a wide range of compositions beyond the ideal formula – $Ca_{10}(PO_4)_6(OH)_2$ (where the Ca:P ratio is 1.67), great caution must be exercised when comparing different results. The exact composition seems to be an important parameter, since the biodegradation rate, for example, depends on it [64]. Tricalcium phosphate – $Ca_3(PO_4)_2$ (TCP) has a Ca:P ratio of 1.5 and is termed a calcium deficient apatite.

Commercially produced powder forms of calcium deficient HA sintered at 800 - 900°C begin to form β - tricalciumphosphate (β-TCP) as densification occurs. At, or near, 1180°C, β-TCP transforms (via an allotropic transformation) into α - tricalciumphosphate (α-TCP). At this point the density decreases slightly due to a volume increase [64]. NB. These transitions only occur in low crystallinity grades of hydroxyapatite.

Figures 2.22 and 2.23 indicate the microstructure of β-TCP and α-TCP, sintered in air at 1100°C and 1200°C respectively.

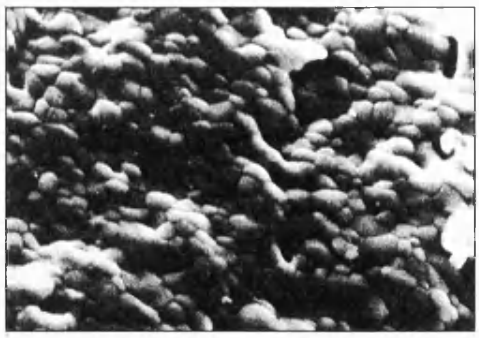

Figure 2.22: SEM micrograph of β-TCP sintered at 1100℃ (x700) [67]

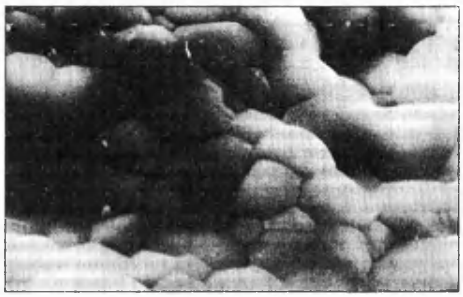

Figure 2.23: SEM micrograph of α-TCP sintered at 1200℃ (x2100) [67]

When the atomic ratio of Ca:P of an initial slurry mix is different from the ideal Ca:P ratio i.e. 1.67, the ceramic body sintered at temperatures in excess of 1000°C is generally composed of several phases such as HA + calcia (CaO) when the Ca:P ratio is greater than 1.67, or HA + TCP when the Ca:P ratio is less than 1.67 [64]. According to Royer et. al [64], TCP appears to play an active role in the strengthening of HA (figure 2.24).

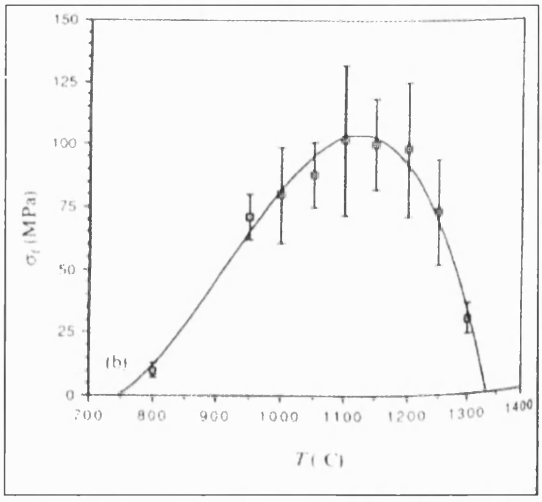

Figure 2.24: Flexural strength as a function of temperature for pure HA, indicating strength increase due to the formation of TCP phases at ~ 1100 – 1200°C, depending on mineral content [64]

On transformation from β-TCP to α-TCP, there is a volume increase that introduces compressive stresses at the surface. Compressive forces can reduce the critical flaw size and increase the corresponding failure strength [104].

At around 1350°C the final theoretical density (~98%) is obtained. For temperatures above 1350°C, the flexural strength breaks down because the samples are degraded following the decomposition of α-TCP into tetracalciumphosphate ($Ca_4P_2O_9$) [64].

The most widely studied CaP ceramics are tricalciumphosphate (TCP), hydroxyapatite (HA) and the newest tetracalciumphosphate (which has lower strengths) [62]. The appeal of the calcium phosphates rests largely with their biocompatibility since they are protein free, offer minimal immunological reactions, foreign body reactions or systemic toxicity have also been reported with their use [89, 104, 105]. The chemical and mineralogical similarity of calcium phosphates with the calcified tissue that they are replacing may provide a template for osseous growth (regeneration of local environment) and/or subsequent remineralisation [106].

There is evidence that biphasic ceramics (consisting of α-TCP or β-TCP in conjunction with HA) are biologically more active than pure HA ceramics alone [104]. Also the biological behaviour of these biphasic CaP ceramics containing β-TCP is superior in terms of new bone formation.

Figure 2.25 shows how the sintering temperature affects both the porosity and the compressive strength of a biphasic ceramic.

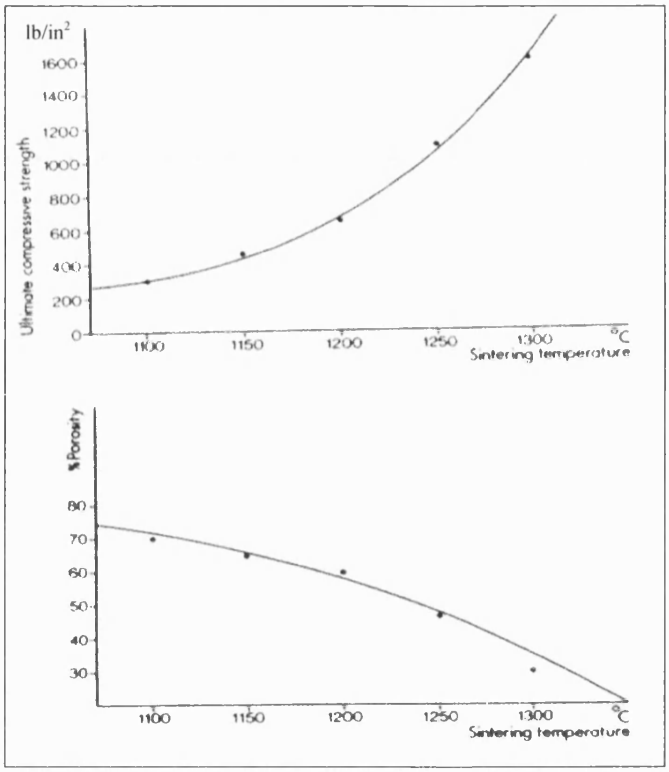

Figure 2.25: The dependency of compressive strength and porosity on temperature [61]

Pores of 1 – 10μm in diameter allow cell ingress in an implant. In conjunction with this a high microporosity volume enhances the wetting of bodily fluids on the implants, which increases the surface area for cell interaction. Porosity ranging from 10 – 100μm in diameter helps develop the propagation of bone growth. For continued vascular growth and osteoid formation, an interconnected pore structure with pore diameters greater than 100μm is required whereby osteoblasts may form the beginnings of bone growth. Some authors claim that larger incidents of interconnecting pore diameters are required i.e. > 300μm for bony ingrowth, and that it is the amount of interconnectivity and the interconnected pore size that determines the success of CaP implants [81, 82, 84]. The design of synthetic bone graft material with a porosity network mimicking that of the bimodal structure of bone (i.e. with a cortical-cancellous porosity distribution), combined with sufficient mechanical strength to withstand the local forces applied on the defect area, is a most important challenge [100].

2.4 Fabrication Techniques for Calcium Phosphate Bioceramics

Fabrication processes for CaP bioceramics vary from mechanical slip cast processes to hydrothermal and chemical processes such as foaming and sol-gel reactions [108-114].

The main challenge when fabricating CaP bioceramics (as far as bone remodelling and continued vascularisation are concerned) is to allow enough interconnected porosity without compromising the structural integrity. There is much more scope for fabrication of cortical bone replicate specimens, as the biological requirements in terms of porosity, are not as demanding as for porous CaP bioceramics [108]. The final step in the fabrication of CaP bioceramics is nearly always sintering by a thermal process. The fabrication processes outlined below are used to produce a green body, which is ready for sintering.

2.4.1 Powder Preparation

There are numerous methods for producing synthetic hydroxyapatite and other forms of CaP powders. However, the favoured production route is termed the wet chemical method.

It derives from the basis that Ca^{2+} and PO_4^{3-} ions react in aqueous solution to form the initial hydroxyapatite [115]. Reaction 1 below shows a classic example of synthesising theoretically pure hydroxyapatite powder with a Ca:P ratio of 1.67 [109].

$$10Ca(NO_3)_2 + 6(NH_4)_3 PO_4 + 2NH_3.H_2O \longrightarrow Ca_{10} (PO_4)_6 (OH)_2 + 20NH_4NO_3 \quad (1)$$

where $Ca(NO_3)_2$ - calcium nitrate
$(NH_4)_3 PO_4$ - ammonium phosphate
$NH_3.H_2O$ - ammonia solution
NH_4NO_3 - ammonium nitrate
$Ca_{10} (PO_4)_6 (OH)_2$ - theoretically pure hydroxyapatite (Ca/P ratio of 1.67)

Calcium nitrate solution is mixed (in drop steps) in stoichiometric proportions into ammonium phosphate solution. This mixture is stirred at a temperature of 90°C. While stirring, ammonia solution is added to keep the pH value at no less than 9 (to avoid formation of CaO). The suspended sediment is then filtered and washed several times until the pH value is equal to approximately 7. This final sediment is dried at 110°C for 3hrs and calcified at 700°C for 3hrs.

The calcified sediment is then dispersed in ethanol solvent and ground for 24hrs. The final hydroxyapatite (HA) powder is dried in air (relative humidity – 50%, temperature – 25°C) [109, 115, 116].

Figure 2.26 shows a TEM micrograph indicating the dimension and sizes of powders produced by the wet chemical method.

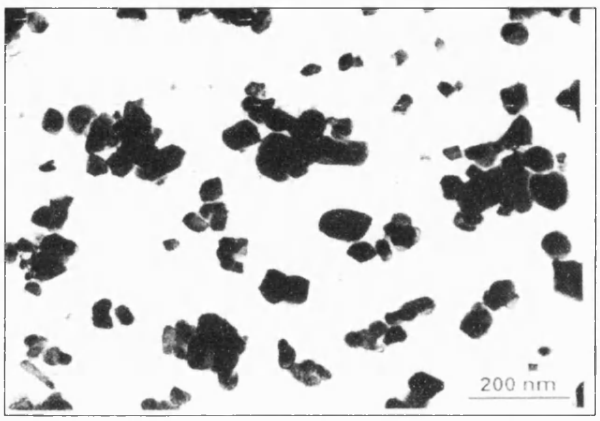

Figure 2.26: TEM of HA powder after calcining at 800°C for 3hrs [116]

The ease and convenience of this process is that it allows Ca/P regulation of the final product. Crystalline or amorphous HA powders can be produced by varying the Ca:P ratio; (e.g. HA – Ca:P ratio 1.67, TCP – Ca:P ratio 1.5), this may also be achieved by including such phases as calcium phosphate hydrate, therefore it is possible to fabricate HA, tricalciumphosphate (TCP) or a biphasic CaP material from the base powders.

Utilisation of these powders allows thermo-chemical procedures for producing CaP bioceramics in both bulk and granular form. Mechanical processes have also been developed (e.g. slip casting and pressing) in order to produce dense CaP bioceramics [114]. Other chemical processes such as foaming by polymerisation reactions to produce porous bioceramics have also been explored.

2.4.2 Foaming and Gelcasting

Foaming is a process whereby gas bubbles are introduced to the slurry in order to encourage interconnectivity of the pores on drying and sintering [110, 117-119]. Ultrasonification of powders by the incorporation of methyl cellulose followed by immediate drying at 90 – 100°C

for 24hrs allows the foaming to occur. Figure 2.27 shows an example of the final HA bioceramic after sintering up to 1350°C [117].

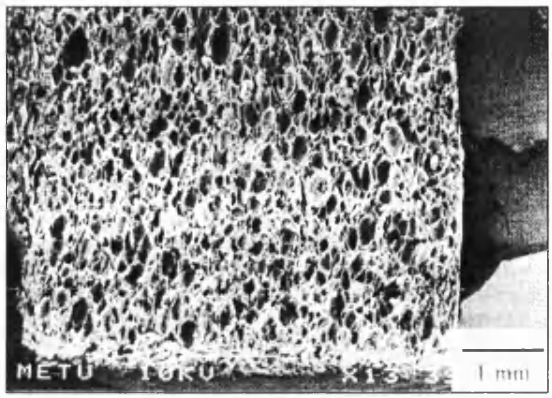

Figure 2.27: SEM micrographs of HA bioceramic produced by foaming [118]

High drying temperatures are required to immobilise the slurry particles therefore less drainage occurs [110]. Figure 2.28 shows a flow chart of the foaming process.

The process offers good structural integrity however the interconnectivity between pores is limited as the polymerisation process is difficult to control.

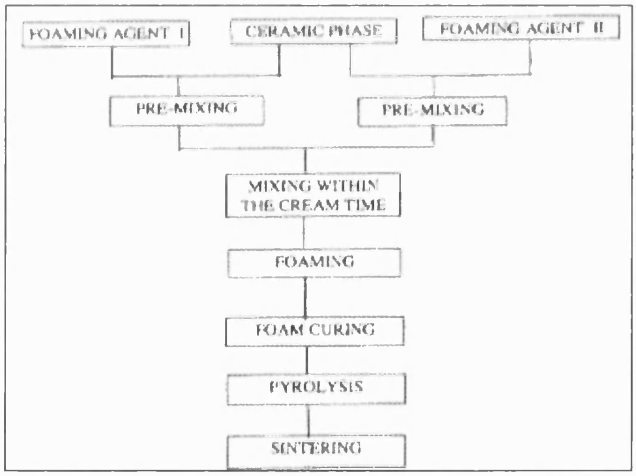

Figure 2.28: Flow chart describing stages of foaming of CaP bioceramics [119]

Gelcasting is very similar to foaming, only that in gelcasting the foam structure produced is more ordered and controlled giving circular pores of varying sizes [120]. After foam formation, polymerisation of the monomers on heating promotes setting. The pore size depends on the time

of polymerisation and can be varied by expansion of the foam prior to polymerisation [113]. Figure 2.29 shows an example of the gelcast structure.

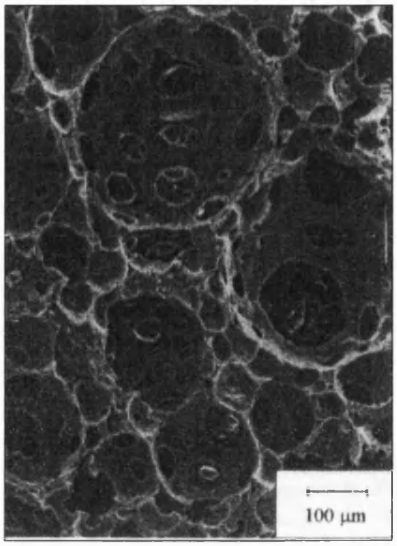

Figure 2.29: CaP bioceramic produced by gelcasting [120]

Ceramic gelcasts can produce porosities ranging between 40-90%, with pore sizes ranging from 30-2000µm [121]. Two different amide monomers, combined with a suitable dispersing agent, allow for optimum polymerisation [111].

2.4.3 Thermochemical Processes

Fabrication procedures that fall into this category utilise chemical interactions, novel pore generators and the use of high temperatures [76, 112, 114, 116].

2.4.3.1 Burnt-out Polymeric Spheres (BurPS)

The aim of this process is to produce porous CaP ceramics with controlled porosity by using various polymeric materials as pore generators [76]. Figure 2.30 shows an example of a HA/α-TCP with PMMA powder as a porosifier.

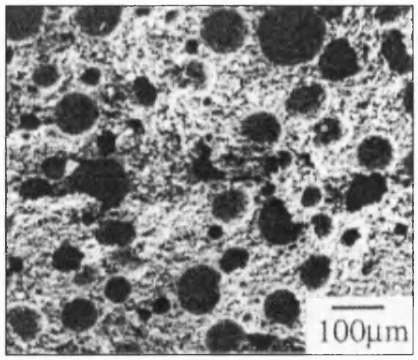

Figure 2.30: HA/α-TCP ceramic with 33.8vol% PMMA powder as porosifier [122]

It is possible to induce pore sizes in the correct size range for osteoconduction (150 - 300μm) by this process. However, the particles will not make contact and therefore the porosity is isolated. Larger number of particles are required to obtain any degree of interconnectivity, however the structural integrity then becomes compromised.

Pore generators used include polyvinyl butyral (PVB), polymethylmethacrylate (PMMA), polyethylene oxide (PEO) and polyvinyl chloride (PVC). Particle sizes can range from 50 – 250μm (±50μm). Usually particles greater than 250μm in diameter can cause cracking between pores, generally weakening the material [76, 122, 123]. Pore generator mixtures can range from 30-60% depending on the amount of porosity required (i.e. density of sample) and strength requirements. The mixed powders (HA and polymer) are then subjected to uniaxial die-pressing at pressures of over 20MPa.

Polyethylene oxide (PEO) is believed to be the powder material that offers the greatest degree of interconnectivity while PMMA is known to create horizontal cracking on pressing, thus compromising the structure [122]. Finally, burn out must be completed in order for the CaP ceramic to be non-toxic and bioactive with the host human tissue.

It is difficult to obtain the correct pore distribution and interconnectivity for BurPS materials to be considered as potential bone replacement materials.

2.4.3.2 Calcium Phosphate Sol-Gels

This process is extremely similar to the preparation of CaP powders using the wet chemical method. CaP sol-gel materials offer a useful method for preparing tailor made coatings and dense CaP [112]. Typically CaP gel can be produced from the reaction given in reaction 2 below:

$$10Ca(NO_3)_2 + 6H_3PO_4 + 2NH_4OH \xrightarrow[\text{r.t.}]{\text{pH 10 -12}} Ca_{10}(PO_4)_6(OH)_2 + 20HNO_3 + 2NH_3 \qquad (2)$$

Figure 2.31 indicates the apparatus and experimental procedure commonly used for gelatinous production of CaP.

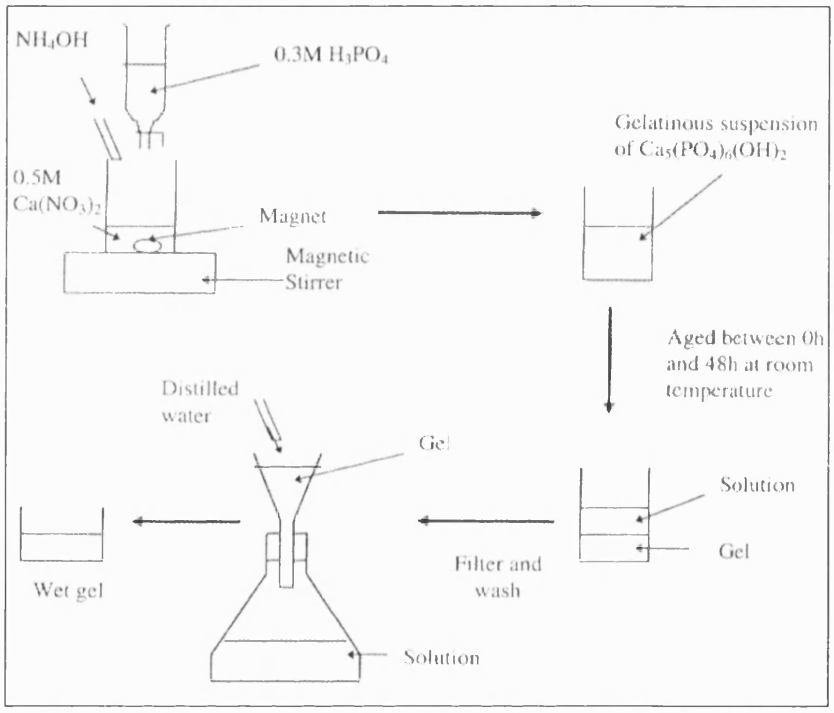

Figure 2.31: The synthesis of CaP gel [124]

A stoichiometrically proportioned amount of phosphoric acid is titrated into a glass beaker containing calcium nitrate. The pH is kept between 10 and 12 by adding ammonium hydroxide at a drop at a time. By ensuring the pH is 10 – 12, development of gelatinous suspension of CaP is facilitated. This suspension is aged at room temperature for 0-48hrs, and is filtered and washed to obtain the correct Ca/P ratio. Pure HA has a Ca/P ratio of 1.67. TCP has a CaP ratio of 1.5

[109]. Limited bioceramics have been prepared using this technique due to the difficulty in obtaining the correct Ca/P ratio.

2.4.3.3 Freeze-drying

The freeze-drying process has been used to produce both dense and porous freeze-cast CaP bioceramics [116] (powder preparation takes place as described in section 2.4.1), by placing the pre-synthesised gel of CaP in liquid nitrogen and at low pressures (3-6 bar, 1 bar ~ 10^5 Pa). An infrared lamp at an intensity in the order of 3000Wm^{-2} accelerates the process. This procedure is maintained for 36-72hrs or until freeze-drying is complete. Figure 2.32 shows sample preparation of freeze-drying.

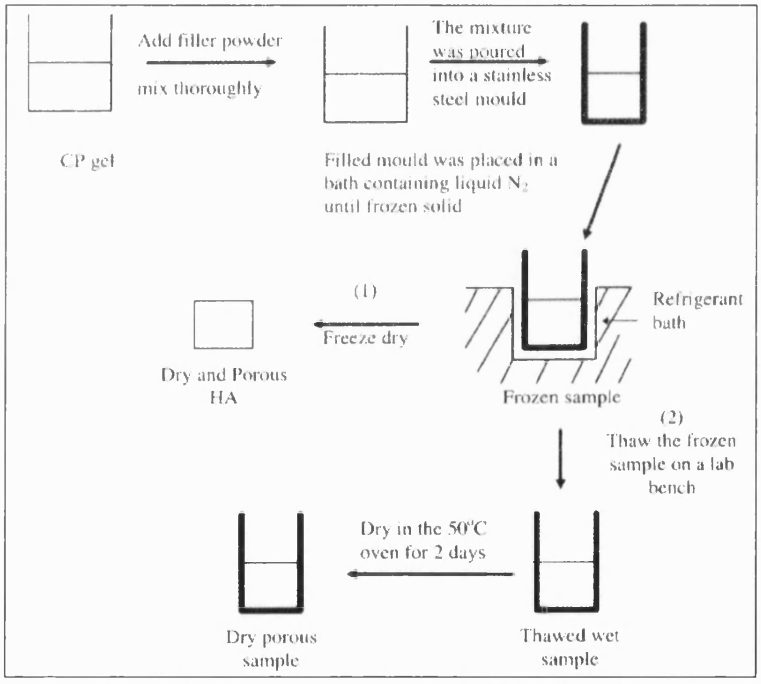

Figure 2.32: Sample preparation of freeze casting [124]

The green compacts thus produced are then heated and sintered for three hours at a temperature range of 1100-1350°C depending on choice of phase composition [116].

In contrast, porous CaP ceramics produced by freeze-drying methods utilise the vaporisation of water vapour as a porosifier. After freeze-drying at –60°C, samples are allowed to thaw, they are then dried in an airflow oven and sintered up to 1350°C [124]. It is difficult to fabricate

bioceramics from this method due to the difficulty in eliminating cracking in the material on thawing.

2.4.4 Mechanical Processing

Both porous and dense CaP ceramics can be produced by a range of physical processes which include slip casting, pressing, extrusion and tape casting [80, 125, 126]. Both these and many other processes utilise the properties of a preformed ceramic slurry. The slurry must be able to flow and form a cast in order to produce a green body. The two most popular mechanical processes are tape and slip casting.

2.4.4.1 Tape Casting

Tape casting is a well known process for producing mechanically robust electronic materials e.g. in capacitators. The process has only been used relatively recently (mid 90's) to fabricate CaP bioceramics [127]. The advantage of the method is that by understanding both slurry rheology and slip properties; it is possible to produce both dense and porous CaP bioceramics. Tailored gradients of porosity ranges have also been produced in CaP bioceramics produced by tape casting [128].

After slurry formation, the slip is cast onto a glass plate by means of a doctor blade. The produced tape, once the solvent has evaporated, contains ceramic powder and the remainder being made up of binders, plasticisers, dispersant and other additives that develop into pore generators on sintering [128, 129]. The green tapes obtained can be fired to produce dense or porous bioceramics depending on the amount of additives present in the slip.

This process is extremely successful in producing dense bioceramics. Porosity may be introduced however it is difficult to maintain the structural integrity of the bioceramic (as with BurPS materials).

2.4.4.2 Slip Casting

Through the development of die-pressing technology to produce CaP bioceramics, difficulties have been encountered when using conventional methods to form complex geometric shapes

[130]. Numerous advantages stem from casting a ceramic slip into a mould. These include controlled geometry, structural uniformity and the minimisation of defect size. Traditionally, slip casting is used for producing dense materials (and can be used to produce dense bioceramics) however understanding slip properties and the thermochemical processes that occur on sintering will allow the production of porous CaP bioceramics to be developed.

As with tape casting, it is difficult to develop interconnected pores without compromising strength [130]. The strength-porosity relationship with respect to slipcast CaP ceramics is shown in figure 2.33. Two different porosifier sizes are used for comparison purposes.

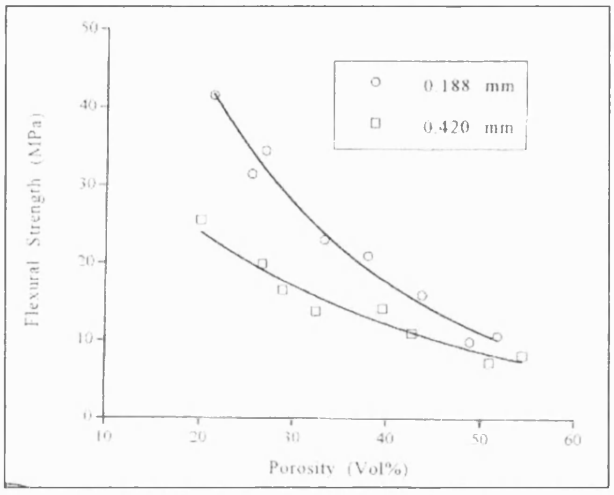

Figure 2.33: Strength-porosity correlation for HA bioceramics with different sized porosifiers [130]

The slurry rheology is of extreme importance in slip casting as this controls the uniformity of the macropore distribution [130]. It is crucial to obtain a porous structure of various sizes (i.e. to facilitate fluid flow, cell development and bony tissue ingress) in order for vascularisation to occur. However, due to the difficulty in obtaining an interconnecting pore distribution, literature regarding the continued ingress of bone cells and tissue is sparse. Slip casting processes however are still successful in producing dense CaP bioceramics (cortical replication) [130].

2.4.5 Open-Pore Ceramics Produced by Foam Replication Method

Since the development and pioneering work of Scwartzwalder and Somers [131, 132], ceramic foam technology and the number of published papers and patents on the subject has increased at

an exponential rate [133] Figure 2.34 indicates this rise in interest and development in ceramic foams.

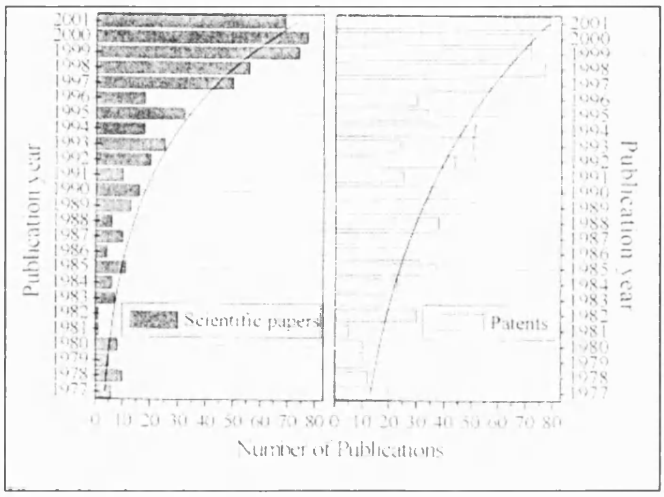

Figure 2.34: The rise in publications in ceramic foam technology since 1977 [133]

According to Gibson and Ashby [5], one can properly speak of ceramics being foams only when the relative density of the material is ≤ 0.3. Such materials consist of 3-dimensional array of polyhedral cells, with diameters ranging from 10-7000μm [5]. The fabrication process however ultimately controls the actual cell size and cell shape. Foams are often classed by the nature and structure of the cells: closed or open. Structurally closed-cell ceramics do not have interconnected pores. Open-celled ceramics guarantee interconnectivity. Figures 2.35 and 2.36 show examples of a closed cell ceramic and an open celled ceramic respectively.

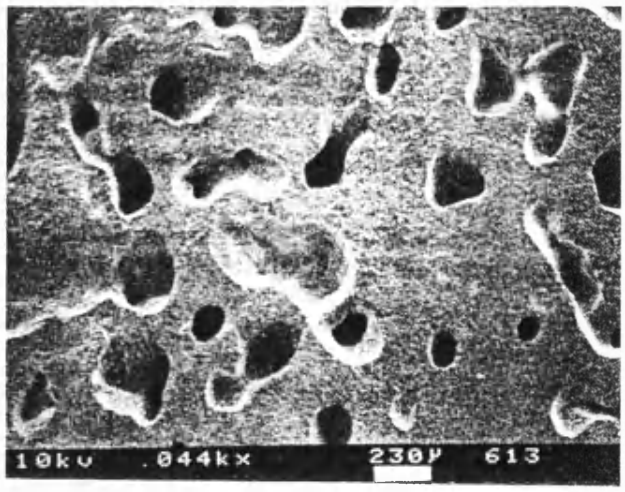

Figure 2.35: Microstructure of closed cell Ca-Mg-Zr phosphate (CMZP) ceramic [108]

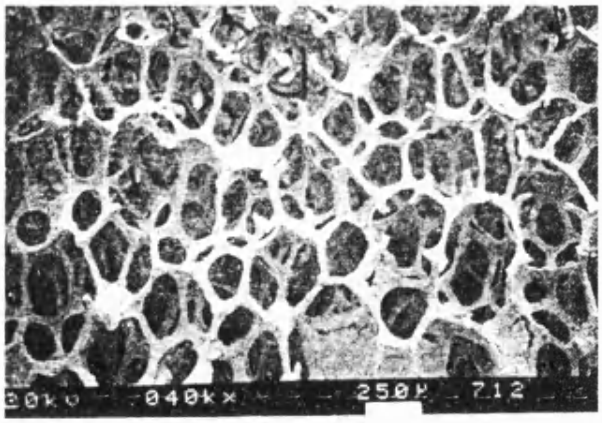

Figure 2.36: Microstructure of open cell Ca – Mg-Zr phosphate (CMZP) ceramic [108]

Ceramic foams can be used in diverse applications such as filters for molten metal, to extract noxious particulates in diesel exhaust gases, as catalyst supports, thermal protection systems, components in solid oxide fuel cells, lightweight sandwich structures and they offer potential as bioceramic graft material [133]. The unique properties of ceramic foams include low density, high surface area to volume ratio (as does cancellous bone), high porosity and high degree of interconnectivity of cells [133]. Common ceramics that are fabricated into ceramic foams include Silicon Carbide, Silicon Nitride, Zirconia and Alumina.

The three main properties of a synthetic bone graft - bioactivity, porosity and strength - are of extreme importance when fabricating bioceramic foams from calcium phosphate (HA, TCP or biphasic HA/TCP). The bioceramic must be able to participate in ionic exchanges in order to promote bone cell activity. Pores greater than 300µm are required for continued bone remodelling and osteogenesis to occur. The bioceramic must be porous enough to allow cell and tissue ingress, but it must also be strong enough to withstand the stresses of the defect area.

A description of the most common method for producing open-pore ceramic foams is now presented.

2.4.5.1 Polymer Foam Replication

This technique involves coating a reticulated polymeric foam by immersing it into a ceramic slurry. The impregnated foam is then compressed to ensure filling of the void space with slurry,

it then passes through a set of rollers to remove any excess slurry. After drying, the polymeric material is burnt off to leave a ceramic foam that structurally resembles that of the polymer template [30, 108, 109, 133, 134].

Figure 2.37 shows a typical flow diagram of the procedure.

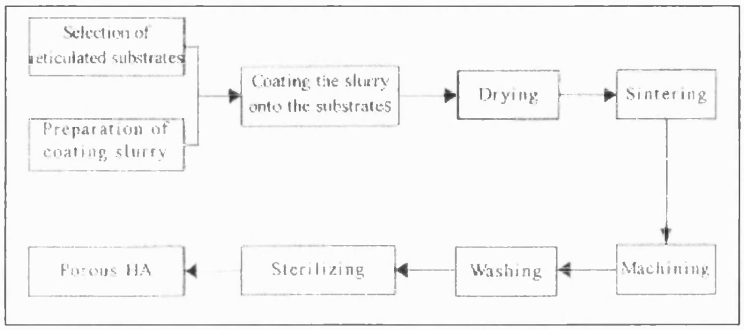

Figure 2.37: Typical flow chart for polymer foam replication procedure [109]

Two aspects are critical to selection of the foam template material. Of the polymeric materials available, polyurethane (PU) is the most attractive. This is due to its low softening temperature and ease of burn out which minimises thermal stresses that may fracture unsintered ceramics [108] and its ability to recover its original shape after impregnation of the slurry.

Figure 2.38 represents the structure of a typical PU foam template.

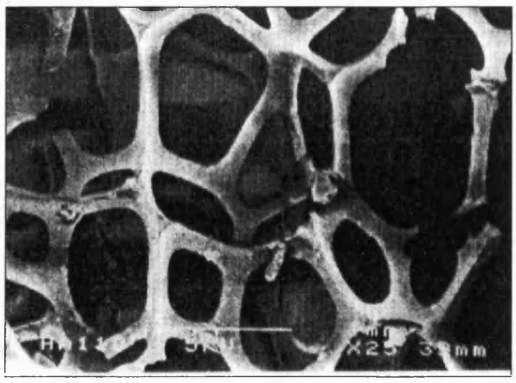

Figure 2.38: Porous structure of PU foam [109]

Two other routes may also be used to process ceramics made by the polymer foam replication method:

1) coating of the foam with a sol-gel or colloidal solution
2) pyrolysing the polymer foam then coating the carbonaceous skeleton with ceramic using chemical vapour infiltration techniques. This process is also known as obtaining ceramic materials from pre-ceramic polymers [108, 133].

The pyrolysis temperature of the PU foam determines the maximum temperature at which the ceramic foams can operate without undergoing further microstructural or dimensional changes (with the exception of densification on sintering) [133]. A slow pyrolysis rate is required (<5°C/min) to allow for gas evolution to occur. On complete burn out of the polymeric foam, a hollow cavity is formed. Three-dimensional reticulates permit the formation of regularly arranged three-dimensional porosity within the struts of the ceramic. Figure 2.39 shows this characteristic.

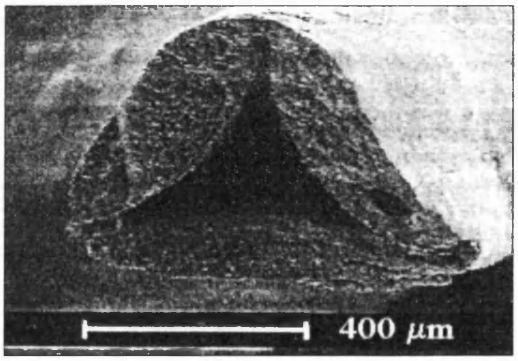

Figure 2.39: Detail of a strut showing the nature of the internal porosity on polymer burn out [133]

The development of the cavities shown in figure 2.39 can significantly reduce the strength of the ceramic according to Griffith's law [135, 136].

2.4.5.2 Strength-Porosity Relationship

By varying the pore size and total porosity of the PU foam template, it is possible to produce ceramics with a wide range of mechanical properties. Figure 2.40 shows an example of such a strength-porosity relationship in porous HA created by centrifuging the impregnated foam instead of rolling through preset rollers.

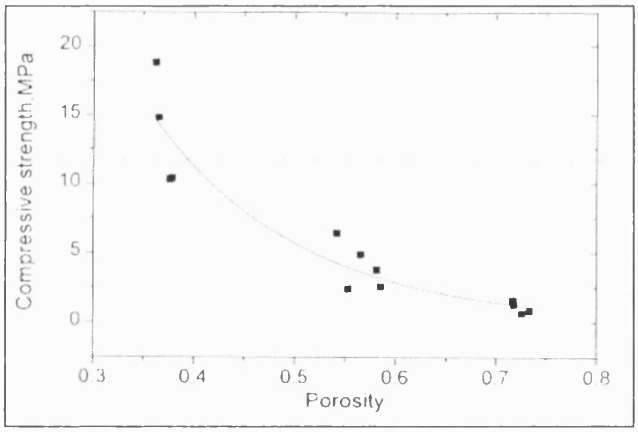

Figure 2.40: Strength-porosity relationship of HA bioceramic [109]

The failure of these materials usually occurs by collapse of a narrow band of cells perpendicular to the loading direction [136]. Experimentally, it has been found that the strength of porous ceramics is decreased in an exponential relationship with porosity. Equation 3 below represents an analytical relationship for the effect of porosity [137].

$$\sigma = \sigma_0.e^{-bP} \quad (3)$$

where σ = applied stress (MPa)
σ_0 = theoretical stress (MPa)
b = constant (~ 4-7)
P = volume fraction of porosity

The sensitivity of the material behaviour to the microstructure of brittle cellular solids, and the need for understanding this relationship is of extreme importance for bone replacement applications [5, 81]. It must be remembered that bone is viscoelastic and the proposed substitute material is ceramic therefore the failure mechanisms for both are completely different.

2.4.5.3 Ceramic Slip Properties of PU Foam Replication Method

During the slip impregnation stage of fabrication, the slip must be fluid enough to enter, fill and uniformly coat the internal three-dimensional structure of the foam. However, if the slip is too viscous then the production of a uniform ceramic green body is difficult. If the viscosity is too low, then the slip flows out of the foam and does not impregnate and satisfactorily coat the struts of the foam [127, 134].

It is suggested that a combination of thixotropic and high viscosity slips are necessary for optimum impregnation of the polymer foam template. The pseudo-plastic nature of a thixotropic slip allows it to flow relatively easily whilst still able to retain sufficient viscosity under static conditions to coat the struts of the PU foam successfully [134].

2.4.5.4 Novel Fabrications using Foam Replication Technique

It is possible to develop the foam replication technique further in order to alter the structural and mechanical properties of the ceramic. Porosity gradients can be incorporated into the PU templates by compression moulding prescribed shapes that geometrically have position dependent porosity [138].

To reduce the occurence of burn out cracks from the PU foam, methods have been developed whereby the ceramic slip is sprayed onto and into the PU substrate. The slip droplets penetrate the PU struts and on sintering the presence of microstructural cracking is reduced [139]. In addition to this, recoating the sintered ceramic using a lower viscosity slip (compared to that used for the first coating on the foam), in order to alleviate the presence of microcracks, has also been employed in an attempt to improve mechanical properties [140]. Work done by Kim, Kim and Knowles [141] also presents research detailing the coating of bioactive porous scaffolds with varying calcium phosphate phases.

Ceramic slip rheology has a profound effect on the properties of the final ceramic foam [135, 140]. It is imperative to produce a thixotropic slip to allow high solid loading contents, which in turn increases the density of the struts and hence increases strength [140].

The foam replication method of producing open cell bioceramics has one major structural advantage over other fabrication procedures such as foaming or gelcasting. The process guarantees interconnected porosity and a structure that closely resembles that of cancellous bone. The PU template can be chosen (or fabricated) so that the pore size is in the correct range for osteoconduction and further bone induction processes such as osteogenesis (i.e. pores 150 - 300μm).

Inherently linked to large pore sizes and a large porosity are poor mechanical strengths. Structural integrity is crucial to bioceramic technology. Continued bone remodelling and

revascularisation of the defect site depends on the presence of the correct pore distribution as described in section 2.3. However, this potential for osseous growth within the implant is useless without the ability of the material to keep its structural form intact and hence its pore distribution intact. Complete burnout of all slip additives and PU foam template is essential for biocompatibility. The biological properties of the CaP powder ultimately affect the bioactivity nature of the ceramic.

2.5 Variability in Strength of Ceramics

The fabrication process that has been chosen, governs the properties of the ceramic materials produced. Ceramics are sensitive to parameters such as binder content, powder content, sintering temperature, sintering time and heating and cooling rates [142]. It is possible that any of these parameters may alter the microstructure of the ceramic and hence its properties.

The failure of ceramic structures under load can be dominated by non-yielding mechanisms. In brittle fracture, there is usually localised and limiting plasticity, and defects are generally macroscopic. The mechanism of brittle fracture usually begins with the initiation of a crack, which normally originates at small flaws on the surface that cause a concentration of stress and the ultimate brittle failure of the material as the crack exceeds the critical crack size for failure. It is therefore imperative in ceramic fabrication to produce defect free products in order to maximise strength.

2.5.1 Strength and Brittle Fracture

In theory, ceramic structures should have outstanding mechanical properties, as the separation of two planes of atoms would determine their strengths. However, in practice, surface flaws (and internal flaws) in the structure, have the most profound effect on lowering the strength of ceramic structures.

2.5.1.1 Theoretical Strength

The theoretical strength of ceramics may be calculated from the stress required to separate two rows of atoms simultaneously across its cross-section. The theoretical strength can be calculated by equation (4):

$$\sigma_{th} = (E\gamma/a_0)^{1/2} \quad (4)$$

where σ_{th} = theoretical strength (MPa)
E = Young's modulus (e.g. HA = 80-110GPa (GNm^{-2}), PSZ = 200GPa)
γ = surface energy (Jm^{-2})
a_0 = interatomic distance between atoms (equal to the apparent diameter of the atom ~ 10^{-10}m)

However, the observed strengths of brittle materials are often much less (~250 times less) than the predicted strengths (equation 4) [143]. When fracture dominates, the fracture stress is exceeded before the yield stress and plastic deformation are limited to the localised high stress areas associated with defects. An applied stress causes elastic strain energy within the material. When a crack propagates, strain energy is released, reducing the overall energy. The energy lost has gone into forming two new surfaces that have been created due to the extension of the crack. The flaws associated with this failure are known as Griffith flaws.

2.5.1.2 Griffith Theory

Griffith used the proposition that an existing crack will propagate under an applied stress if the total energy of the system is lowered. The critical condition is reached when a decrease in the stored elastic energy (U_a) of a stress body, is equivalent to the energy required to create two new surfaces (U_γ) due to fracture. The total energy of the body (U) represents the combined stored elastic energy and the energy required to form two new surfaces. From this analysis, the following results are obtained:

$$U_a = (-\pi\sigma^2a^2)/2E \quad (5)$$

$$U_\gamma = 2 \times (2a\gamma) = 4a\gamma \quad (6)$$

$$U = U_a + U_\gamma \quad (7)$$

where a = Crack size (m)
σ = Critical stress for failure (MPa)
E = Young's Modulus (MPa)
γ = Surface energy (Jm^{-2})

Therefore, the total energy (U) of the body follows equation (8):

$$0 = -(\pi\sigma^2a^2)/2E + 4a\gamma \quad (8)$$

When the energy system is at equilibrium, the change in energy (dU_0) equals zero and is a function of crack length a.

$$\therefore \quad dU_0/da = 0 \quad (9)$$

Thus,

$$\frac{d}{da}(-\pi\sigma^2a^2/E) + (4a\gamma) = 0 \quad (10)$$

$$\Rightarrow \quad \sigma_{crit} = (2E\gamma/\pi a)^{1/2} \quad (11)$$

Since E and γ are constant, crack propagation will take place when the product $\sigma(a)^{1/2}$ exceeds a critical value [143].

2.5.2 Surface Flaws

Experience has shown the most damaging flaws in most ceramic structures occur in association with the surface [143-145]. Surface flaws in ceramics can be produced in the forming process, they can be created during subsequent finishing processes, or simply by poor handling [146]. At sufficiently high loads, existing submicroscopic flaws are propagated under high stress and extend and cause failure [146]. The larger the flaw (or rather its effective zone of influence) the lower will be the strength. Thus, in generating a microstructure, strength can only be optimised by removing as many surface flaws as possible [145].

An important consequence of the Griffith theory is that brittle fracture is initiated at the most serious flaw [143]. The size of flaw that can be tolerated in a ceramic, depends on the 'in service' requirements of the product and the strength required [145]. In the case of a bioceramic, the implant must integrate with the host bone before stress to failure occurs in order to provide full osteoconductive support.

Due to the formation of surface flaws that magnify the stress on loading, and lower the strength of the materials, invariably there is a large scatter in the strengths. Therefore, it is imperative to test large numbers of samples in order to evaluate the scatter found in the results [144]. Hence, it is a necessity to be aware of these structural weaknesses that lower the strengths of ceramics, in order to optimise the material's properties. The first microstructural target for strength should be the reduction in size of surface flaws [144].

2.5.3 Structural Toughening Mechanisms

There have been substantial increases in strength made by achieving control of microstructure. Strengthened ceramics show a dramatic lack of resistance to crack propagation once failure stress is exceeded [143]. A wide range of processes, including the following, can act as strengthening mechanisms used to obtain higher strengths in ceramics:

- Annealing
- Compressive surface stresses
- Minimizing grain size
- Minimizing porosity
- Solid solution hardening [142]

One approach to increasing both strength and reliability in brittle materials is to decrease the characteristic flaw size. As a result reliability increases as smaller flaws can often grow to a limiting size before failure. Much effort has concentrated on improving the surface flaw size population, and the resistance to crack growth, this has been known as 'flaw tolerance' [143].

2.5.3.1 Coatings and Compressive Stresses

Processes for strengthening ceramics by using low expansion coatings or by placing the surface into deliberate compression, results in increases in the nominal stress at which surface flaws act to cause failure [142, 144, 147]. Compressive surface stresses are induced during cooling processes, because the interior volume of the material contracts more than the volume surface; thus placing the surface into compression [144]. This process is successful due to volume changes that occur. Therefore, the stresses are retained in the structure and the material remains stable. The principle criterion for selection of bodies for strengthening by compressive surface stresses is that fracture due to externally applied loads must normally originate at surface flaws [142, 144].

The role of surface flaws in the fracture of ceramics, has led to the development of a number of techniques for inducing compressive surface stresses in ceramic bodies [142, 147]. These include:

- Quenching
- Coatings (e.g. glazing)
- Quenching of coatings
- Ion exchange
- Forming of low expansion solid solution surface layers
- Forming surface layers by reactions or phase transformations, characterised by an increase in volume

Partially stabilised zirconia (PSZ) is an example of such a material in which a phase transformation produces a volume increase (~ 9%), and hence places the surface into compression resisting crack growth. Additions of CaO, MgO or Y_2O_3 partially stabilise the zirconia in the cubic form. On cooling through the transformation range (~1000°C) the unstable body transforms from the tetragonal to the monoclinic cubic structure and places the surface into compression [144].

To achieve the properties required, the selection of chemistry, choice of raw materials and the optimisation of processing towards an ideal target microstructure, must be analysed [145]. The reduction in size or even the elimination of surface flaws in ceramics is paramount in order to achieve high strengths.

2.6 Organometallic Precursors

Organometallic chemistry relates to compounds in which an organic group is attached through carbon to an atom that is less electronegative than carbon (i.e. generally compounds that contain a direct metal-carbon bond) [148, 149]. Organometallic precursor materials are designed to contain structural units of the inorganic material that will be produced. The actual transformation into an inorganic material takes place by a sequence of condensation reactions during heating. At higher temperatures, the material can be crystallised into a thermodynamically stable ceramic [150, 151].

The method consists of making a homogeneous solution of the component organometallic, in a suitable solvent (usually the parent alcohol), and then using a hydrolysis reaction to produce a gel containing the hydrated metal oxide. The gel is dried and sintered to produce a ceramic material at temperatures much lower than that required by conventional melting processes [152, 153].

The advantages of the process include lower sintering temperatures, high purity, uniformity and the ease of application. As the precursor material is in solution e.g. magnesium methoxide (magnesium in solution in methanol), films or coatings may be applied to complex shapes and to a wide range of substrates to optimise for example optical, electrical and mechanical properties [151].

2.6.1 Mechanisms of Ceramic Formation from Organometallic Precursors

Ceramic precursor organometallics based on compositions such as $M(OR)_n$, where M = metal e.g. silicon, sodium, zirconia, R = methyl (CH_3), ethyl (C_2H_5), are popular precursors because they react readily with water to hydrolyse [154]. When dissolved in pure water, water molecules hydrolyse metal cations, M^{z+}, and a hydroxyl ion (OH^-) attaches to the metal atom, according to the hydrolysis reaction (12):

$$M(OR)_n + H_2O \longrightarrow HO - M(OR)_{n-1} + ROH \qquad (12)$$

Depending on the amount of water present, hydrolysis may go to completion, so that all of the OR groups are replaced by OH^- ions [155]. According to reaction (13) if completion occurs:

$$M(OR)_n + H_2O \longrightarrow M(OH)_n + nROH \quad (13)$$

where ROH = alcohol (e.g. CH_3OH methanol)
$M(OR)_n$ = organometallic (e.g. zirconium butoxide $Zr(OR)_4$)
$M(OH)_n$ = metal hydroxide (e.g. magnesium hydroxide $Mg(OH)_2$)

This process can also stop when the metal is only partially hydrolysed – $M(OR)_{n-1}(OH)_n$.

The hydrolysis reaction occurs in organometallics, due to the presence of highly electronegative OR groups (i.e. π electron donors) that stabilise the metal in its highest oxidation state, which leaves the metal very susceptible to nucleophilic attack (i.e. molecules/compounds that like to attach to positive ionic groups) [156].

It is also possible for two partially hydrolysed molecules to link together in a condensation reaction such as in reaction (14). The inorganic metal oxide is formed as a result of the process [156].

$$M(OR)_n - OH + M(OR)_n - OH \longrightarrow M(OR)_n\text{-}O\text{-}_n(RO)M + H_2O \quad (14)$$

By definition, condensation liberates a small molecule, such as water or alcohol. This type of reaction can continue to build larger and larger oxide containing molecules by the process of polymerisation [150, 153] or as it sometimes termed – polycondensation. This eventuality results in a metal oxide network forming.

When sufficient M-O-M bonds are formed, they act co-operatively as colloidal (submicron) particles or a sol. Since the sol is a low viscosity liquid, it can be cast into a mould, or used for coatings or as a film former. With time and increasing temperature, the colloidal particles condense into metal oxide species to form a three dimensional network. The physical characteristics of this gel network depend greatly on the size of particles and extent of cross-linking prior to gelation [150].

Further careful drying of the sol-gel must be carried out to relieve large surface stresses that can form as cracks during drying. Final densification of the gel occurs by sintering at high

temperatures to reduce porosity and surface area. Figure 2.41 shows the structural characteristic changes that occur during processing of sol-gel by this method.

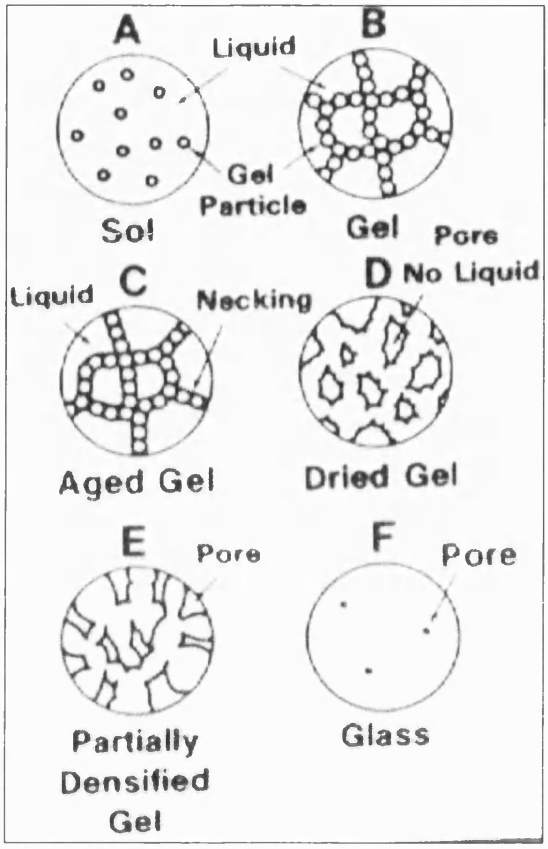

Figure 2.41: Structural changes associated with sol-gel process [156]

2.6.2 Applications of Sol-Gels in Ceramic Technology

Sol-gel and ceramic materials made from organometallic precursors, have been used in the application of glasses, crystalline ceramics and coatings for optimising material properties such as optical, electrical, chemical and mechanical characteristics [157].

The sol-gel process described in this section is particularly suited for numerous applications. The versatility of the process and examples of applications are described here.

2.6.2.1 Sol-Gel Materials Demonstrating Bioactivity

The ability to tailor the chemical properties of the sol-gel by the choice and reaction path of organometallics is an advantage for the production of bioactive sol-gel glasses, as researched by Hench [151, 158]. Bioactive implants that form a mechanically strong bond to bone, are important due to their potential long survivability [158]. Figure 2.42 shows the importance of survivability for the bioactivity of sol-gel implant material.

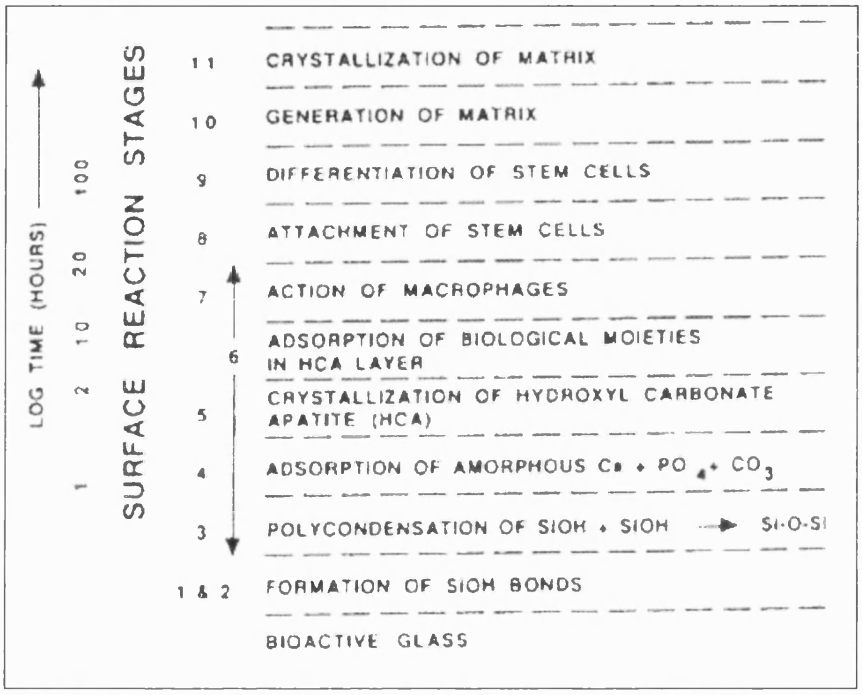

Figure 2.42: Comparison of time dependence on the sequence of bone forming for Si based sol-gel [158]

The most common sol-gel derived glass composition $SiO_2 - CaO - P_2O_5$, has been shown by Hench and West [151] to form hydroxycarbonate apatite bone bridges between the implant and the host bone. Bone activity was found in melt derived ceramics of the same composition [151].

It has been shown that the process described to produce ceramics, from the use of organometallic compounds, makes the materials attractive for producing controlled interactions between inorganic materials and biological molecules [158]. The availability of such low temperature viscous sintering rather than by cooling from a melt, provides the possibility of forming ceramic bodies with unique distributions of phases for specific applications [151, 158].

2.6.2.2 Coatings and Films

The ability for low viscosity sol-gel solutions fabricated from organometallic precursors, to coat large areas and complex geometries, offers possibilities in numerous areas [159]. These include protecting underlying the ceramic, metal or polymer surfaces from harsh chemical environments. It is also possible to produce net shapes and net surface components by casting the solution into precision moulds [160], and by coating large and complex net shapes with precision uniformity [157]. Perhaps the most common thin film forming process involves spin coating of the sol-gel solution required onto a substrate. The presence of atmospheric water immediately causes hydrolysis. On heating to temperatures from 400° - 850°C, an amorphous film crystallises to produce a polycrystalline ceramic. This is the case for the ceramic Barium Titanate. Disadvantages of the processes described using organometallic precursors, include the raw material cost for fabricating large quantities of material and also that gelation, drying and densification are all relatively lengthy processes [161].

The sol-gel process is particularly suited for the preparation of coatings and films. Not only does the use of liquid solutions at room temperature have great advantages, but also the techniques for preparation of multi component homogeneous liquid solutions for a wide range of crystalline and non-crystalline coatings, can be applied to numerous substrates [148].

The ability to modify the surfaces of ceramics so as to alter their response to mechanical forces and to promote strength is attractive in certain applications. With suitable coatings it is possible to increase, for example, the scratch resistance of materials, and similar techniques to provide engineering gradations in chemistry for improved bonding [159]. It may be possible to reduce surface flaws by the flow and viscous sintering of sol-gel derived solution into surface defects, this would strengthen the material.

2.7 Summary of Literature Review Findings

Bone has outstanding properties; it is a dynamic, living material that provides mechanical support, homeostasis, bone remodelling and also regulates ionic reserves in the body. Bone grafts, such as autograft and allograft, are used to treat bone loss, infection and diseased or damaged bone. However, these materials pose problems associated with their use, namely the availability and volume of graft is limited. Allograft procedures risk infection and disease, and autograft procedures increase the pain for the patient, as a second incision site is required. Therefore, there is a need to develop a material that is capable of osteogenesis (bone remodelling), while also offering structural support to the affected area.

Calcium phosphates have been shown to be suitable candidates for the production of bone substitute materials. Their chemical composition resembles that of natural bone and allows ionic exchanges between the implant and host bone demonstrating the ability to form hydroxycarbonate apatite bone "bridges", resulting in secure fixation of the implant. This bioactivity is essential to encourage osteoblastic (bone forming cell) activity. In order for bone remodelling to occur, calcium phosphates must also demonstrate an adequate strength-porosity relationship, to ensure that osteogenesis is possible while also providing a structural matrix for biomechanical support. For continued bone growth to occur, a hierarchial pore structure is required, with pores ranging in size from 150 – 300μm. To sustain osteogenesis, the synthetic material must provide sufficient strength to ensure good fixation between the implant and the host bone structure.

Various different fabrication techniques have been developed to manufacture calcium phosphate ceramics that resemble both cortical bone (dense material) and cancellous bone (porous material). These include numerous thermochemical techniques, such as foaming and gelcasting in addition to mechanical techniques, such as slip casting and tape casting. It has proved to be difficult to provide a bioceramic material capable of providing both a high volume porosity network (with large pores) combined with sufficient strength to support the material during bone remodelling.

However, ceramic fabrication also has limitations due to the presence of surface flaws in the finished articles that lower the strength of the products on loading. These structural weaknesses must be overcome in order to develop successful bone substitute materials. One method to

relieve these surface flaws is to develop coatings or films that place the surface flaws under compression and therefore provide resistance to crack growth and thus increase the strength of the material.

To date, however, there has been limited research conducted to assess the materials properties and design of bone substitute materials to encompass a structural-biological matrix as found in bone grafts. If the complications associated with bone grafting are to be overcome, their root causes must be identified, and, in order to achieve this, consideration must be given to the contributory effects of bone substitute materials and their design.

2.8 Objectives and Aims of Research

The initial objective of the research was to address the need to develop and fabricate calcium phosphate (CaP) bioceramics comprising hydroxyapatite (HA), α-tricalcium phosphate (α-TCP) and β-tricalcium phosphate (β-TCP) with pores in the correct size range for bone formation and bone ingrowth. This necessitated the fabrication of materials with an interconnected macroporosity network (i.e. pores > 10μm), having pores in the size range 150 - 300μm, for continued bone ingrowth within the synthetic bone graft material.

From the literature search, it was found that there are difficulties in combining both the structural and porosity requirements needed for a successful CaP synthetic bone graft material. Thus a further objective of the research was to improve the structural integrity and mechanical properties of the bioceramics produced, without compromising the interconnected macroporosity network needed for bone ingrowth. The use of organometallic precursors as treatments for the CaP bioceramics was used in order to reduce, or even eliminate, surface microcracks that result in structural weaknesses in the materials on loading.

There was a need to develop fabrication processes that could be used to produce bone substitute materials in a variety of sizes, shapes and perhaps, most importantly, chemical composition. The research presented highlights the diversity and range of samples that can be produced by the methods developed.

CaP bioceramics were also fabricated for the production of novel bioceramics for specific clinical applications that include spinal fusion interbody applications, chondylar repairs (in knee defects), granular bioceramic material for use in impaction grafting in revision hip procedures and materials with potential for use in maxillofacial surgery (mandible/jaw reconstruction). This highlights the need to not only develop CaP bioceramics for research purposes in the laboratory but also to develop bioceramics for specific clinical applications that are currently employed by orthopaedic surgeons.

Chapter 3 Materials and Experimental Methods

3.1 Calcium Phosphate Base Powders and their Phases

The base powders used in the research were Grade 118 and Grade 130 forms of hydroxyapatite (HA), supplied by Stryker Orthopaedics. Grade 118 is less crystalline than 130, and contains calcium deficient HA, which permits phase transitions to occur. This allows the final sintered products to consist of β - tricalcium phosphate (β-TCP) and α-tricalcium phosphate (α-TCP). Grade 130 is a stable, crystalline phase of HA and does not thermally transform to TCP. Therefore, using a combination of the two powders one can produce any combination of HA/TCP bioceramic composition. In addition, samples comprising purely HA, α-TCP or β-TCP can be made.

The base phase is HA, chemical formula $Ca_{10}(PO_4)_6(OH)_2$. This can be thermally transformed in its amorphous form (grade 118) to produce β - and α - TCP ($Ca_3(PO_4)_2$), at 900 – 1000°C, β-TCP forms, up to 1180°C this phase is stable. Above 1180°C, it transforms to α-TCP and above 1350°C tetracalcium phosphate is formed. The schematics below indicate the phase transitions that occur on heating of the powders:

$$\text{Grade 118 HA} \xrightarrow{\textit{heat}} \beta\text{-TCP} + \alpha\text{-TCP}$$

Ca deficient, low crystallinity

$$\text{Grade 130 HA} \xrightarrow{\textit{heat}} \text{HA}$$

Crystalline HA phase

It is generally accepted that there is a trade off in properties between the high biological response of β-TCP and the high loading properties of HA. This is summarised in figure 3.1.

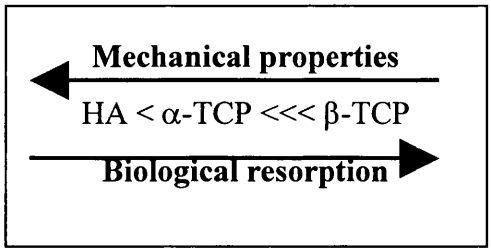

Figure 3.1: Duality between mechanical properties and bioactivity of calcium phosphates

3.2 Polyurethane (PU) Foam

PU reticulated foams obtained from Sydney Heath and Sons Ltd, were used to produce varying densities of bioceramic scaffold material by mimicking the positive or negative image of the foam. A ceramic slip was used to either impregnate or coat the struts of the foams. The foam structures can be described as open and reticulated, and were used in two different pore sizes - 30 and 45 ppi (pores per inch). The PU foams were used as structural templates for the production of open porous bioceramic materials.

3.3 Thermogravimetric Analysis (TGA)

TGA was performed on both 30ppi and 45ppi PU foam in addition to PU foam coated with the bioceramic slip. Samples with a mass of 1mg were placed inside an alumina crucible that was suspended inside a heating chamber. The crucible mass was then measured with increasing temperature, PU foam samples were heated from 1°C to 600°C at a heating rate of 1°C/min. The PU foam coated with bioceramic slip was heated at the same rate but up to a maximum temperature of 1300°C. Step increases in temperature were made every 0.1°C. Plots were subsequently made of mass loss against increasing temperature, in order to evaluate the characteristics of the PU foam and slip coated foam during the sintering cycle.

3.4 Optical and SEM Characterisation

Off cuts from each set of fabricated samples were chosen for further analysis by optical microscopy and scanning electron microscopy (SEM) analysis. The SEM images were later used to analyse the porosity distribution of the samples by image analysis software via computer manipulation (section 3.5).

The off cuts of the fabricated samples described in section 3.8, were either mounted in epoxy resin, cured and then subsequently ground and polished, or cut to size to fit on a plate ready for SEM analysis. These samples were then gold sputtered and immediately analysed by a JEOL 6310 model SEM with an accelerating potential of 15kV.

Both macroporosity and microporosity examination followed. However, concentration focused more on macroporosity analysis, as the macroporosity distribution appears to have a greater influence on the mechanical properties of the samples. However, an extensive examination of both types of distributions, how different sintering temperatures affect them, the drying mechanisms and the type of porosifiers used then followed.

3.5 Image Analysis and Porosity Evaluation

Micrographs produced from SEM analysis, showing both macroporosity and microporosity distribution in the specimens were analysed by the computer software – Optimas 6.1 – to calculate not only the total porosity present in the samples, but also the macro-and microporosity distributions. Other useful data such as the average area equivalent diameter of the pores present, and the size and shape of the porosity have also been analysed.

The images were first scanned into the software and subsequently "cleaned" to produce a sharper image, which in turn results in more efficient and accurate results. This is because the software used identifies colour threshold differences in the micrographs used. By "cleaning" the micrographs via computer manipulation the clarity of each phase (grain and porosity phases) is improved.

The data set of the samples analysed was then exported to an Excel file for further numerical and graphical analysis (e.g. to calculate porosity distributions and to show how the experimental parameters affect the macroporosity and microporosity).

3.6 X-Ray Diffraction (XRD) Analysis

In order to assess the accuracy of the amounts of different phases present in the bioceramics made, a Phillips X-Ray Diffractometer was used by using Cuα radiation with a wavelength of 1.54Å. The data range was set at $20° < 2\theta < 60°$, with a scan step size of 0.01°. This produced a

file containing the counts recorded at each step. These counts were then plotted against the 2θ angles. The strong reflections in the traces were then matched against standard diffraction patterns for all calcium phosphate materials via computer software PDFC 2.00.

3.7 Slip Preparation

In total, six slips have been prepared each with different properties, although more than six slips have been fabricated during the research to optimise the slip properties; it is these specific slips that have been used in the current research. Table 3.1 summarises the slip formulations for the research undertaken. The 45 ppi foams were impregnated with slips that were slightly less viscous than those used for impregnation of 30 ppi foams. This was because 30 ppi foams have larger interconnected pore channels than their 45 ppi counterparts.

For all the slips, the liquid components were added first and stirred vigorously under motorised stirring at 20 rpm. Each form of HA powder (118 and 130) was then added and again vigorously stirred until all powder was incorporated into the slip. Remaining individual dry components were then added and stirred vigorously once again until all the dry materials were incorporated into the slip. Fabrication of the slip was complete once a handful (~ 50g) of zirconia milling media was inserted into the slip ready for ball milling for 24hrs at 20 rpm. The approximate ratio of HA:TCP for the Impact-Impregnated (I.I.), granular and Open Porous Scaffolds (OPS) was 75:25 %. The Spinal Fusion samples fabricated from 118 powder comprised pre-dominantly β-TCP when sintered at 1150°C, and α-TCP at temperatures above 1180°C. The samples fabricated from 130 powder comprised HA.

In order to achieve a thixotropic nature to the slips produced, various binders, plasticisers and surfactants have been employed. Dispex A40 is a non-ionic surfactant that acts as a deflocculant to avoid agglomeration of the slip. Methyl cellulose, polyvinyl alcohol (PVA) and polyvinylpyrrolidone (PVP) are high molecular weight binders that provide stability and aid thixotropy. Polyethylene glycol (PEG) is a plasticiser that gives the slip some fluidilty and helps the movement of the slip. Octyl alcohol is an anti-foaming agent used to avoid the presence of air bubbles and nonyl phenol is used as an aid to adhesion i.e. for slip to adhere to PU foam.

Method of Fabrication		**Impact-Impregnation and Granular Material**		**Open Porous Scaffolds**		**Spinal Fusion – 45 ppi**	
Ingredients	Physical Form	*45 ppi*	*30 ppi*	*45 ppi*	*30 ppi*	*HA Slip*	*TCP Slip*
HA118 (g)	Powder	187.5	225	250	250	0	600
HA130 (g)	Powder	187.5	225	250	250	600	0
H_2O distilled (ml)	Liquid	750	750	500	500	500	500
Dispex A40 (ml)	Liquid	1-2	2-3	12	10	7.5	7.5
PEG (g)	Liquid	-	-	7.5	7.5	10	10
Methyl Cellulose (g)	Powder	-	-	7.5	7.5	10	10
PVA (g)	Powder	-	-	-	-	6	6
PVP (g)	Powder	-	-	-	-	6	6
Octyl alcohol (ml)	Liquid	-	-	-	-	5	5
Nonyl phenol(ml)	Liquid	-	-	-	-	5	5

Table 3.1: Summary of slip formulations for different fabrication methods

3.8 Range of Fabricated Samples

There were five fabrication methods used in the research detailed here, each resulting in different CaP structures. The first fabrication method details a process called Impact-Impregnation (I.I.). The main aim of producing samples using this method was to fabricate HA/TCP bioceramics with a guaranteed interconnected porosity network. This process is described in section 3.8.1. The second method is termed the Open Porous Scaffold (OPS) method. The objective was to produce HA/TCP bioceramics with larger pore sizes and greater volume porosity while retaining the interconnectivity of the pores. This process is detailed in section 3.8.2. The third method follows on from the OPS method and details a process that produces HA, α-TCP and β-TCP bioceramics for a practical application termed Spinal Fusion (SF) Interbody Operations. The fabrication method for SF bioceramics is detailed in section 3.8.3 and shows the diversity and the range of samples that can be produced from the technique developed. Once again the interconnected porosity, as fabricated in the OPS structures, must be retained on fabrication

while improving the mechanical properties. The fourth method again illustrates the diversity of the techniques developed, and the range of materials that can be made. A granular form of the block material fabricated by the I.I. method was produced for the specific purpose of acting as a synthetic alternative for impaction grafting in revision hip operations. This work is detailed in section 3.8.4. The fifth method follows on from the SF method (section 3.8.3), whereby SF sintered samples were treated with a sol-gel solution, with the intention of improving the mechanical properties. The method must not compromise the interconnected porosity network needed for possible bone regeneration that was produced with the earlier methods. The process is detailed in section 3.8.5.

3.8.1 Impact-Impregnation (I.I.) Bioceramics

Twenty samples were prepared for each batch of slip (for 30 and 45 ppi foam samples) thus totalling forty samples (twenty for the 45 ppi samples: ten fired at 1280°C and ten at 1150°C, and twenty for the 30 ppi samples: again, ten fired at 1280°C and ten at 1150°C).

The foams (30 and 45 ppi) were measured and cut to approximate dimensions of 40 x 40 x 15 mm in preparation for impregnation by the milled slurry, and placed overnight in distilled water in order to clean any inclusions off the foam to assist slip adhesion. The foams were then taken out and allowed to dry fully on tissue paper ready for slip impregnation. The washing and drying procedure for the PU foams, described here, was a common part for all the fabrication processes.

A small polyethylene container (~ 200ml in size) was filled half to two thirds full of the slurry from the slip. A cut foam specimen was then introduced to the slurry. The foam was squeezed and dipped into the slurry. During the expansion back to its original shape and size, the slurry impregnated the foam. During this expansion, the foam was placed under the slurry line as to both introduce the slurry to the foam and to remove any air present in the foam.

Tissue paper was then placed as a cover over the container (NB. The lid of the container was not tightened, as this would prevent the airflow necessary through the foam). The container was then systematically impacted against a solid surface to drive out the air from the foam and to improve impregnation. A combination of both firm and light impact were undertaken in an attempt to drive out the air from the foam. The specimen was then removed from the container and placed to dry either on a metal mesh (grill) or on tissue paper. The small container was then topped up

with the slurry from the corresponding slip and the process repeated. This process was repeated for each batch with the corresponding foams.

3.8.2 Open Porous Scaffolds (OPS) Bioceramics

A mechanical plunging machine that was designed and developed specifically for impregnation of the PU foams was used to impregnate the OPS slips, described in table 3.1, for the 30 and 45 ppi foams respectively.

Samples were cut into dimensions of 40mm in length by 25mm in width by 10mm in depth, and washed and dried as for previous methods.

Foam samples were inserted into the mechanical plunging machine, which consisted of a channel where the slip was poured and a plunger controlled by a screw thread action that compressed the foam. The plunger was then drawn down (via the screw thread) and pushed all the slip out of the foam. On subsequent retraction of the plunger, the slip was drawn up into the foam (impregnation) to coat the struts; this process was repeated to ensure the coating of the struts of the foam. This process was known as the dipping process.

The second stage of fabrication was the dripping process. The foam sample was held above the slip bath to allow the excess liquid to seep out of the foam, and to fully coat the struts of the foam. This was possible as the slips used in the production of OPS were not as viscous as the slips used for I.I. fabrication. The foam was drip cast on all sides (one to two minutes on each side) so that struts were coated evenly.

The foam samples were then immediately sprayed with high velocity compressed air (approximately two minutes on each side). This was done to avoid the formation of any closed cells, ensure coating of the foam struts and to aid drying. Interconnectivity between the pores was guaranteed. This was known as the drying stage. Longitudinal and transverse pore shaped samples as well as spherical (or as-received) pore foams, were then fabricated by the same process, as described in the following section.

Finally, the sample was allowed to dry for one minute on each side on tissue paper, at room temperature, to extract all excess moisture.

3.8.2.1 Directionally Elongating Cells of PU Reticulated Foam

In order to mimic the orientated trabecular structure found in cancellous bone, a technique was developed to stretch and elongate the cells of the PU foam. Figure 3.2 shows the apparatus used to directionally elongate the polyurethane foam to produce elongated cells in the polymer template prior to fabrication.

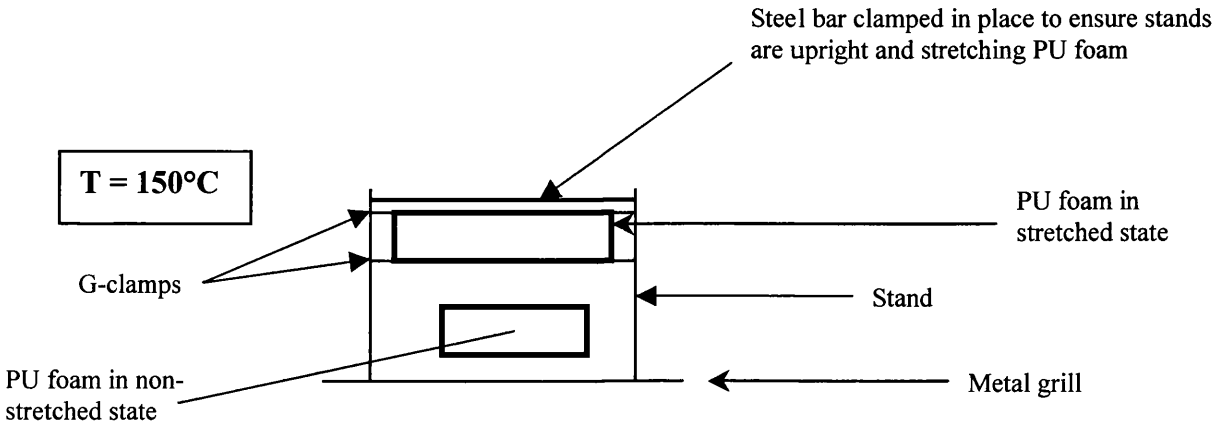

Figure 3.2: Set-up for directional elongation of PU foam

Samples of 30 and 45 ppi PU foams were cut to dimensions of 24cm x 8cm x 2.5cm. The end 2cm were clamped by steel lap joints to enable four G-clamps to slide over two stands all fixed on a metal grill. The stands were stretched in place so that elongation was 30% of the original length, and clamped in place by a steel bar. The whole set-up was then placed in an air flowing oven at 150°C for 15 minutes. The temperature of 150°C was chosen as it is close to the glass transition temperature (200°C) and therefore allows slight chain flow and hence on subsequent cooling the polymer chains were "frozen" in place in their elongated state. The set-up was taken out of the oven and left for 15 minutes in an air-flowing chamber at room temperature. The foam was then taken out of the grips and cut longitudinally to sample dimensions of 40mm x 25mm x 10mm (the same dimensions as for as-received foams). The same sample dimensions were cut at a perpendicular plane to produce transverse samples. The elongation procedure results in changes in the pore geometry of the foam, from mainly spherical to ellipsoidal in shape; this is illustrated below in figure 3.3.

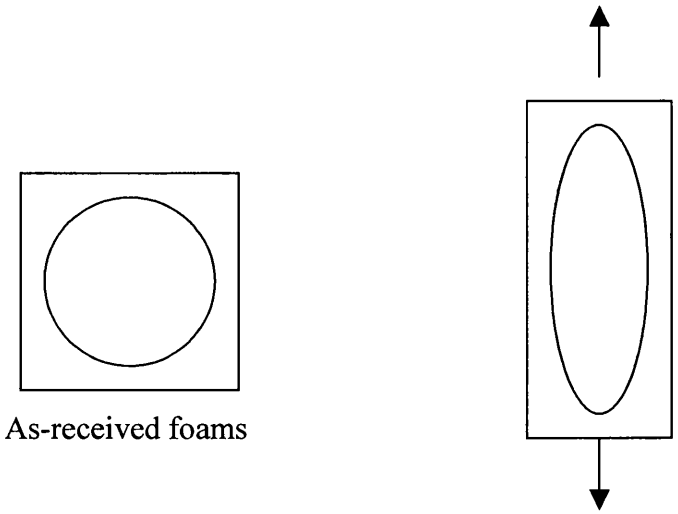

Figure 3.3: The treated foams produce elliptical shaped pores as opposed to the spherical pores present in the as-received (or pre-treated) foams

In total, 120 samples were fabricated by the OPS method producing an open interconnected porous structure resembling a scaffold. Typical mass of samples after the fabrication process and drying on tissue overnight (~15hrs) varied from 3 – 5g. The samples were dried in an oven at 120°C for six hours to ensure all excess moisture was extracted. Typical mass of samples after drying at 120°C varied from 2 – 4g. Final densification masses range from 1.5 – 3.5g.

3.8.3 Spinal Fusion (SF) Bioceramics

The SF method is a further development of the OPS procedure. Cylindrical sections of the 45 ppi PU foam were hot cut using a die of diameter 13mm and length 20mm. These sections of foam were placed in distilled water overnight to ensure that any inclusions were removed from their surface. The foam samples were then treated in the same manner as for the OPS samples and dried on tissue paper in air for one hour under a hot lamp at 75°C ± 5°C.

The second stage of fabrication consists of rolling the cylindrical sample in the same thixotropic slip used for the initial fabrication. This was done to achieve a dense, outer shell protecting the internal interconnected porosity network and to offer mechanical support. Immediately upon completion of rolling and production of a wet coating, samples were placed in tissue paper and rolled gently in order to ensure that the slip did not penetrate the pores, and that cracking due to poor drying could be eliminated. Samples were then left rolled in tissue to dry in air at room temperature for 24 hrs.

3.8.4 Calcium Phosphate (CaP) Granular Material

Angular foam pieces (30 and 45 ppi) were randomly cut (can also be done with die) into shapes ranging in size from 2-4mm, 3-5mm and 4-8mm. These were impregnated and fabricated identically to the I.I. procedure (section 3.8.1). Granules were removed from the slip by sieving and placed on tissue paper in order to remove any excess moisture (one minute on each side). The granules were then placed in an airflow oven at 120°C in order to guarantee that the granules were moisture free so that thermal cracking could be avoided on sintering. All the granules were sintered at 1280°C in order to achieve consistency in the results. Once sintered, the granules were placed in a polyethylene container together with zirconia milling media and ball milled for six hours to round off the edges of the granules. This process optimised the packing potential when die-plunger compression testing was performed.

3.8.5 Sol-Gel Treated SF Bioceramics

SF samples were made and sintered as described in section 3.8.3. A soda sol-gel solution was prepared according to reaction 15:

$$M(OR)_x + xH_2O \longrightarrow M(OH)_x + xROH \qquad (15)$$

where M = metal atom
O = oxygen
R = alkyl group e.g. CH_3, C_2H_5
H = hydrogen

Therefore, by using sodium methoxide as an organometallic compound capable of participating in hydrolysis and condensation reactions to form a sol-gel solution, reaction 16:

$$NaOCH_3 + H_2O \longrightarrow NaOH + CH_3OH \qquad (16)$$

where $NaOCH_3$ = sodium methoxide
NaOH = sodium hydroxide
CH_3OH = methanol (as by product)

Thus, by the stoichiometric equation used, it is possible to calculate the volume of sodium methoxide and water required to form the sol-gel reaction. Therefore, 30g of sodium methoxide

corresponds to 10g of water. The density of sodium methoxide was 0.945g/cm^3 (from Aldrich suppliers), thus:

Volume of sodium methoxide required = mass/density = 30/0.945 = 31.75ml.

Therefore, the volume ratio of sodium methoxide to water used for the sol-gel reaction was 31.75ml: 10ml. These quantities were mixed together in a glass beaker and 0.5g of crushed oxalic acid, which acts as a drying control (i.e. stops film cracking on drying) was added. Raising the temperature speeds up the sol-gel process, and therefore the solution was placed in an airflow oven at 70°C for one hour. Pre-sintered SF samples (HA, α-TCP and β-TCP) were then immersed in the solution mixture and positioned in a vacuum at 70°C for 30 mins to ensure that all air had been expelled from the samples, and the solution could penetrate the entire SF samples. The samples were then removed and quickly spun dried by hand in order to eradicate excess solution and dried in air at room temperature.

3.9 Drying of Samples

The drying of the samples fabricated was carried out in two stages. Drying took place slowly to ensure that surface stresses that cause cracking were relieved, and hence surface cracks were eliminated. The first stage of drying was usually at room temperature (25°C ± 5°C) and the second at a higher temperature (70 – 120°C) to ensure moisture extraction. Slightly different drying procedures were used for different fabrication techniques; these are detailed in the following sections.

3.9.1 I.I. Bioceramics

For comparative purposes two different drying mechanisms were used during the Impact-Impregnation (I.I.) fabrication procedure (section 3.8.1). Half of the samples from each batch/slip were dried on a metal mesh or grill, consisting of circular holes to drain any excess moisture from the foams. The second drying procedure was to dry the specimens on the same metal mesh but this time overlayed with tissue paper in an attempt to extract any excess moisture from the foams and improve the porosity characteristics. The samples were left to dry in air at room temperature for 24 hours and then dried in air at 40°C for a further 24 hours.

3.9.2 OPS Bioceramics

OPS samples were allowed to dry on tissue paper, which was also placed on top of the scaffolds, for 24 hours at room temperature. Following this, OPS samples were then placed in an airflow oven at 120°C for a further 24 hours for moisture extraction.

3.9.3 SF Bioceramics

Cylindrical OPS structures, diameter 13mm ± 1mm, length 20mm ± 1.5mm, prior to fabrication of the dense, outer shell, were dried under a hot lamp at 75°C ± 5°C for one hour. After fabrication of the dense exterior section of the structure, samples were dried in tissue paper and rolled to ensure the entire exterior surface was in contact with the tissue, and left for 24 hours at room temperature. On removal from the tissue paper, the SF samples were then dried in an airflow oven at 120°C for 24 hours.

3.9.4 CaP Granular Material

The granular material, fabricated using the same I.I. procedure, was solely dried on tissue paper in air at room temperature for 24 hrs, and then dried in air at 40°C for a further 24 hrs.

3.9.5 Sol-Gel Treated SF Bioceramics

Sol-gel treated SF bioceramics were dried for 24 hrs under a hot lamp at 75°C ± 5°C. Samples were then freeze-dried, in order to remove any water and methanol (by-product from sol-gel reaction) absorbed within them by a process of sublimation. This involved immersing the samples in liquid nitrogen, with a freezing rate fast enough to avoid the formation of large crystals. They were then placed in the chamber of an Edwards-Pearse Tissue Dryer EPD3, together with phosphorous pentoxide, used to absorb vapour during the freeze-drying process. The chamber was evacuated to 10^{-1} torr, and the temperature lowered to –60°C. This was left overnight, after which the temperature was increased to 25°C and the samples removed. The hot lamp drying and freeze-drying were performed to ensure complete extraction of excess moisture and methanol that was a by-product of the sol-gel process. This ensures that on sintering, surface cracks in the sol-gel surface layer would be eliminated. Samples were then sintered at 500°C and 1100°C – section 3.8.4.

3.10 Sintering of Samples

The sintering regimes that were common to all the fabrication techniques are described in sections 3.10.1 to 3.10.4. First, the PU foam was burnt off and pyrolised at 500°C, followed by densification of the ceramic slip, and finally the samples were cooled at an appropriate rate to produce a structurally strong bioceramic free of defects.

Although the three stages described were constant in the production of the HA/TCP bioceramics, the sintering regimes used, offer some subtle variations.

3.10.1 I.I. Bioceramics and HA/TCP Granular Material

The sintering procedure used for the I.I. bioceramics is shown in figure 3.4. The sintering chamber was heated (from room temperature) at a rate of 60°C/hr for 10 hours. It was then held at 600°C for one hour to ensure that the PU porosifier foam was completely burnt out. The chamber was then set to heat up at a rate of 120°C/hr until the sintering temperature of either 1280°C or 1150°C was reached. This temperature was then held for four hours. The chamber was then programmed to cool to 20°C at a ramp rate of 120°C/hr, and then to shut itself off.

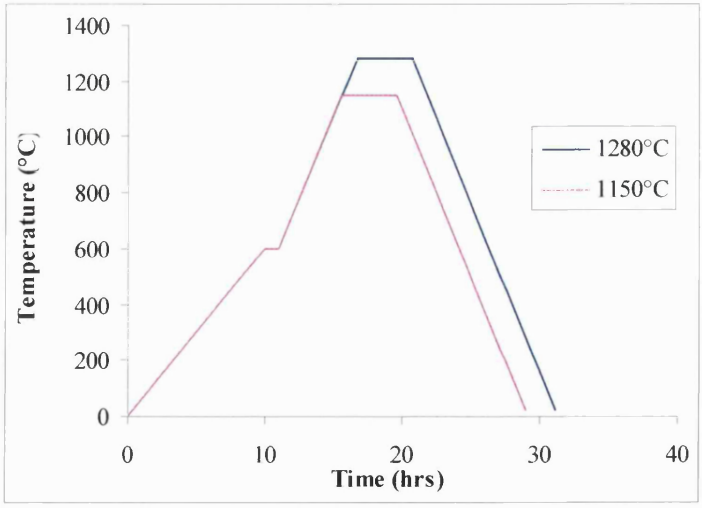

Figure 3.4: Sintering procedure for I.I.bioceramics at 1150°C and 1280°C

3.10.2 OPS Bioceramics

The sintering regime for the OPS bioceramics is shown in figure 3.5. From room temperature, the sintering chamber was heated at a rate of 30°C/hr until 300°C was reached. This temperature was then held for two hours. The chamber was further heated up to 450°C at a ramp rate of 30°C/hr and held for two hours. Further heating occurred up to 600°C at 30°C/hr and this temperature was once again held for two hours. The sintering procedure from this point on was as for the I.I. bioceramics.

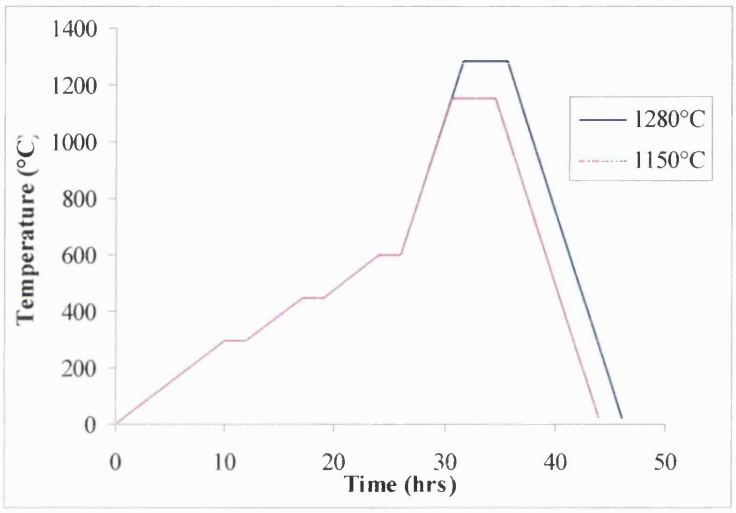

Figure 3.5: Sintering procedure for OPS bioceramics at 1150°C and 1280°C

3.10.3 SF Bioceramics

The sintering regime for the SF bioceramics is shown in figure 3.6. From room temperature, the sintering chamber was heated at 100°C/hr up to a temperature of 120°C. This temperature was held for one hour. The chamber was then set to heat up at a rate of 30°C/hr until 550°C, and this temperature was held for one hour. The chamber then heated up at a rate of 120°C/hr up to the maximum sintering temperature (1150 – 1350°C) and held for two hours. The sintering chamber was then programmed to cool down at a rate of 240°C/hr and shut itself off at 20°C.

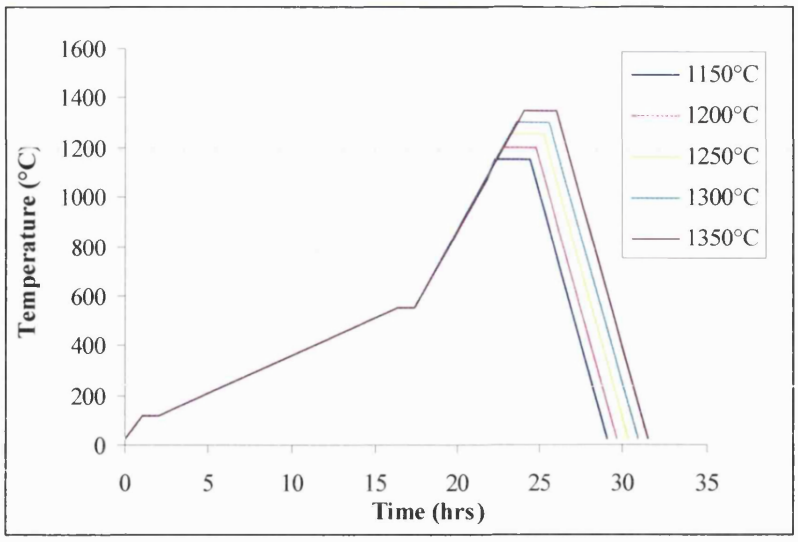

Figure 3.6: Sintering procedure for SF bioceramics at 1150°C - 1350°C

3.10.4 Sol-Gel Treated SF Bioceramics

The sintering regime for the SF bioceramics treated with sol-gel solution is shown in figure 3.7. From room temperature, the sintering chamber was heated at 60°C/hr up to a temperature of 500°C. This temperature was held for 1.5 hrs. The chamber was then set to cool down to room temperature at a rate of 240°C/hr until 20°C. The same sintering regime was used for the sol-gel SF bioceramics sintered at 1100°C.

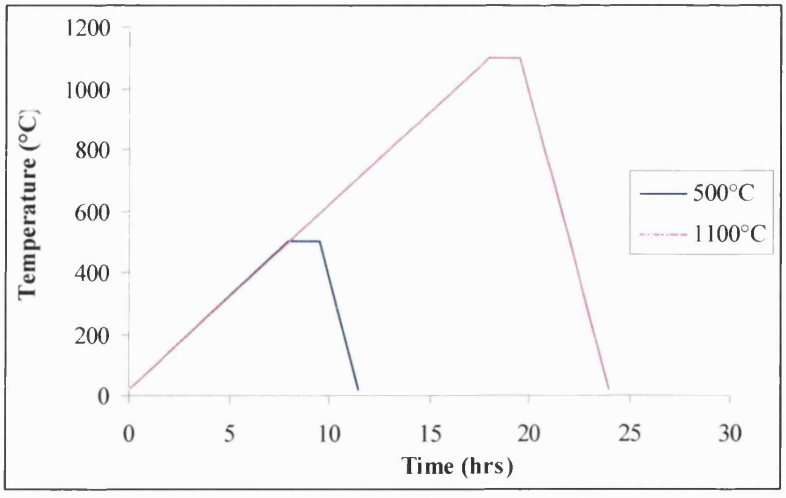

Figure 3.7: Sintering procedure for SF bioceramics treated with sol-gel at 500°C and 1100°C

3.11 Bulk Density Measurements

Bulk density measurements were used, whereby the mass and volumes of the samples were calculated. Apparent density measurements were then made and used only for comparative purposes between all the materials tested.

3.11.1 Impact-Impregnated Samples

The samples (40) were allowed to cool to room temperature and left at this point, in air, for 24 hours to ensure their integrity. They were then machined to form cubes of dimensions of 15 x 15 x 15 mm (or as close as possible to these dimensions). The samples then were ground to the exact dimensions. Simple density measurements were undertaken, as the results were used only as a comparison within the set of samples produced.

Once ground, the dimensions of each sample were measured using a micrometer to ensure the accuracy of each sample. A mean volume for each sample was then calculated. The mass of the cubes were also measured, thus simple density measurements could be made. The cubes were prepared in readiness for compression testing. The offcuts of the samples were used for image analysis and SEM imaging.

3.11.2 Open Porous Scaffolds

Sintered scaffold samples (120) were measured using a micrometer and their masses recorded prior to mechanical testing. The bulk density was then calculated.

3.11.3 SF Bioceramics and Sol-Gel Treated SF Bioceramics

The ends of the SF structures (100) were ground down flat in the same manner as for I.I. samples to ensure that the surfaces were as close to parallel as possible for compression testing. A micrometer was used to measure the mean volume of the materials. The mass was taken and bulk density measurements calculated.

3.12 Mechanical Characterisation

3.12.1 Compression Testing

Compression testing was performed using an Instron 1122 bench-top test machine fitted with a 5kN load cell. Testing was performed under automatic machine control and load was applied axially to the specimens with a crosshead speed of 2mm/min until catastrophic brittle failure occurred. Figure 3.8 illustrates the equipment used.

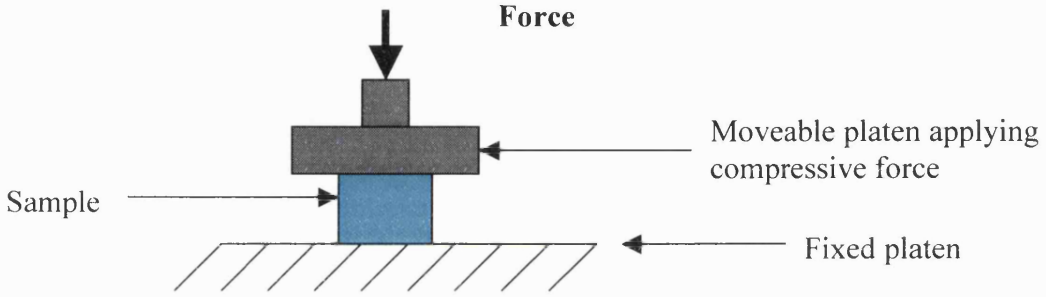

Figure 3.8: Schematic diagram of mechanical testing (compression testing) equipment

The subsequent compressive stress (CS) was then calculated for each specimen:

$$CS = \frac{\text{Maximum force}\quad (N)}{\text{Area of specimen}\quad (m^2)}$$

3.12.2 Three-Point Bend Test

The same Instron machine and machine settings were used as for compression testing, except a three-point bending jig with a distance between rollers of 20mm was used to establish the breaking stress of the OPS. Figure 3.9 illustrates the 3-point bending test set-up.

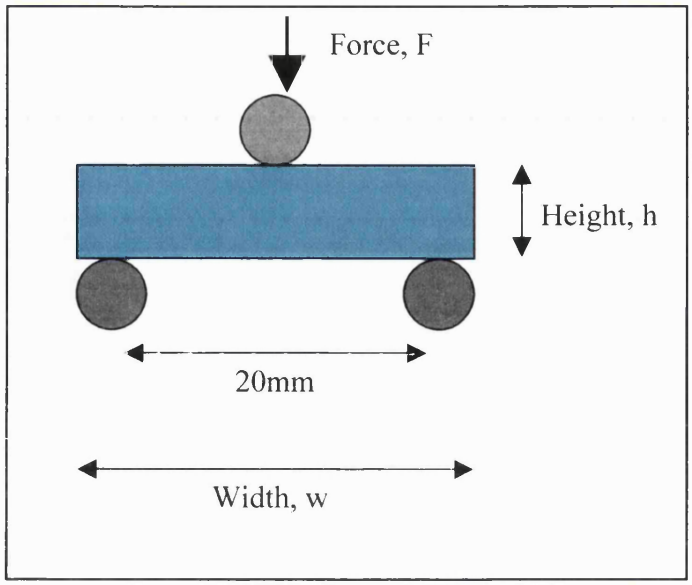

Figure 3.9: Two-dimensional view of 3-point bending test procedure

The maximum breaking stress (σ_B) of each OPS is calculated by equation 17:

$$\sigma_B = F_{max.}.\ (Lc/4I) \qquad (17)$$

where $F_{max.}$ = maximum force at failure (N)
L = distance between rollers (0.02m)
c = distance from cross-sectional centre of scaffold to rollers (m)
I = moment of inertia = $wh^3/12$

3.12.3 Die-Plunger Compression Testing of Granular Material

HA/TCP granules ranging in size from 2-4mm, 3-5mm and 4-8mm were tested by a standard die-plunger compression test. Using a measuring tube, $10cm^3$ of HA/TCP granular material were poured into a hollow tube (die) with a diameter of 20mm, as shown in figure 3.10. It was ensured that all granules had settled in the die before beginning testing. The operating procedure is described below.

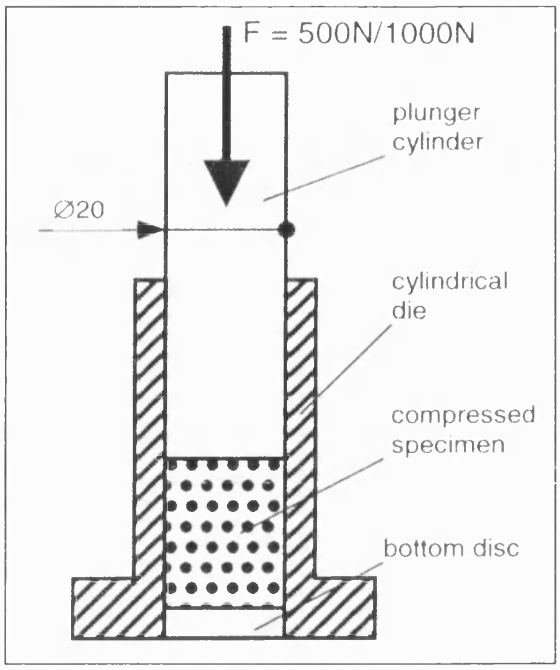

Figure 3.10: Schematic of the die-plunger compression test

To enable accurate conversion of deformation into strain measurements, the starting position of the plunger was noted on each test. Larger particles do not pack well inside the die and on compression granules topple, crush and re-order themselves to give misleading results. The crosshead speed was set at 2mm/min. The following loading cycle was applied for each batch of synthetic granules:

1) Loading to 500N.
2) Force held constant for a relaxation period of 30s.
3) Force released and returned to zero.
4) Steps 1 –3 are repeated.
5) Loading up to 1000N.
6) Force held constant for a relaxation period of 30s.
7) Force released and returned to zero. Retrieval of granular material.

The recorded force and displacement data from the Instron machine (via Marandy software on PC) were subsequently converted into stress and strain measurements and used to calculate the relative compressive modulus between the batches of granules tested. NB. These results are used for comparative purposes only between the granules tested.

3.13 Wicking Experiments

This experiment was carried out to evaluate the wicking properties of samples comprising the three separate phases – HA, α-TCP and β-TCP – in the form of SF samples.

A 2% aqueous solution of methylene blue polychrome (used as an indicator solution) was prepared, and a small amount used to cover the bottom of a petri dish. SF samples were then placed upright in the petri dish and their wicking properties assessed.

HA, α-TCP and β-TCP phases were observed at 1, 10, 40 and 60 minute intervals after being placed in the indicator solution. The length of time taken for the SF phases to be saturated was the factor being determined.

In a separate experiment, SF samples (HA, α-TCP and β-TCP) were left completely submerged in solution for 24 hrs. This was performed to evaluate the mass gain of the samples, due to the uptake of indicator solution.

Chapter 4 Results and Discussion

In this section, the main structural and material property differences between the fabricated samples along with an analysis of the findings is presented. It is useful for the purpose of this research to clarify the meaning of macroporosity and microporosity. Pores with dimensions in the size range 1-10μm are classified as micropores, and those with dimensions greater than 10μm are classed as macropores.

4.1 Image Analysis and Thermogravimetric Analysis (TGA) of PU Foams

This section sets out an analysis of the PU foams used as porosity templates in the fabrication methods. SEM analysis of the porosifier foams and cumulative pore distribution of the foams, as well as TGA analysis were carried out.

4.1.1 Image Analysis of PU Foams

Figures 4.1 and 4.2 shows the structure of the reticulated 45 and 30ppi PU foams by digital photography and from SEM analysis respectively.

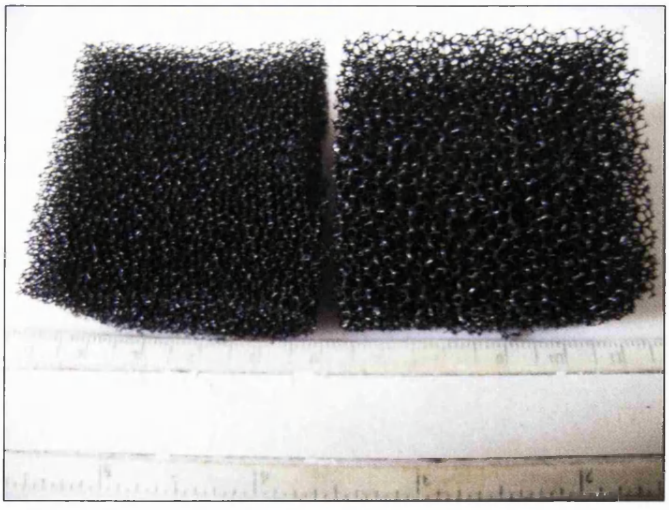

Figure 4.1: 45 and 30 ppi PU foam

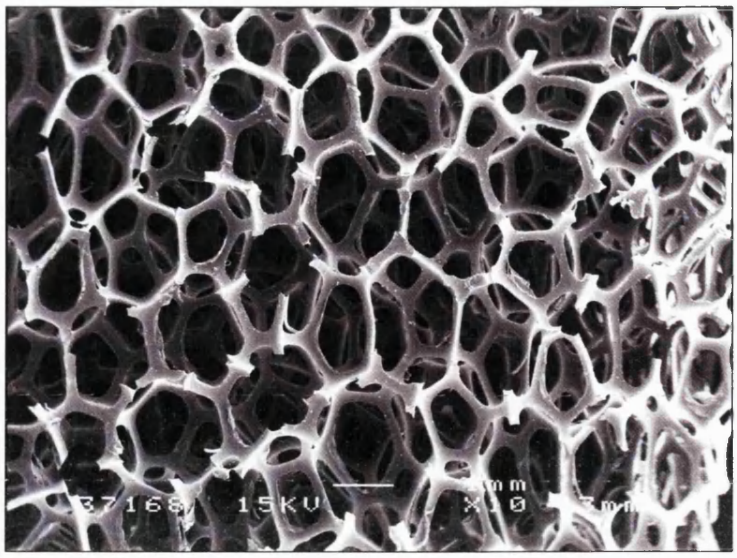

Figure 4.2: SEM image of 45 ppi PU foam

Figure 4.3 show the cumulative pore distribution of the two PU foams used for impregnation by CaP slips.

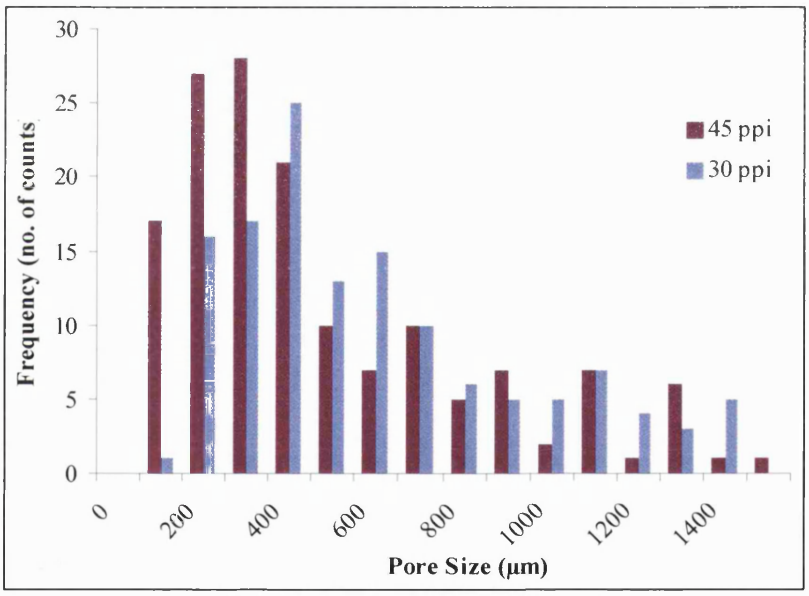

Figure 4.3: Distribution of pores in PU foams prior to fabrication

The mean pore size for the 45 ppi foams was 533.1µm, and the mean pore size for the 30 ppi was 797.7µm. These were calculated as the average from the equivalent area diameter of the pores measured by the Image Analysis software (section 3.5).

The foams offer an excellent template for the production of bone substitute materials. The foams possess interconnected porosity in the correct size range for possible bone ingrowth.

4.1.2 TGA of PU Foams

Figure 4.4 (a) and (b) show the TGA curves for the 30 ppi and 45 ppi foams respectively.

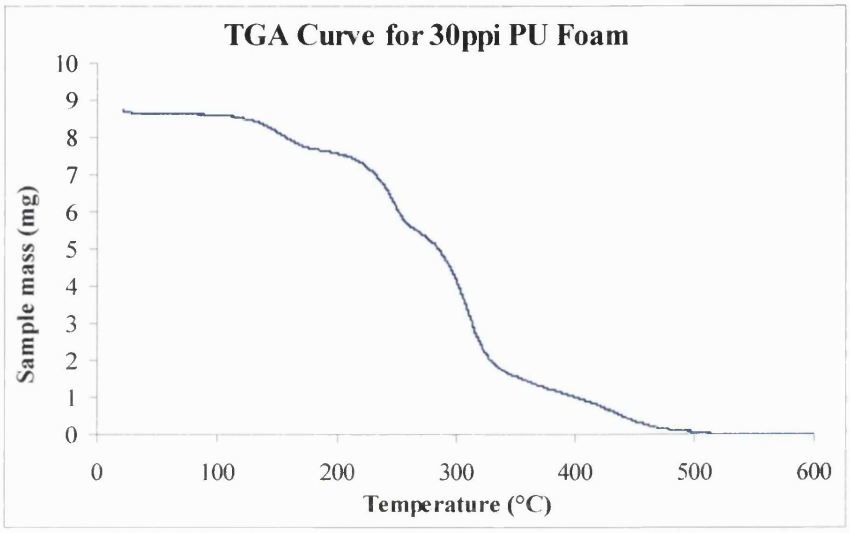

Figure 4.4 (a): TGA curve for 30 ppi foam

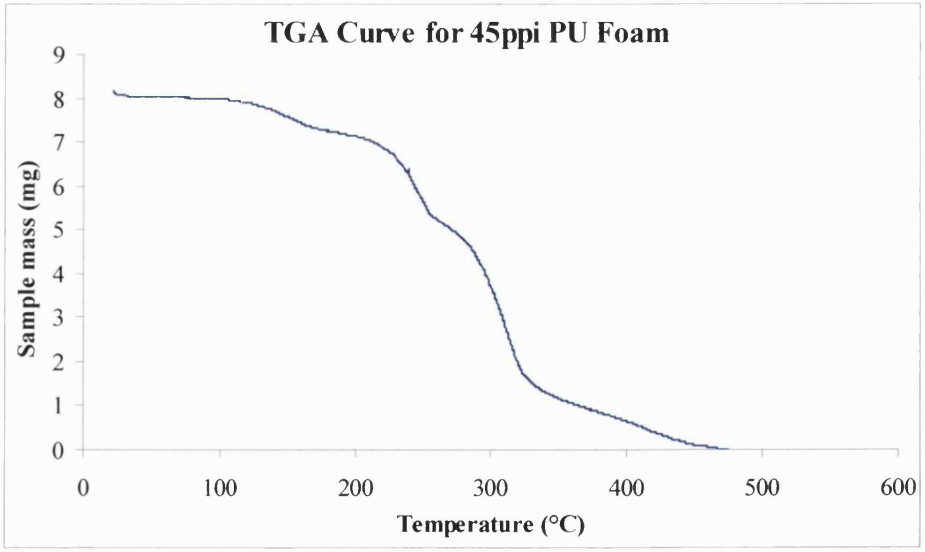

Figure 4.4 (b): TGA curve for 45 ppi foam

These TGA curves indicate similar traces for both grades of foam. Softening begins at 150°C, with sharp decreases in mass from 175°C – 325°C due to molecular side groups such as urethane and allophante groups being burnt away. The foams were burnt out completely at 500°C. Figure 4.5 shows a TGA curve of a 45 ppi foam that has been impregnated by CaP slip.

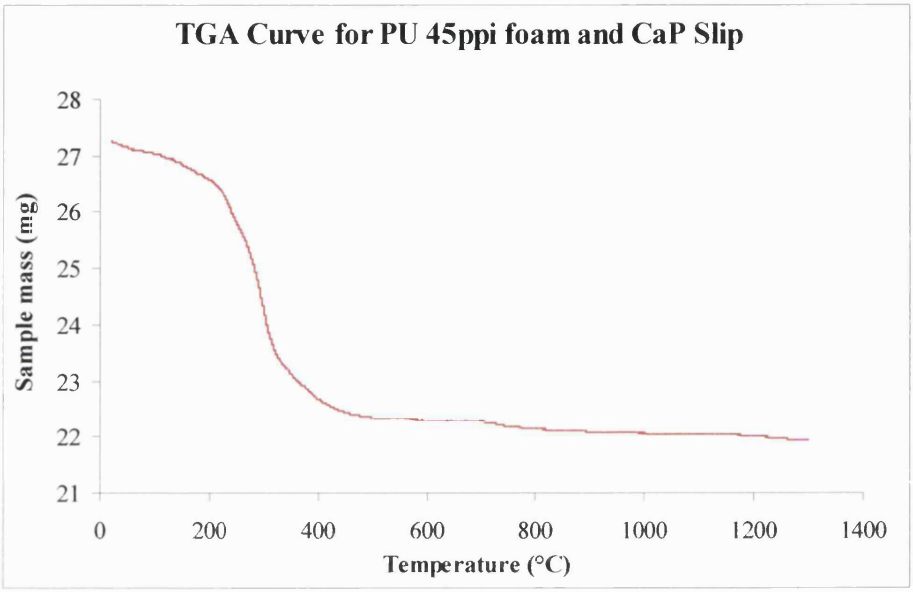

Figure 4.5: TGA curve for 45 ppi foam impregnated with CaP slip

It can be seen from figure 4.5 that the foam follows the same characteristics as shown in figures 4.4 (a) and (b) up until 500°C. Above 500°C, due to dehydroxylation of the CaP slip, the mass steadily decreases until 1300°C. Figure 4.6 shows a detailed view of figure 4.5 in the temperature range 400 – 1300°C. It can be seen that there is a drop in mass at 700°C due to dehydroxylation in the CaP slip. At temperatures above this, there was a steady decrease in mass until ~ 1180°C whereby transformation from β-TCP to α-TCP occurs (section 3.1 and 4.2).

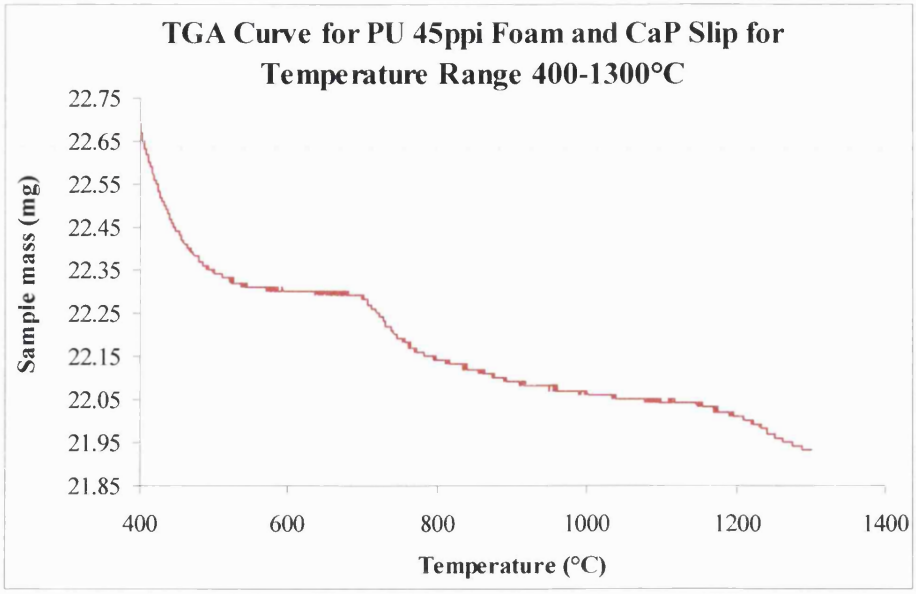

Figure 4.6: TGA curve for 45 ppi foam impregnated with CaP slip from 400-1300°C

4.1.3 Summary of TGA and SEM Analysis of PU Foam

SEM and cumulative pore distribution analysis indicate that the PU reticulated foams are a successful template material to act as a porosifier for bone substitute materials.

The 30 and 45 ppi foams begin to soften at 150°C, with complete material burnout occurring at 500°C. The CaP slip decreases in mass steadily from 700 – 1300°C, with substantial decreases in mass at ~ 700°C as slip densification begins, and at ~ 1180°C when thermal transformation from β-TCP to α-TCP occurred.

4.2 X-Ray Diffraction (XRD) Analysis

XRD analysis was used to evaluate the differences in chemical composition of the base powders, the different CaP phases produced (HA, α-TCP and β-TCP) and the different phases produced in the bioceramics as a result of the sol-gel treatment. The identification of mixed phase materials is more complicated as the strong reflections from different phases overlap and this superposition creates strong reflections and to some degree disguises the distinctive diffraction pattern of the phases present. This makes qualitative identification of the phases present very difficult. This is a limitation of the XRD method that can be resolved by other techniques such as neutron diffraction and EDAX analysis.

4.2.1 Base Powders

The base powders used in the research, supplied by Stryker Orthopaedics, offer versatility in their application and the range of composition of materials that can be fabricated. On sintering, grade 118 allows transformation to TCP. Grade 130 remains predominantly as HA. Figures 4.7 (a) and (b) show XRD traces of the base powders 118 and 130 respectively before sintering.

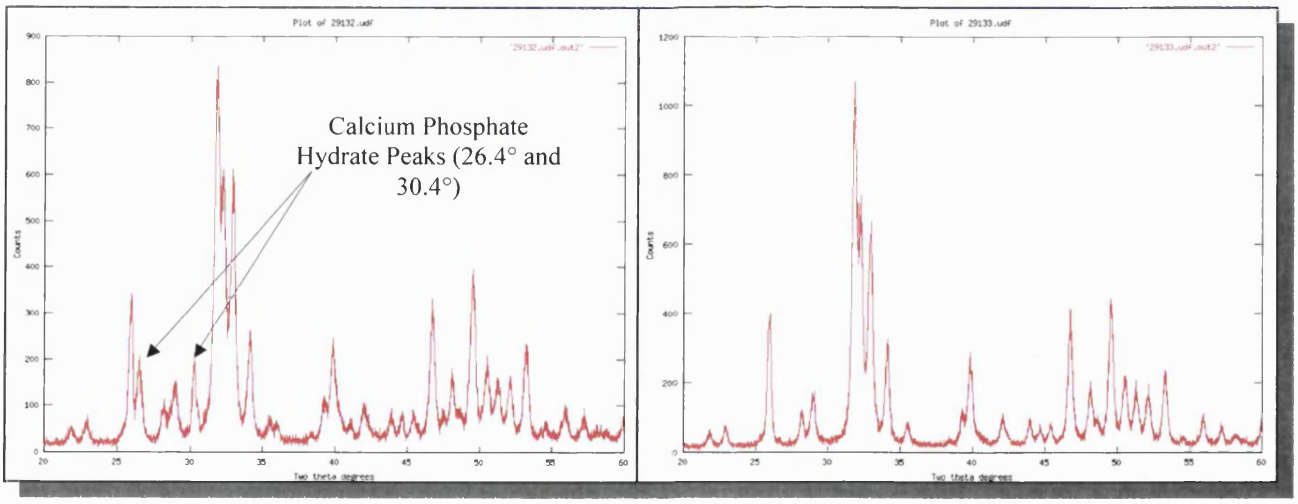

Figure 4.7 (a): XRD trace for grade 118 powder before sintering

Figure 4.7 (b): XRD trace for grade 130 powder before sintering

As indicated on figure 4.7 (a), there were two major calcium phosphate hydrate peaks at 26.4° and 30.4° with the remaining peaks corresponding to HA. The addition of calcium phosphate hydrate lowers the Ca:P ratio below that of the HA stoichiometric ratio of 1.67, and therefore, on

subsequent sintering, thermal transformations allow TCP to form. Grade 130 powders indicate a correlation with the stoichiometric form of HA. Also of note were the low level counts for the background of the 130 powders when compared to 118 powders, this is indicative of a high degree of crystallinity in the former.

Table 4.1 and figure 4.8 show, by the number of counts, the thermal transformation of the base powders 118 and 130 at 1150 – 1350°C. The phases were calculated from the intensity counts of the characteristic peaks of the particular phase to be calculated, divided by the total intensity of the peaks of all three phases present.

%	1150°C		1200°C		1250°C		1300°C		1350°C	
Phase	118	130	118	130	118	130	118	130	118	130
HA	5.6	80.2	4.7	83.2	3.9	85.6	5.4	90.8	5.2	91.2
α-TCP	22.3	6.5	38.7	9.9	40.2	9.8	45.3	6.2	45.5	5.3
β-TCP	72.1	13.3	56.6	6.9	55.9	4.6	49.3	3.0	49.3	3.5

Table 4.1: Thermal transformation of base powders 118 and 130 post-sintering

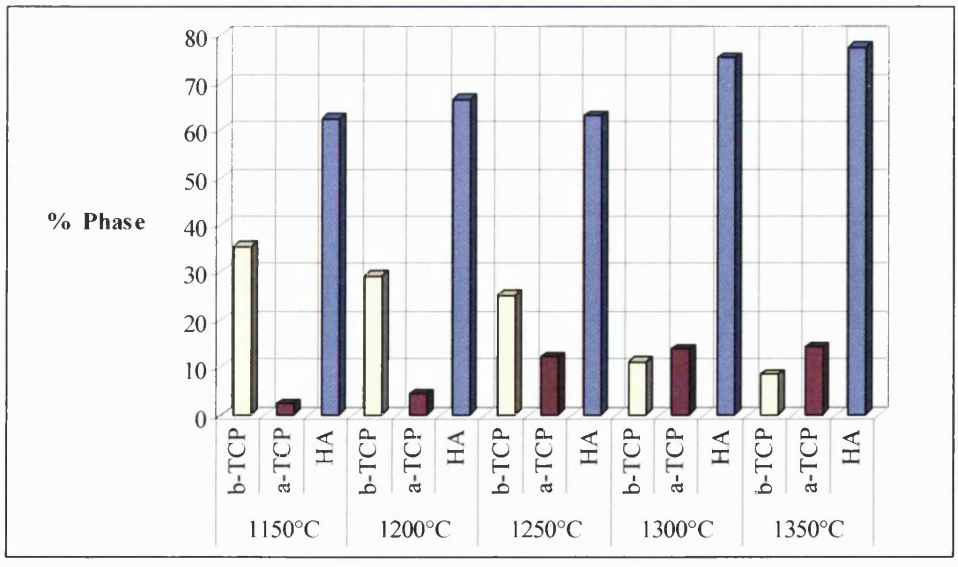

Figure 4.8: Thermal transformations of 50/50 mix of powders 118 and 130

Table 4.1 and figure 4.8 illustrates the increase in the amount of α-TCP with increasing temperature. Table 4.1 shows that powder 118 forms β-TCP at 1150°C. On increasing

temperature, the amount of β-TCP decreases and the amount of α-TCP increases. As discussed in section 3.1, a thermally activated reaction occurs at ~ 1180°C transforming β-TCP to α-TCP. This transformation was due to the lower Ca:P ratio present in the 118 powder, and therefore on sintering the material forms non-stoichiometric calcium phosphate materials i.e. tricalcium phosphate.

The 118 powders sintered at 1150°C transform pre-dominantly into TCP with 72.1% being β-TCP and 22.3% as α-TCP (table 4.1). On further sintering to 1300°C the presence of the α-TCP phase has increased to 45.3%. The formation of α-TCP produces a hard, glassy microstructure that forms from an allotropic transformation due to thermal changes in the β-TCP-to-α-TCP structural change, as described above and in section 3.1. The 130 powders pre-dominantly remain as HA at all temperatures (table 4.1).

4.2.2 CaP Traces

Figures 4.9 (a) to (c) show the XRD traces for the HA, α-TCP and β-TCP phases fabricated in the current research.

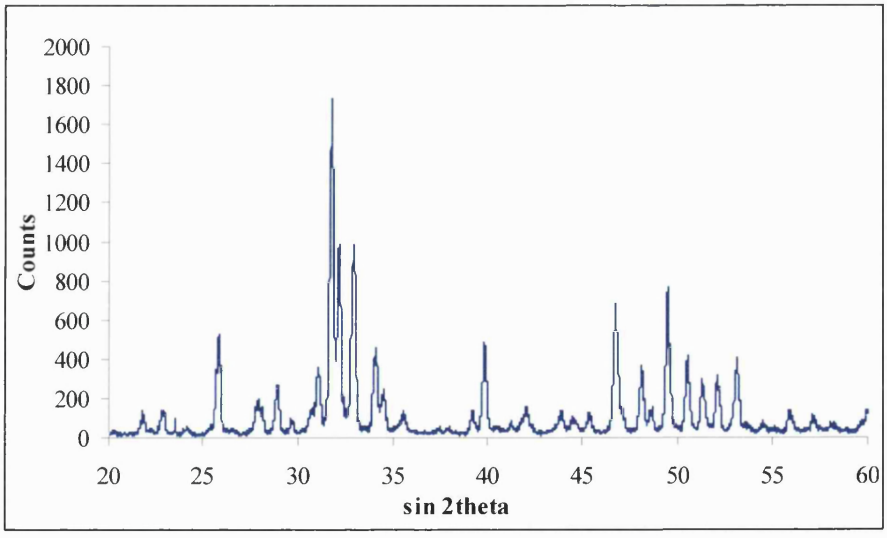

Figure 4.9 (a): XRD trace for HA bioceramic

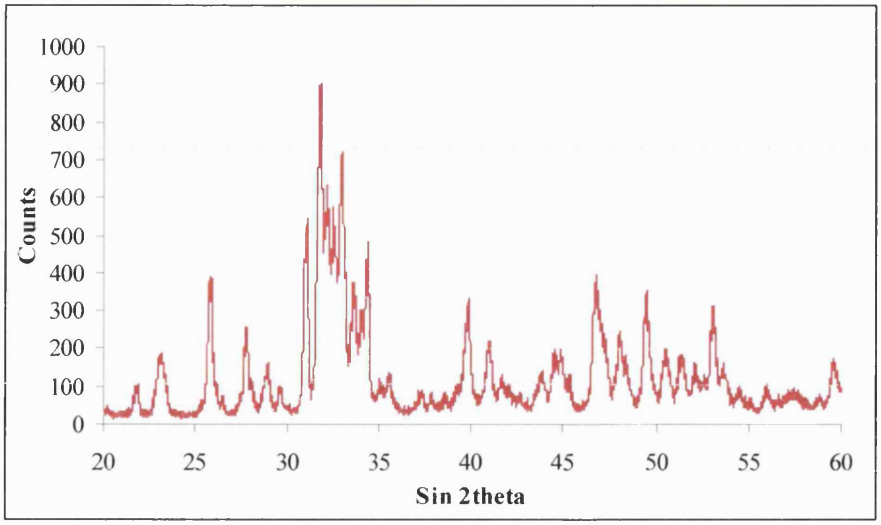

Figure 4.9 (b): XRD trace for α-TCP bioceramic

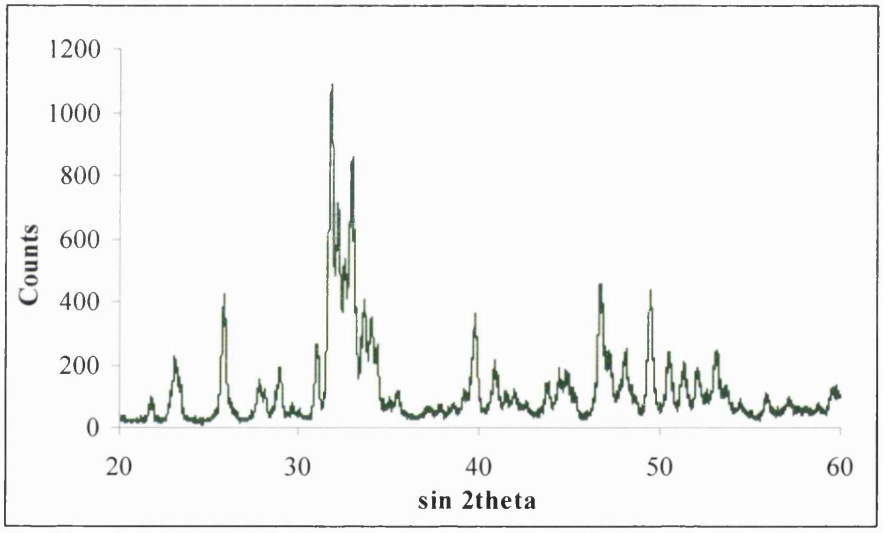

Figure 4.9 (c): XRD trace for β-TCP bioceramic

Figure 4.9 (a) is the XRD trace of the HA phase fabricated from powder 130. There is no indication of the presence of α-TCP or β-TCP peaks. Figure 4.9 (b) is the XRD trace of the α-TCP phase fabricated at 1300°C. The main α-TCP peaks, at 31.1° and 34.3°, give an indication of the quantity of the α-TCP present, as there was no overlap with any of the strong peaks from the smaller amount of β-TCP present. Figure 4.9 (c) illustrates the XRD trace for the β-TCP phase at 1150°C. The main β-TCP peak at 32.2° is characteristic for this structure.

4.2.3 Sol-Gel Treatments

Figure 4.10 shows the XRD traces of the HA, α-TCP and β-TCP phases compared with the traces from samples treated with soda sol-gel.

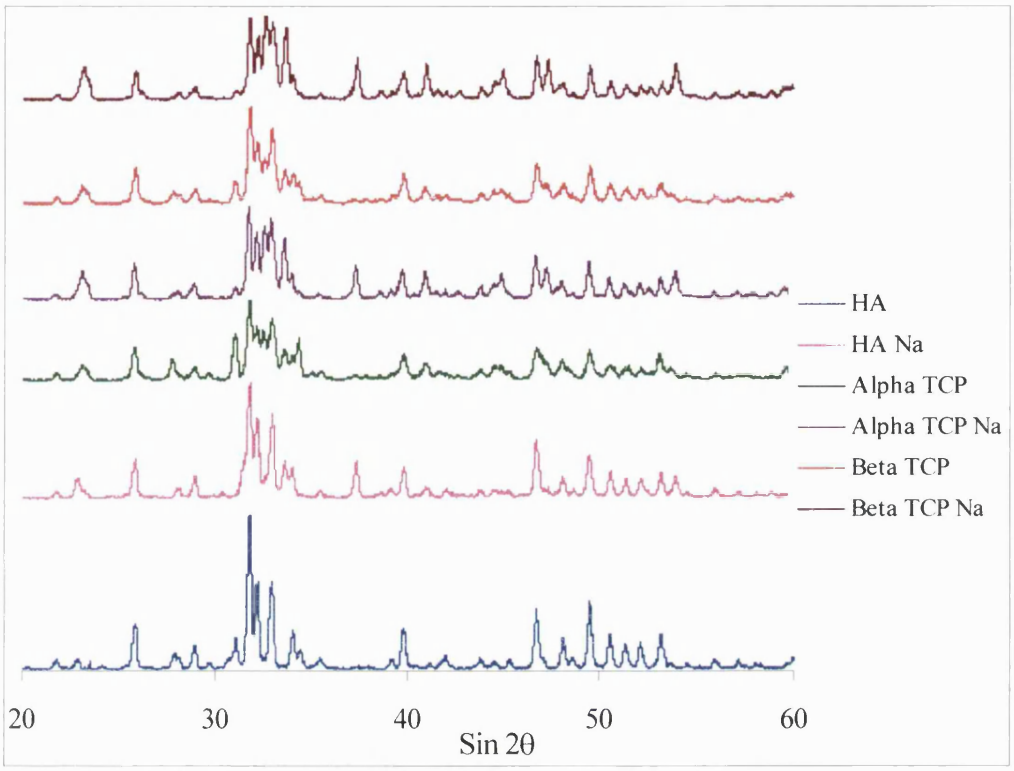

Figure 4.10: Comparison of XRD traces for HA, α-TCP and β-TCP before and after application of the sol-gel

The greatest mechanical strength increases due to the sol-gel treatment, were found with the TCP samples. The XRD traces of these materials indicate a more pronounced change in chemical structure, as only slight changes have occurred in HA samples where, relatively, the strength increases were not as profound. The apatitic structure of the materials produced has been altered due to the sol-gel treatment, most likely sodium phosphate phases have been developed.

At 37.4° there is a peak that is characteristic of those materials treated with soda sol-gel. This peak is present in all three phases treated with the sol-gel solution. This is the only change to the HA structure, however there are numerous more peaks in relation to the TCP structures. These peaks are identified at 44.1°, 45.1° and 47.3°. In addition to these peaks, the peaks from 31.8° -

33° have been altered in intensity. This is due to the fact that there are peaks that overlap with the TCP peaks, hence altering the XRD trace and chemical structure, due to the sol-gel treatment whereby quite possibly sodium phosphate phases have developed.

4.2.4 Summary of XRD Results

Base Powders

Differences in the base powders 118 and 130, were due to the presence of a calcium phosphate hydrate phase in the 118 powder, which ultimately lowered the Ca:P ratio and hence on sintering allows transformation to β-TCP and α-TCP. Grade 130 remains as HA on sintering. At 1150°C, grade 118 powder was pre-dominantly 75% β-TCP and 25% α-TCP. At 1300°C, 50% of the β-TCP thermally transforms to α-TCP. Grade 130 on sintering, remained as HA and only a very small amount of β-TCP was present at 1150°C.

Sol-Gel Treatments

The sol-gel treatments have had the greatest affects on the chemistry of the TCP structures, presumably due to the presence of vacancies in the structure (lower Ca:P ratio). It is these bioceramics that showed the greatest increase in strength on mechanical testing. The large microporosity present in the TCP samples (compared to HA), and thus the ability of the sol-gel to bond to the surface of the TCP, has allowed changes in the structure. This indicates improvements in the structure-property relationship of the bioceramics and correlates with the improved mechanical properties achieved.

4.3 Impact-Impregnated (I.I.) Bioceramics

For the fabrication of I.I. bioceramics, three variables were used in order to ascertain differences in the macroporosity distribution and the resultant effect on mechanical properties. Alterations to the macroporosity distribution included changes to the total volume porosity, the mean pore size and standard deviation of the pore size. The three experimental variables included the different grade of foam porosifiers used during fabrication (30 and 45 ppi), the sintering temperature (1150°C and 1280°C) and the drying medium used (metal mesh or tissue paper). Table 4.2 indicates that there were eight batches of materials produced, and illustrates how the variables were used in the experimental procedure (NB. There were five samples per batch thus totalling forty samples).

	Porosifier Foam Type (ppi)	Drying Method	Sintering temperature (°C)
Batch 1	45	Metal Mesh	1280
Batch 2	45	Tissue Paper	1280
Batch 3	45	Metal Mesh	1150
Batch 4	45	Tissue Paper	1150
Batch 5	30	Metal Mesh	1280
Batch 6	30	Tissue Paper	1280
Batch 7	30	Metal Mesh	1150
Batch 8	30	Tissue Paper	1150

Table 4.2: The batches of samples fabricated from the I.I. procedure

In total, forty samples were fabricated with twenty samples fabricated from 30 ppi foam and twenty from 45 ppi porosifier foams. Half of the samples fabricated from the two different porosifier foams were dried on metal mesh, and the other half were dried on tissue paper. From the samples dried on metal mesh, half were sintered at 1150°C and half at 1280°C. The same sintering procedures were used for the tissue dried samples. Therefore, there were eight different batches of material with five samples per batch totalling forty samples.

Figures 4.11 (a) and (b) show digital camera images of the sintered bioceramics fabricated with the I.I. method. The images show cut sections from the samples illustrating the internal structure of the bioceramics. The large closed porosity that can be seen throughout is the result of poor impregnation in the fabrication stage. The 1150°C samples appeared to be slightly more friable in texture than the 1280°C samples. I.I. samples made from the 30 ppi foams also appeared to be slightly more friable in appearance and nature than the samples made from 45 ppi porosifier foams. This was especially true when dried on the metal mesh instead of the tissue, due to the ease of flow of slurry through the larger pores on the mesh, which leaves an impression on the surface of the dried specimen. All I.I. samples were fired in the same sintering oven.

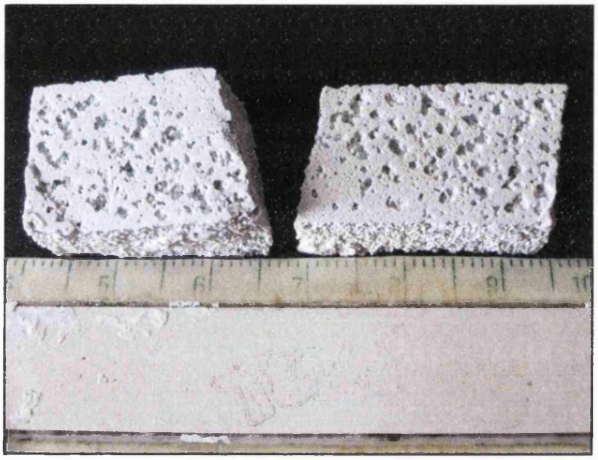

Figure 4.11 (a): I.I. bioceramic sintered at 1280°C. Approximate composition 75% HA, 14% α-TCP, 11% β-TCP

Figure 4.11 (b): I.I. bioceramic sintered at 1150°C. Approximate composition 61% HA, 4% α-TCP, 35% β-TCP

4.3.1 Image Analysis - Macroporosity

The following results show the macroporosity present in the I.I. samples, including examples of the micrographs from SEM analysis and the macroporosity distribution from the I.I. fabrication method.

Sections of the samples from each batch were used to evaluate the macroporosity distribution for that particular batch before sectioned into cubes for compression testing (section 4.3.3). The total cross section was recorded in the form of four SEM images that could be analysed to establish the macroporosity distribution.

The Optimas 6.1 computer software was used for image analysis (as described in section 3.5) on two micrographs that were taken from SEM analysis. These images were scanned into the software and "cleaned up" to improve the clarity of the images and hence the accuracy of the results. The macroporosity distribution was evaluated from four images for each sample (entire area of sample), and the results of the mean pore size, standard deviation pore size and the total volume porosity were correlated to the experimental variables (the sintering temperature, the type of porosifier used and the drying medium).

Tables 4.3 (a) and (b) represent comparative macroporosity distribution data between those samples dried on metal mesh and those dried on tissue paper respectively. It was found that the drying method had the greatest influence on the macroporosity distribution of the I.I. fabricated samples. Drying the I.I. samples on tissue instead of on metal mesh improves the extraction of moisture from the samples, and as a result, the macroporosity of the tissue dried samples was reduced.

The variations found due to the different drying regimes, also affected the standard deviation of the pore size and the maximum pore size found. Those samples dried on metal mesh possessed larger incidences of closed porosity, and it is this porosity caused due to poor drying, that accounts for the disruption in the structure, and as a consequence increases the deviation in the pore size present, table 4.3 (a).

Samples dried on tissue paper have a reduced level of large closed porosity, thus the deviation in the size of the porosity present was reduced, table 4.3 (b). As a consequence, this improved the interconnectivity of the porosity and the accuracy of the measurement of the interconnected bow tie shaped porosity (i.e. the mean pore size). Incidents of larger sized pores were numerous in samples dried on metal mesh when compared to those dried on tissue paper. As a result of this closed porosity from poor drying, the maximum size porosity found in samples dried on metal mesh was substantially larger than those dried on tissue paper.

Approximate Composition of Sample (%)					**Total Volume Porosity (%)**	**Maximum Pore Size (μm)**	**Mean Pore Size (μm)**	**Standard Deviation of Pore Size (μm)**
HA	α-TCP	β-TCP	Sintering temp. (°C)	Porosifier size (ppi)				
75	14	11	1280	45	30.6	1475.4	93.3	161.5
61	4	35	1150	45	17.3	800.5	84.8	107.1
75	14	11	1280	30	19.1	5967.3	113.0	335.5
61	4	35	1150	30	28.3	2926.1	133.6	266.4

Table 4.3 (a): Macroporosity data for I.I. samples dried on metal mesh

Approximate Composition of Sample (%)					**Total Volume Porosity (%)**	**Maximum Pore Size (μm)**	**Mean Pore Size (μm)**	**Standard Deviation of Pore Size (μm)**
HA	α-TCP	β-TCP	Sintering temp. (°C)	Porosifier size (ppi)				
75	14	11	1280	45	21.4	744.3	102.9	108.9
61	4	35	1150	45	10.8	959.1	92.9	73.9
75	14	11	1280	30	9.5	479.4	104.0	78.7
61	4	35	1150	30	6.9	697.1	109.7	78.1

Table 4.3 (b): Macroporosity data for samples dried on tissue paper

Due to poor moisture extraction in the samples dried on metal mesh (compared to those dried on tissue paper), large, circular closed pores were present (from air voidage) that disrupt the interconnectivity of the porosity distribution, provided by the porosifier foam burnout. Drying on tissue reduces the number of incidents of closed porosity and as a consequence offers an improved interconnected porosity network following the burnout of the porosifier foam. Figures 4.12 (a) and (b) show SEM images of sections of samples dried on metal mesh and tissue paper respectively.

The bow tie shaped pores result from porosifier foam burnout (interconnected porosity), and the large circular pores were due to poor moisture extraction and therefore created air voidage and

closed pores on sintering. There was greater clarity in the interconnected porosity network in those samples dried on tissue paper, figure 4.12 (b), as the porosity distribution was not disrupted by the presence of closed porosity.

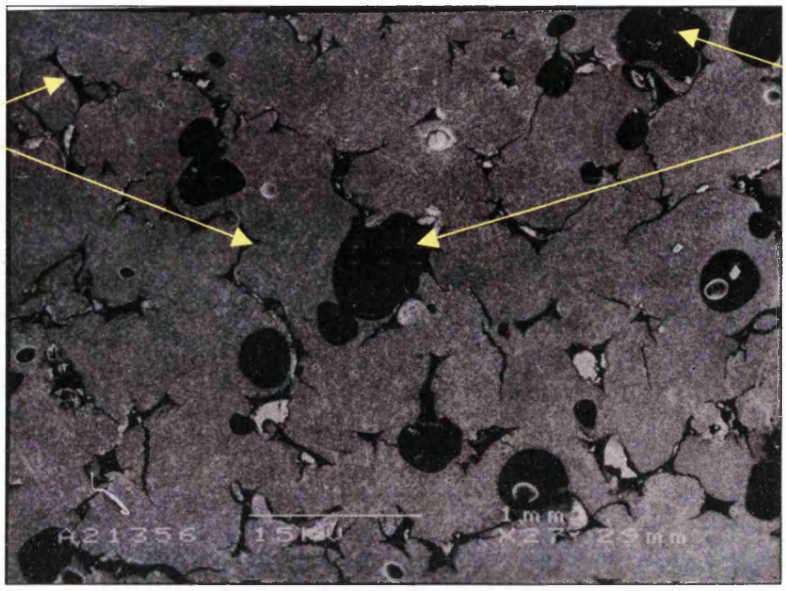

Figure 4.12 (a): SEM micrograph of a section of a 45 ppi sample dried on metal mesh

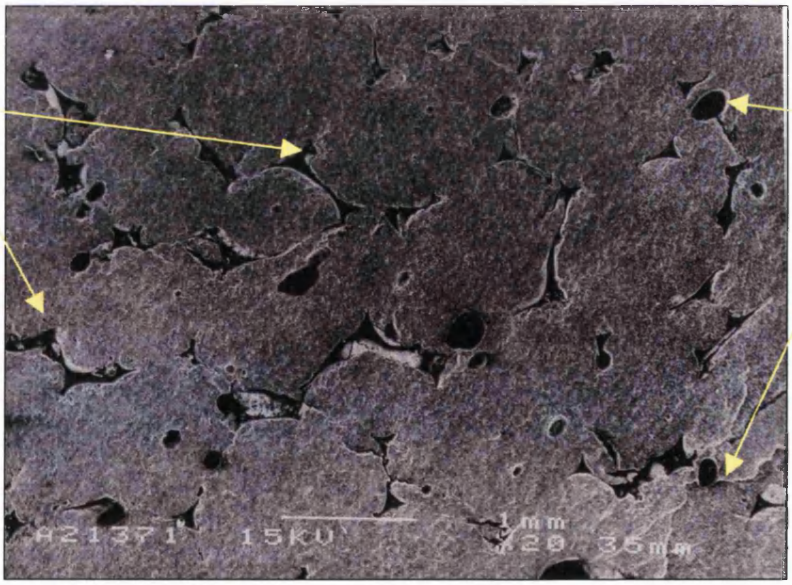

Figure 4.12 (b): SEM micrograph of a section of a 30 ppi sample dried on tissue paper

The mean pore size of the 30 ppi foams was larger than for the 45 ppi foams. The number of interconnected bow tie shaped pores (from foam burnout) was fewer, however they were greater in size. This was a function of the type of porosifier foam used and not the drying method. Both

foam samples possess the same volume of foam and hence the 30 ppi samples possess larger pores created due to foam burnout than for 45 ppi foams, as they were inherently fewer in number.

As a consequence of drying on tissue paper, there were fewer counts of porosity as the number of incidences of closed porosity was reduced. The cumulative pore distribution graphs of those samples dried on metal mesh compared to drying on tissue are shown in figure 4.13. NB. The pore size scale bar has been limited to 500μm although there were counts of porosity above this size. However, these counts were small compared with the rest of the data set, therefore were not included in this comparison.

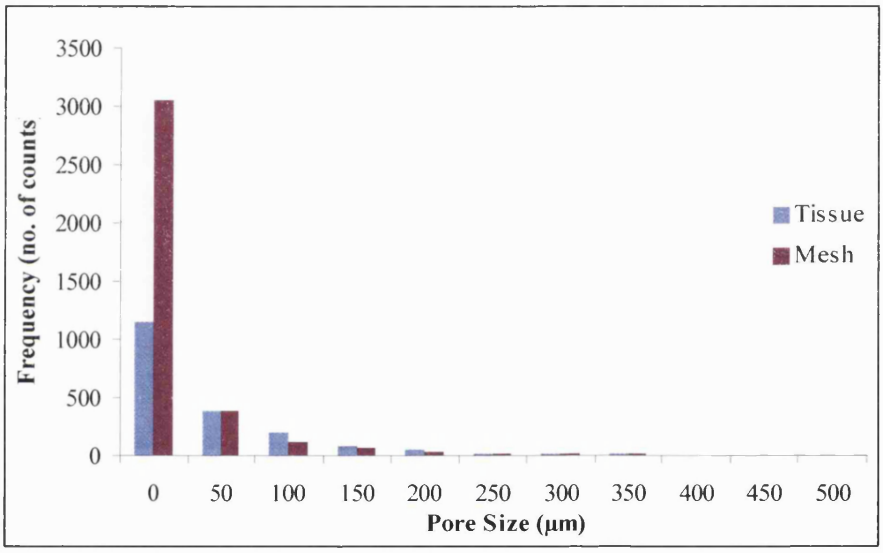

Figure 4.13: Cumulative pore distribution graph for samples dried on metal mesh and tissue paper

The majority of the porosity from the I.I. method was not ideally sized for possible bone substitute material applications. The recognised ideal pore size for bone regeneration to occur is 150 – 300μm, as discussed in sections 2.3 and 2.4. The mean porosity size from all I.I. samples was 104.3μm ± 48.4μm (as a 95% confidence level).

The type of porosifier used pre-dominantly determines the mean pore size of the porosity. It is also worthy to note that drying on metal mesh, which accounts for the presence of closed porosity, and using 30 ppi foams, possess a large deviation in their results.

The 30 ppi impregnated samples possess larger pore channels than those samples fabricated from 45 ppi foams. Therefore, it remained possible that slip would flow out of the foam during drying ("slumping"), thus increasing the mean pore size of the 30 ppi foam samples and the deviation in the result. Moisture extraction due to drying on tissue paper was more sensitive in the 30 ppi foam samples. This effect is shown in figure 4.14 below.

The shape of the porosity was also not ideal for potential bone substitute applications, as the bow tie shaped interconnected pores were larger at their edges than at their centre, suggesting that bone growth would not occur throughout the bioceramic.

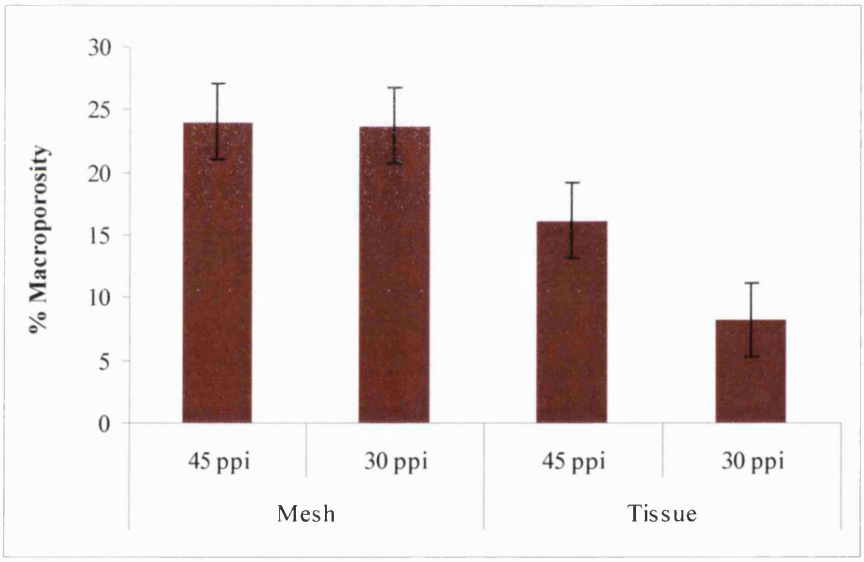

Figure 4.14: Total volume macroporosity of I.I. samples as a function of the drying method used

It can therefore be concluded that the macroporosity distribution fabricated from the I.I. samples does not possess guaranteed interconnected porosity in the correct size range for possible bone remodelling (i.e. 150 – 300μm). This was mainly due to the formation of closed pores due to poor drying on metal mesh. Drying on tissue paper improves the interconnectivity of the porosity and reduces the overall total volume porosity by 51%. The large differences in structure caused by the drying method had the greatest influence over the porosity distribution, the total volume

of porosity present and the deviation found in the result. The type of porosifier used (30 or 45 ppi) pre-dominantly controlled the mean pore size.

4.3.1.1 Accuracy of Macroporosity Measurement

Any errors incurred during image analysis were kept to a minimum due to the use of the Optimas 6.1 imaging software. The software analyses the porosity present by placing colour thresholds on two phases: grain and porosity. Therefore, if the thresholds for each phase are correct then errors with respect to the amount of porosity and the size and shape of the porosity are limited.

However, on one of the samples there appeared scratches (formed during polishing stage) and in another sample some gas porosity was present inside some closed porosity. The software finds it difficult to "see" the difference between the scratches and actual porosity present, as their colour thresholds are similar. Scratches present on one sample could be eliminated from detection by the software by softening the image, thus reducing the presence of the scratches, therefore improving the accuracy of the result.

4.3.2 Image Analysis - Microporosity

The macroporosity plays an active role in bone regeneration and has a strong influence on the mechanical properties of ceramics. However, the microporosity in its own right is an important parameter to focus on, as this is where ingress and migration of fluids and cells occurs. The following results show the microscopic structural features of the I.I. bioceramics, including the microporosity distributions of the samples.

Microstructural SEM analysis was taken from the same samples used in section 4.3.1, so that each batch of samples was analysed against the experimental variables: sintering temperature, drying method and the type of porosifier used. Therefore, a comparison can be made between these variables and the amount of microporosity present.

Tables 4.4 (a) and (b) show comparative microporosity distribution data between samples sintered at 1150°C and at 1280°C respectively. It was found that the sintering temperature had the greatest influence on the microporosity distribution of the I.I. bioceramics.

Approximate Composition of Sample					**Total Volume Porosity (%)**	**Mean Pore Size (μm)**	**Standard Deviation of Pore Size (μm)**
HA (%)	α-TCP (%)	β-TCP (%)	Drying Method	Porosifier size (ppi)			
61	4	35	Mesh	45	37.3	1.8	1.5
61	4	35	Tissue	45	51.6	1.8	1.6
61	4	35	Mesh	30	25.2	1.4	1.1
61	4	35	Tissue	30	34.4	1.5	1.2

Table 4.4 (a): Microporosity data for I.I. samples sintered at 1150°C

Approximate Composition of Sample					**Total Volume Porosity (%)**	**Mean Pore Size (μm)**	**Standard Deviation of Pore Size (μm)**
HA (%)	α-TCP (%)	β-TCP (%)	Drying Method	Porosifier size (ppi)			
75	14	11	Mesh	45	11.6	1.1	0.7
75	14	11	Tissue	45	13.6	1.0	0.8
75	14	11	Mesh	30	35.3	1.5	1.3
75	14	11	Tissue	30	10.2	0.6	0.7

Table 4.4 (b): Microporosity data for samples sintered at 1280°C

The volume porosity present in samples sintered at 1150°C and 1280°C was 37.1% ± 15.1% and 17.7% ± 10.2% respectively (95% confidence level). The large volume microporosity found in the 30 ppi fabricated sample, dried on metal mesh and sintered at 1280°C, was due to the formation of scratches on the surface of the sample during the polishing stage. Image analysis revealed difficulty in reducing the counts of dark areas on the micrograph and therefore unable to distinguish between scratches and actual porosity counts. As a consequence, the deviation in the microporosity present at 1280°C was increased, however, the deviation was greater still in those samples sintered at 1150°C, as there was more scope for error in image analysis due to the granular structure.

Sintering the I.I. samples at 1280°C instead of at 1150°C reduced the total volume microporosity of the bioceramics by 52%. At 1280°C, the samples contain approximately 14% α-TCP, while at 1150°C the bioceramic contains 4% α-TCP, 61% HA and 35% β-TCP (section 4.2). As discussed in sections 3.1 and 4.2, the β-TCP high temperature phase transformation to α-TCP occurs at 1180°C. Figures 4.15 (a) and (b) show SEM micrographs from I.I. bioceramics sintered at 1150°C and 1280°C respectively. It can be seen that there is an inconsistency in the respective microstructures, and therefore the amount of microporosity present in the two samples. An increase in sintering temperature results in a denser microstructure due to the formation of α-TCP (section 4.2).

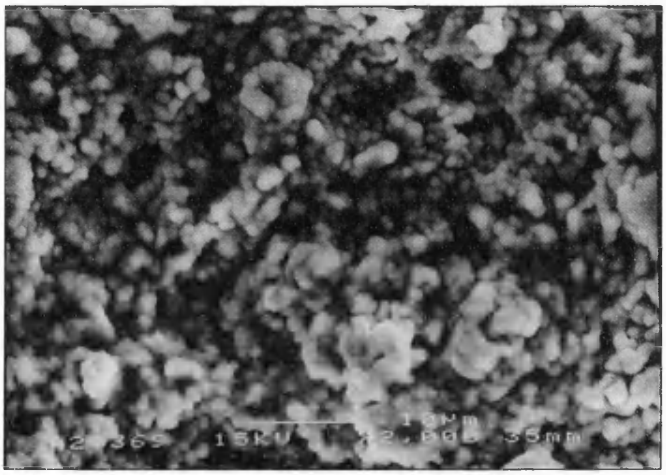

Figure 4.15 (a): Photomicrograph of a section of 61% HA, 35% β-TCP, 4% α-TCP I.I. sample sintered at 1150°C. Scale bar = 10μm

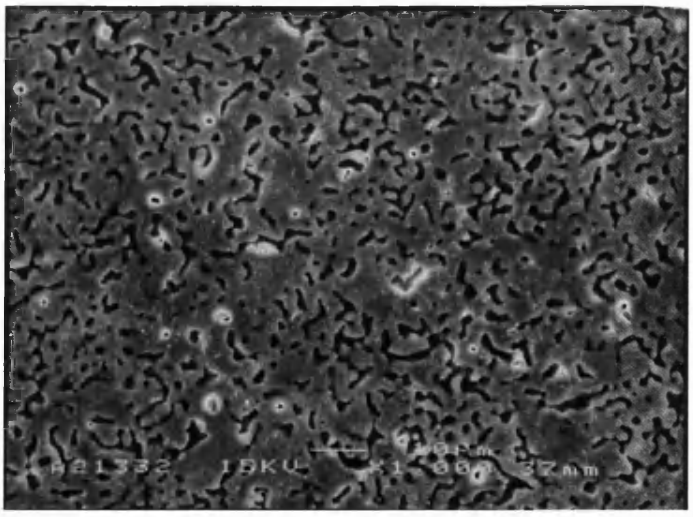

Figure 4.15 (b): Photomicrograph of a section of 75% HA, 14% α-TCP, 11% β-TCP I.I. sample sintered at 1280°C. Scale bar = 10μm

The β-TCP content in samples sintered at 1150°C produces a granular structure, which offers more scope for error in image analysis. This was because it was more difficult to place colour thresholds on the grain structure and microporosity. At 1280°C, due to the presence of calcium phosphate hydrate in the base powder 118 (section 4.2), a thermal phase transformation from β-TCP to α-TCP occurs. This transformation causes microstructural changes driven by grain growth via the elimination of microporosity. As a consequence, samples sintered at 1280°C have 52% less microporosity than those sintered at 1150°C.

The average microporosity present in all samples was 27.4%. The microporosity was found to be independent of the grade of porosifier used and drying method, as the amount of microporosity present in the 45 ppi foam samples and the 30 ppi foam samples was 28.6% and 26.3% respectively. Conversely, as previously discussed, the microporosity is dependent on sintering temperature. The microporosity present in samples sintered at 1150°C and 1280°C was 37.1% and 17.1% respectively. This temperature control over the microporosity of the bioceramics is shown in figure 4.16.

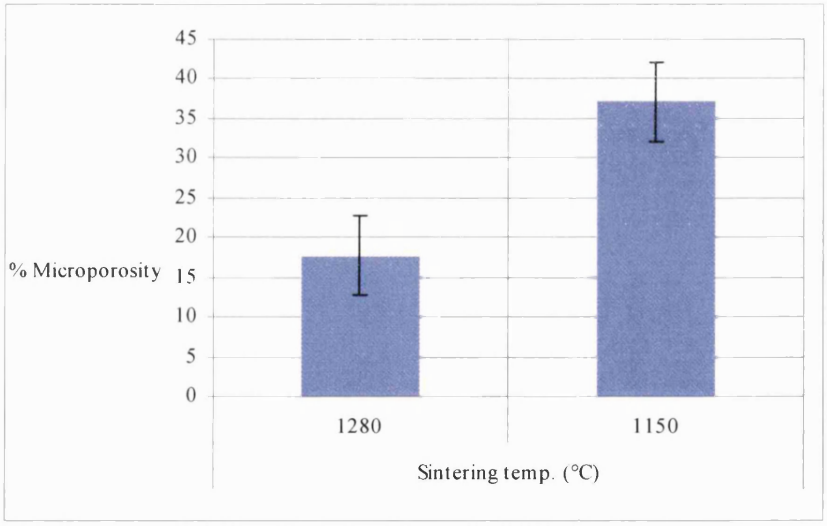

Figure 4.16: Microporosity changes as a function of sintering temperature in I.I. samples

Table 4.4 (a) also indicates that the deviation in the pore size was larger at 1150°C than at 1280°C, table 4.4 (b). In addition, the mean pore size was 0.5μm larger at 1150°C than at 1280°C. Figure 4.17 represents the cumulative pore distributions of the microporosity distribution at 1150°C and at 1280°C.

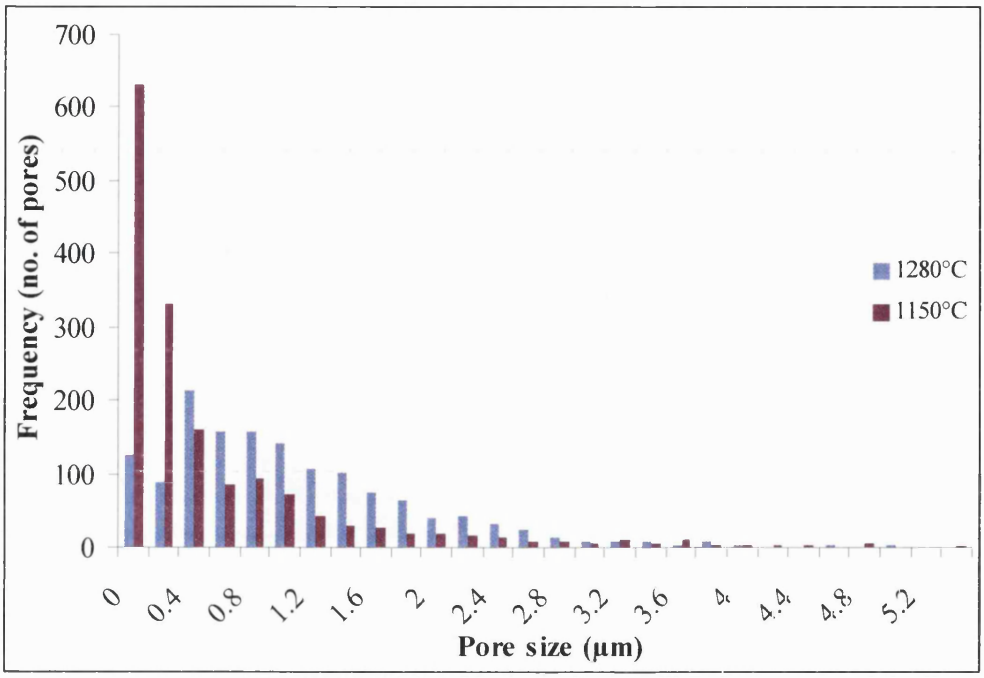

Figure 4.17: Cumulative micropore distribution for all the samples analysed by image analysis

The greater number of counts of porosity from 0 – 0.4µm at 1150°C was due to the discrepancies in image analysis. The granular microstructure due to the lack of formation of α-TCP, where a vitreous reaction occurs, offered a difficult surface for image analysis. Colour thresholds used to identify the grain and porosity would not capture the complete microporosity distribution (i.e. the larger microporosity counts). Therefore, the results for the samples sintered at 1150°C are not as accurate when compared to the samples sintered at 1280°C.

4.3.2.1 Accuracy of Microporosity Measurement

The Optimas 6.1 image analysis software was used for measuring microporosity. As for the macroporosity analysis, colour thresholds were set on the porosity phase and the grain phase. The software can be formatted in this way, to measure the percent porosity present and individual pore sizes. In some of the 1150°C fired samples, the pores were less defined than in the 1280°C fired samples. This posed some problems as the software manipulation had to be employed to soften the image so the software could distinguish between the two phases present (grain structure and porosity).

4.3.3 Strength-Density Relationship of I.I. Bioceramics

All forty samples were tested in compression until failure. The compressive stress was then calculated. The samples were first machined to cubes of 15 x 15 x 15 mm. Table 4.5 shows the results obtained.

Sample batch number	Sintering temperature (°C)	Porosifier size (ppi)	Drying method	**Mean Density (g/cm^3) - 95% Confidence Level**	**Mean Compressive Strength (MPa) – 95% Confidence Level**
1	1280	45	Mesh	**1.46 ± 0.07**	**3.34 ± 1.34**
2	1280	45	Tissue	**1.46 ± 0.10**	**4.66 ± 1.51**
3	1150	45	Mesh	**1.33 ± 0.19**	**5.27 ± 2.82**
4	1150	45	Tissue	**1.37 ± 0.17**	**4.68 ± 2.84**
5	1280	30	Mesh	**1.40 ± 0.11**	**1.90 ± 1.19**
6	1280	30	Tissue	**1.78 ± 0.25**	**9.94 ± 8.05**
7	1150	30	Mesh	**1.15 ± 0.14**	**2.29 ± 1.87**
8	1150	30	Tissue	**1.22 ± 0.21**	**4.18 ± 3.28**

Table 4.5: Summary of mechanical data for I.I. bioceramics

Figures 4.18 (a) to (e) show the strength-density relationships of the samples analysed. Regression analysis was also performed with R – values quoted on the figures indicating a good correlation in particular in those samples fabricated from 30ppi foams, those samples sintered at 1280°C and those samples dried on tissue paper. Figures 4.18 (a) and (b) compare the mechanical properties of I.I. bioceramics fabricated from different grade porosifiers (45 and 30 ppi). Figures 4.18 (c) and (d) compare samples fabricated at different sintering temperatures (1150°C and 1280°C), and figure 4.18 (e) shows the effects of the drying regime on the mechanical properties of the I.I. bioceramics (metal mesh or tissue paper).

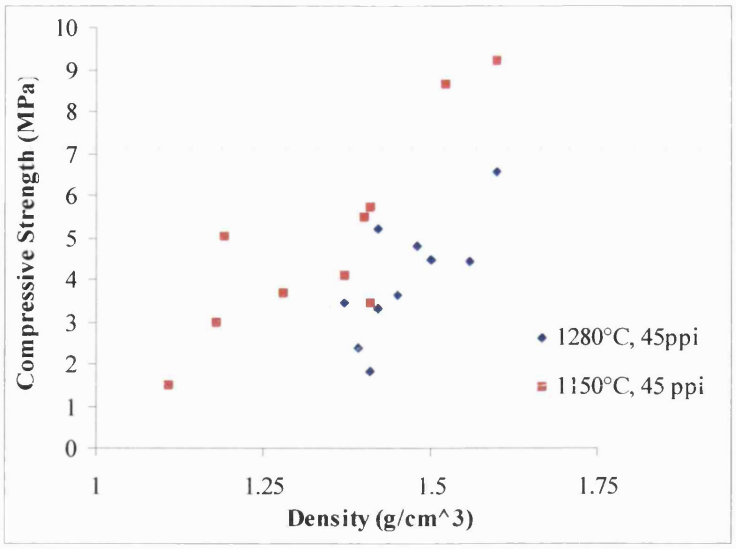

Figure 4.18 (a): Graph indicating strength-density relationship in 45 ppi samples

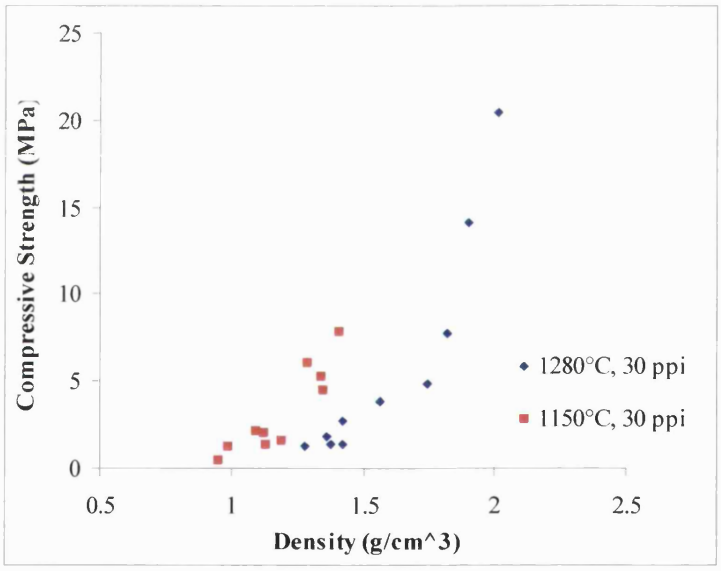

Figure 4.18 (b): Graph indicating strength-density relationship in 30 ppi samples

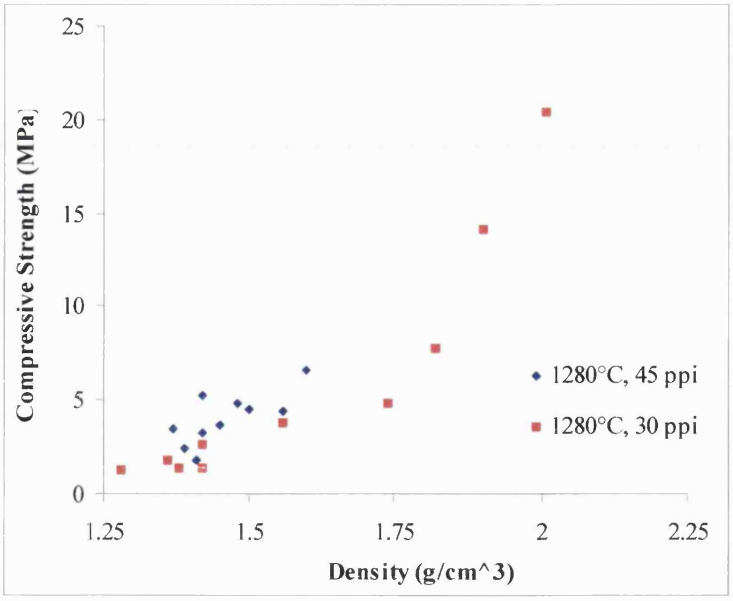

Figure 4.18 (c): Graph indicating strength-density relationship in samples sintered at 1280°C

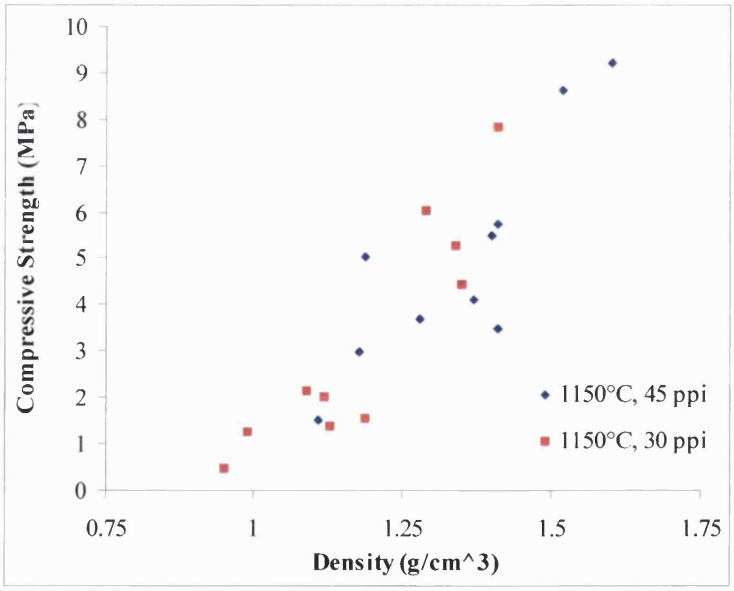

Figure 4.18 (d): Graph indicating strength-density relationship in samples sintered at 1150°C

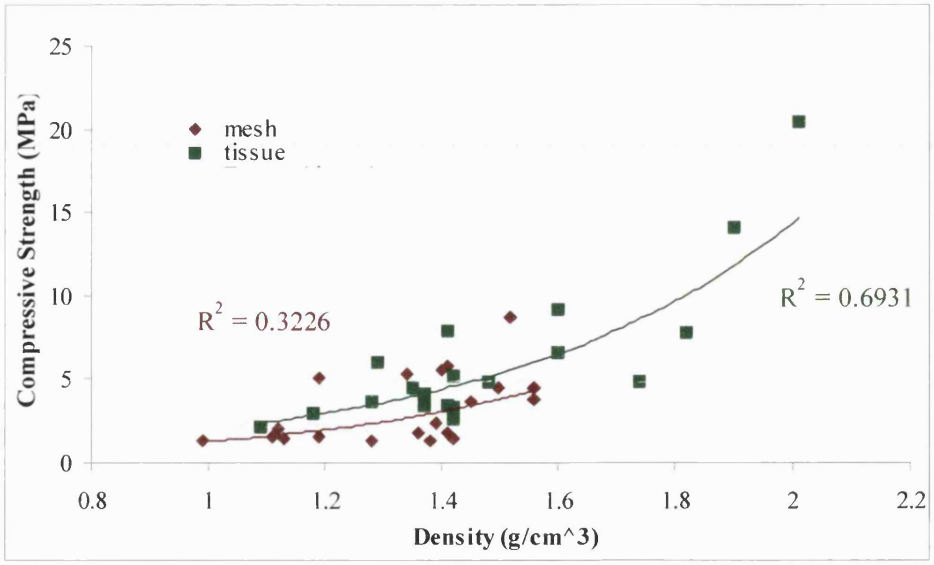

Figure 4.18 (e): Graph indicating strength-density relationship in samples dried on metal mesh and tissue paper

Figure 4.18 (e) illustrates that drying on tissue has reduced the deviation in the results. A polynomial relationship (as described in section 2.4.5.2) was used in order to evaluate the scatter in the results. Regression analysis revealed that the R – value was double that from the samples dried on mesh, as the counts of closed porosity (from poor drying) were eliminated, therefore reducing porosity and increasing strength. Figure 4.18 (b) also shows that the deviation in the compressive stress for the samples made from 30 ppi foams were lower than for 45 foam samples (i.e. high R – value).

All the samples indicate a strength-density relationship whereby an increase in density results in increased strength. Figure 4.19 illustrates the strength-density relationship of all I.I. bioceramic samples. Regression analysis indicates an R-value of 0.76 over the whole sample range. This suggests that a relatively strong correlation is present, however there is also some deviation in the results due to the drying medium used. The polynomial relationship used for figure 4.18 (e) was also used for figure 4.19.

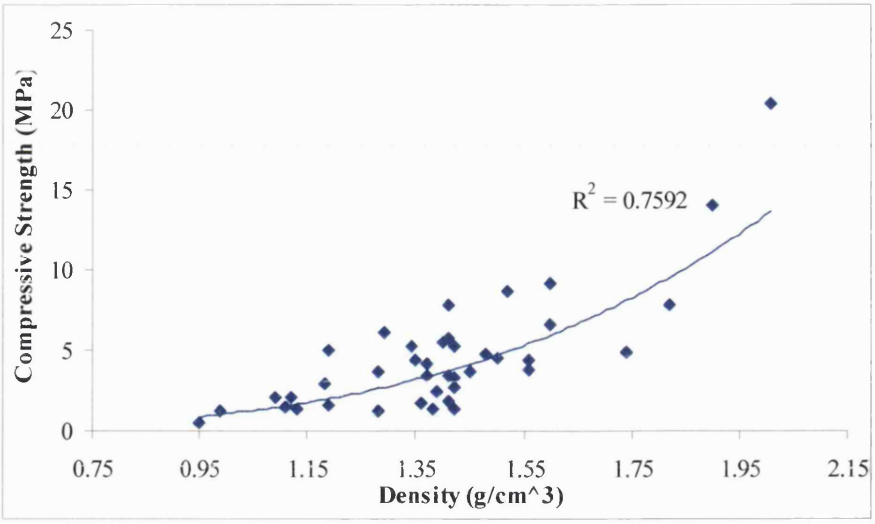

Figure 4.19: Graph indicating strength-density relationship in all I.I. samples

Ceramics inherently have a wide distribution of errors associated with them, mainly due to the nature of internal flaws, their size and distribution, and also due to surface flaws. It has been found that varying the experimental parameters has a profound influence on the structure of the bioceramics and therefore the mechanical properties. The results in table 4.5 have been calculated as 95% confidence levels, indicating that 19 from every 20 samples lie within the range quoted, thus qualifying the results statistically.

An improvement to the experimental method that would reduce the systematic error in the results would be to use rollered platens. Figure 4.20 is a schematic and exaggerated diagram of the situation that occasionally occurred when the surface of the sample was not totally in contact with the platens. This resulted from inaccuracies in the grinding stage of preparing the samples. This could also contribute to some of the large uncertainties and confidence limits measured.

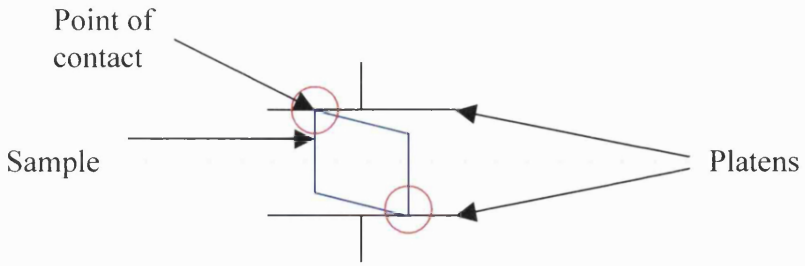

Figure 4.20: Exaggerated schematic of shearing effects that occasionally occurred in samples when prepared samples were not quite parallel

The structural integrity of the samples remained during testing, however, on subsequent handling the samples disintegrated to powder form. It was difficult to measure the modulus of the samples as once they have failed elastically (i.e. the first structural strut) they were deemed out of the elastic region of the material, however the force absorbed by the sample continued to increase until the final remaining material had failed. This is shown graphically below in figure 4.21.

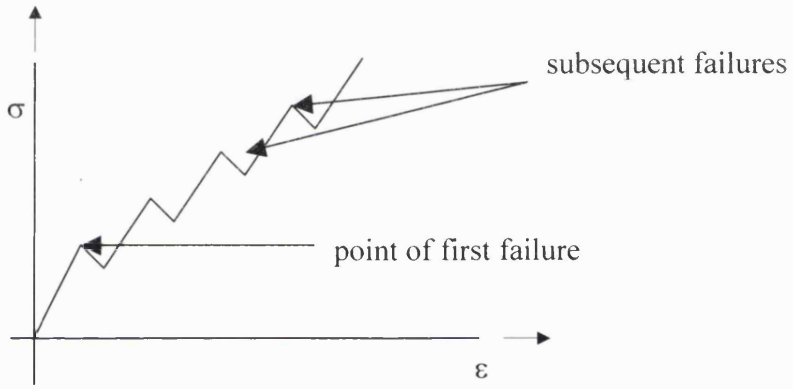

Figure 4.21: Typical load-deformation curve for I.I. bioceramic material

Therefore, the modulus, if measured by the failure of the first structural strut, is not a true reflection of the actual modulus of the sample. For this reason, the modulus of the samples has not been calculated.

Figure 4.22 represents the strength-macroporosity relationship of the samples analysed. As with the strength-density relationship there is a correlation in the results (R - value of 0.80) indicating an increase in porosity results in a decrease in strength.

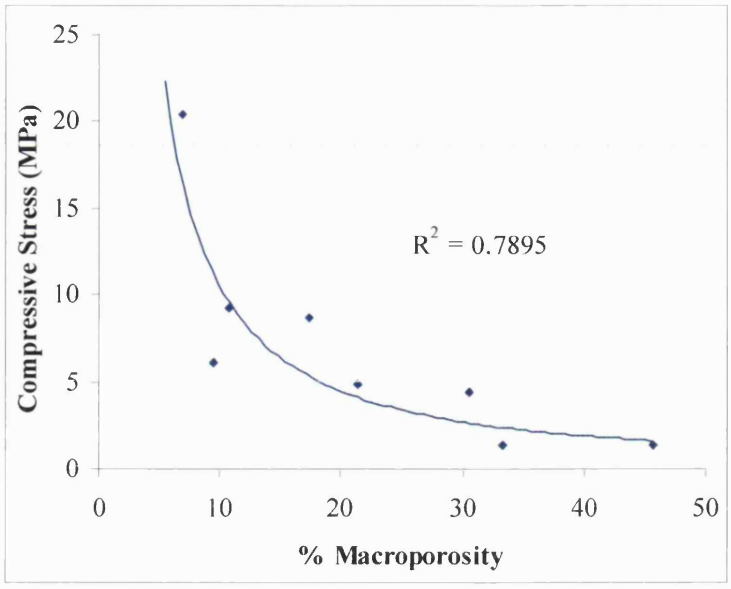

Figure 4.22: Graph indicating the relationship between decreasing porosity, which results in an increase in strength

Figure 4.23 shows the differences in strength in relation to the experimental parameters varied in the research. The 1280°C sintered samples have higher strengths than those sintered at 1150°C, and the type of porosifier used does not affect the compressive strength.

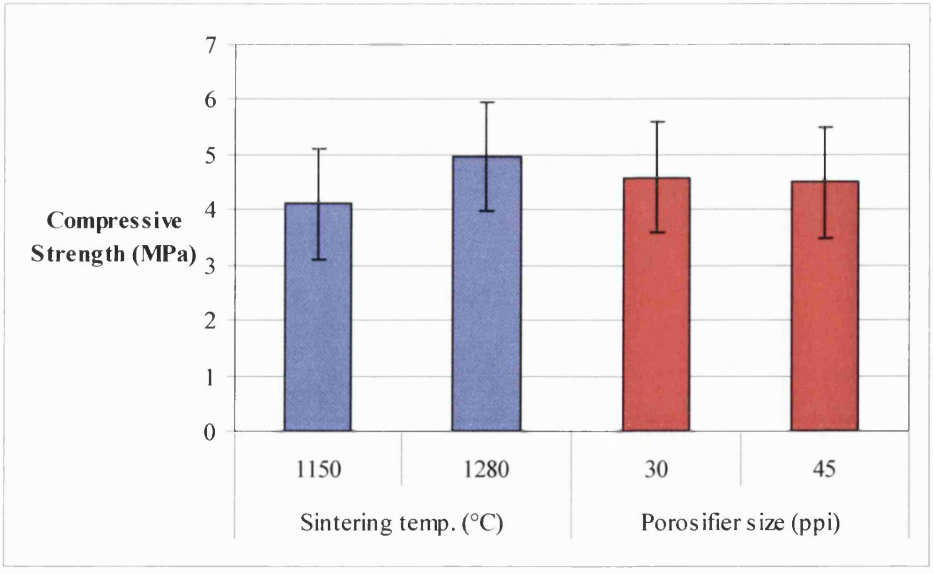

Figure 4.23: Correlation between strength, sintering temperature and the type of porosifier used

4.3.4 Drying Effects on Strength of I.I. Bioceramics

As was shown in section 4.3.1, the drying method used (either metal mesh or tissue paper) had a pronounced effect on macroporosity, and therefore on strength. This is shown in figure 4.24. Both sets of samples sintered at 1280°C and 1150°C have increased strength as a result of drying on tissue.

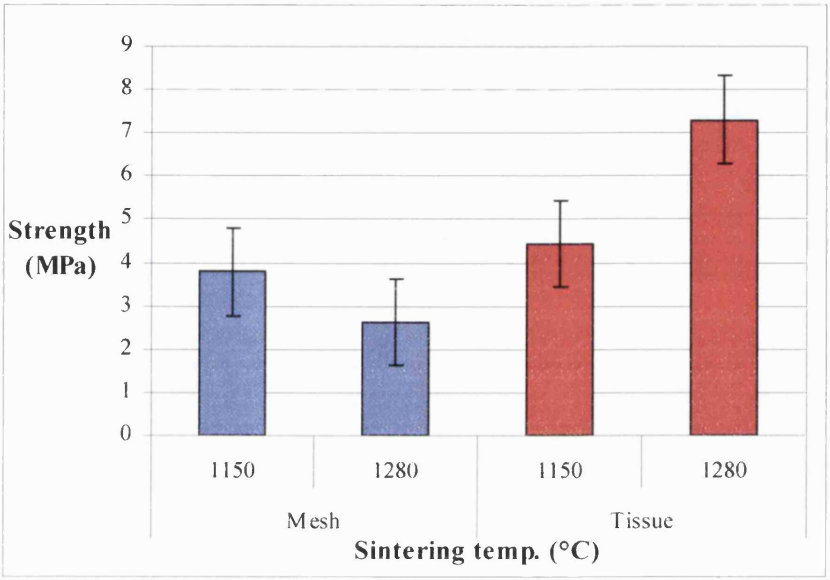

Figure 4.24: Effect of drying on the compressive strength of the I.I. samples

Drying on tissue extracts excess moisture from the samples, and hence there were fewer counts of closed porosity in the samples. As was shown in figure 4.22, a reduction in porosity results in an increase in strength.

4.3.5 Summary of I.I. Bioceramic Results

Fabrication

An interconnected macroporosity network has been fabricated by the impregnation of HA/TCP slips into reticulated PU foams, and the subsequent burnout of PU foam on sintering. This method gives the negative image of the foam in the form of a macropore network in the bioceramic (bow tie shaped pores resulting from the burnout of the PU foam).

Effect of Drying on Macroporosity Network

Drying on tissue extracts a greater volume of moisture from the samples when compared with drying on a metal mesh. Samples dried on metal mesh have a greater number of closed pores that disrupt the interconnected porosity, hence increasing porosity and reducing strength.

The larger sized pore channels in 30 ppi samples allow excess moisture to be extracted easier than in the 45 ppi samples that have smaller pore channels. It is easier to impregnate the 30 ppi foam samples than 45 ppi, as the pore channels are larger. However, there is also a greater possibility for the slip to "slump" out of the foam and leave closed pores that are not representative of the ideal structure (i.e. interconnected bow tie shapes pores from foam burnout). Poor impregnation in some samples leads to an increase in closed porosity resulting in a weaker structure by disrupting the interconnectivity of the porosity in the samples.

The macroporosity in the I.I. bioceramics is dependent on the type of porosifier used and the drying mechanism employed. The macroporosity is independent of the sintering temperature. In addition, the size and shape of the macroporosity was potentially not ideal for bone remodelling purposes, due to the fact that the pores were wider at their edges than at their centres.

Effect of Sintering Temperature and Composition on Microporosity

The microporosity is dependent on the sintering temperature and independent of porosifier type and drying medium. The microporosity network is greater in both size and total volume in those samples sintered at 1150°C than 1280°C, and there was evidence to suggest the formation of a vitreous, glassy structure in 1280°C samples as the micropores are well defined and are clearer

than in 1150°C sintered samples. The thermal transformation at 1180°C from β-TCP to α-TCP, results in a well defined, glassy structure in those samples sintered at 1280°C (75% HA, 14% α-TCP, 11% β-TCP) compared to those at 1150°C (61% HA, 35% β-TCP, 4% α-TCP).

Mechanical Properties

There is a correlation between strength and density in the samples, indicating that an increase in density results in an increase in strength. There is also a strength-porosity relationship, indicating the greater the amount of porosity present, the lower the strength of the bioceramic. The 1280°C sintered bioceramics have greater strengths than those sintered at 1150°C.

Drying has a pronounced effect on mechanical properties. Drying on tissue extracts excess moisture and hence reduces porosity and increases strength. There is a large variation in results due to the fabrication parameters used, e.g. the testing procedure could be improved and hence reduce the uncertainty in the results by using rollered platens on compression testing. This would avoid shearing of samples in some cases where the surfaces of the bioceramic were not ground perfectly flat.

4.3.6 Key Findings

- An interconnected porosity network has been fabricated in HA/TCP bioceramics sintered at 1150°C and 1280°C. The size and shape of the porosity however would require further investigation for potential bone remodelling applications.
- Fabricated I.I. bioceramics have a compressive strength of 4.50 ± 2.86 MPa over a 40 sample size range. The samples possessed a volume macroporosity size range of 7 – 31%, with mean pore sizes ranging from 56 – 152μm.
- The variation in strength was largely due to differences in sintering temperature, drying method and the type of porosifier used, also due to uncertainties in testing procedure.
- The drying method used has been shown to influence the macroporosity distribution and hence has implications with respect to properties such as strength.
- The microporosity was dependent on the sintering temperature used.

Objectives and Aims for Future Research

The following aims and objectives for future research are to be addressed in section 4.4 – Open Porous Scaffold Bioceramics:

- To improve the pore size and shape of the interconnected macroporosity structure, by increasing the total volume macroporosity, pore size and the interconnectivity of the porosity.
- To improve reliability of the bioceramics in both fabrication and testing procedure.
- The ultimate aim of the research is to develop a bioceramic material with an interconnected porosity network, in the correct size range for possible bone remodelling, combined with suitable mechanical properties for load bearing applications.

4.4 Open Porous Scaffold (OPS) Bioceramics

The objectives and aims for future research, detailed at the end of the I.I. results (section 4.3.6), are to be addressed in this section. The focus of research and the aim of the OPS fabrication, was to produce HA/TCP bioceramics with guaranteed interconnected porosity and a total volume porosity, pore size and pore shape in the correct size range for bone remodelling, and in doing so, fabricating a material suitable for bone substitute applications. It was also an objective to produce OPS bioceramics with a structure resembling the orientated nature of cancellous bone (section 3.8.2.1). Figures 4.25 (a) and (b) demonstrate the OPS bioceramics produced by the method described in section 3.8.2.

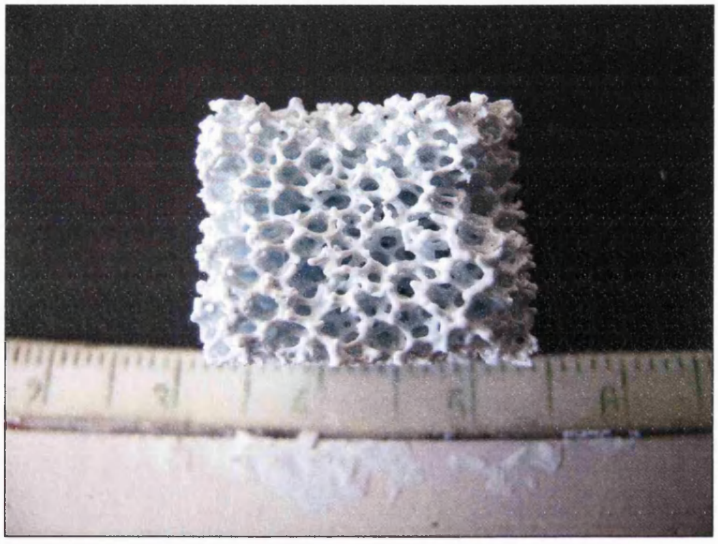

Figure 4.25 (a): 75%HA, 14%α-TCP, 11%β-TCP OPS bioceramic – 30 ppi

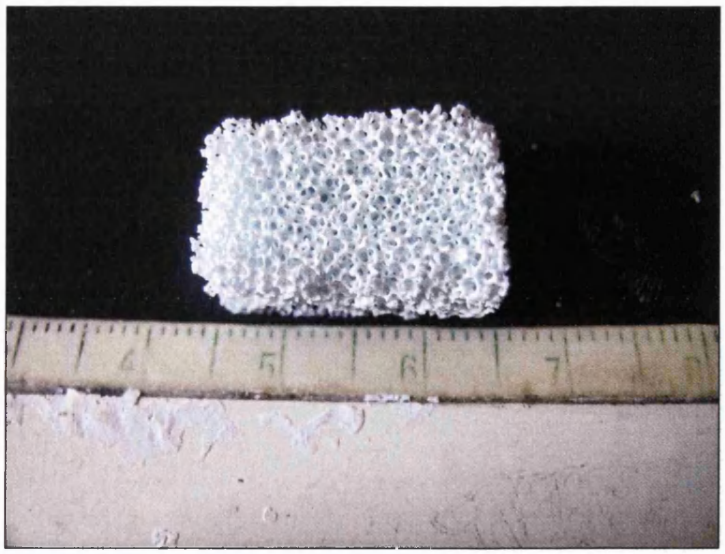

Figure 4.25 (b): 75%HA, 14%α-TCP, 11%β-TCP OPS bioceramic – 45 ppi

For the fabrication of OPS bioceramics, three variables were used in order to ascertain differences in the macroporosity distribution and the resultant effect on mechanical properties (section 4.4.3). The alterations to the macroporosity distribution include changes to the total volume porosity, the mean pore size and standard deviation of the pore size. The three experimental variables include the different foam porosifiers used during fabrication (30 and 45 ppi), the sintering temperature (1150°C and 1280°C) and the shape of porosity due to an elongation procedure detailed in section 3.8.2.1. The porosity shape is stated as normal (N), longitudinal (L) or transverse (T). The mechanical properties will be correlated to the structural findings of the OPS bioceramics. Table 4.6 shows how the variables were used in the experimental procedure.

	Porosifier Foam Type (ppi)	Elongation Procedure	Sintering temperature (°C)
Batch 1	30	N	1280
Batch 2	30	L	1150
Batch 3	30	T	1280
Batch 4	30	N	1150
Batch 5	30	L	1280
Batch 6	30	T	1150
Batch 7	45	N	1280
Batch 8	45	L	1150
Batch 9	45	T	1280
Batch 10	45	N	1150
Batch 11	45	L	1280
Batch 12	45	T	1150

Table 4.6: The batches of samples fabricated from the OPS procedure

In total, 120 samples were fabricated with 60 samples fabricated from 30 ppi foam and 60 from 45 ppi porosifier foams. The samples fabricated from the two different porosifier foams were subjected to an elongation procedure, as described in section 3.8.2.1, to produce orientated structures, labelled L and T on table 4.6. The L and T suffix relates to the formation of

longitudinal (L) and transverse (T) shaped porosity as opposed to the pores in untreated foams that are spherical i.e. N – normal. Half of these unorientated (N) and orientated samples (L and T) were sintered at 1150°C and the other half at 1280°C. Therefore; there were 12 different batches of material with 10 samples per batch totalling 120 samples.

4.4.1 Image Analysis – Macroporosity

The following results show the macroporosity measured in the OPS samples and include examples of the micrographs from SEM analysis and the macroporosity distributions from the OPS fabrication method.

The SEM micrographs also illustrate the structural differences in the samples due to the orientation procedure described in section 3.8.2.1. Sections of the samples from each batch were used to evaluate the macroporosity distribution. The entire surface area of a sample representative of the batch was analysed from four SEM images to assess the macroporosity distribution.

Tables 4.7 (a) and (b) show comparative compositions and macroporosity distribution data for OPS samples fabricated from 30 ppi foams and 45 ppi foams respectively.

The total volume porosity of the OPS was found to be within a suitable range for bone ingrowth as discussed in section 2.3.2. The elongation procedure has had the effect of reducing the total volume porosity within each batch of samples. However, the total volume porosity remains suitably sufficient for bone replacement applications from a porosity distribution stand point i.e. volume porosity (%), size and distribution of pores.

It can be stated from comparing the results in tables 4.7 (a) and (b), that the mean pore size is larger in 30 ppi OPS samples than in 45 ppi.

Approximate Composition of Sample (%)			Experiment Parameters		**Total Volume Porosity (%)**	**Maximum Pore Size (μm)**	**95% Confidence Level Mean Pore Size (μm)**
HA	α-TCP	β-TCP	Sintering Temperature (°C)	Elongation Procedure (normal, longitudinal, transverse)			
75	14	11	1280	N	93.0	3509.4	328.9 ± 60.9
61	4	35	1150	N	87.7	3463.6	263.8 ± 66.8
75	14	11	1280	L	85.3	3725.5	214.0 ± 60.7
61	4	35	1150	L	85.7	2414.9	229.7 ± 38.0
75	14	11	1280	T	78.1	3382.7	295.4 ± 70.8
61	4	35	1150	T	82.0	3571.4	249.4 ± 59.2

Table 4.7 (a): Composition and macroporosity data for OPS samples fabricated from 30 ppi foams

Approximate Composition of Sample (%)			Experimental Parameters		**Total Volume Porosity (%)**	**Maximum Pore Size (μm)**	**95% Confidence Level Mean Pore Size (μm)**
HA	α-TCP	β-TCP	Sintering temp. (°C)	Elongation Procedure (normal, longitudinal, transverse)			
75	14	11	1280	N	84.1	1887.6	242.8 ± 62.6
61	4	35	1150	N	80.2	2334.9	241.8 ± 95.7
75	14	11	1280	L	73.6	3701.0	210.0 ± 62.5
61	4	35	1150	L	77.4	2382.8	146.2 ± 59.1
75	14	11	1280	T	83.0	2927.1	220.6 ± 57.5
61	4	35	1150	T	79.3	3444.2	215.7 ± 36.7

Table 4.7 (b): Macroporosity data for OPS samples fabricated from 45 ppi foams

The macro-structure of the OPS samples is determined by the type of porosifier used (30 or 45 ppi), not the sintering temperature or elongation procedure used in order to produce orientation in the porosity. Figure 4.26 shows the volume porosity of the OPS samples.

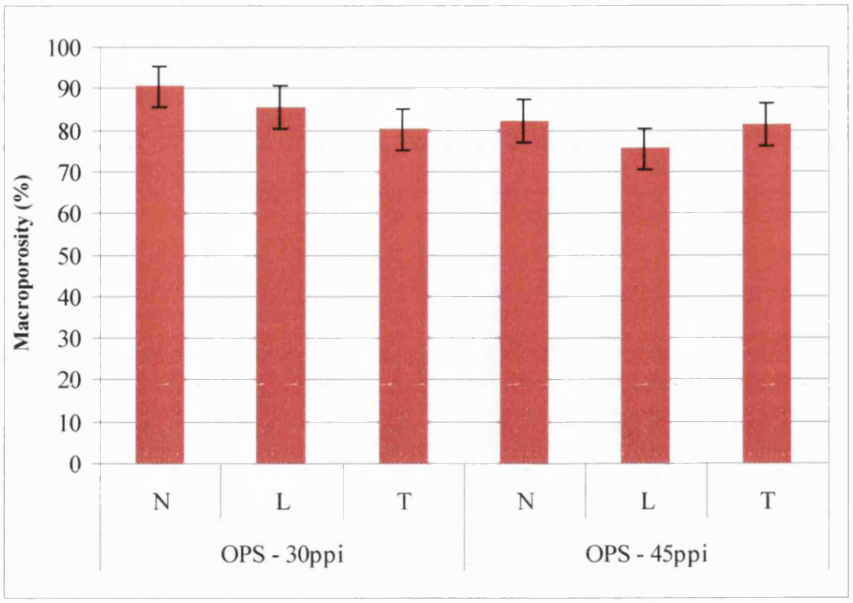

Figure 4.26: Total macroporosity volume (%) of OPS samples

One of the main aims of this section of research was to guarantee the interconnectivity of the porosity in OPS samples. Figures 4.27 (a) to (f) show SEM images of the OPS samples and illustrate both the improved pore shape of the porosity and the degree of interconnectivity of the samples. The orientation in the elongated samples is also illustrated.

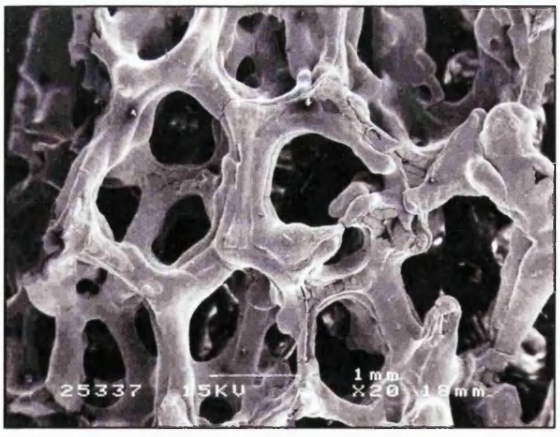

Figure 4.27 (a): OPS 30 ppi N sample

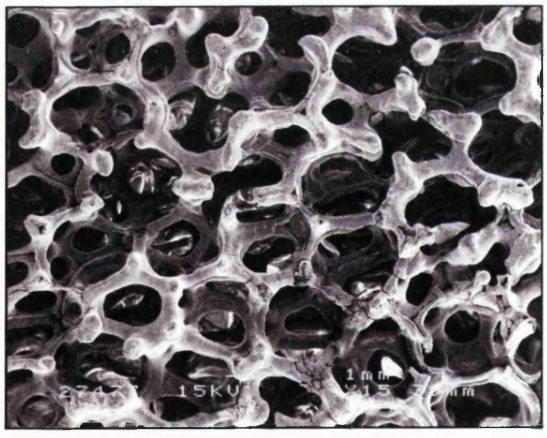

Figure 4.27 (b): OPS 45 ppi N sample

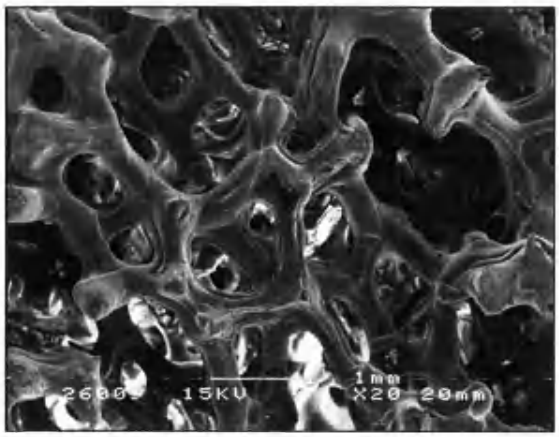

Figure 4.27 (c): OPS 30 ppi L sample

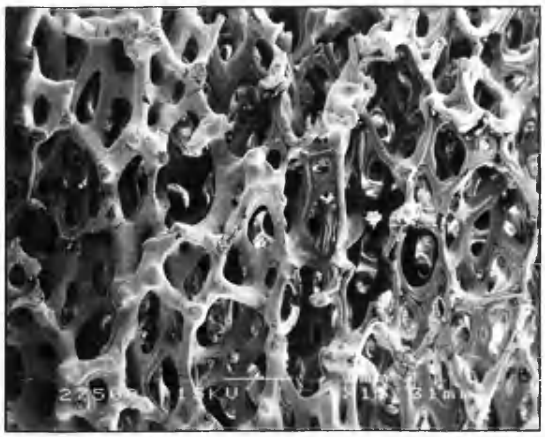

Figure 4.27 (d): OPS 45 ppi L sample

Figure 4.27 (e): OPS 30 ppi T sample

Figure 4.27 (f): OPS 45 ppi T sample

The cumulative pore distribution for the OPS samples, shown in figure 4.28, again clarifies the obvious advantages in pore size for possible bone substitute applications of the OPS samples. It demonstrates a wide porosity distribution with pores ranging in size from 180 – 300μm.

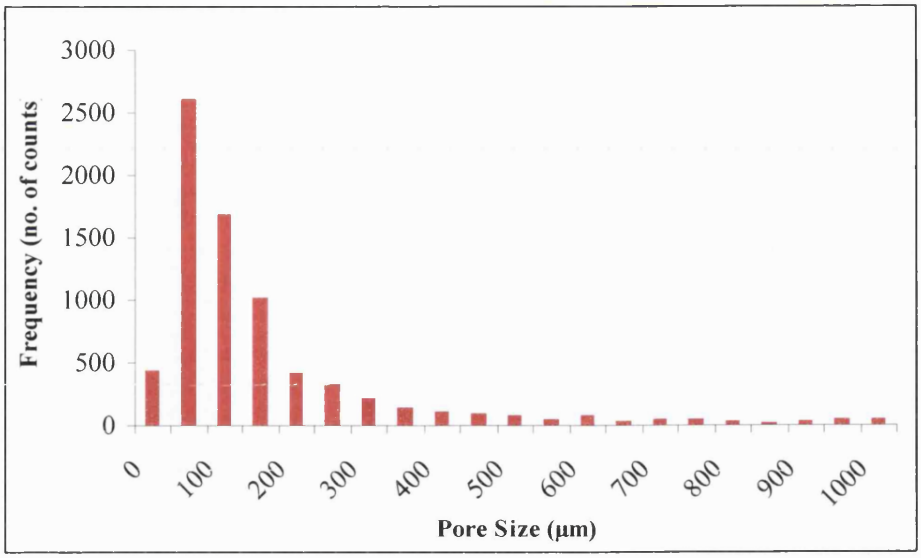

Figure 4.28: Cumulative pore distribution graph for OPS samples

4.4.1.1 Accuracy of Macroporosity Measurement

There were difficulties found with measuring the macroporosity in some OPS samples due to the high volume porosity present and the three dimensional structure. The image analysis software uses colour contrast to measure porosity, so that the struts of the samples appear white and the pores black. In some cases however, struts would overlap with underlying pores varying the amount of porosity that could be measured. In these cases equation 17 was used to evaluate the macroporosity present:

$$\text{Total porosity} = \frac{\text{theoretical density of phase produced} - \text{apparent density}}{\text{theoretical density of phase produced}} \times 100\% \qquad (17)$$

Theoretical density of HA: 3.16g/cm^3
Theoretical density of α-TCP: 3.07g/cm^3
Theoretical density of β-TCP: 2.86g/cm^3 [109]

4.4.2 Image Analysis - Microporosity

As the same base powders were used for the production of I.I. and OPS bioceramics, it was confirmed from OPS microstructural analysis that the sintering temperature had determined the amount of microporosity present (as was found in the I.I samples). Therefore, it is only necessary to show the distribution of microporosity with respect to sintering temperature (1150°C and 1280°C). Microstructural SEM carried out on the same samples used in section 4.4.1. Four SEM images of the microporosity distribution from each sample used for analysis, as the microporosity distribution within the samples was consistent.

Tables 4.8 (a) and (b) show comparative microporosity distribution data between those samples sintered at 1150°C and at 1280°C respectively. It was found that the sintering temperature had the greatest influence on the microporosity distribution of the OPS bioceramics.

Approximate Composition of Sample (%)			Experimental Parameter	**Total Volume Porosity (%)**	**Mean Pore Size (µm)**	**Standard Deviation of Pore Size (µm)**
HA	α-TCP	β-TCP	Porosifier size (ppi)			
61	35	4	30	25.2	1.4	1.1
61	35	4	45	34.4	1.5	1.2

Table 4.8 (a): Microporosity data for OPS samples sintered at 1150°C

Approximate Composition of Sample (%)			Experimental Parameter	**Total Volume Porosity (%)**	**Mean Pore Size (µm)**	**Standard Deviation of Pore Size (µm)**
HA	α-TCP	β-TCP	Porosifier size (ppi)			
75	14	11	30	10.2	0.6	0.7
75	14	11	45	13.6	0.9	0.8

Table 4.8 (b): Microporosity data for OPS samples sintered at 1280°C

It was found that it is the sintering temperature that governs porosity at the microstructural level. The volume of microporosity present in samples sintered at 1150°C and 1280°C was 29.8% and 11.9% respectively. Increasing the sintering temperature to 1280°C from 1150°C reduced the total volume of microporosity of the OPS bioceramics by 60.1%. Figures 4.29 (a) and (b) show SEM images of the microstructures of the OPS bioceramics sintered at 1150°C and 1280°C. The decrease in the amount of microporosity with increasing temperature is illustrated in figure 4.30.

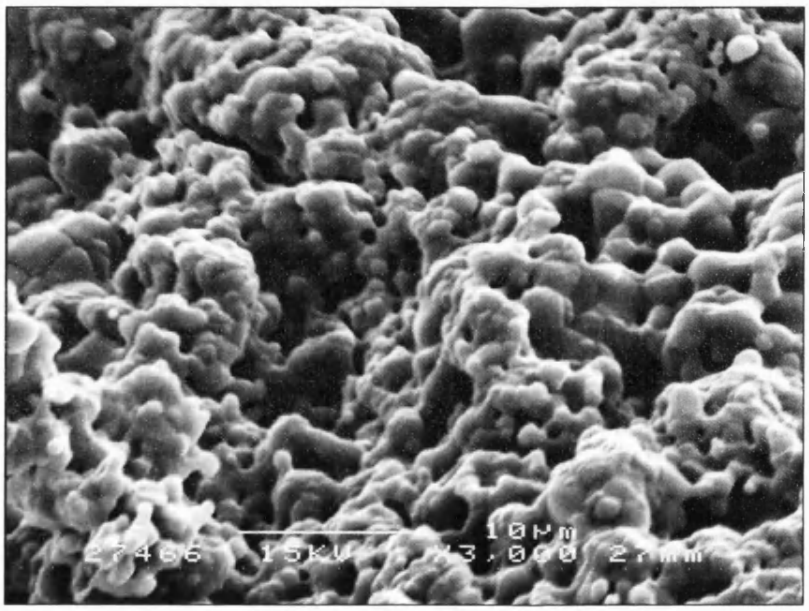

Figure 4.29 (a): Photomicrograph of a 61% HA, 39% TCP OPS sample sintered at 1150°C. Scale bar = 10μm

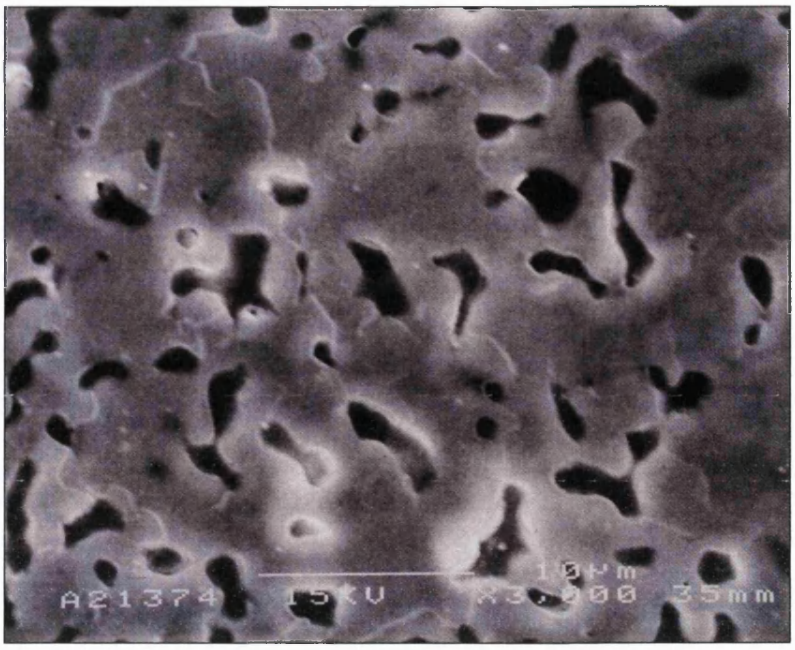

Figure 4.29 (b): Photomicrograph of a 75% HA, 25% TCP OPS sample sintered at 1280°C. Scale bar = 10μm

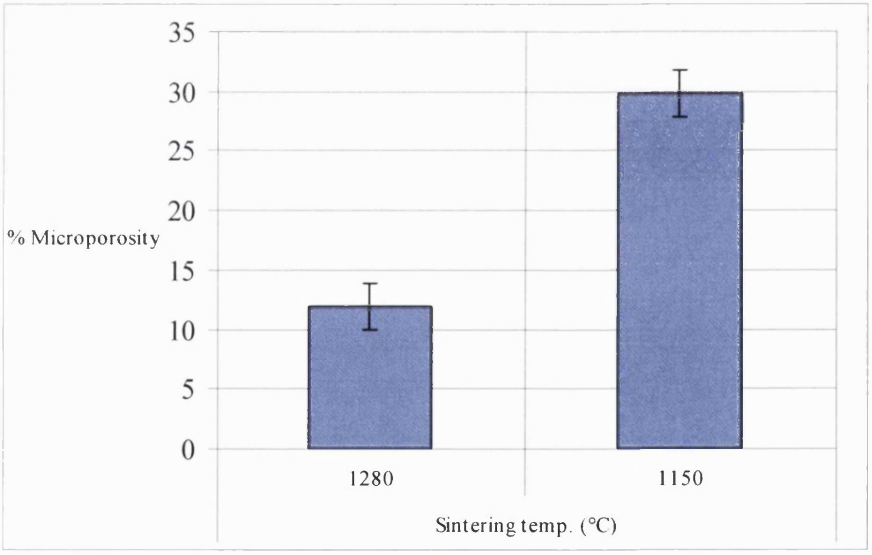

Figure 4.30: Microporosity changes as a function of sintering temperature in OPS samples

As a consequence of the thermal transformation of grade 118 powder to α-TCP at 1180°C (section 4.2), the microporosity of the OPS samples has been reduced. As discussed in section 4.3.2, the β-TCP content in samples sintered at 1150°C produces a granular structure that appears less dense than the microstructure obtained when samples are sintered at 1280°C. At 1280°C, due to microstructural changes driven by grain growth via the elimination of

microporosity, because of the formation of α-TCP, samples have less microporosity than those sintered at 1150°C. The pores at 1280°C are clearly defined, figure 4.29 (b), however at 1150°C, figure 4.29 (a), the pores appeared in the form of a granular structure and lacked clarity. Figure 4.31 shows the cumulative pore distributions of the microporosity distribution at 1150°C and at 1280°C.

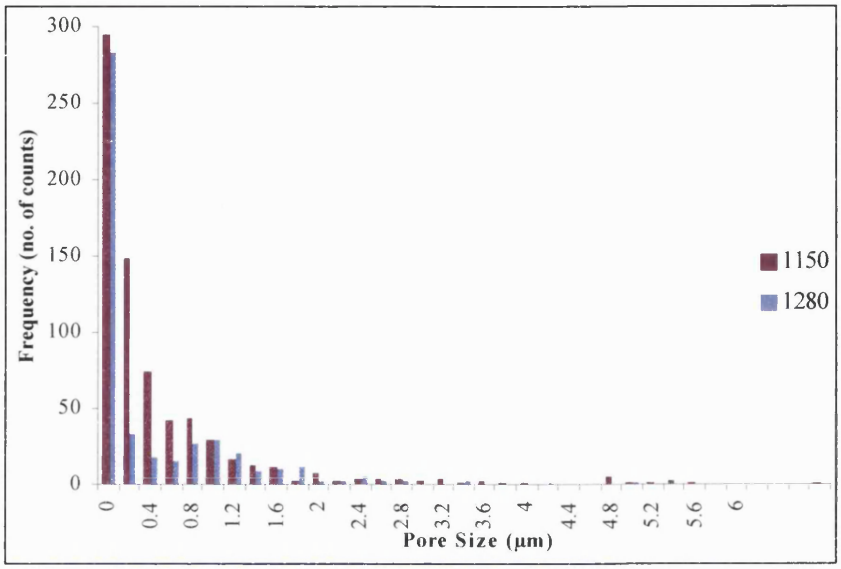

Figure 4.31: Cumulative micropore distribution for all OPS samples analysed by image analysis

The cumulative microporosity distribution of OPS samples are dependent in both pore size and size range on sintering temperature. This was found to be due to the thermal transformation of non-stoichiometric CaP to α-TCP, resulting in microstructural changes decreasing microporosity at higher sintering temperatures.

4.4.2.1 Accuracy of Microporosity Measurement

The granular microstructure due to the lack of formation of α-TCP at 1150°C, offered a difficult surface for image analysis. Colour thresholds used to identify the grain and porosity would not capture the complete microporosity distribution (i.e. the larger microporosity counts). The software was formatted to measure the percent porosity present and individual pore sizes. On some of the 1150°C fired samples, the pores were less defined than in the 1280°C fired samples.

This posed some problems as the software manipulation had to be employed to soften the image so the software could distinguish between the two phases present (grain structure and porosity).

4.4.3 Strength-Density Relationship of OPS Bioceramics

In total, 120 samples had a breaking stress of 0.32MPa ± 0.01MPa at 95% confidence levels. Table 4.9 shows the breaking stresses of all samples tested.

Porosifier type (ppi)	Elongation Procedure	Sintering Temperature (°C)	**Mean Bulk Density (g/cm^3)**	**Standard Deviation of Apparent Density (g/cm^3)**	**Mean 3-Point Bend Strength (MPa)**	**Standard Deviation of Strength (MPa)**
30	N	1150	0.43	0.02	0.34	0.11
30	L	1150	0.37	0.02	0.28	0.06
30	T	1150	0.38	0.04	0.31	0.05
30	N	1280	0.46	0.04	0.37	0.10
30	L	1280	0.41	0.04	0.30	0.06
30	T	1280	0.45	0.04	0.40	0.07
45	N	1150	0.33	0.03	0.20	0.04
45	L	1150	0.31	0.02	0.28	0.04
45	T	1150	0.31	0.02	0.33	0.10
45	N	1280	0.40	0.02	0.33	0.05
45	L	1280	0.38	0.03	0.33	0.06
45	T	1280	0.37	0.03	0.35	0.08

Table 4.9: Summary of mechanical data for OPS bioceramics

Figure 4.32 shows that those samples sintered at 1280°C have higher densities and strengths than those at 1150°C. The strengths reported are low, but there was evidence from 95% C.L. that the fabrication procedure was consistent and reliable.

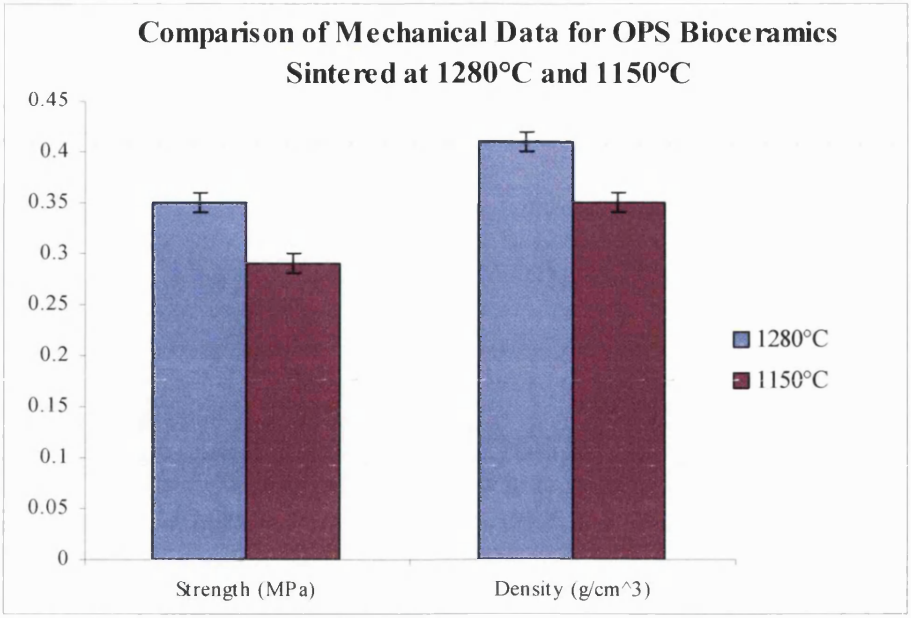

Figure 4.32: Strength-density comparison for OPS bioceramics sintered at 1280°C and 1150°C

In producing an open porous structure with porosity in a suitable size range for bone remodelling, the mechanical property requirements have been compromised and substantially reduced. The OPS samples possess sufficient pore volume, pore size and interconnectivity for possible bone ingrowth, they also have shown limitations due to their low strengths. The mechanical properties of the OPS bioceramics are currently not sufficient for loading purposes in the body.

4.4.4 Surface Flaws Associated with OPS Fabrication

Detailed SEM analysis revealed the presence of surface flaws in the struts of the OPS structures that could be seen to significantly affect the mechanical properties. Figures 4.33 (a) to (d) illustrate these microcracks that on loading collapse and result in low strengths.

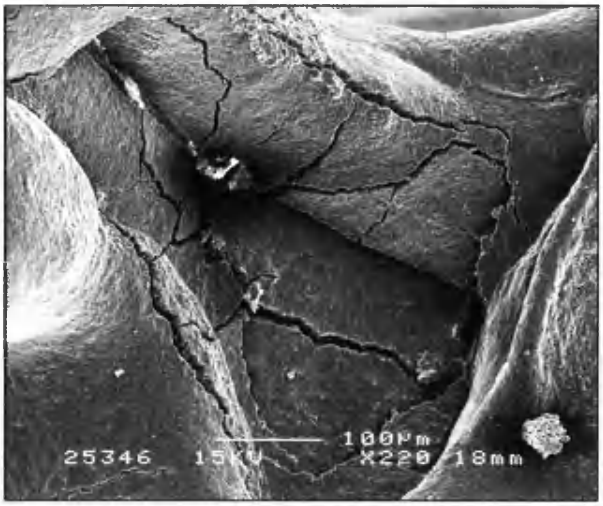

Figure 4.33 (a): Formation of microcracks on surface of OPS – 30ppi N

Figure 4.33 (b): Formation of microcracks on surface of OPS – 45ppi L

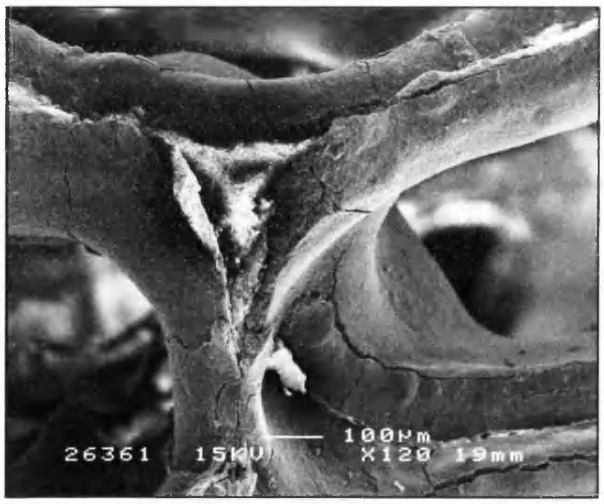

Figure 4.33 (c): Formation of microcracks on surface of OPS – 45ppi T

Figure 4.33 (d): Formation of microcracks on surface of OPS – 30ppi L

The microcracks appear to form primarily at areas where numerous struts converge. These are termed triple point junctions, as usually three struts meet at areas of high PU foam concentration. On heating, the PU foam flows and meets at these triple point junctions, under its own surface energy. Further heating (at ~ 500°C) forces the PU foam to form gaseous products that escape from the ceramic scaffold structure. This creates structural weaknesses, mainly at triple point junctions where there were high concentrations of PU foam, which on further sintering cause surface stresses and formation of microcracks. The high stresses cannot be relieved by viscous flow of the ceramic and hence microcracks form.

On loading, these microcracks grow and converge until the crack length increases, lowering the stress to cause failure and decreasing the overall strength of the bioceramic. This explains why there were no substantial differences in strength between the untreated OPS samples and those subjected to orientation procedures. It was hypothesised that those samples with elliptical shaped pores (instead of spherical pores) would have lower strengths due to the higher stress concentrations at their tips. However, due to the consistent presence in all OPS bioceramics of the aforementioned microcracks, strengths were consistently low throughout the whole range of samples, irrespective of their geometry.

It is these microcracks that must be reduced in size, or even eliminated, in order to improve the mechanical properties of the OPS bioceramics. However, this must be achieved without compromising the interconnected macroporosity structure successfully fabricated for possible bone remodelling purposes.

4.4.5 Summary of OPS Bioceramics Results

Fabrication

An interconnected macroporosity network resembling that of cancellous bone has been successfully fabricated. An orientated structure resembling the directional differences (due to loading) in cancellous bone has also been fabricated. The benefits of producing an open porous structure with pores in a an appropriate size range for bone remodelling (150 – 300μm) has been off-set by the limitations of the material for load bearing capabilities.

Macroporosity Network

The total volume macroporosity in OPS bioceramics was 74-93%. The size and shape of the porosity is more favourable for potential bone ingrowth, with pores that are circular and possess a wide porosity distribution from 177-299μm (95% confidence levels).

Mechanical Properties

Those scaffolds sintered at 1280°C possessed higher strengths than those sintered at 1150°C. It was the formation of microcracks formed on sintering that was the dominating factor predisposing samples to failure. This also explained why the OPS bioceramics had such unpredictable low strengths throughout the sample range. The fabrication procedure was consistent and reliable.

4.4.6 Key Findings

- A high volume interconnected macroporosity network (resembling that of cancellous bone) was successfully fabricated.
- The process offered consistent and reliable results, however the mechanical properties of the OPS bioceramics were not sufficient for load bearing applications.
- The formations of microcracks on sintering at triple point junctions on the interconnected struts, were the reason for the consistent low strengths reported.

Objectives and Aims for Future Research

The following aims and objectives for future research are to be addressed in sections 4.5 and 4.6 – Spinal Fusion Bioceramics and Sol-Gel Treated Spinal Fusion Bioceramics respectively:

- To improve the structure-property relationship of the bioceramics without compromising the successful fabrication of the interconnected porosity network that is needed for any possible bone regeneration.
- To reduce/eliminate the microcracks on the surface of the OPS in order to improve mechanical properties.
- To fabricate bioceramics, utilising the technology developed, for practical and clinical applications.

4.5 Spinal Fusion (SF) Bioceramics

The objective of this section of research was to produce a bioceramic for a specific practical application i.e. for spinal fusion interbody operations, by improving the structure-property relationship of the material. This was achieved by increasing the density of the OPS bioceramics whilst retaining the interconnected macroporosity network successfully fabricated previously for the OPS samples (section 4.4). Figure 4.34 (a) and (b) illustrates scanned images of the SF structures produced.

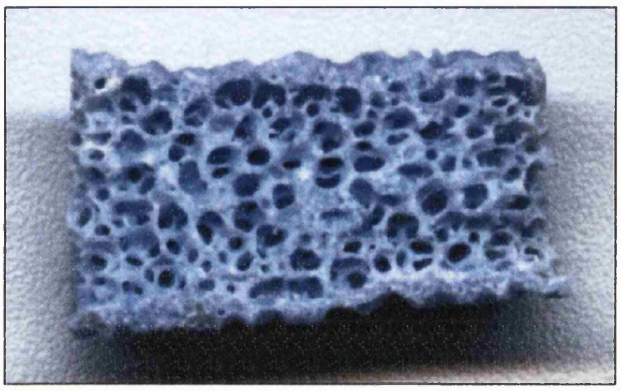

Figure 4.34 (a): Longitudinal section of 91% HA SF sample sintered at 1300°C. Scale 1cm = 2.5mm

Figure 4.34 (b): Cross-sectional view of 83% HA SF sample sintered at 1200°C. Scale 1cm = 2.5mm

4.5.1 Image Analysis - Macroporosity

The method used to fabricating the SF bioceramics consisted of developing an outer dense shell surrounding an internal porosity network – see figures above and section 3.8.3. The internal porosity structure was formed by exactly the same method as for the OPS bioceramics. Therefore, the interconnected macroporosity distribution matched that of the OPS structures formed by using the 45 ppi porosifiers.

The following results show the macroporosity measured in the SF samples and includes examples of the micrographs from SEM analysis and the macroporosity distribution from the SF fabrication method. Sections of the samples from each batch were used to evaluate the macroporosity distribution. The entire surface area of the macroporosity distribution of the sample representative of the batch was analysed from four SEM images.

Table 4.10 shows the composition and comparative macroporosity distribution data between the fabricated SF samples.

Base Powder	HA (%)	α-TCP (%)	β-TCP (%)	Sintering Temperature (°C)	**Total Volume Porosity (%)**	**95% Confidence Level Mean Pore Size (μm)**	**Maximum Pore Size (μm)**
118	6	22	72	1150	81.1	210.6 ± 62.3	2871.5
118	5	39	57	1200	90.2	234.7 ± 55.4	2569.1
118	4	40	56	1250	73.4	223.5 ± 48.9	2110.5
118	5	45	50	1300	84.5	218.8 ± 78.9	2928.6
118	5	46	49	1350	74.8	221.8 ± 88.4	3333.5
130	83	10	7	1200	86.1	219.4 ± 47.1	2858.7
130	86	10	4	1250	75.9	214.2 ± 59.7	2329.6
130	91	6	3	1300	86.4	243.9 ± 92.8	2437.7
130	91	5	4	1350	92.2	236.4 ± 74.6	3046.3

Table 4.10: Composition and macroporosity data for SF samples fabricated from 45 ppi foams

The following SEM micrographs, figures 4.35 (a) - (c), illustrate the macroporosity network of the SF bioceramics. As was illustrated in table 4.10, the total volume porosity and mean pore size lie within the same size range as for the OPS 45 ppi samples, table 4.7 (b), section 4.4.1.

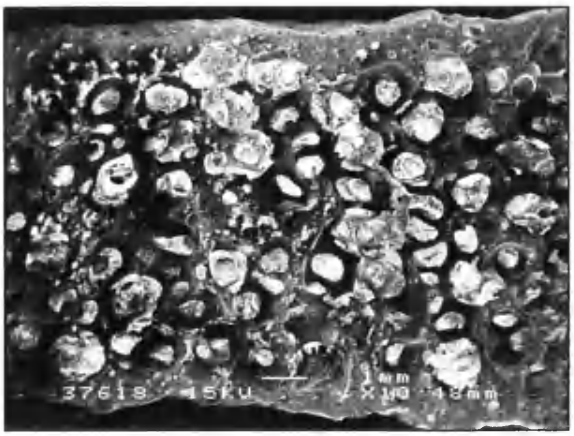

Figure 4.35 (a): 91% HA SF bioceramic sintered at 1300°C

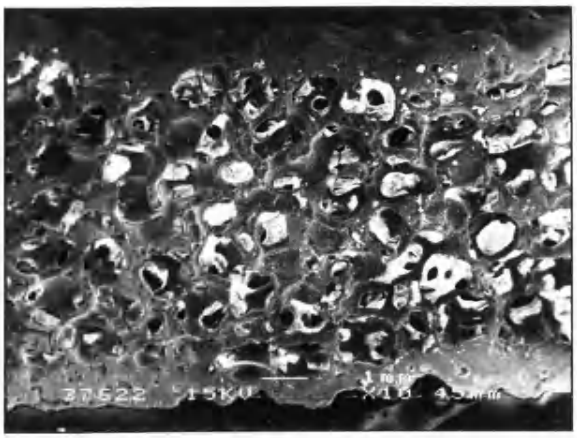

Figure 4.35 (b): 46% α-TCP, 49% β-TCP SF bioceramic

Figure 4.35 (c): 72% β-TCP, 22% α-TCP SF bioceramic

As can be seen from figures 4.35 (a) to (c), the internal macroporosity structure is identical to that for the OPS bioceramics (exact method) as illustrated in section 4.4.1. Figure 4.36 shows the cumulative macropore distribution from image analysis for the SF bioceramics. This is identical to the distribution for those OPS bioceramics fabricated from the 45 ppi foam porosifiers (figure 4.32, section 4.4.1).

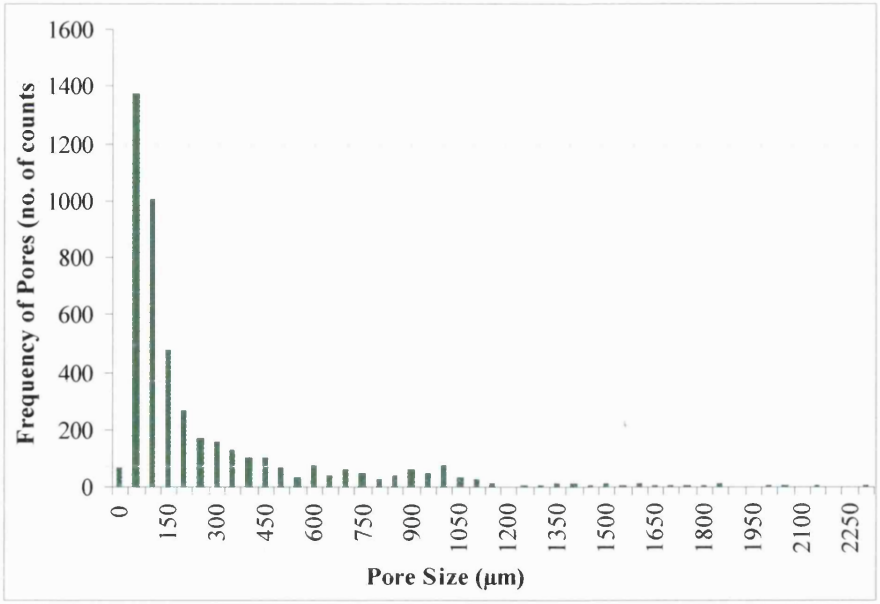

Figure 4.36: Cumulative pore distribution for SF bioceramics

The mean pore size range for the OPS samples was 177 – 299µm and for SF samples was 157 – 292µm, thus the OPS and SF samples offer a suitable structural template for bone substitute applications. There were far greater counts of porosity in an appropriate size range for bone growth (150 – 300µm), therefore producing a hierarchial porosity structure resembling the structure of cancellous bone.

Figures 4.37 shows an SEM micrograph that is representative of the whole batch, illustrating the boundary between the dense outer shell and the internal macroporosity network, indicating that the interior macroporosity network was not compromised.

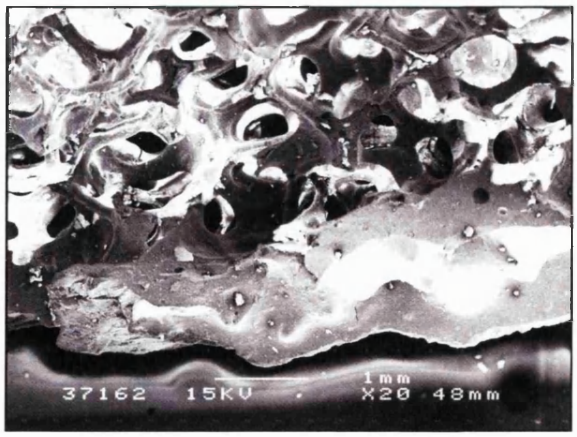

Figure 4.37: 91% HA SF bioceramic

It is important to note that the fabrication of an outer dense shell has not compromised the interconnectivity of the macroporosity network. There is a definite distinction between the dense shell, which offers mechanical support, and the internal interconnected macroporosity network that is needed for bone regeneration.

Macrostructural SEM analysis also suggested evidence of similar microcracks formed on sintering as found in OPS bioceramics. Figures 4.38 (a) and (b) show the effects of foam burnout and the formation of subsequent stresses as surface microcracks on cooling.

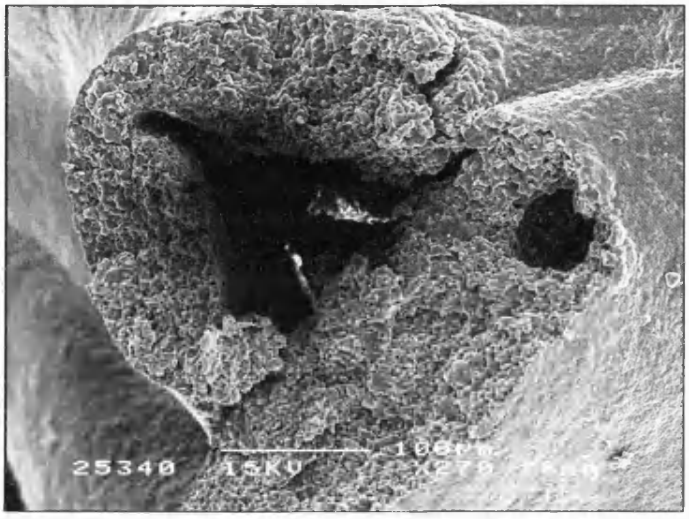

Figure 4.38 (a): Formation of microcracks on surface of 91% HA SF sample

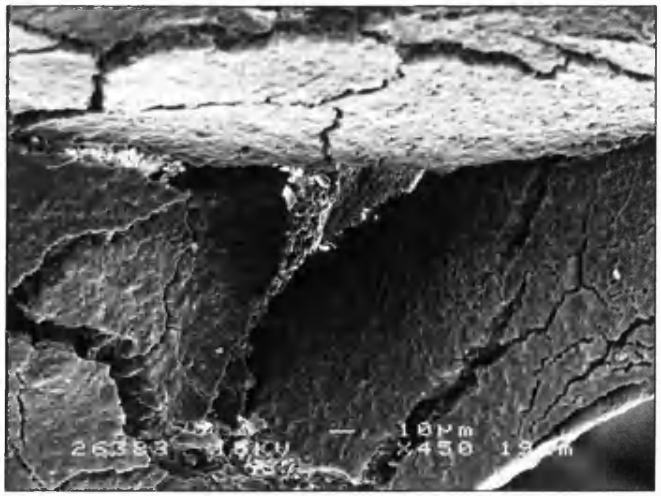

Figure 4.38 (b): Formation of microcracks on surface of 46% α-TCP, 49% β-TCP SF sample

4.5.2 Image Analysis – Microporosity

As the same base powders were used for the production of I.I., OPS and SF bioceramics, it was confirmed that the sintering temperature determined the amount of microporosity present. Therefore, it is only necessary to show the distribution of microporosity with respect to sintering temperature. Microstructural SEM analysis was taken from the same samples used in section 4.5.1. Four SEM images of the microporosity distribution from each sample were taken for analysis, as the microporosity distribution within the samples was consistent.

Table 4.11 shows the composition and comparative microporosity distribution data between the SF samples. It was found that the sintering temperature had the greatest influence on the microporosity distribution of the SF bioceramics.

Base Powder	HA (%)	α-TCP (%)	β-TCP (%)	Sintering Temperature (°C)	**Total Volume Porosity (%)**	**Mean Pore Size (μm)**	**Standard Deviation of Pore Size (μm)**
118	6	22	72	1150	31.2	1.4	1.0
118	5	39	57	1200	19.4	1.0	0.8
118	4	40	56	1250	15.0	1.0	0.7
118	5	45	50	1300	11.5	0.8	0.7
118	5	46	49	1350	3.8	0.4	0.2
130	83	10	7	1200	20.2	1.1	0.7
130	86	10	4	1250	13.8	1.0	0.8
130	91	6	3	1300	10.9	0.9	0.8
130	91	5	4	1350	3.4	0.5	0.3

Table 4.11: Composition and microporosity data for SF samples

As discussed in sections 4.2, 4.3.2 and 4.4.2, the β-TCP content in samples sintered at 1150°C produces a granular structure that appears less dense than the microstructure sintered at temperatures higher than this. At 1180°C, due to microstructural changes driven by grain growth via the elimination of microporosity (because of formation of α-TCP) samples possess less

microporosity than those sintered at 1150°C. These microstructural changes, due to sintering temperature, are shown in figures 4.43 (a) to (e).

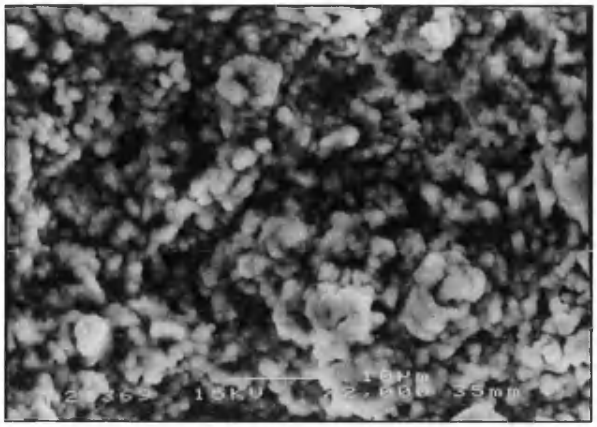

Figure 4.43 (a): SF bioceramic sintered at 1150°C

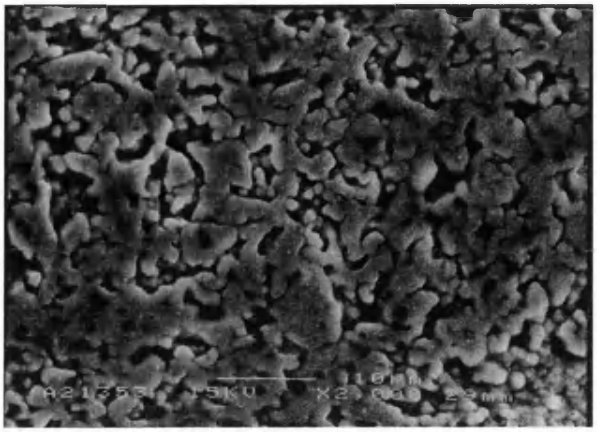

Figure 4.43 (b): SF bioceramic sintered at 1200°C

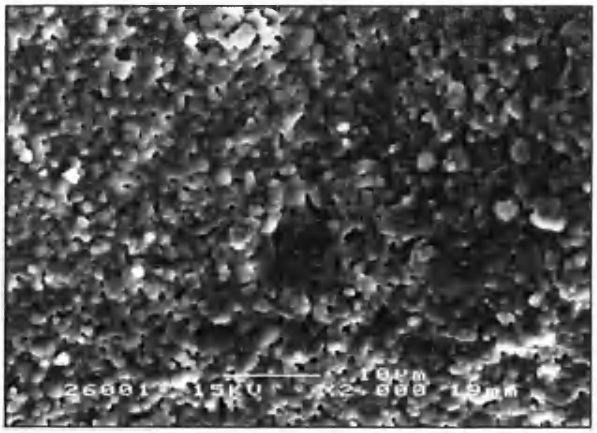

Figure 4.43 (c): SF bioceramic sintered at 1250°C

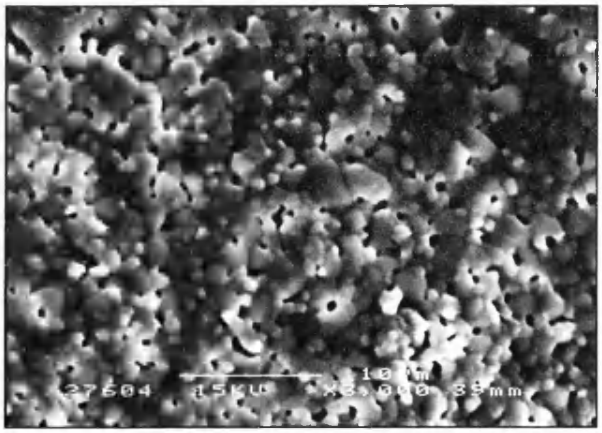

Figure 4.43 (d): SF bioceramic sintered at 1300°C

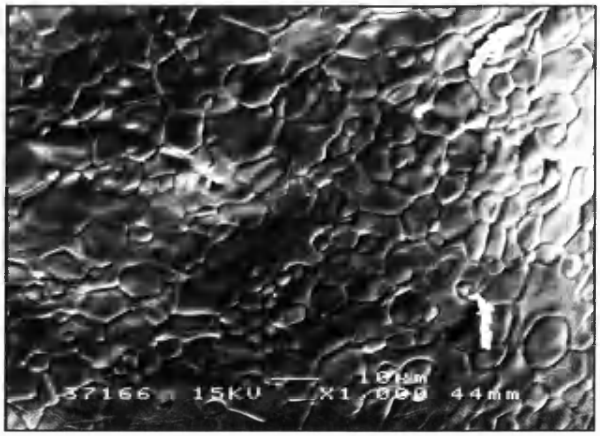

Figure 4.43 (e): SF bioceramic sintered at 1350°C

The decrease in the amount of microporosity with increasing temperature, due to the formation of α-TCP is illustrated in figure 4.44.

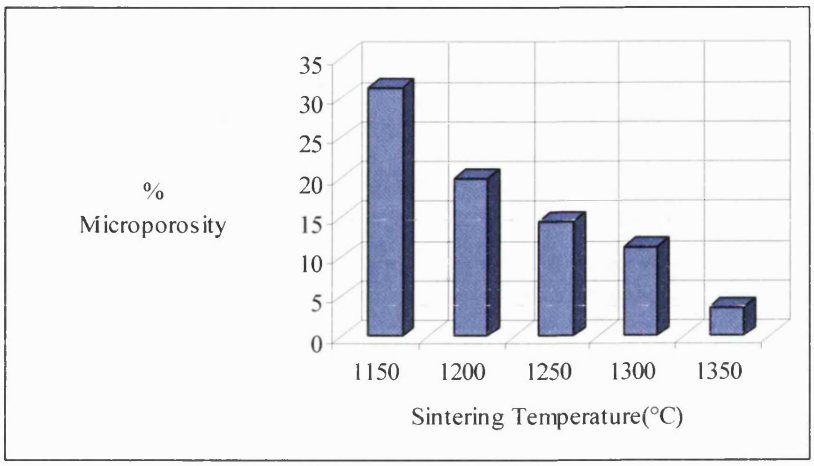

Figure 4.44: Microporosity changes as a function of sintering temperature in OPS samples

Figure 4.45 shows the cumulative pore distributions of the microporosity distribution of the SF samples. The cumulative microporosity distribution in I.I., OPS and SF samples are similar in both pore size and size range, and was found to be dependent on sintering temperature. This was found to be due to the thermal transformation of non-stoichiometric CaP to α-TCP, resulting in microstructural changes decreasing microporosity.

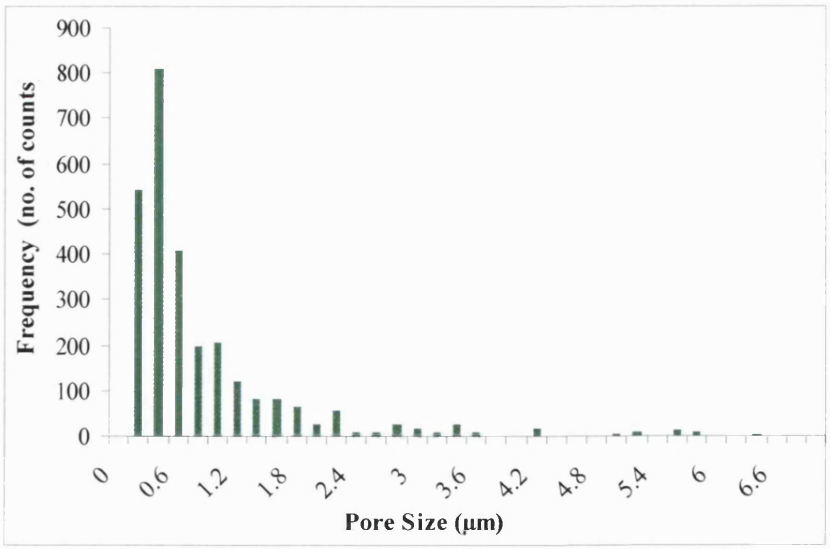

Figure 4.45: Cumulative micropore distribution for all SF samples

4.5.3 Strength-Density Relationship of SF Bioceramics

In total 100 SF bioceramics were compression tested with rollered platens, and found to have a compressive strength of 2.85MPa ± 0.52MPa, with an apparent density of 0.99g/cm^3 ± 0.05g/cm^3. Table 4.12 is an analysis of the mechanical properties of all the samples compression tested, by quoting 95% confidence intervals for the results. This analysis represents the normal distribution for the samples, and states that only 5% of the sample lies outside the range quoted. Table 4.13 shows a summary of the mechanical properties of the three phases produced (HA, α-TCP, β-TCP) from the base powders.

	Bulk Density (g/cm^3) (95% Confidence Level)		Compressive Strength (MPa) (95% Confidence Level)	
Sintering Temperature (°C)	HA	α-TCP	HA	α-TCP
1200	0.96 ± 0.06	0.92 ± 0.04	2.89 ± 0.16	2.54 ± 0.63
1250	1.00 ± 0.05	1.00 ± 0.04	2.96 ± 0.33	2.63 ± 0.53
1300	1.06 ± 0.04	1.04 ± 0.05	3.81 ± 0.80	2.68 ± 0.54
1350	1.08 ± 0.07	1.06 ± 0.04	4.33 ± 0.98	3.29 ± 0.93

Table 4.12: Mechanical data for HA and α-TCP SF bioceramics sintered at 1200°C, 1250°C, 1300°C and 1350°C

Phase	Bulk Density (g/cm^3) (95% Confidence Level)	Compressive Strength (MPa) (95% Confidence Level)
HA	1.03 ± 0.06	3.50 ± 0.57
α-TCP	0.99 ± 0.05	2.73 ± 0.60
β-TCP	0.94 ± 0.05	2.31 ± 0.39

Table 4.13: Summary of mechanical data for SF bioceramics

Figure 4.46 graphically illustrates the compressive strength of each batch of bioceramics produced by the SF method.

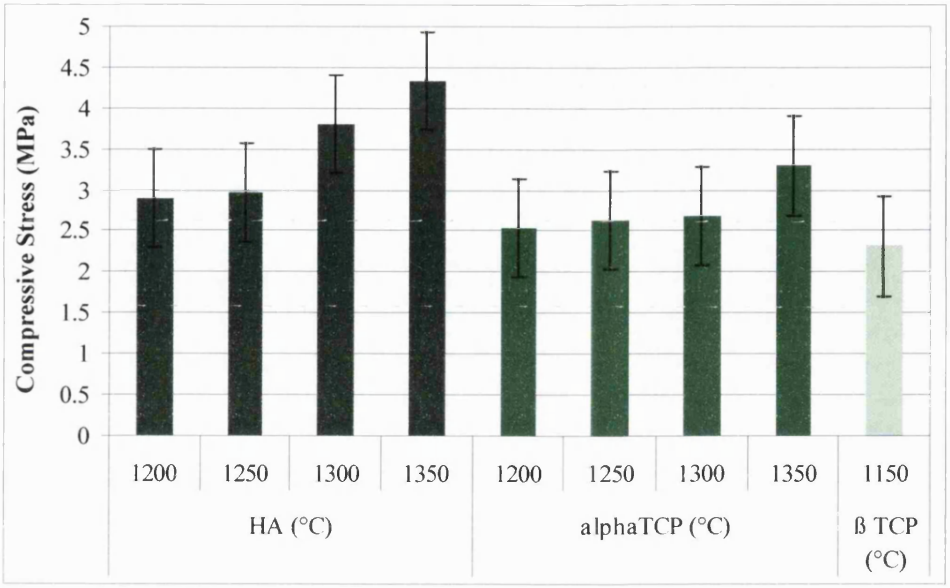

Figure 4.46: Mechanical properties of each batch of SF bioceramic

Figures 4.47 (a) and (b) represent the strength-density and strength-porosity relationships respectively of the SF bioceramics compared to the OPS bioceramics.

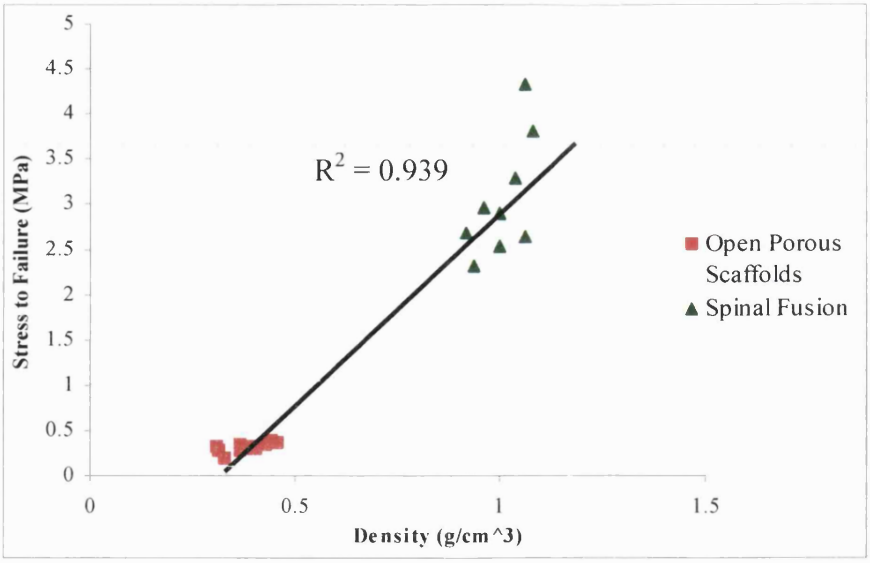

Figure 4.47 (a): Strength-density relationship for OPS and SF samples

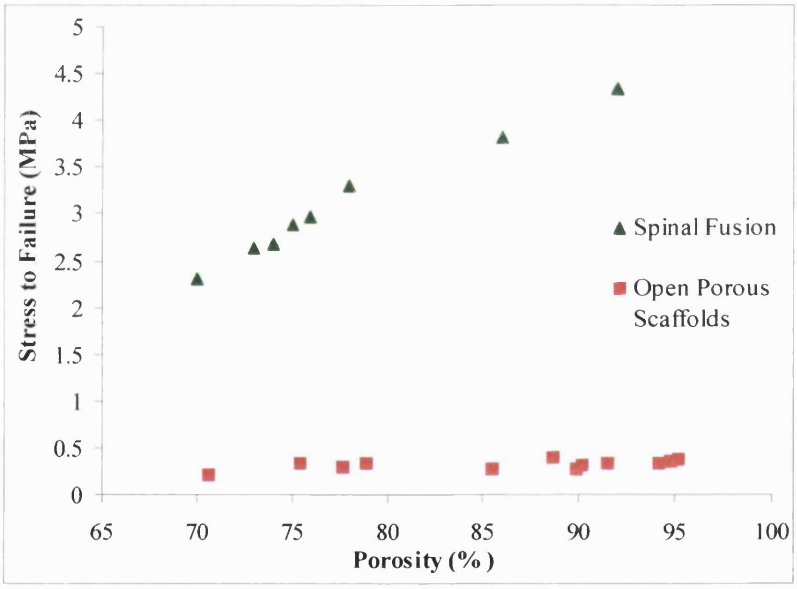

Figure 4.47 (b): Strength-porosity relationship for OPS and SF samples

Figure 4.47 (a) illustrates that the SF bioceramics correlate with strength-density relationships as for OPS samples. Regression analysis on the data gave an R-value of 0.939 indicating a good correlation of the results. Figure 4.47 (b) indicates that the SF method has not compromised the interconnected macroporosity network formed from the OPS process, while increasing the strength of the SF bioceramics.

Figure 4.48 shows the effect of a phenomenon termed stress shielding. Note that the integrity of the internal interconnected porosity structure remains consistent and interconnected, even after failure. It has also been found that failure occurs in the outer dense shell of the SF bioceramics. This is an important phenomenon that would have implications for possible future practical applications, as the interior porosity network needed for bone regeneration was protected and retained its structural integrity on failure.

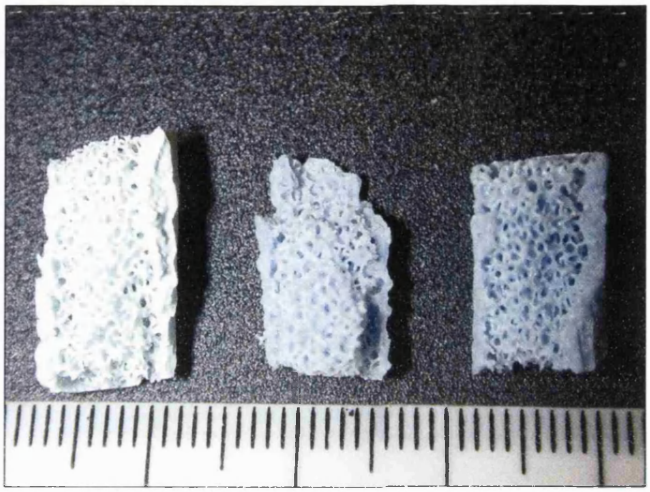

Figure 4.48: Range of failed SF samples after compression testing – left to right: HA 1200°C, HA 1300°C, HA 1350°C

4.5.4 Summary of SF Bioceramics Results

Fabrication

The SF method developed, which produces a dense outer shell surrounding a cylindrical OPS interior, does not compromise the interconnected macroporosity network needed for possible bone regeneration. The SF samples had a distinct boundary between the dense outer shell and the interior porosity network. On stressing, the outer dense shell "protects" the interior macroporosity network by resisting the stress on compression. This was important as the interconnected macroporosity network was retained and remained structurally intact. This phenomenon is termed stress shielding.

Macroporosity Network

The total volume macroporosity of SF samples was identical to those fabricated by the OPS bioceramics prepared with 45 ppi porosifiers, which was 73-92%. Similar macropore sizes were also evident, ranging from 50 – 1000μm, with a mean pore size range from 157 – 292μm.

Mechanical Properties

SF bioceramics had improved mechanical properties in comparison to OPS bioceramics due to an increase in the density of the samples without compromising the interconnected porosity network. Compressive strengths were reported as 2.85MPa ± 0.52MPa with apparent densities of $0.99g/cm^3 \pm 0.05g/cm^3$.

The SF bioceramics show a direct strength-density correlation with the OPS samples previously fabricated, so that an increase in density results in increased strength (figure 4.78). The process offers consistency and reliability in both the fabrication procedure and the testing method. Due to the use of rollered platens much of the systematic error found with the compression testing of the I.I. bioceramics was eliminated. Surface microcracks on the struts, formed on sintering, remain present and it is these together with the microstructure of the dense shell (i.e. microporosity and grain growth evolution) that control strength.

4.5.5 Key Findings

- SF bioceramics for specific, clinical applications have been successfully fabricated (i.e. for spinal fusion interbody operations).
- The SF bioceramics had an identical, internal, interconnected macroporosity network to the OPS bioceramics previously fabricated. This porosity was in the correct size for potential bone regeneration within the bioceramic.
- The strength of the SF bioceramics was improved, compared to the OPS bioceramics with the same porosity (i.e. the porosity network was not compromised during fabrication). However, further improvements to the structure of the samples need to be addressed e.g. surface microcracks.

Objectives for Future Research

The following aims and objectives for future research are to be addressed in sections 4.6 and 4.7 – Sol-Gel treated SF Bioceramics and Calcium Phosphate Granular Material respectively:

- To improve the structure-property relationship of the bioceramics by addressing the issue of surface microcracks created on sintering, and hence ultimately to improve the mechanical properties of the bioceramics. This needs to be achieved without compromising the interconnected macroporosity network.
- To fabricate further bioceramics for clinical applications, such as a granular form of the materials produced, for use in impaction grafting.

4.6 Sol-Gel Treated SF Bioceramics

The objective of this research was to address the issue of surface microcracks that are the cause of structural weakness. By reducing, or eliminating these microcracks, the critical crack lengths that magnify stress on loading are reduced and hence strength increased.

4.6.1 Image Analysis - Macroporosity

The method used in the fabrication of the sol-gel treated SF bioceramics consisted of fabricating SF bioceramics (as in section 4.5), and thermally treating with a sol-gel solution to reduce or eliminate surface microcracks that cause structural weakness on testing. The internal porosity structure was formed by exactly the same method as for the OPS bioceramics. Therefore, the interconnected macroporosity distribution is identical to the OPS structures formed by using the 45 ppi porosifiers.

Figures 4.49 (a) to (c) show images of the SF bioceramics treated with sol-gel solution. HA, α-TCP and β-TCP samples were treated with sodium methoxide solution (detailed in section 3.8.5) and sintered at 500°C and 1100°C.

Figure 4.49 (a): 91% HA SF bioceramics treated with sol-gel. Left to right: untreated, sintered at 500°C, sintered at 1100°C

Figure 4.49 (b): 46% α-TCP SF bioceramics treated with sol-gel. Left to right: untreated, sintered at 500°C, sintered at 1100°C

Figure 4.49 (c): 72% β-TCP SF bioceramics treated with sol-gel. Left to right: untreated, sintered at 500°C, sintered at 1100°C

The following results show the composition and macroporosity measured in the SF samples and includes examples of the micrographs from SEM analysis and the macroporosity distribution from the SF fabrication method. Sections of the samples from each batch were used to evaluate the macroporosity distribution. The entire surface area of the macroporosity distribution of the sample representative of the batch was analysed from four SEM images. Table 4.14 shows the composition and comparative macroporosity distribution data between the fabricated SF samples.

Sintering Temperature of Soda Sol-Gel (°C)	HA (%)	α-TCP (%)	β-TCP (%)	**Total Volume Porosity (%)**	**95% Confidence Level Mean Pore Size (μm)**	**Maximum Pore Size (μm)**
500	91	6	3	89.4	228.8 ± 77.2	2675.5
500	5	46	49	90.2	211.1 ± 88.6	2435.9
500	6	22	72	93.8	220.4 ± 47.5	2198.2
1100	91	6	3	81.2	213.9 ± 54.7	2726.4
1100	5	46	49	75.6	243.3 ± 71.6	3105.3
1100	6	22	72	82.6	234.4 ± 90.3	2967.7

Table 4.14: Composition and macroporosity data for SF samples fabricated from 45 ppi foams

During fabrication, the low viscosity sol-gel solution flows throughout the macroporosity and does not compromise the interconnectivity of the porosity network. Figure 4.50 shows an SEM micrograph, indicative of the batch of sol-gel treated SF bioceramics, demonstrating the macroporosity structure of the samples after soda sol-gel treatment. As was illustrated in table 4.14, the total volume porosity and mean pore size lie within the same size range as for the OPS and SF samples.

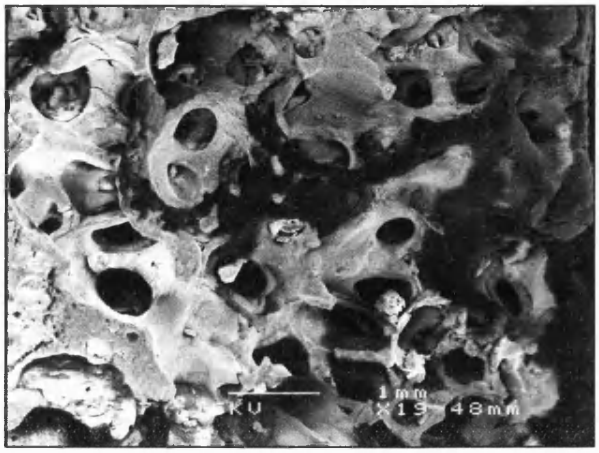

Figure 4.50: 46% α-TCP treated with sol-gel at 500°C

Figure 4.51 shows the cumulative macropore distribution from the SF bioceramics treated with sol-gel solution. Macropores were similar in size range to those found in OPS and SF untreated bioceramics (50-1000μm). The porosity distribution is identical to that for OPS and SF bioceramics fabricated from the 45 ppi foam porosifiers. Therefore, the treatment by sol-gel solution to increase strength by reducing or eliminating surface microcracks, has not compromised the interconnectivity, the pore size or the total volume of the porosity network (table 4.14).

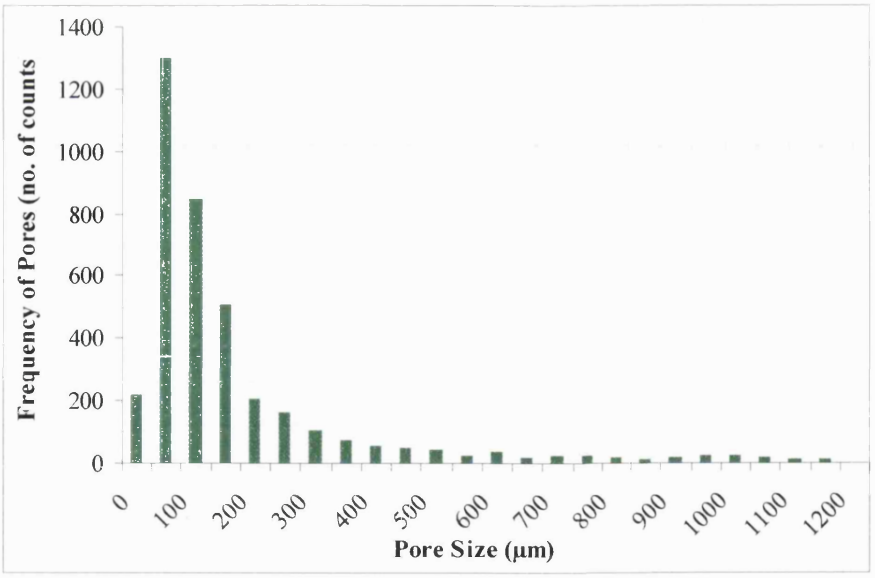

Figure 4.51: Cumulative Pore Distribution for SF samples Treated with Soda sol-gel

Figure 4.52 (a) and (b) demonstrate the improvement in microstructure due to the sol-gel treatment. The figures illustrate structural changes around triple point junctions where surface microcracks would usually be present. In OPS and SF bioceramics, it was these areas that predominantly indicated PU foam burnout and subsequent microcrack formation on further sintering, and hence reduced strength. However, figures 4.52 (a) and (b) illustrate the reduction in size and in some instances the total elimination of the microcracks previously identified as a structural weakness on loading.

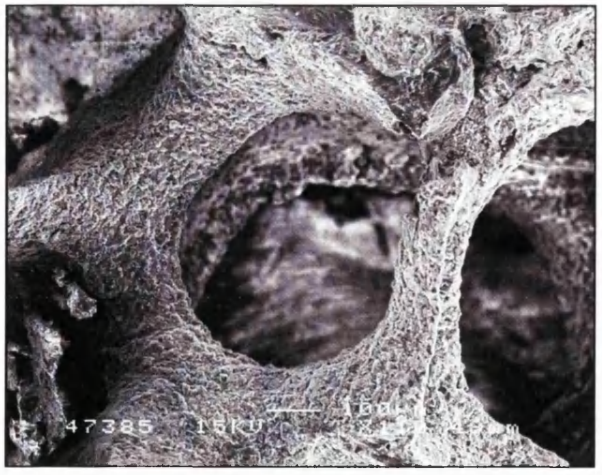

Figure 4.52 (a): Microstructure of a HA treated SF sample at 500°C

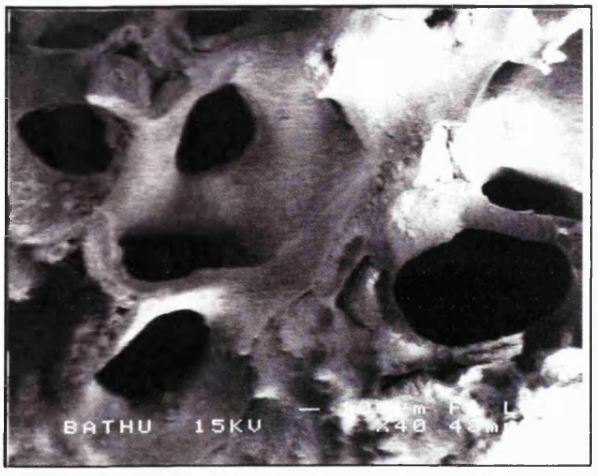

Figure 4.52 (b): Microstructure of a β-TCP treated SF sample at 1100°C

4.6.2 Image Analysis - Microporosity

Microstructural SEM analysis revealed a change in surface structure when compared to SEM micrographs from OPS and SF bioceramics (sections 4.4.2 and 4.5.2 respectively). The structural differences were most notable in TCP, and in particular the high microporosity β-TCP bioceramics. Figures 4.53 (a) and (b) show the microstructural changes caused by the sol-gel treatment.

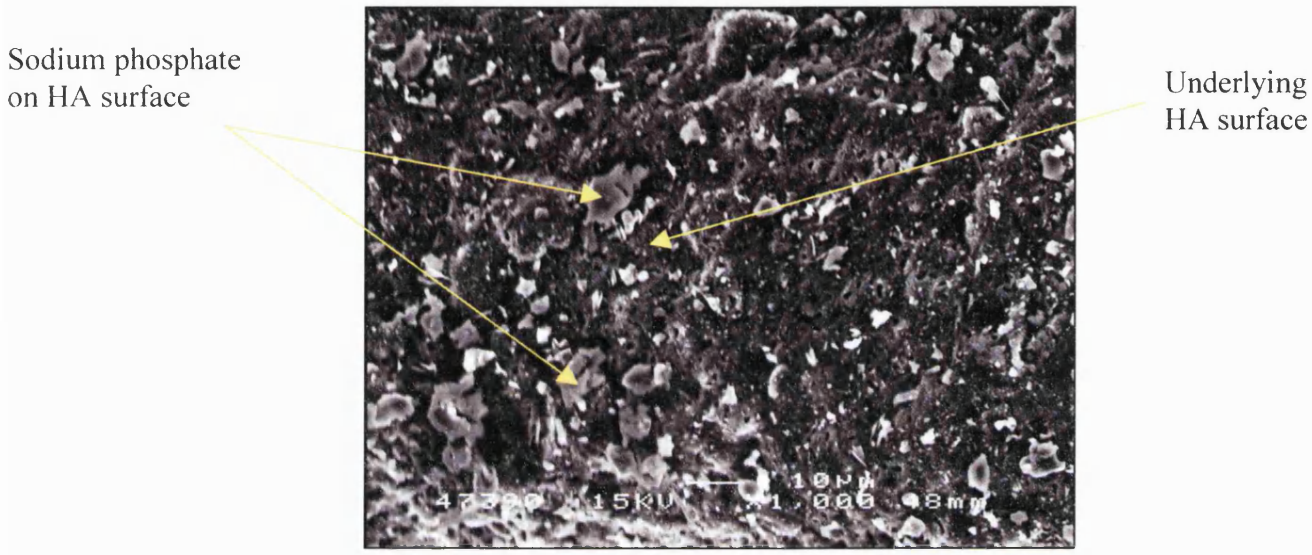

Figure 4.53 (a): Microstructure of HA sol-gel treated and sintered at 500°C

Figure 4.53 (b): Microstructure of β-TCP sol-gel treated and sintered at 1100°C

The sodium phosphate crystals sit on the surface of the HA sample as a second phase, figure 4.53 (a). Analysis of the crystals by EDX during SEM analysis revealed their composition as sodium phosphate. The β-TCP image, figure 4.53 (b), shows that the surface structure has been altered due to the treatment, and therefore the soda sol-gel has been incorporated into the structure. The 1100°C sintered samples had 24.9% less microporosity than those sintered at 500°C, as table 4.15 illustrates. The treatment of sol-gel solutions on the surface of the sintered bioceramics, has produced a polycrystalline surface layer that was more prominent on the high microporosity TCP and in particular the β-TCP structures. A less profound effect was observed for α-TCP samples due to the denser, more crystalline, microstructure.

	Microporosity (%)	
SF phase	**500°C**	**1100°C**
HA	18.8	12.3
α-TCP	21.1	19.5
β-TCP	16.8	10.9

Table 4.15: Microporosity changes due to sol-gel treatment

Figure 4.54 shows the cumulative micropore distribution for the sol-gel treated SF bioceramics. The majority of the microporosity was less than 3μm in size, however some minor incidences of larger microporosity were observed.

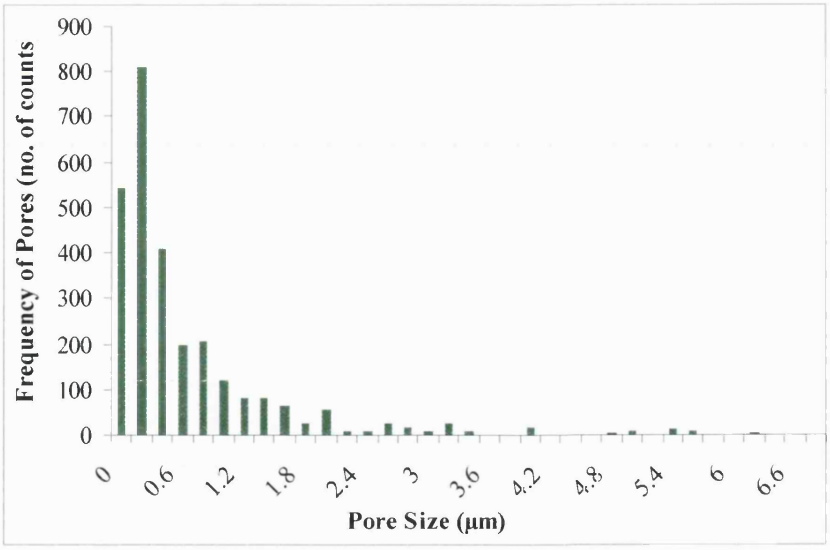

Figure 4.54: Microporosity distribution for sol-gel treated SF bioceramics

4.6.3 Strength-Density Relationship for Sol-Gel Treated SF Bioceramics

In total, 60 SF sol-gel treated bioceramics were compression tested (with rollered platens), and found to have a compressive strength of 5.94MPa ± 1.06MPa, the samples were analysed as a normal distribution. Apparent densities of 1.51g/cm^3 ± 0.22g/cm^3 were found. Table 4.16 shows the mechanical properties of all batches of samples analysed, and the strength increases made when compared to SF bioceramics that were not treated.

SF Bioceramic Treated with Soda Sol-Gel		95% C.L. Bulk Density (g/cm^3)	95% C.L. Compressive Stress (MPa)	Strength increases over original SF bioceramics (%)
500°C	HA	1.71 ± 0.31	6.01 ± 1.54	71.7
	α-TCP	1.28 ± 0.11	4.72 ± 0.83	72.9
	β-TCP	1.14 ± 0.15	4.46 ± 1.09	75.6
1100°C	HA	1.76 ± 0.25	7.50 ± 0.78	114.3
	α-TCP	1.55 ± 0.30	6.28 ± 1.15	130.0
	β-TCP	1.59 ± 0.22	6.69 ± 0.99	163.4

Table 4.16: Mechanical properties and strength increases for SF bioceramics treated with sol-gel against those untreated

The average strength increases for the treated SF bioceramics was 105% greater than those SF bioceramics previously fabricated (section 4.5). However, the greatest strength increases occurred in those coatings sintered at 1100°C, and in particular the β-TCP bioceramics. Figure 4.55 shows the mechanical properties data as a comparison between untreated SF bioceramics and treated SF bioceramics in sol-gel solution.

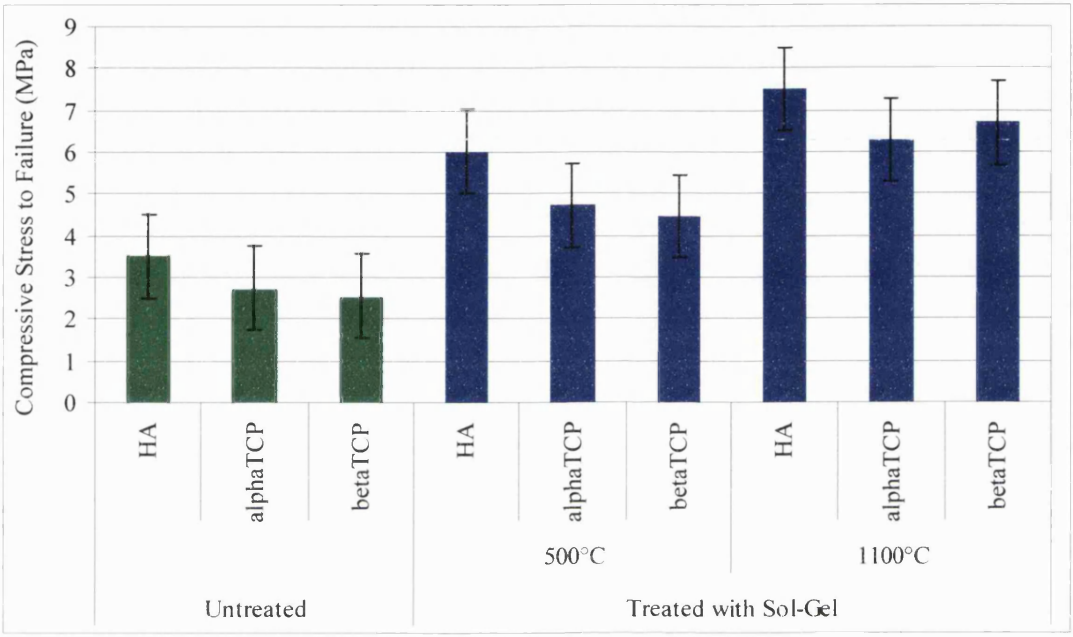

Figure 4.55: Comparison of mechanical property data for untreated and treated SF bioceramics

Strength increases in samples produced by the sol-gel method have been made without compromising the interconnected macroporosity network, as shown in figure 4.56, which shows the strength-porosity relationship of the bioceramics produced. Figure 4.57 shows the strength-density relationship of the bioceramics and demonstrates that the process was consistent with previously fabricated bioceramics. Regression analysis established that the samples possessed an R-value of 0.967, indicating an excellent correlation between strength and density for the OPS, SF and SF treated samples fabricated in this research.

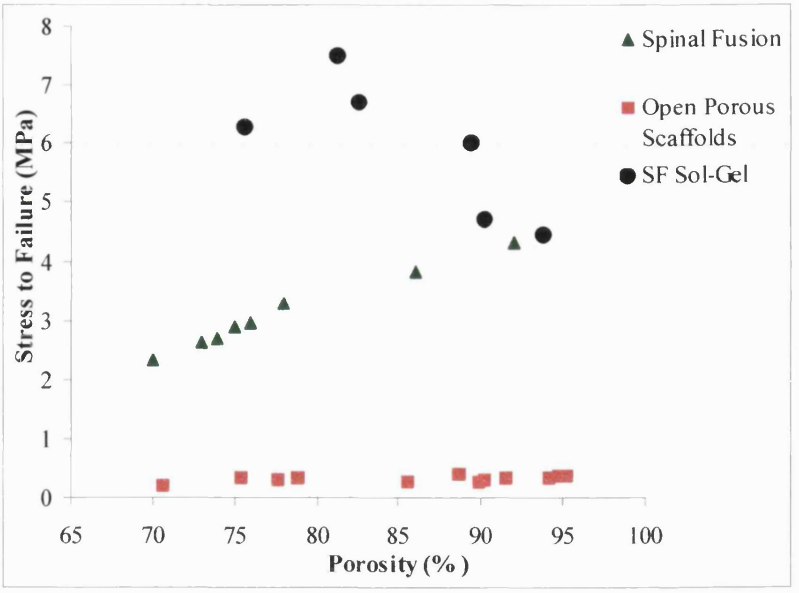

Figure 4.56: Strength-porosity relationship of SF treated bioceramics

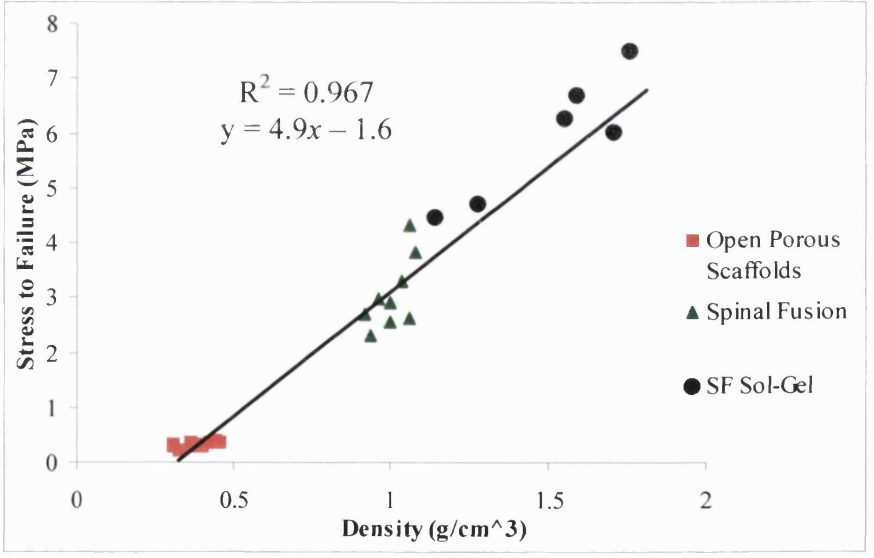

Figure 4.57: Strength-density relationship of SF treated bioceramics

4.6.4 Summary of SF Sol-Gel treated Bioceramics

Fabrication

The sol-gel treatment successfully increased the strength of the SF bioceramics without compromising the interconnected macroporosity network. The soda sol-gel solution changed the colour of the surface of the SF bioceramics on sintering. On failure, the deep interiors of the samples retain the colour of their original phases (e.g. HA – blue, TCP – white). Hence, it can be hence stated that the soda sol-gel only affects the surface of the structure, and therefore primarily addresses the surface microcracks previously identified as sources of weakness.

Structure-Property Relationship

The structure-property relationship of the bioceramics has been improved by reducing in size, and in some instances eliminating completely, the surface microcracks previously identified as the cause for structural weakness. Microstructural analysis revealed the formation of a polycrystalline phase on the TCP samples. The solution was able to adhere to the surface of these high microporosity samples with more success than for HA samples (crystalline surface) and hence reduce or eliminate surface microcracks and increase strength.

Mechanical Properties

Those SF treated bioceramics sintered at 1100°C had an average compressive strength of 6.82MPa, those sintered at 500°C had compressive strength of 5.06MPa. The average compressive strength of all the samples analysed by 95% confidence levels, was 5.94MPa ± 1.06MPa, with a bulk density of 1.51g/cm^3 ± 0.22g/cm^3.

The average strength increase in comparison to untreated SF bioceramics was 105%, with the greatest strength increase of up to 163% for the high microporosity β-TCP samples.

4.6.5 Key Findings

- The sol-gel solution treatment has increased the strength of the SF bioceramics without compromising the interconnected macroporosity network required for possible bone regeneration.
- The strength increases were possible due to improvements made in the structure-property relationship. Low viscosity sol-gel solutions flow into the microcracks previously identified as structural weak points for failure. As a result, the microcracks are reduced in size or even eliminated.
- Microstructural analysis revealed structural changes to the SF bioceramics, revealing a polycrystalline phase on the surface of the SF bioceramics (especially on high microporosity β-TCP samples).

Objectives for Future Research

The following aims and objectives for future research are to be addressed in sections 4.7 and 4.8 – Calcium Phosphate Granular Material and Wicking Properties respectively:

- To fabricate further CaP bioceramics from the methods developed for practical and clinical applications e.g. granular material for possible use in impaction grafting.
- To evaluate the wicking properties of the CaP phases produced (HA, α-TCP and β-TCP), and to identify a possible correlation between microporosity and the wicking properties of the materials.

4.7 CaP Granular Material

CaP granules (varying in size from 2-8mm) were fabricated by using the I.I. method and die-plunger compression tested up to 500N and 1000N respectively as detailed in sections 3.8.4 and 3.12.3. A commercially available product, manufactured by Stryker Orthopaedics termed BoneSave®, was also tested by the same compression test, and the results compared.

4.7.1 Image Analysis of Granular Material

Figures 4.58 (a) to (d) show images of the granular material fabricated. Figure 4.58 (a) illustrates the commercially available product BoneSave®. Figures 4.58 (b) to (d) show the 75% HA, 14% α-TCP and 11% β-TCP granular material fabricated from the I.I. method (sintered at 1300°C), with sizes ranging from 2-4mm, 3-5mm and 4-8mm respectively.

Figure 4.58 (a): Granular BoneSave® material – 2-4mm in size

Figure 4.58 (b): Granular material from I.I. method – 2-4mm in size

Figure 4.58 (c): Granular material from I.I. method – 3-5mm in size

Figure 4.58 (d): Granular material from I.I. method – 4-8mm in size

The granular material fabricated has identical porosity to the block material formed from the I.I. method described in section 4.3. The macroporosity is generated due to the burnout of the polymer PU foam that leaves the negative image of the foam as the interconnected porosity network. The macroporosity in BoneSave® granules is generated due to the burnout of the isolated porosifier, and is not interconnected.

4.7.2 Die-Plunger Compression Tests

The following results were used for comparative purposes only between the HA/TCP granules fabricated and the BoneSave® granules. The compressive moduli calculated were not the true materials properties of the granules. This was due to the fact that the granules on loading would topple and re-order themselves. Table 4.17 represents the relative moduli of the materials tested by die-plunger compression testing. This also explains the sudden drops in stress on the stress-strain curves in figures 4.59 (a) to (d).

Bone Substitute Material Tested	Relative Modulus up to 500N of Loading (GPa)	Relative Modulus from 500 – 1000N of Loading (GPa)
BoneSave®	29.5	45.1
HA/TCP 2 – 4mm	49.6	66.5
HA/TCP 3 – 5mm	40.3	66.4
HA/TCP 4 – 8mm	5.9	35

Table 4.17: Mechanical data (for comparison purposes only) for granular material tested

The low relative modulus reported from the 4-8mm sized granules was due to the large degree of toppling, crushing and re-ordering of the granules on loading. Figure 4.59 (d) shows the constant re-ordering of these larger sized granules by the constant drops in stress on the stress-strain curve. These affects were less pronounced for the smaller sized granules in particular the 2-4mm sized granules, that provide a more consistent and predictable mechanical response relative to the larger diameter granules.

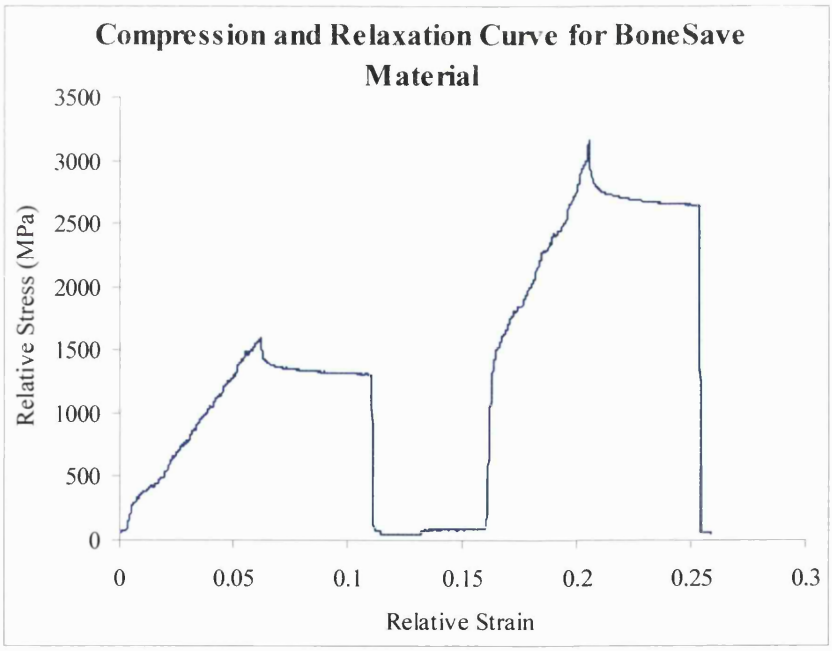

Figure 4.59 (a): Stress-strain curve for BoneSave® material – 2-4mm in size

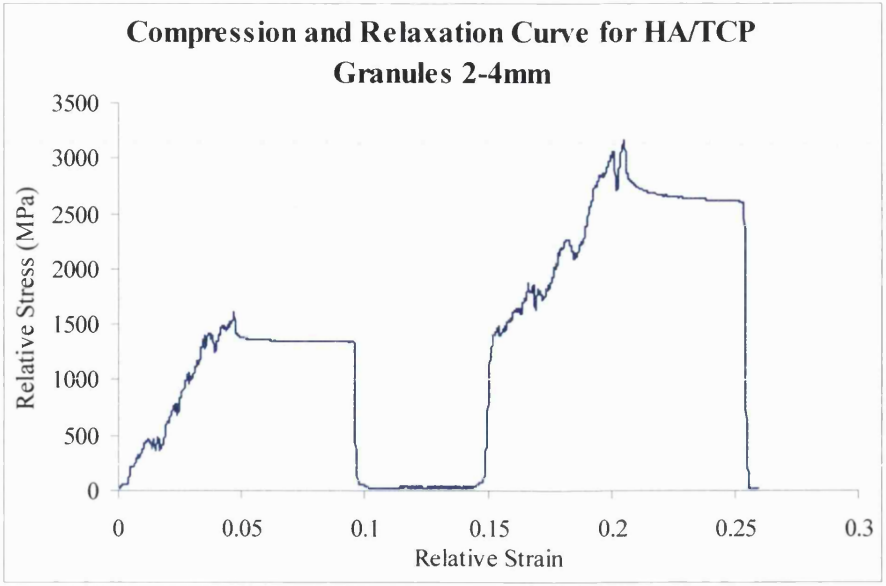

Figure 4.59(b): Stress-strain curve for 2-4mm sized HA/TCP granular material

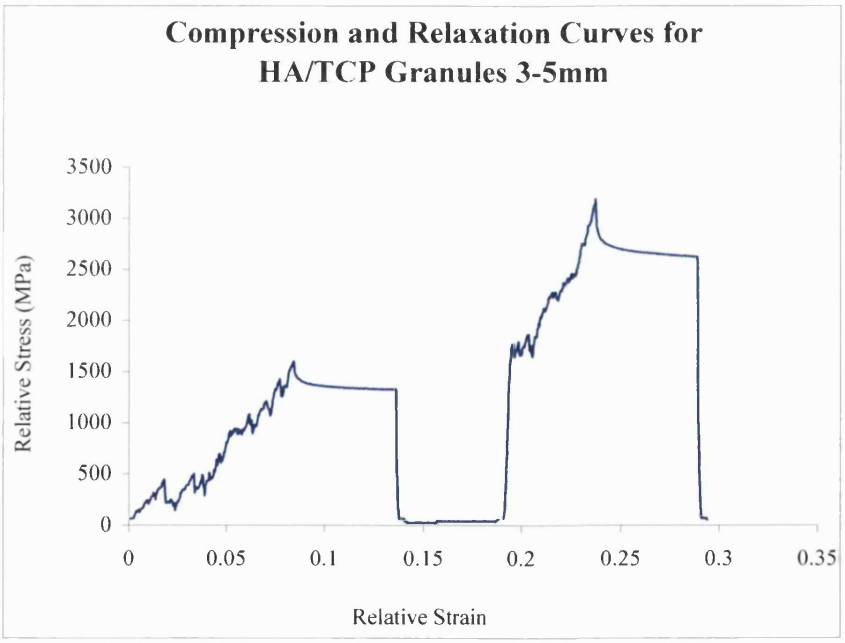

Figure 4.59 (c): Stress-strain curve for 3-5mm sized HA/TCP granular material

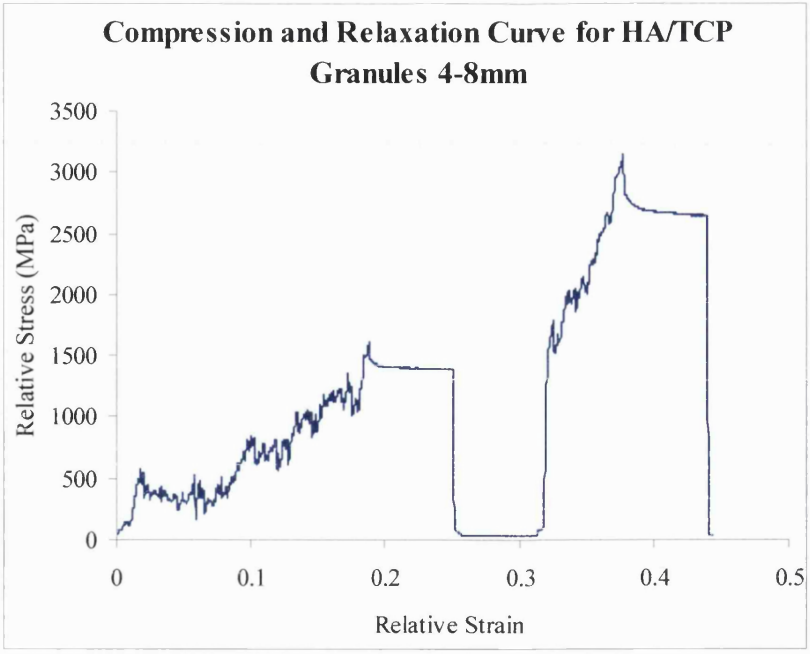

Figure 4.59 (d): Stress-strain curve for 4-8mm sized HA/TCP granular material

The stress-strain curves shown above were for comparison purposes only between each batch and the values given for relative moduli in table 4.17, and do not reflect the true material properties of the materials. It can be seen from the graphs that the 2-4mm and 3-5mm HA/TCP granules have improved mechanical integrity when compared to BoneSave®, and suggests that these materials would possibly have advantages over BoneSave® if used for impaction grafting. The fabricated granules from the I.I. method have the added advantage over BoneSave® that they have interconnecting as opposed to isolated porosity.

4.7.3 Summary of CaP Granular Material Results

Fabrication

HA/TCP granules ranging in size from 2-8mm, have been successfully fabricated with interconnected porosity, and superior mechanical properties compared to a commercially available product termed BoneSave®, which does not have interconnected porosity. The base powders (118 and 130) used in I.I. HA/TCP granular fabrication, were the same base powders as used in the production of BoneSave®.

Mechanical Properties

The material properties analysed were not the true material properties due to the toppling effect of the granules on loading. Therefore, the results were only for comparison within the batch of material tested. I.I. HA/TCP 2-4mm and 3-5mm size granules, demonstrated improved mechanical resistance to loading when compared to BoneSave®. The results indicate that, for this testing procedure, the I.I. HA/TCP granules offer an improved material for possible use in impaction grafting. This has been concluded on the basis of the combination of improved mechanical resistance and the presence of interconnected porosity.

4.7.4 Key Findings

- HA/TCP granules with an interconnected porosity network and varying in size from 2-8mm have been successfully fabricated.
- The fabricated granules offer improved mechanical resistance when compared to a commercially available product - BoneSave®. This combined with the improved interconnected porosity network, suggests the possibility of an improved material for impaction grafting.

4.8 Wicking Experiments

The following results have been obtained from simple wicking experiments, in order to evaluate the potential of the HA, α-TCP and β-TCP SF bioceramics to wick up fluids. The samples have identical macroporosity, but due to the nature of the microstructure of the phases (i.e. different sintering temperatures) they have varying amounts of microporosity; HA has the least, then α-TCP and β-TCP have the greatest amount of microporosity. A methylene blue indicator solution was used as the wicking fluid. A saturation test and mass gain test was performed.

4.8.1 Saturation Results

It was immediately noticeable upon immersion the three phases in the indicator solution that the TCP samples began to wick up the solution. HA did not wick up at the same rate as the TCP samples. Figures 4.60 (a) to (e) show images of the bioceramics before, during and after saturation. The samples were removed after 60 minutes immersion. Figure 4.60 (a) shows HA, α-TCP and β-TCP from left to right, in the remainder of the images the order of samples from left to right is α-TCP,β-TCP and HA.

Figure 4.60 (a): Samples prior to saturation

Figure 4.60 (b): Samples after 1min saturation

Figure 4.60 (c): Samples after 10min saturation

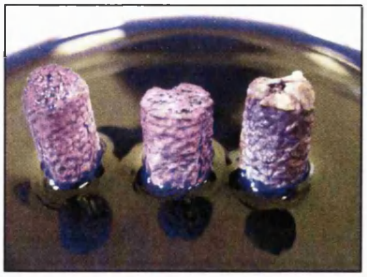

Figure 4.60 (d): Samples after 40min saturation

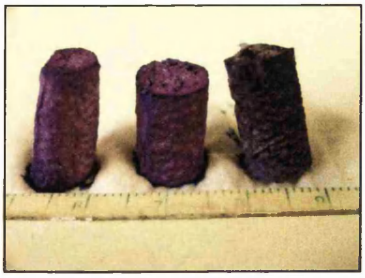

Figure 4.60 (e): Samples after 60min saturation

Table 4.18 shows the time taken for the samples to be fully saturated along with the respective sintering temperatures and microporosities.

Bioceramic Phase	Time for Saturation (minutes)	% Microporosity	Sintering Temperature (°C)
HA	50	9.5	1300
α-TCP	20	17.5	1300
β-TCP	2	32.0	1150

Table 4.18: Saturation times as a function of microporosity

The HA (low microporosity) SF bioceramic wicks up 25 times slower than the β-TCP (high microporosity) SF bioceramic. Figure 4.61 shows a plot of saturation time versus microporosity for the phases produced.

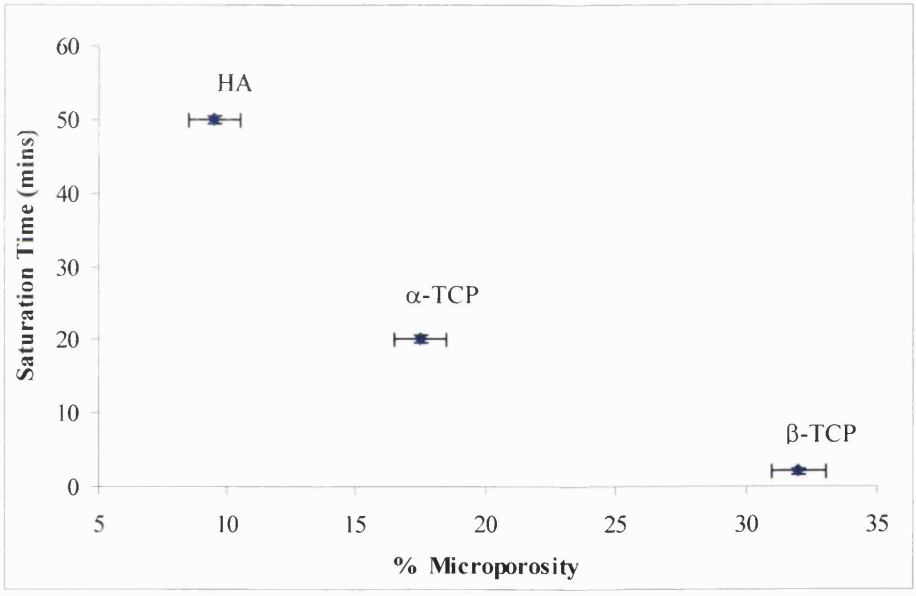

Figure 4.61: Comparison of saturation times against microporosity for phases produced

4.8.2 Mass Gain Results

Separate HA, α-TCP and β-TCP SF bioceramics were immersed in indicator solution in a petri dish and left for 24 hours in order to evaluate the mass gain of the samples. Figure 4.62 illustrates the bioceramics before and after immersion for 24 hours.

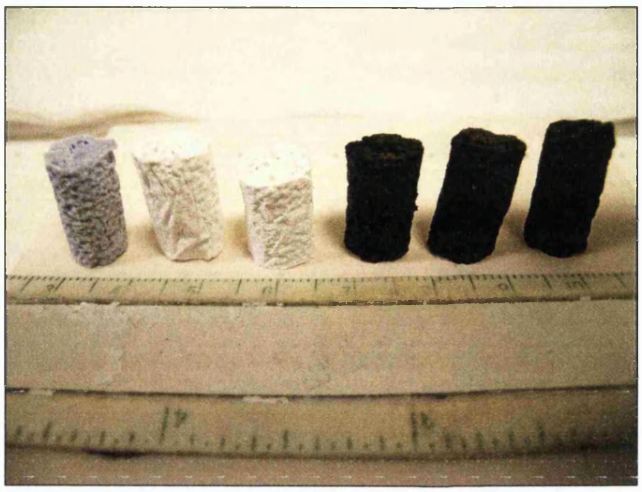

Figure 4.62: HA, α-TCP and β-TCP SF bioceramics before and after immersion in indicator solution for 24 hours

Table 4.19 below represents the mass gain results as a function of microporosity in the phases. Figure 4.63 represents a plot of mass gain against microporosity for the respective phases produced.

Bioceramic Phase	Mass Prior (g)	Mass After (g)	% Mass Gain	% Microporosity	Sintering Temperature (°C)
HA	1.45	2.02	39.3	9.5	1300
α-TCP	1.33	2.02	51.9	17.5	1300
β-TCP	1.06	1.92	81.1	31.0	1150

Table 4.19: Mass gain results as a function of microporosity

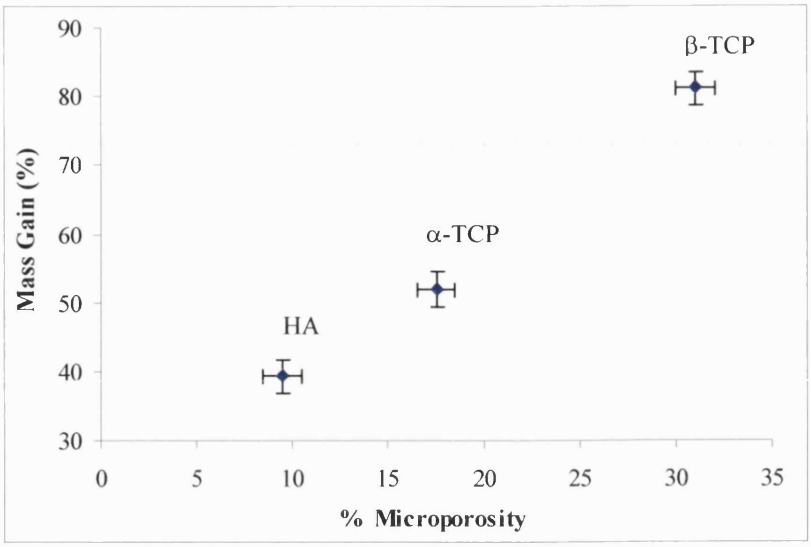

Figure 4.63: Comparison of mass gain versus microporosity for phases produced

As all the samples have the same macroporosity; both the saturation and mass gain experiments demonstrate that the wicking properties of the bioceramics are a function of the microporosity.

4.8.3 Summary of Wicking Experiment Results

In summary, the main findings from the wicking experiments were as follows:

- The HA bioceramics wick up to 25 times slower (i.e. to be fully saturated) compared to β-TCP bioceramics.
- After 24 hours immersion in indicator solution the HA, α-TCP and β-TCP bioceramics increased in mass by 39%, 52% and 81% respectively.
- The results suggest there is a correlation between the microporosity of the bioceramics and their wicking properties.

Chapter 5 General Discussion and Conclusions

At this point it is useful to return to the main aims and objectives of the research that will be addressed in this section:

1) To produce CaP bioceramics based on hydroxyapatite (HA), α-tricalcium phosphate (α-TCP) and β-tricalcium phosphate (β-TCP) with a guaranteed interconnected network of macropores in the appropriate size range (i.e. 150 - 300μm) for bone formation and re-vascularisation.
2) To improve the structure-property relationship (i.e. with the ultimate aim of improving mechanical properties) of the fabricated bioceramics without compromising the interconnected macroporous network vital for bone ingrowth.
3) To develop bioceramics for specific clinical applications including for example spinal fusion interbody operations, maxillofacial procedures, chondylar defects and granular material as a bone graft substitute.

5.1 Analysis of the Interconnected Macroporosity Network

There is a need to develop an interconnected macroporosity network in bone substitute materials resembling that of cancellous bone to act as a scaffold to aid bone formation, ingrowth and re-vascularisation in a diseased or damaged site. The importance of fabricating an interconnected porosity network is a key issue addressed by numerous authors [45, 47, 49, 50, 63]. As seen in table 2.2 (p.33), few fabrication methods successfully produce CaP bioceramics with a guaranteed interconnected macroporosity combined with sufficient mechanical properties for use in load-bearing applications. Therefore, the first objective of the research was to fabricate such a porosity network in the CaP bioceramics.

5.1.1 Comparing the Macroporosity Network of the Bioceramics Produced

Switching the focus of research from producing dense Impact-Impregnated (I.I.) bioceramics with a low volume interconnected network of porosity, to producing Open Porous Scaffold (OPS) bioceramics with a high volume interconnected network of porosity, has proved successful from the point of view of developing a porosity structure with the potential for bone remodelling. It must not be overlooked that the internal porosity network in Spinal Fusion (SF)

bioceramics is identical to that in the OPS bioceramics. Figure 5.1 compares the porosity distributions of I.I. bioceramics with the OPS bioceramics (identical structure to internal SF bioceramics). Table 5.1 indicates how changing the fabrication procedure has produced CaP bioceramics with an improved porosity size distribution that is acceptable for bone ingrowth.

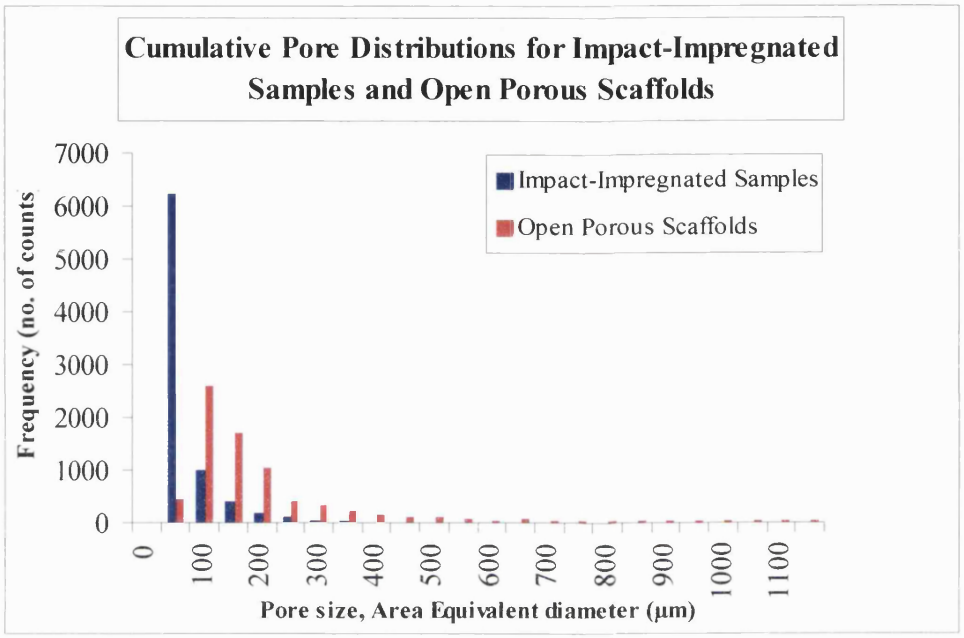

Figure 5.1: Comparison of porosity distributions for Impact-Impregnated samples and OPS

Pore range (µm)	Total % porosity of Impact-Impregnated Samples	Total % porosity of Open Porous Scaffolds
0-150	90.9	12.5
150-450	9.0	79.3
450+	0.1	8.2

Table 5.1: Comparison of changes in porosity in dense (I.I) and porous (OPS) samples

It is generally accepted (and has been discussed in chapter 2.3) that a pore size range of 150-300µm is appropriate for vascularised growth within a bioactive ceramic [61, 65, 73]. Figure 5.2 indicates the differences in the porosity size range between the I.I. dense bioceramics and the high volume porosity OPS bioceramics.

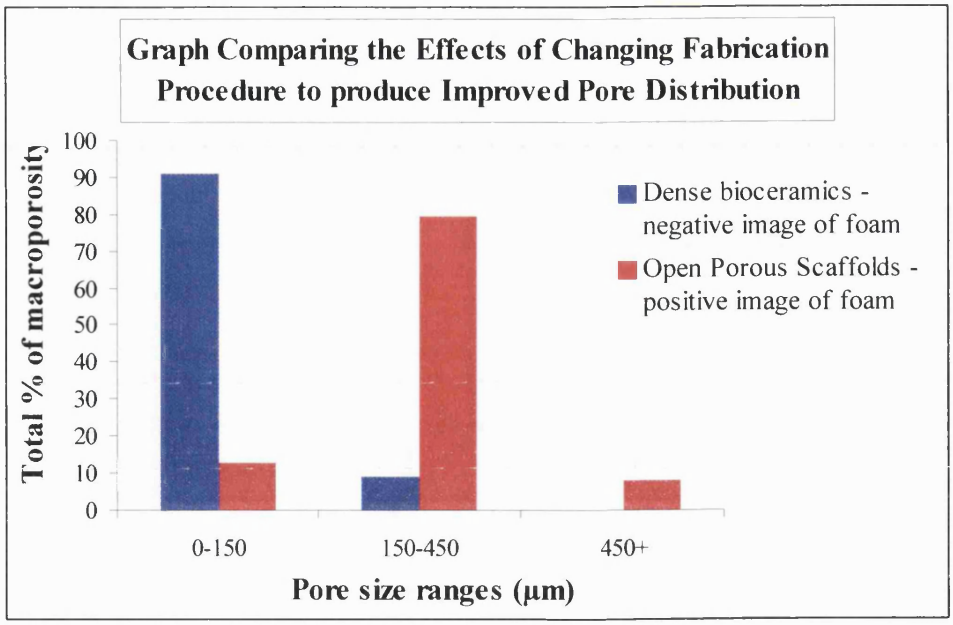

Figure 5.2: Improved pore size range in OPS compared with Impact-Impregnated samples

The objective of producing the I.I. bioceramics was to impregnate and substantially fill the spaces of the polyurethane (PU) foam with the ceramic slip, then to burn out the reticulated PU foam to leave an interconnected porosity network resembling the structure of the foam. Hence the majority of the porosity lies in the 0-150µm size range, as this is the size range of the PU struts burnt out on sintering. Figure 5.3 illustrates this structure.

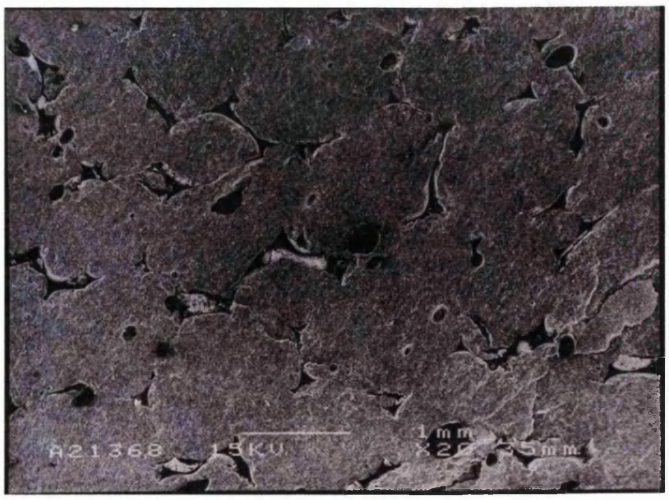

Figure 5.3: Structure of I.I. bioceramics indicating the bow-tie shaped pores not ideal in shape for potential bone remodelling

By producing the OPS and SF bioceramics from the same foam template (and therefore same porosity distribution), that is by impregnating and coating the slip on to the struts of the foam resembling the positive porosity image of the foam, the majority of the porosity is in the appropriate size range (150-300μm) and shape for bone formation and ingrowth. Figure 5.4 illustrates an example of the OPS and SF structures produced.

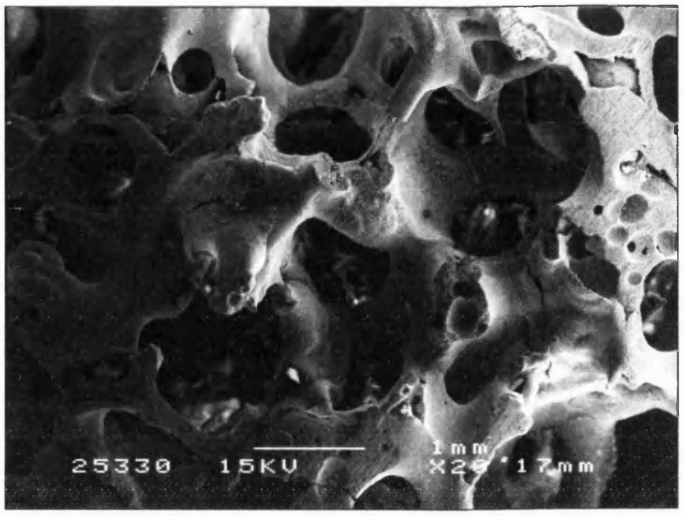

Figure 5.4: Structure of OPS bioceramic indicating the high volume porosity structure and good pore size and shape

Figures 5.1 and 5.2 clearly indicate the structural advantages as far as bone remodelling is concerned with switching the focus of research to produce OPS and SF bioceramics, in that a porosity distribution in the appropriate size range for bone ingrowth has been produced. Figures 5.5, 5.6 and 5.7 are expanded sections of figure 5.1. From these it can be seen that OPS and SF bioceramics have a much more appropriate pore size distribution than I.I. samples in terms of potential for bone remodelling.

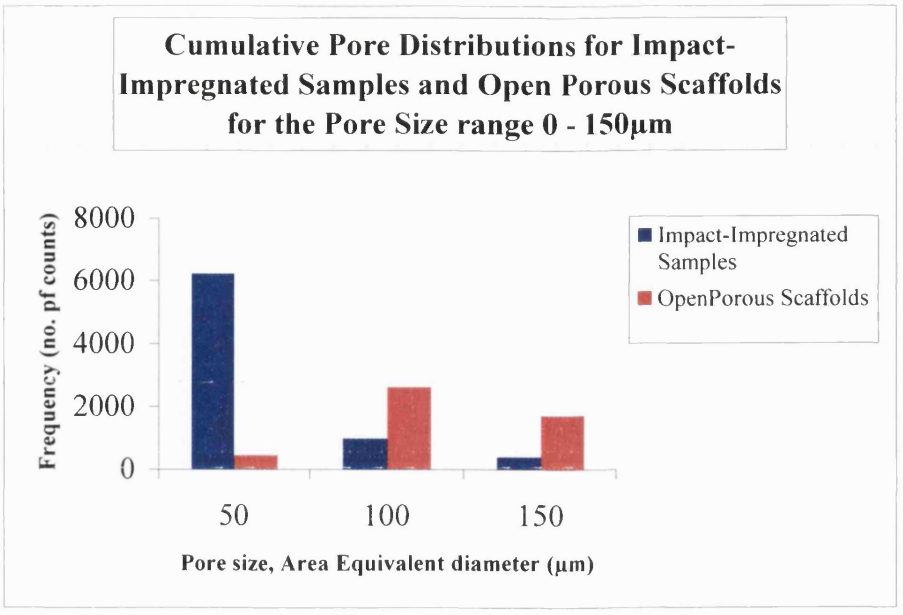

Figure 5.5: Cumulative pore distribution for size range 0-150µm

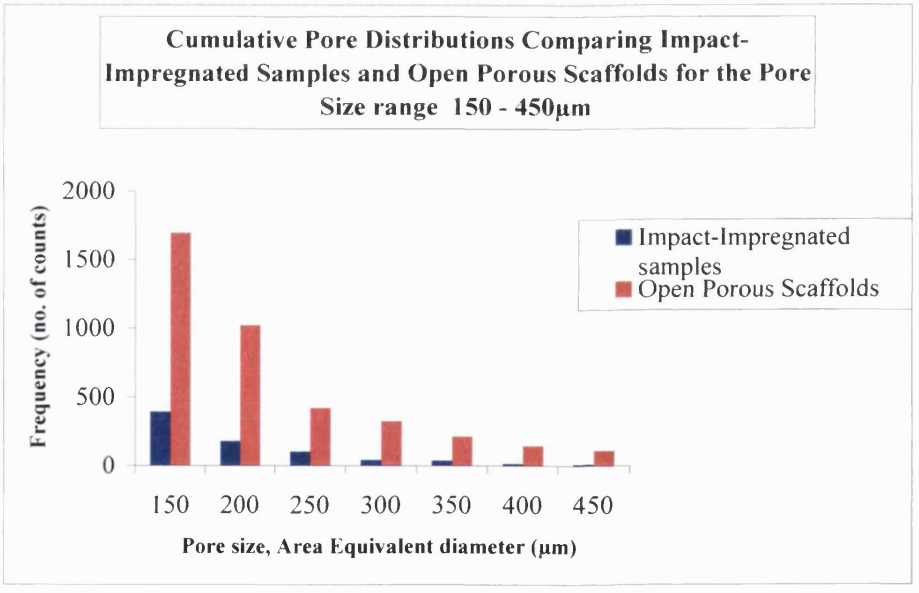

Figure 5.6: Cumulative pore distribution for size range 150-450µm

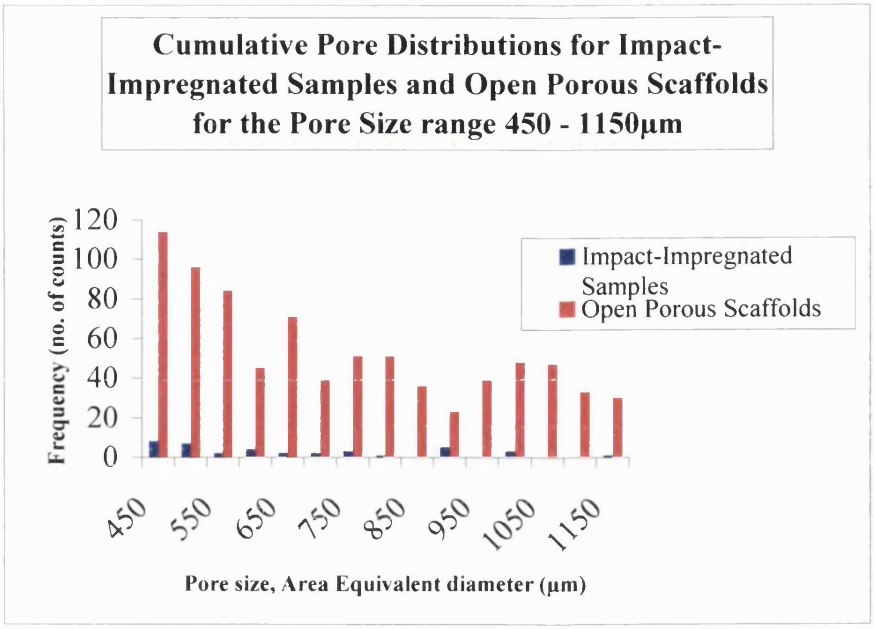

Figure 5.7: Cumulative pore distribution for size range 450-1150µm

This is not to say that the I.I. bioceramics do not have a role to play as a possible bone substitute materials. These dense bioceramics have similar porosity distributions to those found in cortical bone, where one function of the porosity is to distribute nutrients (through cylindrical Haversian systems) to facilitate bone ingrowth. Figure 5.8 illustrates the difference in macroporosity produced in the samples from the different fabrication procedures. This reiterates the point that fabricating OPS and SF bioceramics (SF bioceramics identical in porosity structure to OPS) results in a bone substitute material with greater volume porosity and an improved pore size distribution to encourage bone growth.

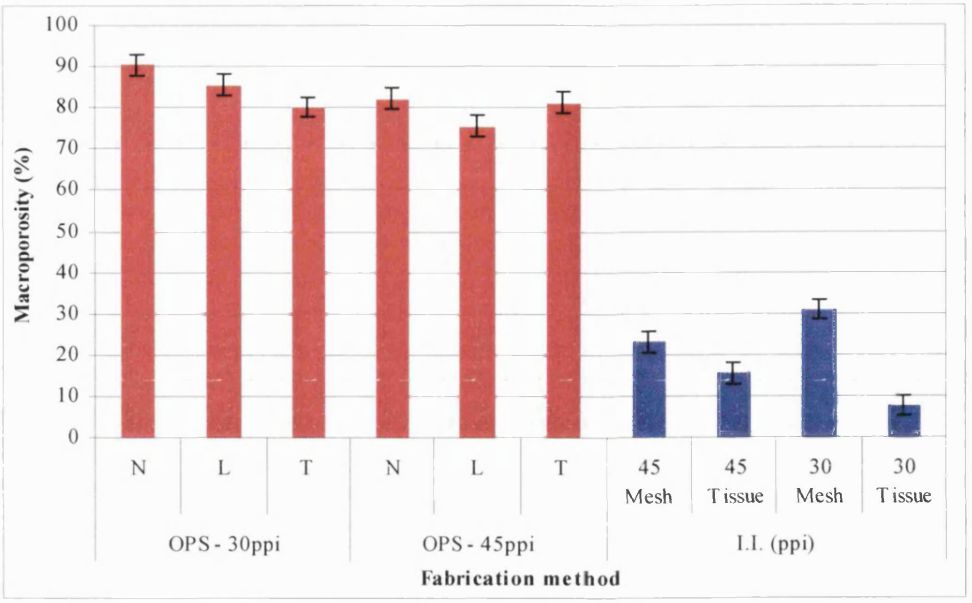

Figure 5.8: Comparison of macroporosity in I.I. and OPS samples

For the I.I. bioceramics, it is the drying mechanism that is the main influence on macroporosity. Drying on tissue rather than on metal mesh extracts all excess moisture from the samples and reduces the possibility of closed porosity occuring. Typical macroporosity in I.I. bioceramics ranges from 7-31% compared with 72-93% for OPS and SF bioceramics.

To summarise, the switch to producing OPS and SF bioceramics has resulted in the fabrication of samples with an interconnected macroporosity network in the appropriate size range for bone formation and ingrowth. The first objective of the research was therefore achieved.

5.2 Structure-Property Relationships of Bioceramics Produced

The following section will focus on the second objective of addressing the structure-property relationship of the bioceramics and how to improve the relationship in order to improve the mechanical properties without compromising the interconnected macroporosity network. The same approach of addressing the structure-property relationship is used to assess the sol-gel treated SF bioceramics. In addition, x-ray diffraction (XRD) analysis and scanning electron microscopy (SEM) were used to examine microstructural changes resulting from the treatment employed.

5.2.1 Comparing the Structure-Property Relationships of I.I., OPS and SF Bioceramics

The mechanical properties of CaP ceramics, as with all engineering ceramics, are highly dependent on the processing route as a consequence of the effects of processing on the microstructure of the final product. The sintering temperature, the type of porosifier used, the drying route taken and the resultant macropore distribution will all affect the microstructure and hence the mechanical properties of the samples produced. Table 5.2 summarises the mechanical properties, apparent densities and total volume porosity of the bioceramics fabricated.

Bone Substitute	**Impact-Impregnation**	**Open Porous Scaffolds**	**Spinal Fusion**	**Spinal Fusion treated with Sol-Gel**
Strength 95% C.L. (MPa)	4.50 ± 2.86	0.30 ± 0.01	2.92 ± 0.60	5.94 ± 1.06
Bulk Density 95% C.L. (g/cm^3)	1.50 ± 0.60	0.35 ± 0.05	1.01 ± 0.05	1.51 ± 0.22
Volume Porosity (%)	7 - 31	75 - 95	70 - 92	72 – 94
Sample Size	40	120	100	60

Table 5.2: Summary of mechanical data from fabricated samples

It can be seen from table 5.2 that by shifting focus to OPS and SF methods that the porosity requirements of the bioceramics and the reproducibility and hence consistency has been improved, however strength has decreased. The large variations found in the I.I. samples were primarily due to the drying effects and the dependence on sintering temperature. The level of porosity is similar in OPS and SF bioceramics as the same PU template was used as was discussed in section 5.1.1. There is evidence of a strength-density and strength-porosity relationship as illustrated by figures 5.9 and 5.10 respectively.

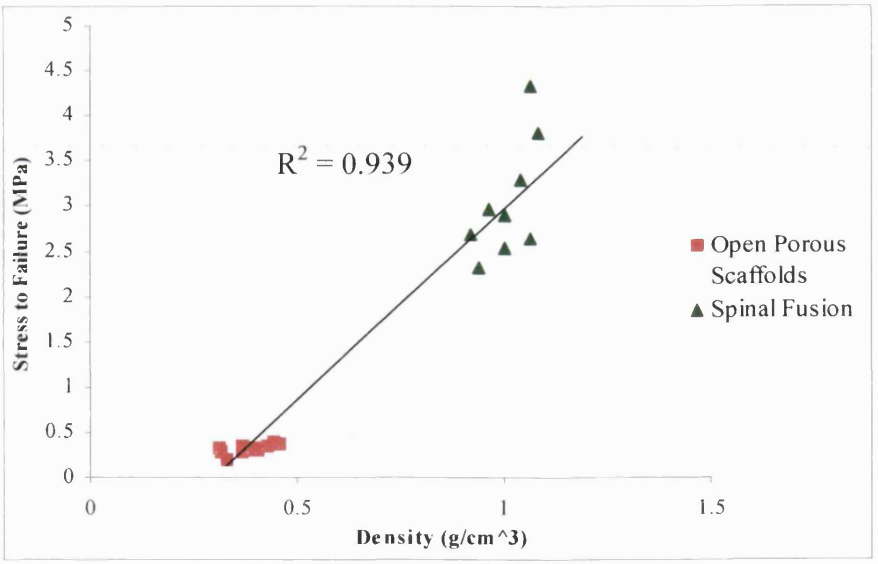

Figure 5.9: Graph illustrating strength-density relationship of OPS and SF bioceramics produced

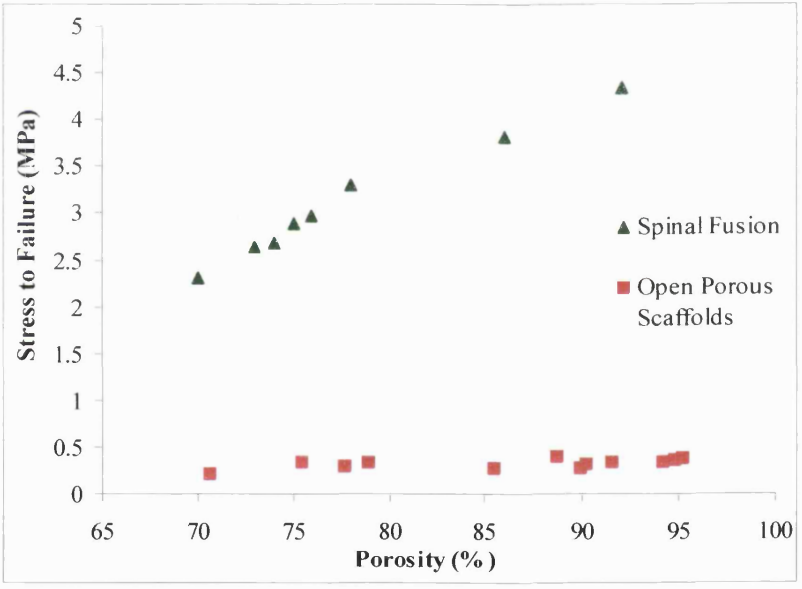

Figure 5.10: Graph illustrating strength-porosity relationship of OPS and SF bioceramics produced

The increase in density in SF bioceramics was due to the fabrication of a dense shell surrounding an OPS cylindrical specimen, which has increased strength without compromising the interconnected porosity network. On loading, the dense outer shell acts as a stress-shield and supports the interior open porosity. This is an important criterion on stressing as the interconnected macroporosity network necessary for bone ingrowth was retained even on failure. Figure 5.11 indicates this important phenomenon.

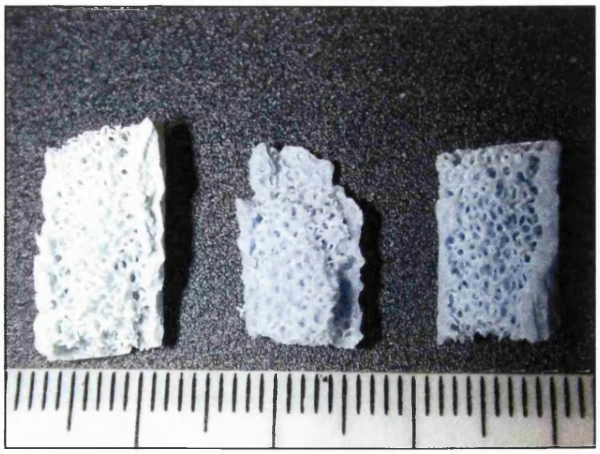

Figure 5.11: Stress-shielding phenomenon in failed HA SF bioceramics whereby interior porosity network is retained as the outer dense shell supports stress

It is the outer dense shell that provides the majority of the support for stress on loading. It was established by SEM analysis that grain growth and microporosity were temperature dependent. This temperature dependency is shown in figures 5.12 through to figure 5.14, whereby an increase in temperature results in a reduction in microporosity from 31.2% at 1150°C to 3.6% at 1350°C (see table 4.11, p.141).

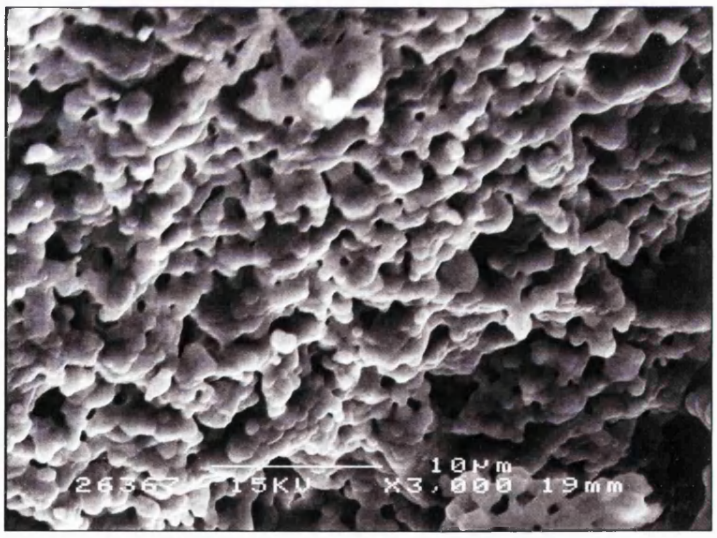

Figure 5.12: Microstructure of SF bioceramics at 1150°C indicating high microporosity

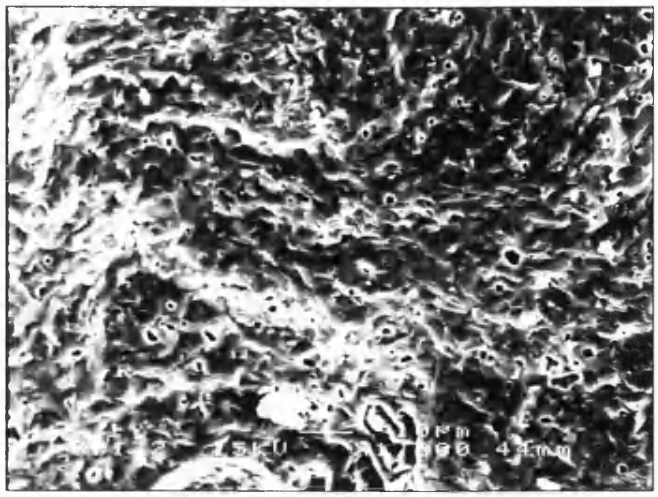

Figure 5.13: Microstructure of SF bioceramics at 1250°C indicating a reduction in microporosity with increase in sintering temperature

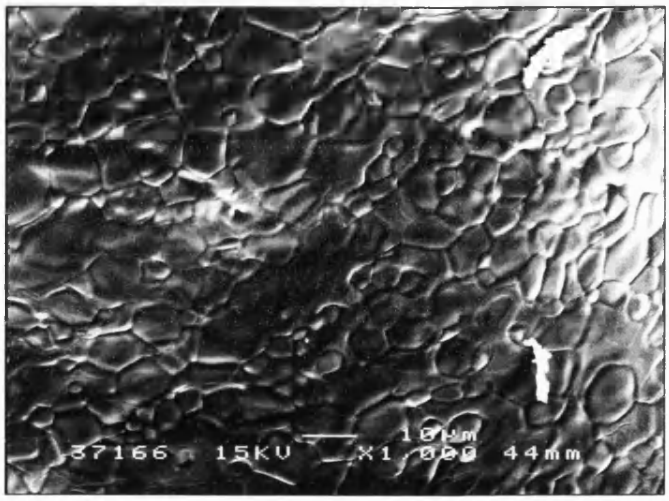

Figure 5.14: Microstructure of SF bioceramics at 1350°C indicating low microporosity

The switch to fabricating OPS as opposed to I.I. bioceramics has successfully resulted in samples with a high volume interconnected macroporosity network with pores in the appropriate size range for bone ingrowth. However, as table 5.2 indicates the strength properties of the OPS samples have dramatically lowered even though the process has become more reproducible. The formation of microcracks on sintering at areas of high concentration of PU foam, termed triple point junctions, created structural weaknesses that were the cause of such unpredictable and variable low strengths. Figure 5.15 shows an example of these microcracks that are commonplace through out the structure. In OPS (and SF bioceramics) it is the presence of these small flaws that severely limit the mechanical properties of the bioceramic. Hence there is a need to improve the structure-property relationship still further.

Figure 5.15: Microcrack formation on sintering creating structural weaknesses lowering mechanical properties

Under loading, the microcracks formed grow until they collapse and cause brittle failure. The success of producing an interconnected macroporosity network for bone ingrowth has affected the structure-property relationship and resulted in a structurally weak material and hence low mechanical properties.

The strength properties achieved in the OPS and SF bioceramics were insufficient to meet the demands for clinical application. Therefore, research switched focus to address the surface microcracks that are the cause of structural weakness, and hence to improve the structural properties of the OPS and SF bioceramics with the aim of increasing mechanical properties without compromising the interconnected macroporosity network.

5.2.2 Structure-Property Improvements to SF Bioceramics due to Sol-Gel Treatment

The second objective to be fulfilled by the research was to improve the structure-property relationship without compromising the interconnected macroporosity network essential for bone ingrowth.

It has already been described how microcrack formation on sintering in OPS an SF bioceramics is responsible for the consistent low strengths found on stressing in these high volume porosity

samples. These are partially responsible for failure in SF bioceramics due to the stress shielding by the outer dense shell.

The sol-gel method involves treating the SF bioceramics with a low viscosity solution that flows into the micropores and surface microcracks of the specimen and on sintering forms a polycrystalline structure that reduces or even eliminates the structural weaknesses previously identified. Figures 5.16 and 5.17 show the strength-density and strength-porosity relationships of the sol-gel treated samples compared to the previously fabricated samples.

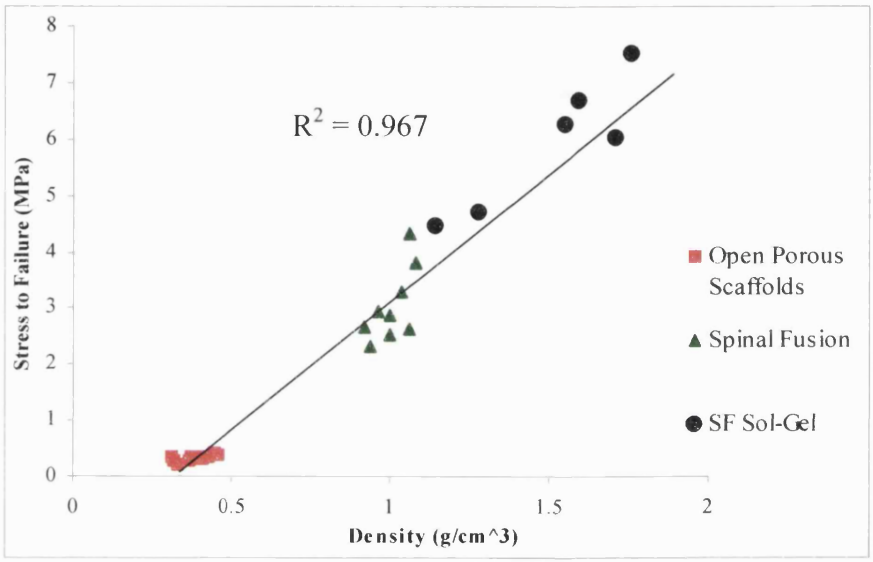

Figure 5.16: Graph showing strength-density relationship of OPS, SF and sol-gel treated SF bioceramics

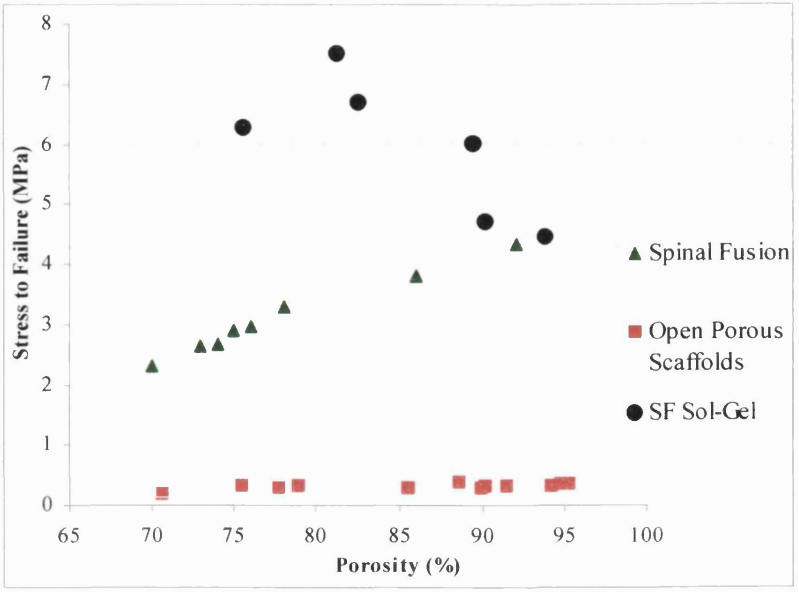

Figure 5.17: Graph showing strength-porosity relationship of OPS, SF and sol-gel treated SF bioceramics

It is important to note that the sol-gel treated SF bioceramics have increased strengths without compromising the interconnected macroporosity network (figure 5.17). Table 5.2 emphasizes this point. As with producing the SF bioceramics, there is a strength-density correlation that is a coinciding theme throughout the research.

Figure 5.18 shows a strength-density graph of all the untreated and treated SF bioceramics, and figure 5.19 summarises the strength differences between the two fabrication procedures and samples treated with sol-gel at 500°C and 1100°C.

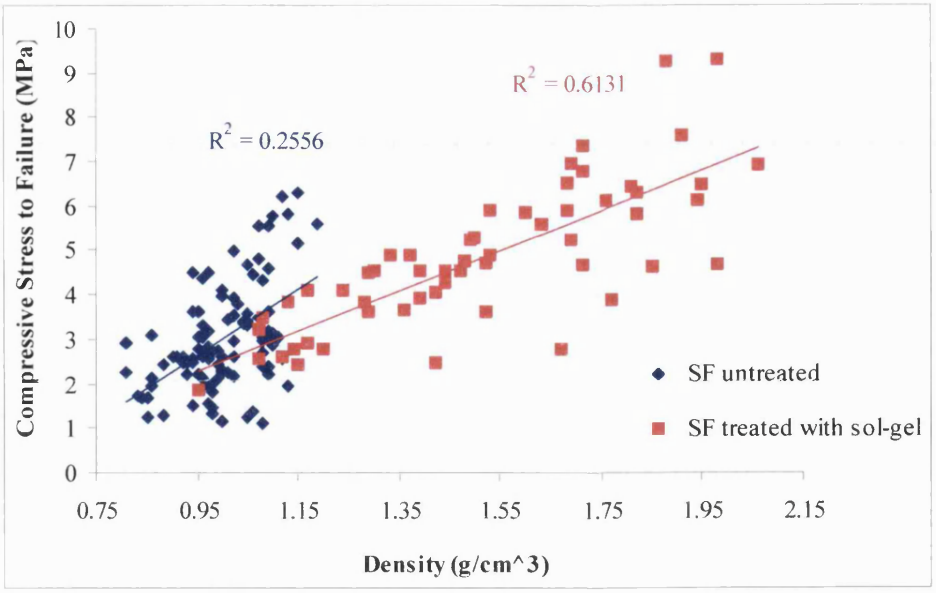

Figure 5.18: Strength-density data for all SF bioceramics

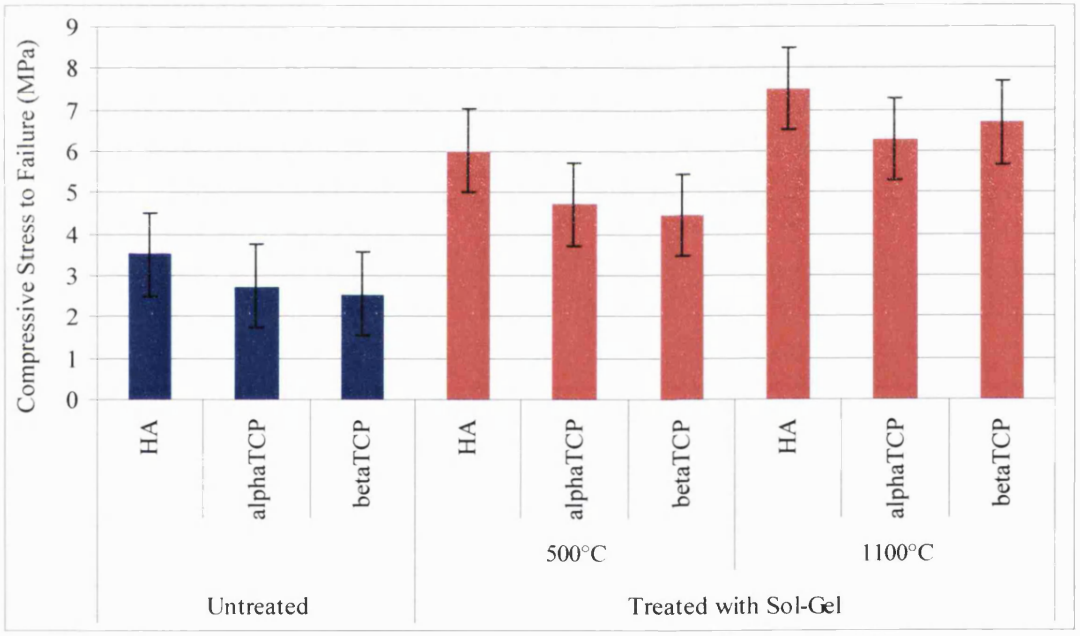

Figure 5.19: Summary of all SF bioceramics results

Figure 5.19 indicates not only that treating the SF bioceramics with a sodium methoxide sol-gel solution has increased strength, but also that those samples treated and sintered at 1100°C have higher strengths than those sintered at 500°C. However, this graph also shows that the high microporosity TCP samples are the most sensitive to the sol-gel treatment as they show the greatest relative increase in strength. This is particularly true for the high microporosity β-TCP bioceramics. This suggests that the sol-gel solution has reacted and changed the surface structure

of the TCP bioceramics more than the HA bioceramics due to the larger microporosity present. Hence, the ability of the oxide formed to bond to the surface and therefore reduce or eliminate the microcracks previously identified as weak points, has increased the strength of the bioceramics.

SEM and XRD analysis confirmed the structural and chemical changes that accompanied the increase in strength. It must be noted that the sol-gel treatment has not compromised the interconnected macroporosity network; this is confirmed from figure 5.17.

Figures 5.20 and 5.21 show the structural differences before and after the treatment with soda sol-gel. Both SEM images are taken from areas one would expect to find microcracks i.e. at triple point junctions. Figure 5.20 demonstrates this phenomenon clearly. Conversely, figure 5.21 shows a similar area as for figure 5.20 where microcracks would be expected. As a result of the sol-gel treatment not only have the microcracks been reduced but also eliminated.

Figure 5.20: Microcrack formation on sintering in SF untreated bioceramic

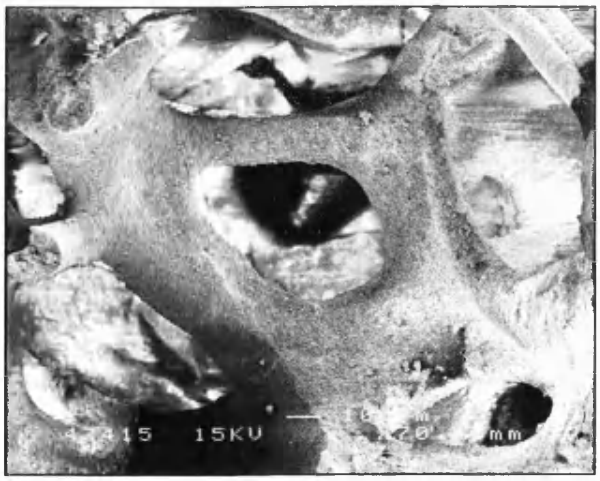

Figure 5.21: Elimination of microcracks and change in surface structure due to sol-gel treatment

Another example of the effect of this treatment is shown in figures 5.22 and 5.23. Figure 5.22 shows the microcracks common in untreated bioceramic scaffolds and figure 5.23 a similar area where microcracks would be expected. However, the sol-gel treatment has eliminated these structural weaknesses and altered the surface structure of the SF bioceramics.

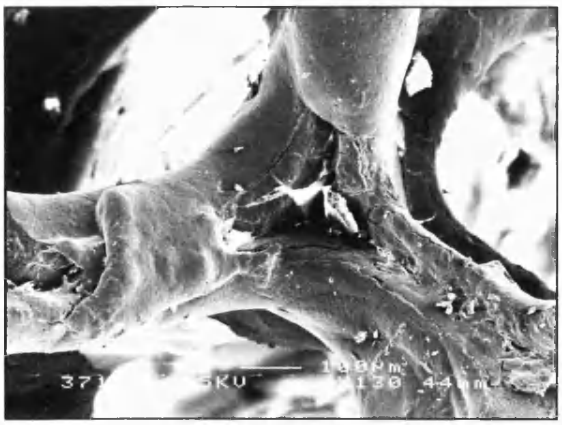

Figure 5.22: Presence of microcracks at triple point junctions in SF bioceramics

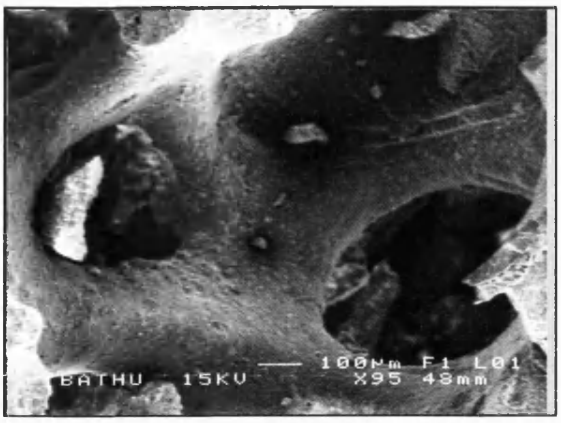

Figure 5.23: Elimination of microcracks and formation of amorphous phase on surface of bioceramic

At higher magnifications it is possible to distinguish the difference in surface structure between untreated and treated SF bioceramics. This is indicated in figures 5.24 (before treatment with sol-gel) and figure 5.25 (after sol-gel treatment).

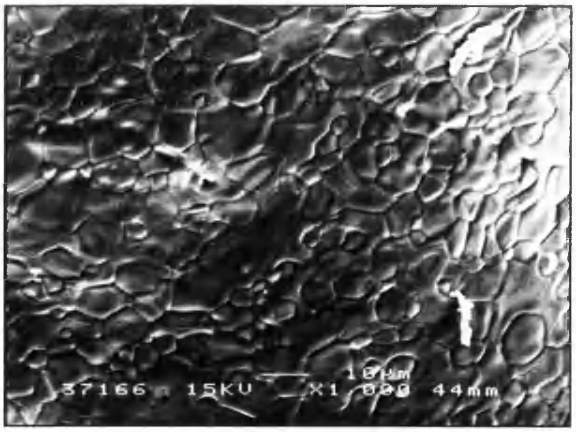

Figure 5.24: Vitreous, glassy surface of 46% α-TCP SF bioceramic

Figure 5.25: Formation of polycrystalline structure at surface of α-TCP SF bioceramic

These structural differences were most notable in the TCP samples and in particular β-TCP bioceramics due to the larger microporosity compared to HA bioceramics. As a result the greater strength increases were found in the β-TCP bioceramics e.g. sol-gel treated β-TCP bioceramics at 1100°C have strength increases of 160% without compromising the interconnected macroporosity network.

Figure 5.26 indicates the XRD analysis of the untreated and treated SF bioceramics.

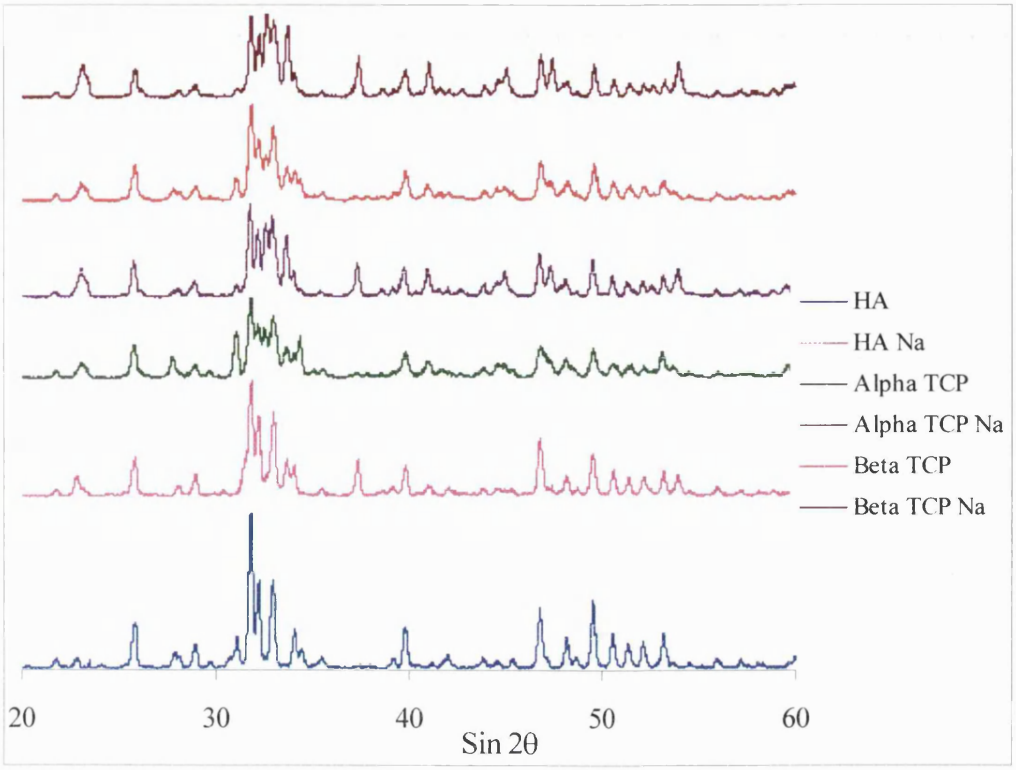

Figure 5.26: Comparison of XRD data for SF samples untreated and SF samples treated with sol-gel

It can be noted that the greatest evidence of for structural and chemical differences is in the TCP phases and it is these that also demonstrate the greatest strength increases as a result of the sol-gel treatment. The large amount of microporosity in these phases, (shown by SEM micrographs) and thus superior ability of sol-gel to bond to surface of TCP bioceramics, has altered the chemical structure of the phase. This structural and chemical alteration is shown in figure 5.27 at 31.5° - 33.5° where the apatitic structural group in TCP samples has been altered due to the reaction with the soda sol-gel. Conversely, the HA XRD traces do not indicate a change in the apatitic group and therefore the chemical and structural changes are not as marked as for the TCP samples. The strength increases in HA bioceramics are not as great as for the TCP and in particular the high microporosity β-TCP bioceramics.

The structural and hence mechanical property improvements due to the treatment of soda sol-gel, via the elimination of microcracks and the altering of the chemical structure, has improved the

mechanical properties of the SF bioceramics without compromising the interconnected macroporosity network needed for bone ingrowth. This was a main objective of the research as the initial fabricated bioceramics with an improved porosity structure were structurally weak.

Table 5.3 illustrates the structural and mechanical properties of the sol-gel treated SF bioceramics compared to selected materials from table 2.2 (p.33).

Material	Cortical bone	Cancellous bone	Endobon®	HA/ TCP	HA	HA	**Sol-gel treated SF bioceramics**
Content	Apatite (+ mineral impurities) *	Apatite (+mineral impurities) *	HA	HA/ TCP (60/40)	HA	HA	**HA, α-TCP, β-TCP**
Density (g/cm^3)	1.6 - 2.1	0.05 – 1.0	0.4 – 1.2	0.6 – 0.9	0.3 –0.8	0.03 – 0.06	**1.3 - 1.7**
Compressive Strength (MPa)	100 – 230	2 – 12	1.11	5.0 – 7.0	1.6 – 3.3	0.05	**4.9 – 7.0**
Youngs Modulus (GPa)	7 – 30	0.05 – 0.1	0.2 – 3.1	-	-	-	**-**
Volume porosity (%)	5 – 10	40 - 95	10 – 40	40 – 60	72 - 90	> 95	**72 – 94**
Interconnected or isolated porosity?	Int.	Int.	Int.	Isol.	Int.	Int.	**Int.**
Pore size range (μm)	10 – 200	10 – 1000 **	100 – 400	100 - 400	15 - 120	50 - 500	**50 – 1000 +**
Reference	Rho et. al. [15]	Rho et. al. [15]	Hing et. al. [63]	Liu [123]	Sepulve da [121]	Binner [110]	**Current Research**

* The content of bone varies due to its location in the body.
** Porosity size range in bone can be greater than this.

Table 5.3: Comparison of structural and mechanical properties of some current bone replacement materials with the sol-gel treated bioceramics fabricated in current research

It can be seen from table 5.3 that the open porous SF treated bioceramics have similar structures from the point of view of volume porosity, interconnected porosity and pore size range to other materials produced in the field i.e. by Sepulveda [121] and Binner [110]. However the sol-gel treated SF samples have improved mechanical resistance compared to these materials. When compared to a commercially available product, Endobon®, the material produced from the current research has improved structural characteristics (i.e. volume porosity and pore size range) and also improved compressive strength. The sol-gel treated SF bioceramics has similar mechanical properties to materials developed by Liu [123], however the materials produced by the current research has improved structural characteristics compared to this material i.e. interconnected porosity, high volume porosity, pore size range. It can also be seen from table 5.3

how the materials produced by the current research closely approximate the structural and mechanical properties of cancellous bone.

The materials produced from the current research offer a significant advancement in the field as a superior range of materials has been produced with appropriate structural characteristics for bone ingrowth that also exhibit a diversity of applications.

5.3 Microporosity Evaluation and Wicking Properties of SF Bioceramics

The microporosity present in the bioceramics produced has two important roles. Firstly, there is potential for the microporous materials to be used as drug carriers so that diseased or damaged bone can be treated *in-vivo* by the release of bone morphogenetic proteins through the microporous structure. Secondly, the amount of microporosity present is an indication to how well the bioceramics wick up fluid, an important element when considering the potential biocompatibility of a material.

5.3.1 Microporosity Dependence on Sintering Temperature

The microporosity distribution of all samples analysed is shown in figure 5.27. Although the pores <2μm are more numerous, the pores >2μm provide a greater contribution to the volume fraction of microporosity.

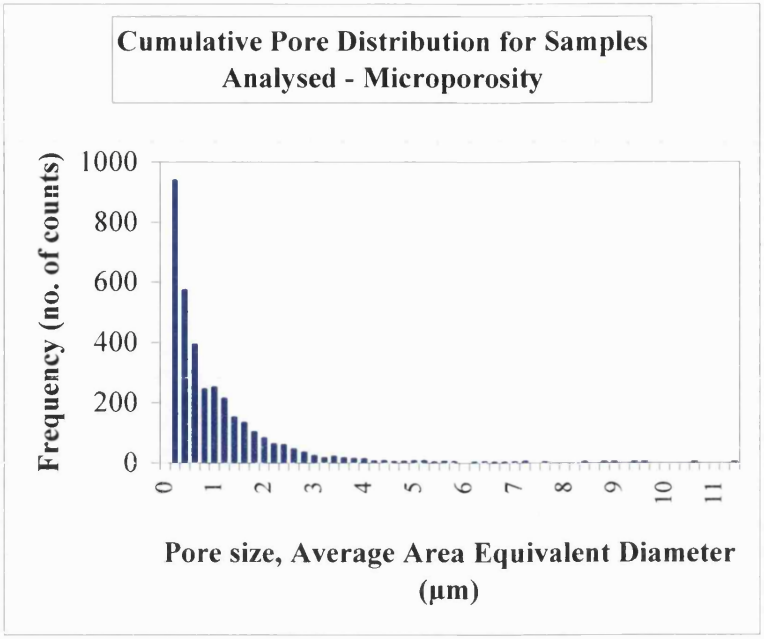

Figure 5.27: Cumulative micropore distribution of all the samples analysed

The microporosity was found to be dependent on sintering temperature and independent of the type of porosifier used or drying mechanism. The microporosity changes seen above 1180°C correspond to an increase in grain growth, particularly in the calcium deficient grade 118 HA powders. Figures 5.28, 5.29 and 5.30 illustrate the differences in microstructure at 1150°C, 1250°C and 1350°C in SF bioceramics, indicating the reduction in microporosity with increased sintering temperature.

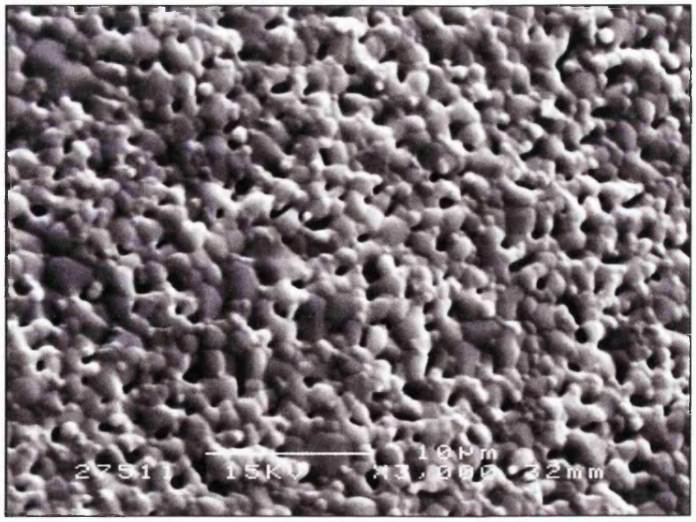

Figure 5.28: Microporous structure of 1150°C sintered SF bioceramic

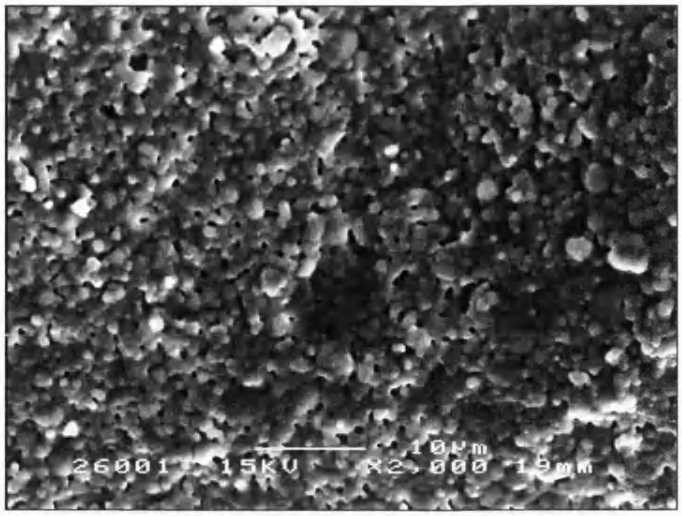

Figure 5.29: Microporous structure of 1250°C sintered SF bioceramic

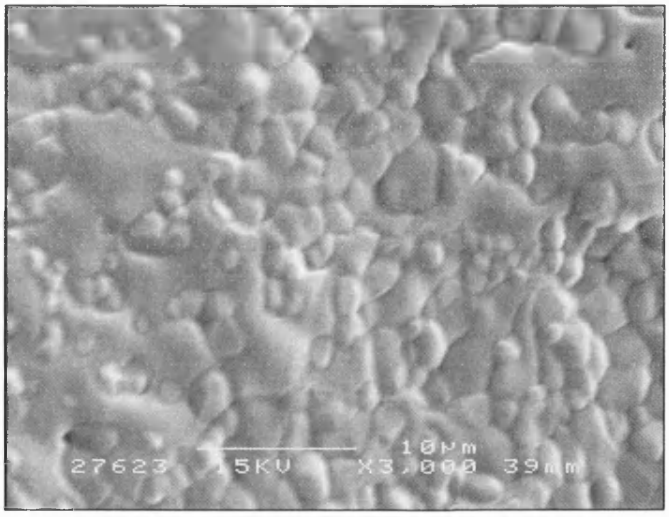

Figure 5.30: Microporous structure of 1350°C sintered SF bioceramic

The predominant phase in 1150°C sintered samples with grade 118 powders is β-TCP. Above 1180°C a vitreous reaction occurs that forms a hard, glassy α-TCP phase. A further increase in sintering temperature (figure 5.30) reduces the microporosity still further due to coalescence of grains. The micrographs demonstrate how sensitive the base powders are to sintering temperature and the importance of absolute control over the temperature ramp rate and overall temperature inside the sintering oven for phase control.

Figure 5.31 indicates the dependency of microporosity by sintering temperature and the independence from the porosifier used. The 1280°C fired bioceramics have 52% less microporosity than their 1150°C counterparts.

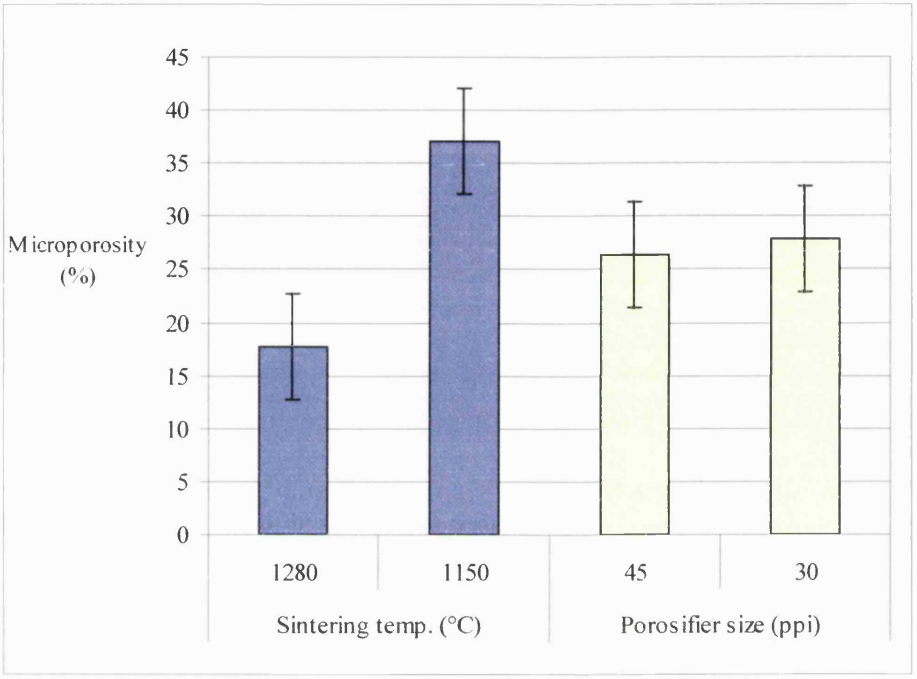

Figure 5.31: Graph showing how the experimental parameters affect the microporosity in the samples

The presence of α-TCP in the 1280°C fired samples, which introduces a volume increase on formation and hence a smaller grain size, is a possible explanation for the difference in microporosity, as the number of sites for micropores to nucleate is smaller. Another argument is the possibility of forming a vitreous, glassy phase resulting from mass flow and the coalescence of grains at high temperatures.

The microporosity in the 1280°C fired samples is more clearly defined. However, in the 1150°C fired samples, where there is no transformation to α-TCP, the grains appear to cluster together in clumps (i.e. no vitreous formation and hence no coalescence of grains) leaving the microporosity to be less defined and randomly distributed in pockets surrounded by clustered grains. This adds weight to the argument that at high temperatures the coalescence of grains is predominantly the driving force for the reduction in microporosity with increasing temperature.

5.3.2 Wicking Experiments and Relationship to Microporosity

Wicking experiments were performed to evaluate how the microporosity affects the wicking properties of the three phases (HA, α-TCP and β-TCP). For example, as an indication to the relative solubility of the three phases, it is reported in the literature that HA is 20 times less soluble than β-TCP [50].

It was found from the wicking experiments that β-TCP samples were fully saturated after two minutes of immersion in a methylene blue indicator solution. HA samples were fully saturated after 50 minutes of immersion. Therefore, HA which has 52% less microporosity than β-TCP wicks up 25 times slower. This coincides with the solubility results reported *in-vivo* in the literature [42]. Figure 5.32, 5.33 and 5.34 show images of the samples prior to immersion, during immersion and after immersion respectively.

Figure 5.32: SF bioceramics prior to immersion

Figure 5.33: SF bioceramics during immersion

Figure 5.34: SF bioceramics after immersion

In a separate experiment, samples were left immersed for 24 hours to ensure full saturation of the samples by the indicator solution. After 24 hours HA, α-TCP and β-TCP bioceramics increased in mass by 39%, 52% and 81% respectively. This confirms the relationship between microporosity and wicking properties i.e. an increase in microporosity correlates with an increase in wicking properties.

5.4 Fabricated Bioceramics for Practical and Clinical Applications

It is necessary not only to produce bioceramics purely for laboratory research, but also to transfer that research and technology into the manufacture of bioceramics for clinical applications. This was another objectives of this research laid out in section 2.8, whereby research concentrated upon four practical areas. These being, the development and compression testing of synthetic CaP granules (from the I.I. method) for impaction grafting in revision hip operations, block material for potential use in maxillofacial surgery (jaw reconstruction), cylindrical graft material for spinal fusion interbody operations and also a synthetic alternative for non-load bearing chondylar defects in the knee joint.

The need to produce these practical synthetic graft materials also illustrates the diversity of the process, and that not only the size and shape of the samples can be tailored (as well as porosity distributions), but the chemical composition can also be altered for specific biological and mechanical requirements.

5.4.1 CaP Granules for Impaction Grafting

As the supply of allograft material is limited and allograft is also of poor quality, there is a need to develop an alternative material for impaction grafting in revision hip operations. The two grades of powders used in the present study (118 and 130 – both supplied by Stryker Orthopaedics) are also used as base powders in a commercially available synthetic granular alternative to allograft for use in impaction grafting developed by Stryker Orthopaedics and named BoneSave®. BoneSave® has been proven to be biocompatible with bone and has excellent wicking properties. However it does not have interconnected macroporosity. CaP granules fabricated via the I.I. method were produced in similar size ranges to BoneSave® and both materials were then compression tested using a die-plunger and their mechanical properties

compared. Figure 5.35 illustrates an example of the stress-strain curves of the fabricated CaP granules from the I.I. method and the BoneSave® granules. Table 5.4 shows the respective modulus of each size range against that for BoneSave®. The study was carried out in order to evaluate the relative mechanical response under compression loading of the material fabricated as part of the current research programme compared to that of BoneSave®.

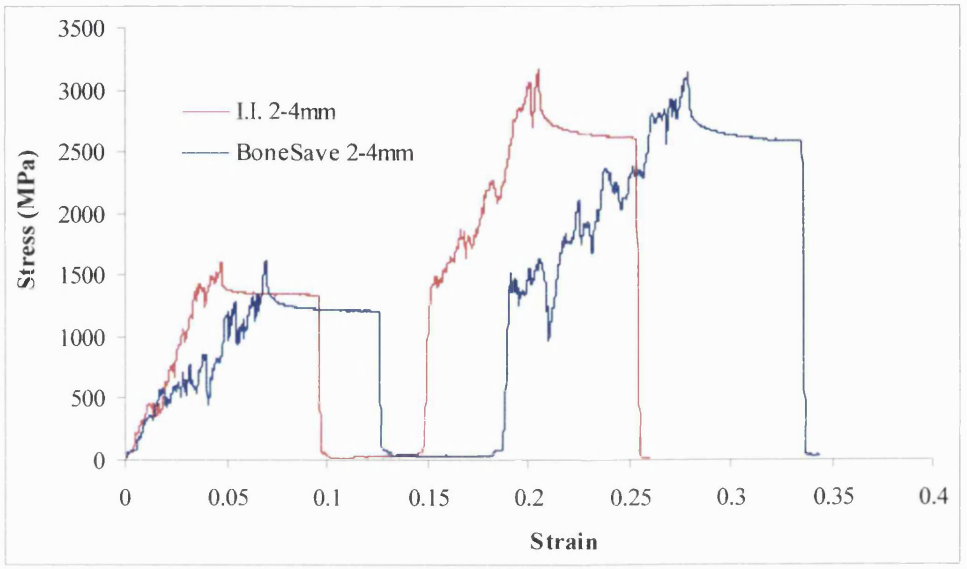

Figure 5.35: Die-plunger compression test for CaP granules fabricated from I.I. method and BoneSave®

Bone Substitute	Modulus up to 500N (GPa)	Modulus from 500 – 1000N (GPa)
BoneSave®	29.5	45.1
2 – 4mm sized CaP granules	49.6	66.5
3 – 5mm sized CaP granules	40.3	66.4

Table 5.4: The respective moduli for the two different granules tested

The granules produced using the I.I. method had a higher compressive modulus relative to BoneSave®. This is particularly true for the 2-4mm sized granules. Larger sized granules tend to shear at the edges as they topple and re-order themselves on loading hence have a lower compressive modulus. It must be noted that the moduli reported are not the true material moduli due to the toppling effect of the granules on testing. The results are purely relative within the batch tested.

The research has successfully fabricated granules that are similar in size to current/commercial alternatives for impaction grafting, but with higher compressive moduli. The fabricated granules have the added advantage over BoneSave® of having interconnected porosity.

5.4.2 Block Graft Material for Maxillofacial Operations

Maxillofacial operations or jaw reconstruction surgery, offer a vast area of application for synthetic bone graft materials. With the difficulty in shaping allograft material, due to its relatively high mechanical properties and the extra surgical site required for autograft procedures, there is a need to develop a bone substitute that can be specifically tailored for individual requirements in order to fabricate blocks, wedges and space fillers at the time of surgery. Figures 5.36 and 5.37 show I.I. bioceramics that have interconnected macroporosity and that have been ground down very simply and quickly to produce different shapes that could be used as space fillers in maxillofacial operations.

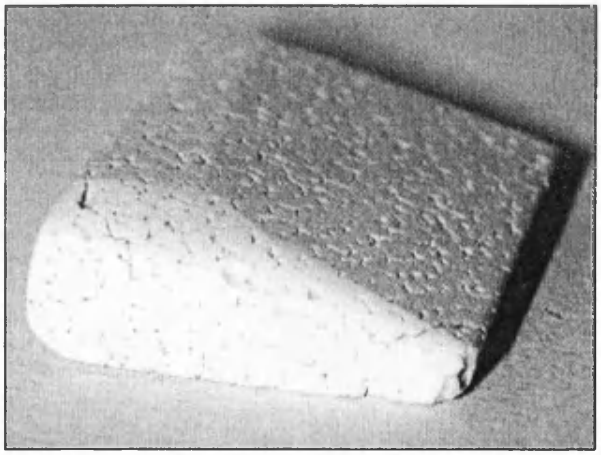

Figure 5.36: A wedge of β-TCP I.I. bioceramic ground down for potential use in maxillofacial operations. Scale: 1cm = 2mm

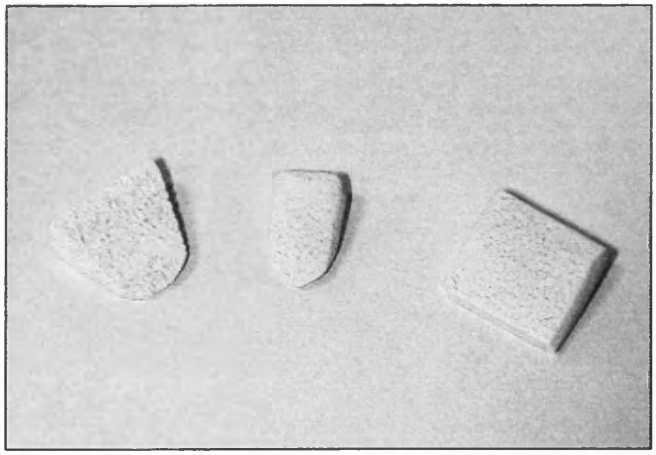

Figure 5.37: Further examples of the varying shapes that can be produced from the I.I. procedure. HA bioceramics are shown in this figure. Scale: 1cm = 1cm

The above images once again illustrate the diversity of the process in producing a broad range of sizes and shapes for specific operations. In addition, chemical compositions can also be tailored by using the two different base powders – 118 and 130.

5.4.3 Spinal Fusion Interbody Graft Material

In certain surgical procedures in the spine, cylindrical spinal fusion graft material is required to assist bone ingrowth between vertebrae in the spinal column e.g. for broken spinal discs that have been ruptured into the spinal column. At present hollow metal (usually titanium) cylindrical cages 8-12mm in diameter and 12-20mm in length are filled with allograft material in order to aid bone growth between the two vertebrae. There are perceived advantages in developing an alternative in the form of the bioceramic components similar to those developed in the current research programme. Figures 5.38 to 5.40 illustrate the type of material fabricated and the type of structure that could be used in this type of surgery.

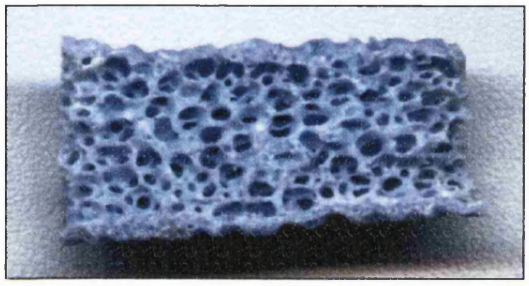

Figure 5.38: Example of HA SF bioceramic produced by current method cut longitudinally

Figure 5.39: SF bioceramic image taken from above

Figure 5.40: Examples of HA, α-TCP and β-TCP SF bioceramics

The samples have an internal interconnected macroporosity network resembling cancellous bone with a 1-3mm thick outer dense shell to promote structural integrity. Results from the present research showed that untreated SF bioceramics (no sol-gel treatment) had an average compressive stress of 3MPa, with those SF bioceramics treated with soda sol-gel having

compressive stresses averaging 6MPa. This was achieved by improving the structure-property relationship of the bioceramics without compromising the interconnected macroporosity network.

5.4.4 Chondylar Defects

These non-load bearing samples are required for filling in defects in knee joints whereby diseased cartilage and bone (e.g. due to severe degenerative arthritis) has been worn away to leave defects. These space fillers ideally should have interconnected porosity in the correct size range for bone formation and ingrowth (i.e. 150 - 300μm). Examples of porous scaffolds fabricated in this research are shown in figures 5.41 and 5.42 below.

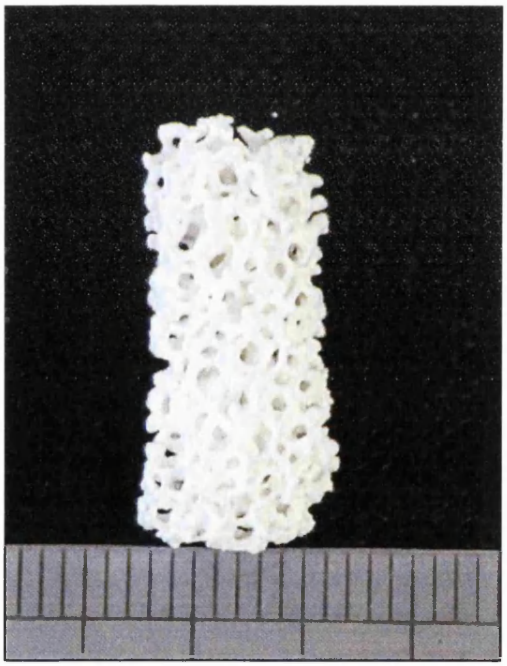

Figure 5.41: Porous scaffold bioceramic produced from 30 ppi porosifier and sintered at 1150°C

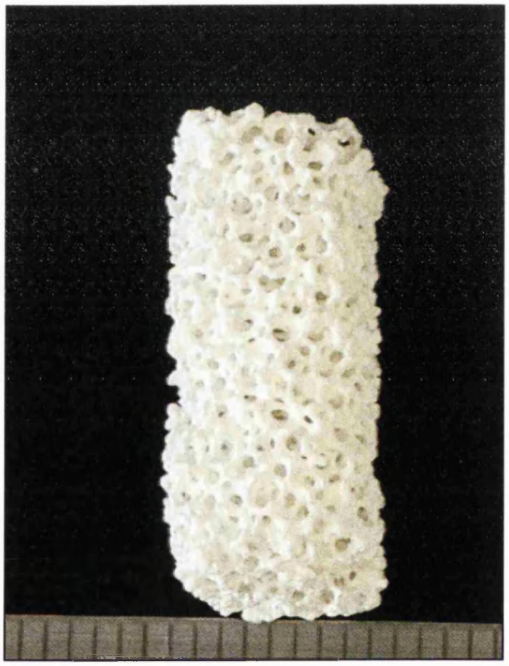

Figure 5.42: Porous scaffold bioceramic produced from 45 ppi porosifier and sintered at 1150°C

The samples shown above are cylindrical versions of the OPS bioceramics or conversely, SF bioceramics without the dense outer shell. The dense outer shell is not incorporated, as these samples are required for non-load bearing applications, although SF bioceramics could also be used.

The range of samples described here highlights the diversity of the process developed in this research. Size and shape can be tailored as well as the chemical composition and interconnected porosity distributions. Producing bioceramics with the correct interconnected pore size range for bone ingrowth, combined with appropriate mechanical properties, suggests that the bioceramics have the potential to be successful bone substitute materials.

5.5 Conclusions

The main aims and objectives of the research have been successfully achieved. These were to fabricate HA/TCP bioceramic scaffolds of varying geometries, with open, interconnected pores in the appropriate size range for potential bone formation, that also have sufficient mechanical strength to withstand load-bearing activities *in-vivo*.

This study confirmed the potential of the fabricated bioceramics for use as bone substitute materials. The research was driven by both the need to supplement the materials structure-property relationship, and also by clinical needs. However, the research has been directed towards structural improvements, resulting in improved mechanical properties.

The initial aim of this research was to produce HA/TCP bioceramics with an interconnected porosity in the correct size range for possible bone formation and ingrowth. This was achieved by the development of Impact-Impregnated (I.I.) bioceramics. However, the size of the porosity along with the low total volume porosity, was not ideal for bone remodelling.

In developing novel techniques to producing Open Porous Scaffold (OPS) bioceramics, a high volume interconnected porosity network was successfully fabricated, resembling that of cancellous bone. This offered an improved pore size, shape and porosity structure, when compared to the I.I. bioceramics. The formation of microcracks on sintering, on the interconnected struts, combined with low densities, lowered the stress to cause failure, and therefore lowered the mechanical properties of the OPS bioceramics. These properties were not adequate for possible load-bearing applications.

However, the techniques developed in producing OPS bioceramics were used to retain the same porosity network for Spinal Fusion (SF) bioceramics. These samples were produced for a specific clinical application with improvements made to the mechanical properties, by the

fabrication of a dense outer shell protecting the interior porosity network and increasing density. This was achieved without compromising the structure of the interior porosity network.

Further treatment of these SF bioceramics by the use of sol-gel solutions, resulted in further improvements to the microstructure, for example, by addressing the issue of surface microcracks. The interconnected macroporosity network was not compromised by this method. Hence, the SF bioceramics treated with sol-gel solution had increased mechanical properties due to improvements made in the structure-property relationship. Therefore, the potential for these bioceramics to be used in load-bearing applications is enhanced.

In addition to manufacturing HA/TCP bioceramics with varying geometries and adequate load-bearing capabilities and porosity requirements, materials for other clinical applications have also been produced. These include granular material for use as an alternative to a commercially available product BoneSave®, developed by Stryker Orthopaedics. In a comparison between BoneSave® and the granular material developed in this research, the developed granular material had improved mechanical resistance to loading. Cylindrical OPS samples have been produced for possible use in non-weight bearing chondylar repair. In addition, I.I. bioceramics in the form of wedges for potential use in maxillofacial applications have also been developed. This illustrates the diversity of applications possible with the materials developed, and the range of sample geometries that can be fabricated.

To conclude, the materials developed in the current research programme offer structural and mechanical advantages over other bioceramic materials. The fabrication procedure guaranteed an interconnected macroporosity network within the HA/TCP scaffold and high volume porosity, with pores in the appropriate size range for bone ingrowth. This was combined with adequate mechanical properties for possible load-bearing applications. Superior ranges of materials suitable for a diversity of applications have therefore successfully been developed.

5.5.1 Future Work

The results from the current programme indicate the need for further research in the following areas:

- Biological/Dissolution Studies
- Further Improvements to the Structure-Property Relationship
- Composition and Orientation

Biological/Dissolution Studies

- Due to the nature of the microporous structure of the materials produced (in particular high microporosity β-TCP bioceramics), there is a possibility of using the materials as a base for drug carriers (such as bone morphogenetic proteins), to enable diseased or infected bone to be treated via a drug release mechanism through the micropores. This shows promise especially in the β-TCP bioceramics due to their large surface areas at the microstructural level and excellent wicking properties.
- A simulated body fluid study is required in order to assess the potential of the fabricated bioceramics to participate in ionic interactions to form CaP deposits on its surface. The commercially available product BoneSave® is produced from the same powders used in this study, and hence it would be assumed that the bioceramics fabricated in this research would behave in a similar manner both *in-vitro* and *in-vivo.*
- A study of the effect on the dissolution on the strength properties of the materials produced would also be required. Materials could be removed from a simulated body fluid after set periods e.g. one day, four days, one week, one month etc, and mechanically tested.
- In addition to simulated body fluid tests and *in-vivo* experiments on the HA/TCP bioceramics produced, it would be necessary to run a comparison study between the SF bioceramics and those SF bioceramics treated with sol-gel solution with improved mechanical properties. Any strength improvements due to surface or microstructural changes would ultimately affect the potential biological response of the bioceramics. This would be required to be researched both *in-vitro* and *in-vivo.*

Further Improvements to the Structure-Property Relationship

- In order to improve the mechanical properties without compromising the hierarchial porosity size range, many different processes such as compression treatment by plasma spraying, flame glazing or ion exchange whereby smaller ions are exchanged in the atomic lattice inducing compressive stresses by solid solution hardening (e.g. Zr) may be researched to reduce the potential of crack growth on loading.
- To evaluate crack lengths that determines failure (i.e. Griffith flaws) in the bioceramics produced, and to perform a study to investigate the strength improvements due to changes in size of the Griffith flaws.
- Low thermal coefficient expansion coatings, that on cooling place the surface of a material under compression, and hence improve the mechanical properties by stunting crack growth, is also an area of future research.

Composition and Orientation

- A compositional change to the apatite structure in CaP bioceramics induces not only structural and mechanical changes, but also affects the dissolution and biocompatibility of the materials. The introduction of materials that exhibit such effects as piezoelectricity and ferroelectricity could be of use in the body as polarised materials aid bone growth at an accelerated rate [162].
- To continue the research started in the current programme on altering the orientation of the porosity within the OPS bioceramics. Sol-gel treatments (as used in the SF research) could be employed to evaluate how elliptical shaped pores affect the strength of the bioceramics as opposed to those scaffolds with spherical shaped pores.

Chapter 6 References

[1] Cowin, S. C. (2001). *Bone Mechanics Handbook 2nd Edition.* CRC Press

[2] Cowin, S. C. (1989). *Bone Mechanics Handbook 1st Edition.* CRC Press

[3] Netter, F. H. (1987). *The Netter Collection of Medical Illustrations Vol. 8. Part I.* Novartis – Union Graphics Inc.

[4] Odgaard, A., Weinans, H. (1995). *Bone Structure and Remodelling.* World Scientific

[5] Gibson, L. J., Ashby, M. F. (1999). *Cellular Solids: Structure and Properties. 2nd Edition.* Cambridge University Press.

[6] An, Y. H., Draughn, R. A. (2000). *Mechanical Testing of Bone and the Bone-Implant Interface.* CRC Press.

[7] Minaur, N. J. (1998). *Methotrexate and Bone Formation and Turnover in Rheumatoid Arthritis.* Ph.D. Thesis, University of Bath.

[8] Junqueiria, L. C., Carneiro, J., O'Kelly, R. (1998). *Basic Histology 9th Edition.* Appleton and Lange, Stanford, Connecticut.

[9] Torun-Kose, G., Korkusuv, F., Hasirici, V. (2002). Bone Generation via Tissue Engineering. **In:** *17th European Society for Biomaterials Conference*, Barcelona, Spain 11-14th Sept. 2002, p. P238.

[10] Pecile, A., de Barnard, B. (1989). Bone Regulatory Factors. **In:** *NATO Series A: Life Sciences*, 2-12 May 1989, p. AS1

[11] Hall, B. K. (1990). *Bone Volume I: The Osteoblast and Osteocyte.* The Telford Press

[12] Cornell, C. N., Lane, J. M. (1998). Current Understanding of Osteoconduction in Bone Regeneration. *Clinical Orthopaedic and Related Research*, **355S**, pp. 267-273.

[13] Nicholson, P. H., Chang, X. G., Lowet, G., Boonen, S., Davie, M. W., Dequeber, J., van der Peere, G. (1997). Structural and Material Mechanical Properties of Human Vertebrae Cancellous Bone. *Medical Engineering and Physics,* **19** (8) pp. 729-737.

[14] Jensen, K. S., Mosekilde, L. S., Mosekilde, L. E. I. F. (1990). A model of Vertebral Trabecular Bone Architecture and its Mechanical Properties. *Bone*, **11**, pp. 417-423.

[15] Rho, J. Y., Kuhn-Spearing, L., Zioupos, P. (1998). Mechanical Properties and the Hierarchial Structure of Bone. *Medical Engineering and Physics,* **20**, pp. 92-102.

[16] Gibson, L. J. (1985). The Mechanical Behaviour of Cancellous Bone. *Journal of Biomechanics,* **18** (5) pp. 317-328.

[17] Habal, M. B., Reddi, A. H. (1992). *Bone Grafts and Bone Substitutes.* Saunders, London

[18] Evans, F. G. (1973). *Mechanical Properties of Bone.* Charles C. Thomas, Springfield Il.

[19] Meade, J. B., Cowin, S. C., Klawitter, J. J., Vanburskirk, W. C., Skinner, H. B. (1984). Bone Remodelling due to Continuously Applied Loads. *Calcified Tissue International,* **36**, pp. S25-S30.

[20] Urist, M. R. (2002). Bone: Formation by Autoinduction. *Clinical Orthopaedic and Related Research*, **395**, pp. 5-10.

[21] Simske, S. J., Ayers, R. A., Bateman, T. A. (1997). Porous Materials for Bone Engineering. *Materials Science Forum*, **250**, pp. 151-182.

[22] Goldberg, V. M. (2000). Selection of Bone Grafts for Revision THA. *Clinical Orthopaedic and Related Research*, **381**, pp. 68-76

[23] Habal, M. B., Reddi, A. H. (1992). *Bone Grafts and Bone Substitutes.* Saunders, London, pp. 220.

[24] Habal, M. B., Reddi, A. H. (1992). *Bone Grafts and Bone Substitutes.* Saunders, London, pp. 79.

[25] Habal, M. B., Reddi, A. H. (1992). *Bone Grafts and Bone Substitutes.* Saunders, London, pp. 6.

[26] Habal, M. B., Reddi, A. H. (1992). *Bone Grafts and Bone Substitutes.* Saunders, London, pp. 278.

[27] Habal, M. B., Reddi, A. H. (1992). *Bone Grafts and Bone Substitutes.* Saunders, London, pp. 14.

[28] Tadman, J.(Ed.). (2002). Hip Revision. *Arthritis Today,* No. 118, pp. 12-14.

[29] Benjamin, J., Engh, G., Parsley, B., Donaldson, T., Coon, T. (2001). Morselised Bone Grafting of Defects in Revision TKA. *Clinical Orthopaedics and Related Research,* **392**, pp. 62 - 67.

[30] Habal, M. B., Reddi, A. H. (1992). *Bone Grafts and Bone Substitutes.* Saunders, London, pp. 21.

[31] Schreurs, B. W., Sloof, T. J. J. H., Garderuers, J. W. M., Buma, P. (2001). Acetabular Reconstruction with Bone Impaction Grafting and a Cemented Cup – 20 years' experience. *Clinical Orthopaedics and Related Research,* **393**, pp. 202-215.

[32] Hoeffel, D. P., Rubash, H. E. (2000). Revision TKA. *Clinical Orthopaedics and Related Research,* **380**, pp. 116-132.

[33] Bradley, G. W. (2000). Revision TKA by Impaction Bone Grafting. *Clinical Orthopaedics and Related Research,* **371**, pp. 113-118.

[34] Harris, W. H. (1992). The First 32 years of Total Hip Replacement. *Clinical Orthopaedics and Related Research,* **274**, pp. 6-11.

[35] Callaghan, J. J. (1992). Total Hip Athroplasty. *Clinical Orthopaedics and Related Research*, **276**, pp. 33 – 40.

[36] Boldt, J. G., Dilawari, P., Agarwal, S., Drabu, R. J. (2001). Revision THA using Impaction Bone Grafting with Cemented Non-Polished Stems and Charnley Cups. *Journal of Arthroplasty,* **16** (8), pp. 943-952.

[37] Stulberg, S. D. (2002). Impaction Grafting – Doing it Right. *Journal of Arthroplasty,* **17** (4), pp. 147-152.

[38] Ullmark, G., Orbrant, K. J. (2002). Histology of Impacted Bone-Graft Incorporation. *Journal of Arthroplasty,* **17** (2), pp. 150-157.

[39] Garino, J. P. (2002). The Use of Impaction Grafting in Revision TKA. *Journal of Arthroplasty,* **17** (4), pp. 94-97.

[40] Dennis, D. A. (2002). The Structural Allograft Composite in Revision TKA. *Journal of Arthroplasty,* **17** (4), pp. 90-93.

[41] Smit, T. H., Mueller, R., van Dijk, M., Wuisman, P. I. J. M. (2002). Changes in Trabecular Bone Architecture During Spinal Fusion. **In:** *17th European Society for Biomaterials Conference*, Barcelona, Spain 11-14th Sept. 2002, p. L9.

[42] Yamamuro, T. (Ed.), Hench, L. L., Wilson, J. (1990). *Handbook of Bioactive Ceramics Vol. II: Calcium Phosphate Hydroxylapatite Ceramics.* CRC Press Boston, pp. 345-354.

[43] Wang, J., Chen, W., Li, Y., Fan, S., Weng, J., Zhang, X. (1998). Biological Evaluation of Biphasic Calcium Phosphate Ceramic Vertebral Laminate. *Biomaterials,* **19** (15), pp. 1387-1392.

[44] Habal, M. B., Reddi, A. H. (1992). *Bone Grafts and Bone Substitutes.* Saunders, London, pp. 7.

[45] Simske, S. J., Ayers, R. A., Bateman, T. A. (1997). Porous Materials for Bone Engineering. *Materials Science Forum*, **250**, pp. 151-182.

[46] Reis, R. L., Lunha, M. H., Fernandes, R. N., Correia, A. M. (1997). Treatments to Induce the Nucleation and Growth of Apatite-like layers on Polymeric Surfaces and Foams. *Journal of Mat. Sci.: Mat. In Med.,* **8**, pp. 897-905.

[47] Hench, L. L. (1998). Bioceramics. *Journal of American Ceramic Society,* **81** (7), pp. 1705-1728.

[48] Ravaglioli, A., Krajewski, A. (1997). Implantable Porous Bioceramics. *Materials Science Forum,* **250**, pp. 221-230.

[49] Jarcho, M. (1981). Calcium Phosphate Ceramics as Hard Tissue Prosthesis. *Clinical Orthopaedics and Related Research,* **157**, pp. 259-278.

[50] LeGeros, R. Z. (2002). Properties of Osteoconductive Biomaterials: Calcium Phosphate. *Clinical Orthopaedics and Related Research,* **395**, pp. 81-98.

[51] Hench, L. L., Wilson, J. (1993). *An Introduction to Bioceramics.* World Scientific.

[52] Yamamuro, T. (Ed.), Hench, L. L., Wilson, J. (1990). *Handbook of Bioactive Ceramics Vol. II: Calcium Phosphate Hydroxylapatite Ceramics.* CRC Press Boston.

[53] Qu, S. X., Leng, Y., Guo, X., Cheng, J., Chen, W., Yang, Z. J., Zhang, X. D. (2002). The Ultrastructure Analysis of Heterotopic Osteogenesis in Porous Biphasic Calcium Phosphate Ceramics. **In:** *Bioceramics 14: Key Eng. Mat., No. 218-2, pp. 613-616.*

[54] Fabbri, M., Celotti, G. C., Ravaglioli A. (1995). HA based Porous Aggregates: Physico-Chemical Nature, Structure, Texture and Architecture. *Biomaterials*, **16**, pp. 225-228.

[55] Willmann, G. (1996). Medical Grade HA: State of the Art. *British Ceramic Transactions,* **95** (5), pp. 212-216.

[56] Daculsi, G. (2003). Why Develop Biphasic Calcium Phosphate Bioceramics in place of HA or β - TCP? *Journal of Mat. Sci.: Mat. in Med.,* **14**, pp. iii-iv.

[57] LeGeros, R. Z., Cin, S., Rchamizadeh, R., Mijares, D., LeGeros, J. P. (2003). Biphasic Calcium Phosphate Bioceramics: Preparation, Properties and Applications. *Journal of Mat. Sci.: Mat. in Med.,* **14**, pp. 201-209.

[58] Klein, C., de Groot, K., Chen, W. Q., Li, Y. B., Zhang, X. D. (1994). Osseous Substance Formation Induced in Porous Calcium Phosphate Ceramics in Soft Tissues. *Biomaterials,* **15** (1), pp. 31 – 34.

[59] Vaccario. A. R. (2002). The Role of the Osteoconductive Scaffold in Synthetic Bone Grafts. *Orthopedics,* **25** (5), pp. 571-578.

[60] Bonassar, L. J., Vacanti, C. A. (1998). Tissue Engineering: The First Decade and Beyond. *Journal of Cellular Biochemistry Supplements,* **30/31**, pp. 279-303.

[61] de Groot, K. (1982). Ceramics Based on Calcium Phosphates. **In:** *Ceramics in Surgery: Proceedings of the 2nd International Symposium on Bioceramics,* Lignano Sabbiadoro, Italy, 16 – 19th June 1982 (Vincenzini, P. ed.), pp. 79 – 91.

[62] Burg, K. J. L., Porter, S., Kellam, J. F. (2000). Biomaterial Developments for Bone Tissue Engineering. *Biomaterials,* **21** (23), pp. 2347 – 2359.

[63] Hing, K. A., Best, S. M., Bonfield, W. (1999). Characterisation of Porous Hydroxyapatite. *Journal of Materials Science: Materials in Medicine*, **10** (3), pp. 135 – 145.

[64] Royer, A., Vigiue, J. C., Heughebaert, M., Heughebaert, J. C. (1993). Stoichiometry of Hydroxyapatite: Influence on the Flexural Strength. *Journal of Materials Science: Materials in Medicine,* **4**, pp. 76 – 82.

[65] Liu, D. M. (1997). Influence of Porous Microarchitecture on the in-vitro dissolution and Biological Behaviour of Porous Calcium Phosphate Bioceramics. *Materials Science Forum,* **250**, pp. 183-208.

[66] Manjubala, I., Sastry, T. P. (2002). Structural and Morphological Analysis of Functionally Graded Calcium Phosphate Bioceramics. **In:** *Bioceramics 14: Key Eng. Mat, No. 218-2, pp. 89-92.*

[67] Duff, E. J., Grant, A. A. (1980). Apatite Ceramics for use in Implantation. **In:** *Mechanical Properties of Biomaterials: Proceedings to a conference by the Biomaterials Group of the Biological Engineering Society,* Keele University, Sept. 1978 (Hastings, G. W., and Williams, D. F., ed.), pp. 465 – 476. John Wiley and Sons Ltd.

[68] Gomes, M. E., Salgado, A., Godinho, J. S. et al. (2002). Evaluation of the Mechanical Properties and Biological Response to Osteoblastic Cells of Starch based Scaffolds for Bone Tissue Engineering Applications. **In:** *17th European Society for Biomaterials Conference*, Barcelona, Spain 11-14th Sept. 2002, p. P237.

[69] Wolke, J. G. C., van der Waerden, J. P. C. M., den Bakker, J. E. N., Jansen, J. A. (2002). Bone Behaviour to Calcium Phosphate Fillers. **In:** *17th European Society for Biomaterials Conference*, Barcelona, Spain 11-14th Sept. 2002, p. P153.

[70] Yuan H., van den Doel, M., van Blittersmijk, C. A., de Groot, K., de Bruijn, J. C. (2002). A Comparison of Two Calcium Phosphate Ceramics as Bone Tissue Engineering Scaffold in Goats. **In:** *17th European Society for Biomaterials Conference*, Barcelona, Spain 11-14th Sept. 2002, p. T159.

[71] Gerber, T. H., Yraybova, T., Henbel, K. O., Bienengraber, V. (2002). A New Bone Grafting Material Involved in Bone Remodelling. **In:** *17th European Society for Biomaterials Conference*, Barcelona, Spain 11-14th Sept. 2002, p. T24.

[72] Annaz, B., Hing, K. A., Kayser, M., Buckland, T., Di Silvio, L. (2002). In-vitro Assessment of Porous HA as a Bone Substitute. **In:** *17th European Society for Biomaterials Conference*, Barcelona, Spain 11-14th Sept. 2002, p. T20.

[73] Klein, C., de Groot, K., Chen, W. Q., Li, Y. B., Zhang, X. D. (1994). Osseous Substance Formation Induced in Porous Calcium Phosphate Ceramics in Soft Tissues. *Biomaterials,* **15** (1), pp. 31 – 34.

[74] Yuan, H. P., de Bruijn, J. D., Li, Y. B., Feng, J. Q., Yang, Z. J., Zhang, X. D., de Groot, K. (2001). Bone Formation Induced by Calcium Phosphate Ceramics in Soft Tissue of Dogs: A Comparative Study Between Porous α - TCP and β - TCP. *Journal of Materials Science: Materials in Medicine,* **12** (1), pp. 7 – 13.

[75] Kuon, S. H., Jun, Y. K., Hong, S. H., Lee, I.S., Kim, H.E., Won, Y.Y. (2002). Calcium Phosphate Bioceramics with Various Porosities and Dissolution Rates. *Journal of the American Ceramic Society,* **85** (12), pp. 3129-3131.

[76] O'Kelly, K., Tancred, D., McCormack, B., Carr, A. (1996). A Quantitative Technique for Comparing Synthetic Porous Hydroxyapatite Structures and Cancellous Bone. *Journal of Materials Science: Materials in Medicine,* **7** (4), pp. 207 – 213.

[77] Klein, C., de Groot, K., Chen, W. Q., Li, Y. B., Zhang, X. D. (1994). Osseous Substance Formation Induced in Porous Calcium Phosphate Ceramics in Soft Tissues. *Biomaterials,* **15** (1), pp. 31 – 34.

[78] Holden, G. F. (1980). Tissue Reaction to the Bioceramic Synthos. **In:** *Mechanical Properties of Biomaterials: Proceedings to a conference by the Biomaterials Group of the Biological Engineering Society,* Keele University, Sept. 1978 (Hastings, G. W., and Williams, D. F., ed.), pp. 445 - 456. John Wiley and Sons Ltd.

[79] Hing, K. A., Best, S. M., Tanner, K. E., Bonfield, W., Ravell, P. A. (1997). Biomechanical Assessment of Bone Ingrowth in Porous Hydroxyapatite. *Journal of Materials Science: Materials in Medicine,* **8** (12), pp. 731 – 736

[80] Liu, D. M. (1996). Control of Pore Geometry on Influencing the Mechanical Properties of Porous HA Ceramic. *Journal of Material Science Letters,* **15**, pp. 419 – 421.

[81] Denhollader, W., Patka, P., Klein, C. P. A. T., Heidendal, G. A. K. (1991). Macroporous Calcium Phosphate Ceramics for Bone Substitutes – A Tracer Study on the Biodegradation with ^{45}Ca Tracer. *Biomaterials*, **12** (6), pp. 569 – 573.

[82] Martin, R. I., Brown, P. W. (1995). Mechanical Properties of HA formed at Physiological Temperatures. *Journal of Materials Science: Materials in Medicine,* **6**, pp. 138 – 143.

[83] Daculsi, G., Laboux, O., Malard, O., Weiss, P. (2003). Current state of the art of Biphasic Calcium Phosphate Bioceramics. *Journal of Mat. Sci.: Mat. in Med., **14**, pp. 195-200.*

[84] Richart, O., Descamps, M., Liebetran, A. (2000). Macroporous Calcium Phosphate Ceramics: Optimisation of the Porous Structure and its Effect on the Bone Ingrowth in a Sheep Model. **In:** *Bioceramics: Proceedings of the 13th International Symposium on Ceramics in Medicine*, Bologna, Italy, 22 – 26 Nov. 2000, pp. 425 – 428.

[85] Yuan H. P., De Bruijn, J. D., Zhang, X. D., van Blitterswijk, C. A., de Groot, K. (2001). Use of an Osteoinductive Biomaterial as a Bone Morphogenetic Protein Carrier. *Journal of Materials Science: Materials in Medicine,* **12** (9), pp. 761-766.

[86] Martinetti, R., Belpassi, A., Nataloni, A., Piconi, C. (2000). Porous Hydroxyapatite Cell Carrier for Tissue Engineering. **In:** *Bioceramics: Proceedings of the 13th International Symposium on Ceramics in Medicine*, Bologna, Italy, 22 – 26 Nov. 2000, pp. 507 - 510.

[87] Werner, J., Linner-Kremer, B., Friess, W., Greill, P. (2002). Mechanical Properties and *In-Vitro* Cell Compatibility of HA Ceramics with Graded Pore Structure. *Biomaterials,* **23** (21), pp. 4285-4294.

[88] Blom,A. W., Grimm, B., Cunningham, J., Miles, A. W., Learmonth, I.D. (2002). In-vitro Testing of BoneSave, a Ceramic Bone Graft Substitute for use in Impaction Grafting. **In:** *Bioceramics 14: Key Eng. Mat, No. 218-2, pp. 417-420.*

[89] Hing, K. A., Best, S. M., Tanner, K. E., Bonfield, W., Revell, P. A. (1999). Quantification of Bone Ingrowth Within Bone Derived Porous HA Implants of Varying Density. *Journal of Materials Science: Materials in Medicine*, **10** (10 – 11), pp. 663 – 670.

[90] Li, S. H., de Groot, K., Layrdle, P. (2002). Bioceramic Scaffold with Controlled Porous Structure for Bone Tissue Engineering. **In:** *Bioceramics 14: Key Eng. Mat, No. 218-2, pp. 25-29.*

[91] Gatti, M. A., Monari, E., Salvatori, R., Martinetti, R., Belpassi, A. (2002). Porous HA devices: Experimental study in sheep. **In:** *17th European Society for Biomaterials Conference*, Barcelona, Spain 11-14th Sept. 2002, p. P151.

[92] Newesely, H., Osborn, J. F. (1980). Structural and Textural Implications of Calcium Phosphate in Ceramics. **In:** *Mechanical Properties of Biomaterials: Proceedings to a conference by the Biomaterials Group of the Biological Engineering Society,* Keele University, Sept. 1978 (Hastings, G. W., and Williams, D. F., ed.), pp. 457 - 464. John Wiley and Sons Ltd.

[93] van Blitterswijck, C.A., Hesseling, S.C., Grote, J. J., Koerten, H. K., de Groot, K. (1990). The Biocompatibility of Hydroxyapatite Ceramics: A Study of Retrieved Human Middle Ear Implants. *Journal of Biomedical Materials Research*, **24**, pp. 433 – 453.

[94] Richart, O., Descamps, M., Liebetrau, A. (2002). Preparation and Mechanical Characterisation of HA Monodispersed Macroporous Structure. Influence of Interconnection and Macroporous Diameters. **In:** *Bioceramics 14: Key Eng. Mat, No. 218-2, pp. 9-12.*

[95] Le Huec, J. C., Schaeverbebe, T., Clement, D., Faber, J., Le Rebellar, A. (1995). Influence of Porosity on the Mechanical Resistance of Hydroxyapatite Ceramics under Compressive Stress. *Biomaterials,* **16** (2), pp. 113 – 118.

[96] Gibson, R., Ke, S., Hing, K. A. (2002). Characterisation of Mono- and Biphasic Calcium Phosphate Granules. **In:** *Bioceramics 14: Key Eng. Mat, No. 218-2, pp. 625-628.*

[97] Grimm, B., Miles, A. W., Turner, I. G. (2001). Optimising a HA/TCP ceramic as a Bone Graft Extender for Impaction Grafting. *Journal of Materials Science: Materials in Medicine,* **12**, pp. 929-934.

[98] Grimm, B., Gozzard, C., Miles, A. W., Turner, I. G. (2002). Comparing Compression Properties of Bone Grafts, Ceramic Grafts and Graft Mixes for Impaction Grafting. **In:** *17th European Society for Biomaterials Conference*, Barcelona, Spain 11-14th Sept. 2002, p. L10.

[99] Grimm, B., Miles, A. W., Turner, I. G., Blom, A. W. (2002). In-vitro Endurance Testing of Bone Graft Materials for Impaction Grafting. *Key Engineering Materials,* **218-220**, pp. 375-378.

[100] Tampieri, A., Celotti, G., Sprio, S., Delcogliario, A., Franzese, S. (2001). Porosity graded HA Ceramics to Replace Natural Bone. *Biomaterials,* **22** (11), pp. 1365-1370.

[101] Gabriel-Chu, T. M., Orton, D. G., Hollister, S. J., Feinberg, S. E., Hollaran, J. W. (2002). Mechanical and in-vivo Performance of HA Implants with Controlled Architectures. *Biomaterials,* **23**, pp. 1283-1293.

[102] Liu, D. M. (1996). Fabrication and Characterisation of Porous Hydroxyapatite Granules. *Biomaterials,* **17** (20), pp. 1955 – 1957.

[103] Arita, I.H., Wilkinson, D. S., Mondragon, M. A., Castano, V. M. (1995). Chemistry and Sintering Behaviour of thin HA Ceramics with Controlled Porosity. *Bioamterials,* **16**, pp. 403-408.

[104] Heime, G., Griss, P., Jentshura, G., Werner, E. (1980). Bioinert and Bioactive Ceramics in Orthopaedic Surgery. **In:** *Mechanical Properties of Biomaterials: Proceedings to a conference by the Biomaterials Group of the Biological Engineering Society,* Keele University, Sept. 1978 (Hastings, G. W., and Williams, D. F., ed.), pp. 207 - 215. John Wiley and Sons Ltd.

[105] Duff, E. J., Grant, A. A. (1980). Apatite Ceramics for use in Implantation. **In:** *Mechanical Properties of Biomaterials: Proceedings to a conference by the Biomaterials Group of the Biological Engineering Society,* Keele University, Sept. 1978 (Hastings, G. W., and Williams, D. F., ed.), pp. 465 – 476. John Wiley and Sons Ltd.

[106] Pitto, R. P. (2000). Bone Graft Substitutes for Acetabular Reconstruction in Revision THA. **In:** *Bioceramics: Proceedings of the 13th International Symposium on Ceramics in Medicine*, Bologna, Italy, 22 – 26 Nov. 2000, pp. 947 – 950.

[107] Wang, J., Chen, W., Li, Y., Fan, S., Weng, J., Zhang, X. (1998). Biological Evaluation of Biphasic Calcium Phosphate Ceramic Vertebral Laminate. *Biomaterials,* **19** (15), pp. 1387-1392.

[108] Hirschfield, D. A., Li, T. K., Liu, D. M. (1996). Processing of Porous Oxide Ceramics. *Porous Ceramic Materials, Key Engineering Materials,* **115**, pp. 65-79.

[109] Tian, J. T., Tian, J. M. (2001). Preparation of Porous HA. *Journal of Materials Science,* **36** (12), pp. 3061-3066.

[110] Binner, J. G. P., Reichert, J. (1996). Processing of HA Ceramic Foams. *Journal of Materials Science,* **31** (19), pp. 5717 – 5723.

[111] Padilla, S., Roman, J., Vallet-Reggi, M. (2002). Synthesis of Porous HA by Combination of Gelcasting and foams burnout methods. *Journal of Materials Science: Materials in Medicine,* **13**, pp. 1193-1197.

[112] Haddow, D. B., James, P. F., van Noort, R. (1998). Sol-Gel derived CaP coatings for Biomedical Applications. *Journal of Sol-Gel Science and Technology,* **13**, pp. 261-265.

[113] Ruan, C. Y., Chen, Y. F., Xie, Y. S. (2002). Preparation of Porous HA Ceramics by a Stereo-mold method. *High Performance Ceramics 2001, Key Engineering Materials,* **224-226**, pp. 441-444.

[114] Dabbarah, F., El Zein, A. R., Chaput, C. (2002). A New Method of Preparation of CaP bioceramics. **In:** *Bioceramics 14: Key Eng. Mat, No. 218-2, pp. 17-20.*

[115] Tagai, H., Aoki, H. (1980). Preparation of Synthetic HA and Sintering of Apatite Ceramics. **In:** *Mechanical Properties of Biomaterials: Proceedings to a conference by the Biomaterials Group of the Biological Engineering Society,* Keele University, Sept. 1978 (Hastings, G. W., and Williams, D. F., ed.), pp. 477 - 488. John Wiley and Sons Ltd.

[116] Lu, H., Qu, Z., Zhou, Y. (1998). Preparation and Mechanical Properties of Dense Polycrystalline HA through Freeze-drying. *Journal of Materials Science: Materials in Medicine,* **9** (10), pp. 583-587.

[117] Ozgur Engin, N., Cuneyt Tas, A. (2000). Preparation of Porous $Ca_{10}(PO_4)_6(OH)_2$ and β - $Ca_3(PO_4)_2$ Bioceramics. *Journal of the American Ceramic Society,* **83** (7), pp. 1581-1584.

[118] Ozgur Engin, N., Cuneyt Tas, A. (1999). Manufacture of Macroporous Calcium Hydroxyapatite Bioceramics. *Journal of the European Ceramic Society,* **19**, pp. 2569-2572.

[119] Peng, H. X., Fan, Z., Evans, JRG. (2000). Factors Affecting the Microstructure of a Fine Ceramic Foam. *Ceramics International,* **26** (8), pp. 887-895.

[120] Innocentini, M. D. M., Sepulveda, P., Salvini, V. R., Pandolfeeli, V. C., Coury, J. R. (1998). Permeability and Structure of Cellular Ceramics: A comparison between two preparation techniques. *Journal of the American Ceramic Society,* **81** (12), pp. 3349-3352

[121] Sepulveda, P., Bressiani, A. H., Bressiani, J. C., Meseguer, L. (2002). Synthesis and Properties of Ceramic Foams for Hard Tissue Repair. **In:** *Bioceramics 14: Key Eng. Mat, No. 218-2, pp. 413-416.*

[122] Yasuda, H. Y., Mhara, S., Nishiyama T., Terashita, N., Umakoshi, Y. (2002). Preparation of HA based composites by Colloidal Process. *Tissue Engineering for Therapeutic Use 6,international Congress Series,* No. 1243, pp. 155-160.

[123] Liu, D. M. (1997). Fabrication of Hydroxyapatite Ceramic with Controlled Porosity. *Journal of Materials Science: Materials in Medicine*, **8** (4), pp. 227 – 232.

[124] Zakaria, F. A. (2000). *Sintering and Microstructure Property Relationships of Porous Hydroxyapatite.* PhD Thesis. University of Bath.

[125] Rodriguez-Lorenzo, L. M., Vallet-Reggi, M., Ferreira J. M. F., Ginebra, M. P. (2002). HA ceramic bodies with Tailored Mechanical Properties for Different Applications. *Journal of Biomedical Materials Research,* **60** (1), pp. 159-166.

[126] Koh, Y. H., Kim, H. W., Kim, H. E. (2002). Fabrication of Macrochanneled HA Bioceramic by a Coextrusion Process. *Journal of the American Ceramic Society,* **85** (10), pp. 2578-2580.

[127] Antsiferov, V. N., Ovchinnikova, V. I. (1997). Optimisation of the Rheological Properties of Suspensions for the Production of Open Cell Foamed Ceramics. *Refractories and Industrial Ceramics,* **38** (3-4), pp. 111-114.

[128] Carotenuto, G. (1998). Dense/Porous layered Hydroxylapatite Ceramic for Orthopaedic Device Coating Prepared by Tape Casting. *Advanced Performance Materials,* **5**, pp. 171-181.

[129] Roncari, E., Galassi, C., Pinasco, P. (2000). Tape Casting of Porous HA Ceramics. *Journal of Materials Science Letters,* **19**, pp. 33-35.

[130] Liu, D. M. (1998). Preparation and Characterisation of Porous HA bioceramics via a Slip Casting route. *Ceramics International,* **24**, pp. 441-446.

[131] Schwarzwalde, K., Somers, A. V. (1963). Methods of Making Porous Ceramic Articles. *U.S. Patent No. 3,090,094.*

[132] Rice, R. W., Kahn, M., Shadwell, D. E. (1987). Ceramic Body with Ordered Pores. *U. S. Patent No. 4,683,161.*

[133] Colombo, P., Hellmann, J. R. (2002). Ceramic Foams from Preceramic Polymers. *Materials Research Innovations,* **6** (5-6), pp. 260-272.

[134] Zhu, X. W., Jiang, D. L., Tan, S. H. (2002). The control of slurry rheology in the processing of reticulated porous ceramics. *Materials Research Bulletin,* **37** (3), pp. 541-553.

[135] Zhu, X. W., Jiang, D. L., Tan, S. H. (2002). An Innovative Approach for Improving the Reliability of Reticulated Porous Ceramics. *Journal of Materials Science and Technology,* **18** (1), pp. 89-92.

[136] Brezny, R., Green, D.J. (1993). Uniaxial Strength Behaviour of Brittle Cellular Materials. *Journal of American Ceramic Society,* **76** (9), pp. 2185-2192.

[137] Kingery, W. D. (1960). *Introduction to Ceramics.* John Wiley and Sons, New York, pp.621.

[138] Cichocki Jr., F. R., Trumble, K. P., Rodel, J. (1998). Tailored Porosity Gradients via Colloidal Infiltration of Compression-Molded Sponges. *Journal of American Ceramic Society,* **81** (6), pp. 1661-1664.

[139] Jayasinghe, S. N., Edirisinghe, M. J. (2002). A Novel Method of Forming Open Cell Ceramic Foams. *Journal of Porous Materials,* **9**, pp. 265-273.

[140] Zhu, X. W., Jiang, D. L., Tan, S. H., Zhang, Z. Q. (2002). Improvement in the Strut Thickness of Reticulated Porous Ceramics. *Journal of American Ceramic Society,* **84** (7), pp. 1654-1656.

[141] Kim, H. W., Kim, H. E., Knowles, J. C. (2004). Bioactive Porous Bone Scaffolds Coated with Biphasic Calcium Phosphates. *Key Engineering Materials,* pp. 1103 – 1106.

[142] Kircher, H. P. (1979). *Strengthening of Ceramics – Treatments, Tests and Design Applications.* Marcel Dekker, New York, p. 12.

[143] Chang, Y. M., Birnie III, D, Kingery, W. D. (1997). *Physical Ceramics – Principle for Ceramic Science and Engineering.* John Wiley and Sons.

[144] Kircher, H. P. (1979). *Strengthening of Ceramics – Treatments, Tests and Design Applications.* Marcel Dekker, New York, p. 208.

[145] Cahn, R. W., Haasen, P., Kramer, E. J. (Eds.). (1996). *Materials Science and Technology – A Comprehensive Treatment. Volume 17A – Processing of Ceramics – Part I.* Wiley – VCH. p. 7.

[146] Bowen, H. K. (1980). Basic Research Needs on High Temperature Ceramics for Energy Applications. *Materials Science and Engineering,* **44**, pp. 1 – 56.

[147] Kircher, H. P. (1979). *Strengthening of Ceramics – Treatments, Tests and Design Applications.* Marcel Dekker, New York, p. 158.

[148] Bradley, D. C., Mehrota, R. C., Gaur, D. P. (1978). *Metal Alkoxides.* Academic Press, London.

[149] Haiduc, I., Zuckerman, J. J., de Gruyter, W. (Eds.). (1985). *Basic Organometallic Chemistry.* John Wiley and Sons.

[150] Bradley, D. C. (1989). Metal Alkoxides as Precursors for Electronic and Ceramic Materials. *Chemical Review,* **89**, pp. 1317 – 1322.

[151] Hench, L. L., West, J. K. (1990). The Sol-Gel Process. *Chemical Review,* ***90***, pp. 33 – 72.

[152] Mehrota, R. C. (1988). Polymetallic Alkoxides – Precursors for Ceramics. *Materials Research Society Symposium Proceedings,* **121**, pp. 81 – 91.

[153] Dislich, H., Laine, R. M. (1988). Technical Conversion of Alkoxides to Oxides, Yesterday, Today and Tomorrow. *Transformation of Organometallics into Common and Exotic Materials: Design and Activation,* Martinus Nijhoff Publishers, pp. 236 – 249.

[154] Brinker, C. J., Scherer, G. W. (1990). *Sol-Gel Science – The Physics and Chemistry of Sol-Gel processing.* Academic press, New York, NY, p. 2.

[155] Brinker, C. J., Scherer, G. W. (1990). *Sol-Gel Science – The Physics and Chemistry of Sol-Gel processing.* Academic press, New York, NY, p. 43.

[156] Brinker, C. J., Scherer, G. W. (1990). *Sol-Gel Science – The Physics and Chemistry of Sol-Gel processing.* Academic press, New York, NY, p. 25.

[157] Ulrich, D. R., Laine, R. M. (1988). Technical Conversion of Alkoxides to Oxides, Yesterday, Today and Tomorrow. *Transformation of Organometallics into Common and Exotic Materials: Design and Activation,* Martinus Nijhoff Publishers, pp. 207 - 235.

[158] Hench, L. L. (1997). Sol-Gel Materials for Bioceramic Applications. *Current Opinion in Solid State and Materials Science,* **2**, pp. 604 – 610.

[159] Uhlmann, D. R., Zelinski, B. J. J., Wnek, G. E. (1984). The Ceramisist as Chemist – Opportunities for New Materials. *Materials Research Society Symposium Proceedings,* **32**, pp. 59 – 70.

[160] Sepulveda, P., Jones, J. R., Hench, L. L. (2002). Bioactive Sol-Gel Foams for Tissue Repair. *Journal of Biomedical Materials Research,* **59**, pp. 340 – 348, John Wiley and Sons.

[161] Mackenzie, J. D., Pope, E. J. A., Sakka, S., Klein, L. C. (1994). Present and Future Directions in Sol-Gel Science and Technology. *Ceramic Transactions,* **55**, pp. 25 – 31.

[162] Kobayashi, T., Nakamura, S., Yamashita, K. (2001). Enhanced Osteobonding by Negative Surface Charges of Electrically Polarised Hydroxyapatite. *Journal of Biomedical Materials Research,* **57**, pp. 477 – 451.

APPENDIX

Presentation Conferences

1. Gittings, J. P., Turner, I.G., Miles, A. W. (2004). Development of Bone Substitute Materials – Calcium Phosphate Scaffold Materials. *Abstract and Poster for the Proceedings of the British Orthopaedic Research Society, Bristol, U.K.,* March 2004.

2. Gittings, J. P., Turner, I.G., Miles, A. W. (2004). Development of Bone Substitute Materials – Calcium Phosphate Scaffold Materials. *Proceedings of the 7th World Biomaterials Congress, Sydney, Australia,* May 2004.

3. Gittings, J. P., Turner, I.G., Miles, A. W. (2004). Calcium Phosphate Open Porous Scaffold Bioceramics. *Abstract and Poster for the Proceedings of the 17th International Symposium on Ceramics in Medicine – Bioceramics 17, New Orleans, U.S.A,* December 2004.

Publications

4. Gittings, J. P., Turner, I.G., Miles, A. W. (2005). Calcium Phosphate Open Porous Scaffold Bioceramics. *Key Engineering Materials*: **284 – 286**, pp. 349 – 352. Trans. Tech. Publications, Switzerland.

1. Gittings, J. P., Turner, I.G., Miles, A. W. (2004). Development of Bone Substitute Materials – Calcium Phosphate Scaffold Materials. *Poster and Abstract for the Proceedings of the British Orthopaedic Research Society, Bristol, U.K.,* March 2004.

Development of Bone Substitute Materials – Calcium Phosphate Scaffold Materials

Gittings, J. P.[1], Turner, I. G.[1], Miles, A. W.[2]

[1] Department of Engineering and Applied Science, [2] Department of Mechanical Engineering, University of Bath, Bath, BA2 7AY, U.K.

Introduction

Joint replacement procedures such as revision impaction grafting are stretching allograft bone stocks to their limits [1]. The need for synthetic alternatives that offer a structural and biological matrix for graft incorporation is paramount for future bone replacement and reconstruction surgery [2].

Hydroxyapatite/tricalcium phosphate (HA/TCP) synthetic bone graft alternatives have been shown to be biocompatibie with bone [3]. The presence of an interconnected porosity network has a strong influence on the osteoinductive potential of these synthetic bone graft materials [4].

Early work by the authors focused on an impact-impregnation (I.I.) technique to produce a dense bioceramic [5]. The current study describes the production of open porous scaffold (OPS) calcium phosphate ceramics that possess an interconnected open porous network in the required size range for osteoid growth and revascularisation.

Materials and Methods

Two grades of calcium phosphate powder were blended together to form a HA/TCP ceramic slip which was then ball milled for 24hrs with zirconia milling media. This slip was used to impregnate polyurethane (PU) foam via a mechanical plunging procedure. The impregnated foam was held above the slip bath in order for the slip to flow and coat the struts of the foam. The samples produced were then dried on tissue paper and treated with high velocity compressed air to avoid the formation of any closed cells. The impregnated blocks were dried at 120°C for 15hrs.

The PU foams were graded as 30 and 45 ppi (pores per inch). The slip viscosity ranged from 6000 – 8000 cps (measured with a Brookfield Viscometer, spindle no. 5 and at 10rpm).

Samples were sintered slowly up to 500°C to ensure PU burnout was complete. Sintering continued up to 1280°C to ensure densification. Final sintered dimensions were 40x25x10mm. Image analysis was performed using optical microscopy and scanning electron microscopy (SEM) analysis. Mechanical testing was performed by 3 point bending using an 1122 Instron machine. Figure 1 shows a typical example of the HA/TCP bioceramic scaffold produced.

Figure 1: Interconnected porosity of HA/TCP bioceramic scaffold produced by current method

Results

Typical macroporosity in the bioceramic scaffolds varied from 40-70% with over 79% of porosity lying in the size range 150-450μm in area equivalent diameter. The fabrication procedure guaranteed interconnected porosity. Figure 2 represents the porosity distribution of the open porous scaffolds (OPS) compared to those reported earlier by the impact-impregnation technique i.e. dense bioceramics [5].

The average pore size acknowledged for facilitating osteogenesis (i.e. > 300μm) has been met by the present fabrication technique.

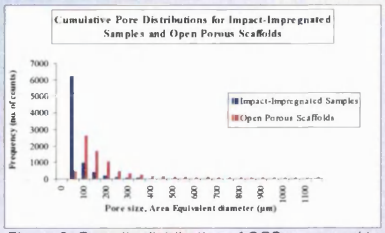

Figure 2: Porosity distribution of OPS compared to dense bioceramics previously produced

Figure 3 represents the strength-porosity relationship between the OPS and impact-impregnated bioceramics. Figure 4 illustrates the strength-density correlation in the calcium phosphate bioceramics produced.

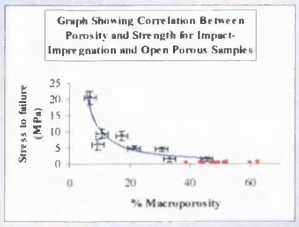

Figure 3: Strength-Porosity relationship for OPS and I.I. bioceramics

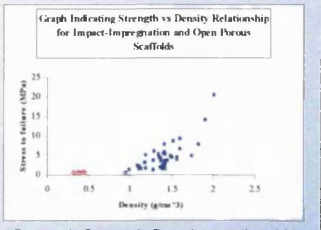

Figure 4: Strength-Density relationship for OPS and I.I. bioceramics

One hundred and twenty samples possessed a breaking stress, with a 95% confidence level, of 0.30MPa±0.01MPa. The low strengths reported were due to the formation of blow-out holes at triple point junctions on the interconnected struts. Figure 5 illustrates this phenomenon which is typical in all bioceramic scaffolds produced. A small applied stress may be magnified many times at the tip of a crack reducing the strength of the overall bioceramic.

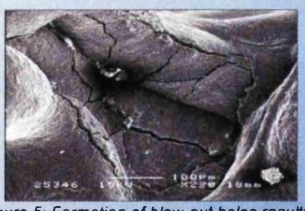

Figure 5: Formation of blow-out holes resulting in poor strengths due to critical crack formation

Conclusions

HA/TCP bioceramics with interconnected porosity in the size range appropriate for bone ingrowth have been successfully produced. The fabrication procedure has proved to be reliable and consistent. Future work will focus on eliminating microcracks in order to optimise mechanical properties.

Acknowledgments

The authors would like to thank the University of Bath and Stryker Howmedica Osteonics for their support.

References

[1] Hing et al. (1997). J. Mat. Sci.: Mat. Med., **8**(12) pp. 731 – 736.

[2] Klein et al. (1994). Biomaterials, **15**(1) pp. 31 – 34.

[3] Wang et al. (1993). J. Mat. Sci.: Mat. Med., **4**(2) pp. 150 – 158.

[4] Le Huec et al. (1995). Biomaterials, **16**(2) pp. 113 – 118.

[5] Casey et al. (2002). Proc. of 17th ESB Conference, Barcelona, p.P146.

UNIVERSITY OF BATH

centre for orthopaedic biomechanics

Development of Bone Substitute Materials – Calcium Phosphate Scaffold Materials

Gittings, J. P.[1], Turner, I. G.[1], Miles, A. W.[2]

[1] Department of Engineering and Applied Science, University of Bath, Bath, BA2 7AY, U.K
[2] Department of Mechanical Engineering, University of Bath, Bath, BA2 7AY, U.K.

Introduction

Joint replacement procedures such as revision impaction grafting and spinal fusion interbody operations are stretching allograft bone stocks to their limits [1]. The need for synthetic alternatives that offer a structural and biological matrix for graft incorporation are paramount for future bone regeneration procedures [2].
Synthetic bone graft alternatives that offer biocompatibility to the host bone (i.e. a biological response) such as hydroxyapatite/tricalcium phosphate (HA/TCP), in addition to possessing an interconnected porosity network have been shown to have a strong influence on the osteoinductive potential of these materials [3, 4, 5].
The current method allows the production of calcium phosphate ceramic components (CPC) that possess an interconnected open porous network in the required size range for osteoid growth and revascularisation.

Materials and Methods

The method can be described as the reticulated foam technique, whereby two grades of calcium phosphate powder are blended together to form a HA/TCP ceramic slip. The slip is then ball milled for 24hrs with zirconia milling media. This slip is used to impregnate polyurethane (PU) foam via a mechanical plunging procedure. The impregnated foam is then held above the slip bath in order for the slip to flow and coat the struts of the foam. The impregnated foam is then dried on tissue paper and treated with high velocity compressed air to avoid the formation of any closed cells.
Samples are dried at 120°C for 15hrs. The PU foams are graded as 30 and 45ppi (pores per inch). The slip viscosity ranges from 6000 – 8000 cps (measured with a Brookfield Viscometer, spindle no. 5 and at 10rpm).
Samples are sintered slowly until 600°C to ensure PU burnout is complete. Sintering continues up to 1280°C to ensure densification. Image analysis was performed using optical microscopy, digital photography and SEM analysis. Mechanical testing was performed by 3 point bending using an 1122 Instron.

Results

Figure 1 shows the macroporosity generated by the process (scale bar is 1mm). Macroporosity in the samples varies from 40 – 70%. Typical pore sizes far exceed 300μm (the pore size acknowledged as that needed for osteogenesis) – see figure 2. Approx. 79% of all pores were between 150 – 450μm in area equivalent diameter.
Typical strut thicknesses ranging from 100 – 500μm were also reported, as was a strut thickness-pore size-mechanical strength relationship.

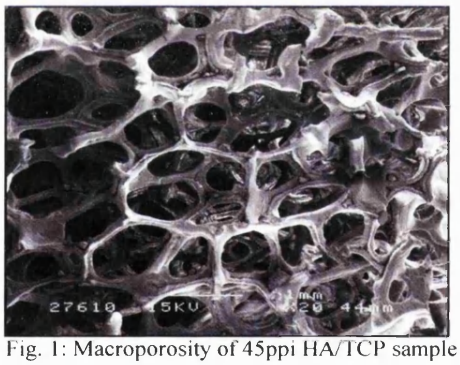

Fig. 1: Macroporosity of 45ppi HA/TCP sample

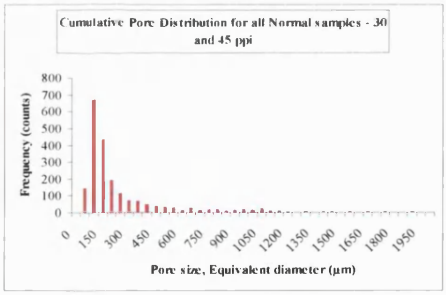

Fig. 2: Pore distribution of samples

One hundred and twenty samples possessed a breaking stress with a 95% confidence level of 0.30MPa±0.01MPa (error margin of just 3%). The low strengths reported are due to the formation of blow-out holes at triple point junctions on the interconnected struts.

Conclusions

Major requirements for replacement bone materials have been met including a wide range of interconnected porosity from 50 – 1000μm. Bioactivity combined with an excellent porosity size range suggests excellent possibility of osteogenesis. In addition this fabrication procedure offers consistency and reliability. Future work will look at improving strength of these open porous calcium phosphate based ceramics.

Acknowledgments

The authors would like to thank the University of Bath and Stryker Howmedica Osteonics for their support.

References

[1] Hing et al. (1997). J. Mat. Sci.: Mat. Med., **8**(12) pp. 731 – 736.
[2] Klein et al. (1994). Biomaterials, **15**(1) pp. 31 – 34.
[3] Wang et al. (1993). J. Mat. Sci.: Mat. Med., **4**(2) pp. 150 – 158.
[4] Le Huec et al. (1995). Biomaterials, **16**(2) pp. 113 – 118.
[5] Liu et al. (1996). J. Mat. Sci. Let., 15, pp. 4

2. Gittings, J. P., Turner, I.G., Miles, A. W. (2004). Development of Bone Substitute Materials – Calcium Phosphate Scaffold Materials. *Poster for the Proceedings of the 7th World Biomaterials Congress, Sydney, Australia,* May 2004.

DEVELOPMENT OF BONE SUBSTITUTE MATERIALS – CALCIUM PHOSPHATE SCAFFOLD MATERIALS

UNIVERSITY OF BATH

centre for orthopaedic biomechanics

Gittings, J. P.[1], Turner, I. G.[1], Miles, A. W.[2]

[1] Department of Engineering and Applied Science, [2] Department of Mechanical Engineering, University of Bath, Bath, BA2 7AY, U.K.

Tel. +44(01225)386196. E-mail: eapjpg@bath.ac.uk, I.G.Turner@bath.ac.uk, A.W.Miles@bath.ac.uk

Introduction

The concept of surgical replacement of diseased or damaged bone with a synthetic substance into which bone ingrowth can occur in order to effect a permanent repair is extremely attractive in orthopaedics.

Hydroxyapatite/tricalcium phosphate (HA/TCP) synthetic bone graft alternatives have been shown to be biocompatible with bone [1]. The presence of an interconnected porosity network has a strong influence on the osteoinductive potential of these synthetic bone graft materials [2].

Early work by the authors focused on an Impact-Impregnation (I.I.) technique to produce a dense bioceramic [3]. The current study describes the production of open porous scaffold (OPS) calcium phosphate ceramics that possess an interconnected open porous network in the required size range for bone ingrowth.

Materials and Methods

Two grades of calcium phosphate powder were blended together to form a HA/TCP ceramic slip which was then ball milled for 24hrs. This slip was used to impregnate polyurethane (PU) foam via a mechanical plunging procedure. The impregnated foam was held above the slip bath in order for the slip to flow and coat the struts of the foam. The samples produced were then dried on tissue paper and treated with high velocity compressed air to avoid the formation of any closed cells. Figure 1 illustrates this procedure. The impregnated blocks were dried at 120°C for 15hrs.

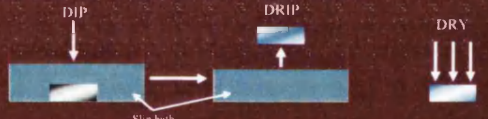

Figure 1: Schematic of fabrication procedure for OPS

The PU foams were graded as 30 and 45 ppi (pores per inch). The slip viscosity ranged from 6000 – 8000 cps (measured with a Brookfield Viscometer, spindle no. 5 and at 10rpm).

Samples were sintered slowly up to 600°C to ensure PU burnout was complete. Sintering continued up to 1280°C to ensure densification. Final sintered dimensions were 40x25x10mm. Image analysis was performed using optical microscopy and scanning electron microscopy (SEM). Mechanical testing was performed by 3 point bending using an 1122 Instron machine. Figures 2 and 3 show typical examples of the HA/TCP bioceramic scaffolds produced.

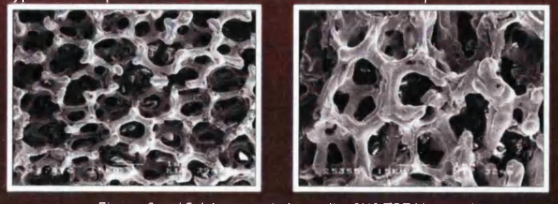

Figures 2 and 3: Interconnected porosity of HA/TCP bioceramic scaffolds produced by current method

Results and Discussion

Typical macroporosity in the bioceramic scaffolds varied from 40-70% with over 79% of porosity lying in the size range 150-450μm in area equivalent diameter. The fabrication procedure guaranteed interconnected porosity. Figures 4 and 5 represent the porosity distributions of the open porous scaffolds (OPS) compared to those reported earlier by the Impact-Impregnation technique i.e. dense bioceramics [3].

The average pore size acknowledged for facilitating osteogenesis (i.e. > 300μm) has been met by the present fabrication technique.

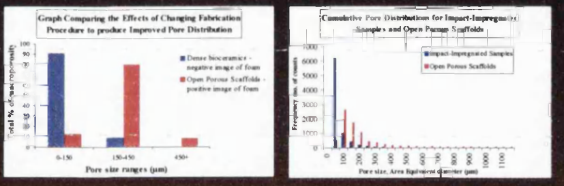

Figures 4 and 5: Porosity distribution of OPS compared to dense bioceramics previously produced

Figure 6 represents the strength-porosity relationship between the OPS and Impact-Impregnated bioceramics. Figure 7 illustrates the strength-density correlation in the calcium phosphate bioceramics produced.

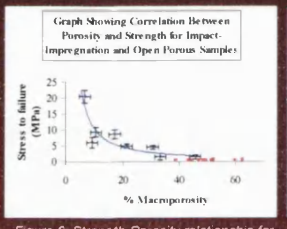

Figure 6: Strength-Porosity relationship for OPS and I.I. bioceramics

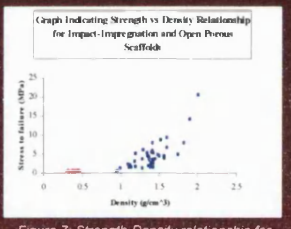

Figure 7: Strength-Density relationship for OPS and I.I. bioceramics

One hundred and twenty samples possessed a breaking stress, with a 95% confidence level, of 0.30MPa ± 0.01MPa. The low strengths reported were due to the formation of microcracks at triple point junctions on the interconnected struts due to thermal shrinkage. Figures 8 and 9 illustrate this phenomenon which is typical in all the bioceramic scaffolds produced. A small applied stress may be magnified many times at the tip of a crack reducing the strength of the overall bioceramic. It is the presence of these small flaws that severely limit the strength of the bioceramic.

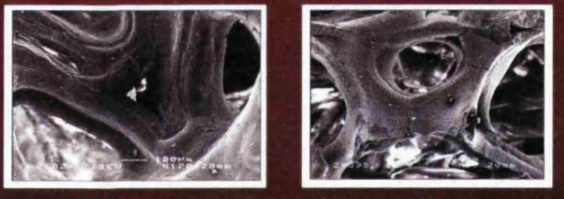

Figures 8 and 9: Formation of microcracks resulting in poor strengths due to critical crack formation

Conclusions

HA/TCP bioceramics with interconnected porosity in the size range appropriate for bone ingrowth have been successfully produced. The fabrication procedure has proved to be reliable and consistent. Future work will focus on eliminating microcracks in order to optimise mechanical properties.

Acknowledgments

The authors would like to thank the University of Bath and Stryker Howmedica Osteonics for their support.

References

[1] Jarcho. (1981). Clin. Orth. Rel. Res., **157**, pp. 259 – 278.

[2] Hing et al. (1997). J. Mat. Sci. – Mat. in Med., **8** (12), pp. 731 - 736.

[3] Casey et al. (2002). Proc. of 17th ESB Conference, Barcelona, p. P146.

3. Gittings, J. P., Turner, I.G., Miles, A. W. (2004). Calcium Phosphate Open Porous Scaffold Bioceramics. *Poster and Abstract for the Proceedings of the 17th International Symposium on Ceramics in Medicine – Bioceramics 17, New Orleans, U.S.A,* December 2004.

CALCIUM PHOSPHATE OPEN POROUS SCAFFOLD BIOCERAMICS

UNIVERSITY OF BATH

Gittings, J.P., Turner, I.G., Miles, A.W.

centre for orthopaedic biomechanics

Centre for Orthopaedic Biomechanics, Department of Mechanical Engineering, University of Bath, BATH, BA2 7AY, U.K.

E-mail: J.P.Gittings@bath.ac.uk, I.G.Turner@bath.ac.uk, A.W.Miles@bath.ac.uk

Introduction

Synthetic calcium phosphate (CaP) bioceramics have been used successfully as bone substitute materials for over thirty years. The majority of CaP bioceramics are based on hydroxyapatite (HA) and tricalcium phosphate (TCP) [1]. Factors such as porosity, biocompatibility and structural integrity are of critical importance in the development of bioactive calcium phosphates [2].

This study involves fabricating CaP ceramics that combine both a porosity network appropriate for bone regeneration and mechanical properties that give structural integrity to the bioceramics. Open porous scaffolds (OPS) were produced with orientated porosity in order to replicate the structure found in trabecular bone. It was hypothesised that different shaped pores would result in a range of strengths, as elliptical shaped pores would decrease the stress to cause failure and hence be weaker than CaP OPS with spherical pores. Figure 1 shows typical examples of the HA/TCP bioceramic scaffolds produced.

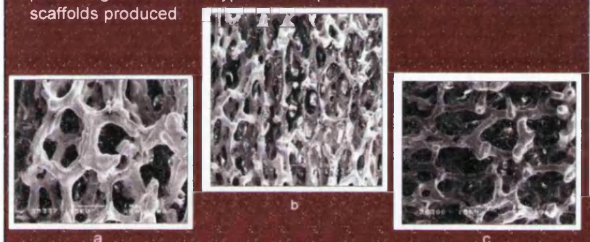

Figure 1. CaP OPS from left to right: (a) 30N 1280°C, (b) 45L 1150°C, (c) 30T 1280°C.

Materials and Methods

Two different calcium phosphate powders (118 and 130) were blended to form thixotropic ceramic slips. The 118 CaP powder is non-crystalline and undergoes phase transformations to ß- and α-TCP on sintering. Powder 130 is highly crystalline and on sintering forms HA. The process used to fabricate the OPS is shown in figure 2. The CaP thixotropic slips were used to coat the cells of the reticulated polyurethane (PU) foams. This was achieved with the aid of a mechanical plunging device designed specifically to allow the slip to penetrate throughout the open porous structure of the foam. The foams were then held above the slip bath for the slip to seep out of the foam. Careful turning allows complete wetting of the struts of the foam. The final stage was to spray the samples with high velocity compressed air in order to avoid the formation of closed cells and to dry the scaffold structure. In this way the pore interconnectivity of the dried scaffolds is guaranteed. The work detailed is covered under British Patent Application no. 0318901.6

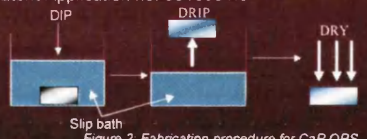

Figure 2. Fabrication procedure for CaP OPS

In order to achieve the orientated structure observed in cancellous bone, a technique was developed to elongate the cells of PU reticulated foam prior to fabrication. Sheets of foam were stretched and thermally transformed to produce elliptical shaped pores. This produced PU scaffolds with pore structures classed as normal i.e. untreated foam (N), longitudinal (L) or transverse (T) as described in figure 1. The PU foams were graded as 30 or 45 ppi (pore per inch). The untreated foams possessed spherical pores ranging in size from 850-1500µm.

Further drying at 110°C for 24hrs and subsequent sintering at 1150°C or 1280°C (depending on the phase required) produces the CaP OPS bioceramic. Image analysis was performed using optical microscopy and scanning electron microscopy (SEM). Mechanical testing was performed by 3 point bending using an 1122 Instron machine.

Results and Discussion

One hundred and twenty OPS samples with an interconnected macroporosity network were produced. Figure 3 shows the broad distribution of pore sizes in the samples analysed; it can be seen that the majority of pores fall in the 150-300µm size range appropriate for bone ingrowth and overall shows a hierarchal pore structure with a size range from 50-1000µm. A volume porosity of 40-70% was reported. Figure 4 gives a summary of the mechanical properties for the OPS produced. The results are given as 95% confidence levels and indicate consistent low strength and a low apparent density. Those samples sintered at 1280°C possess slightly greater strengths than those sintered at 1150°C due to the allotropic transformation to α-TCP at high temperatures. The consistently low strengths reported indicate a different failure mechanism than that originally hypothesised i.e. due to the elongation of PU foam.

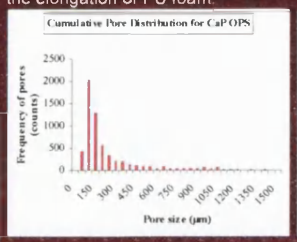

Figure 3. Macropore distribution of CaP OPS

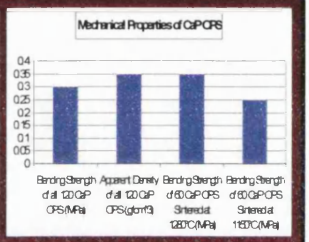

Figure 4. Mechanical data summary for CaP OPS

It was hypothesised in the initial stages of this work, that the elliptical shaped pores would create higher stress concentration factors at their tips than the spherical pores of the untreated foams, hence decreasing their resistance to mechanical stress. However, SEM studies revealed the low strengths reported were due to the formation of microcracks during thermal shrinkage on cooling. Figure 5 shows examples of the thermal shrinkage due to sintering and the resulting weakness in the scaffold structure thus created. On stressing, these microcracks severely limit the strength of the bioceramic. Therefore, the mechanical properties of the OPS were not controlled by the different shaped pore structures as hypothesised, but by the microcracks formed due to thermal shrinkage. This explains the consistently low strengths measured.

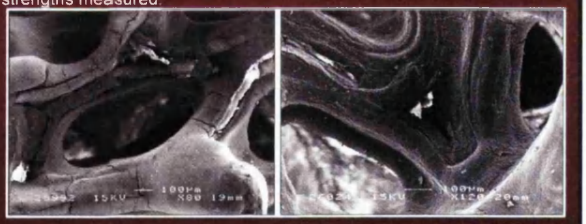

Figure 5. Formation of microcracks lowering the strength of the CaP OPS bioceramic

Conclusions

OPS have pores typically in the size range 150 – 300µm and 40 – 70% porosity by volume. The majority of pores were in the appropriate size range for bone ingrowth. The mechanical properties of the samples produced were found to be low. Elongating the pore structure in transverse and longitudinal directions did not affect the total porosity of the bioceramics or their mechanical properties. Further work will focus on the elimination of the microcracks present in order to optimise the properties of the materials produced.

Acknowledgments

The authors would like to thank the University of Bath and Stryker Howmedica Osteonics for their support.

References

[1] D. M. Liu. Materials Science Forum. Vol. 250 (1997), p.183.

[2] M. Jarcho. Clinical Orthopaedics and Related Research. Vol. 157 (1981), p.259.

CALCIUM PHOSPHATE OPEN POROUS SCAFFOLD BIOCERAMIC

Gittings, J. P., Turner, I. G., Miles, A. W.

Department of Mechanical Engineering, University of Bath, Bath, BA2 7AY, U.K.

Introduction

Calcium phosphate (CaP) ceramics, such as hydroxyapatite/tricalcium phosphate (HA/TCP), possessing an interconnected porosity network in the appropriate size range for promoting bone ingrowth offer the possibility of a structural/biological matrix for replacing diseased or damaged bone. The bioceramic must possess mechanical integrity to avoid failure whilst offering a bioactive surface for bone ingrowth.

The objective of the current study was to produce a HA/TCP bioceramic that imitated the orientated trabecular structure found in cancellous bone. The structure-property relationship of these bioceramics was then analysed. It was hypothesised that the mechanical properties would be linked to the shape of the pore structure due to the orientation of the open porous scaffolds (OPS). The current research was compared to previous work that produced HA/TCP dense bioceramics with an interconnected porosity network.

Materials and Methods

In order to achieve the elongated structure resembling cancellous bone, a technique was developed to elongate the cells of polyurethane (PU) reticulated foam. PU foams provided the substrate for the production of HA/TCP bioceramics and were graded as 30 or 45ppi (pores per inch). The PU foams possessed spherical pores ranging in size from 850-1500μm. These were stretched and thermally transformed in order to produce elliptical shaped pores. Following this procedure, 120 foam samples were cut to dimensions of 40mm x 25mm x 10mm in both longitudinal and transverse directions. This produced HA/TCP scaffolds with pore structures classed as normal i.e. untreated foam (N), longitudinal (L) or transverse (T).

A thixotropic ceramic slurry was produced in order to achieve optimum coating of the PU foam walls. Foam samples were impregnated with the aid of a mechanical plunging device that compressed the foam sample in order to draw the slurry into the foam and coat its structure. The samples produced were then dried on tissue paper and treated with high velocity compressed air to ensure the interconnectivity of the porosity network. Drying of the final samples occurred at 120°C for 15hrs followed by sintering up to 1280°C. Scanning electron microscopy and image analysis was used to assess the porosity distribution and 3-point bending was used to evaluate the mechanical properties.

Results and Discussion

OPS bioceramics possessed an interconnected macroporosity network of 30-60% with bending strengths of 0.16-0.56MPa. Typical pore sizes of OPS were in the size range 200-600μm. The fabrication of CaP OPS produced a wide range of macroporosity in the correct size range for ossification processes to occur. The dense bioceramics previously manufactured had an interconnected macroporosity network of 7-31%, pore size range of 50-200μm and compressive strengths of 1-21MPa. Figure 1 illustrates the difference in macroporosity produced from the elongation fabrication procedure.

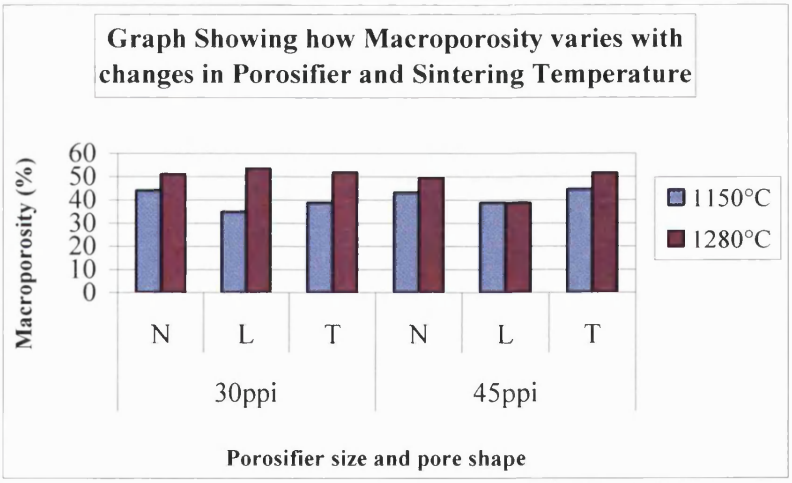

Figure 1: Variations between the normal (N), longitudinal (L) and transverse (T) shaped pore bioceramic

It was hypothesised that the shape of the pore structure would influence the mechanical properties of the HA/TCP OPS produced. However, the low strengths reported were due to the formation of microcracks during thermal shrinkage on cooling. On stressing, these microcracks severely limit the strength of the bioceramic. Therefore, the mechanical properties of the OPS were not controlled by the different shaped pore structures as hypothesised, but by the microcracks formed due to thermal shrinkage.

Conclusions

The HA/TCP bioceramics produced possess an interconnected porosity network between 100-1000μm+ in size and 30-60% by volume. Elongating the pore structure did not effect the total porosity of the bioceramics. Strengths were low due to microcrack formation on sintering. Further work will address the elimination of these microcracks that magnify stress and cause failure.

Acknowledgements

The authors wish to thank the University of Bath and Stryker Howmedica Osteonics for their support.

4. Gittings, J. P., Turner, I.G., Miles, A. W. (2005). Calcium Phosphate Open Porous Scaffold Bioceramics. *Key Engineering Materials*: **284 – 286**, pp. 349 – 352. Trans. Tech. Publications, Switzerland.

Calcium Phosphate Open Porous Scaffold Bioceramics

Gittings, J. P.[1, a], Turner, I. G.[1, b], Miles, A. W.[2, c]

[1] Dept. of Engineering and Applied Science, University of Bath, BATH, BA2 7AY, U. K.
[2] Dept. of Mechanical Engineering, University of Bath, BATH, BA2 7AY, U. K.

Keywords: Calcium Phosphate, Hydroxyapatite, α-tricalcium phosphate, β-tricalcium phosphate, bioceramic

Abstract

Calcium phosphate (CaP) ceramics possessing an interconnecting porosity network in the appropriate size range for vascularisation offer the possibility of providing a structural matrix for replacement of diseased or damaged bone. Such bioceramics must possess sufficient mechanical strength to avoid failure whilst offering a bioactive surface for bone regeneration. The objective of the current study was to produce a hydroxyapatite/tricalcium phosphate (HA/TCP) bioceramic that imitated the orientated trabecular structure found in cancellous bone. The structure-property relationship of these bioceramics was then analysed. It was hypothesised that the mechanical properties would be linked to the shape of the pore structure due to the orientation of the open porous scaffolds (OPS) produced. OPS bioceramics possessed an interconnected macroporosity network of 40-70% by volume with bending strengths of 0.30MPa ± 0.01MPa and apparent densities of 0.35g/cm^3 ± 0.05g/cm^3. Typically, pore sizes in the range of 150-300μm were produced. The fabrication of CaP OPS resulted in a wide range of macroporosity in the correct size range for osseointegration to occur. Elongating the pore structure did not affect the total porosity of the bioceramics. Strengths were low due to microcrack formation on sintering and not due to the shape of the pores present in the scaffold as initially hypothesised.

Introduction

Synthetic CaP bioceramics have been used successfully as bone substitute materials for over thirty years [1]. The majority of CaP bioceramics are based on hydroxyapatite (HA) and tricalcium phosphate (TCP) [2, 3]. The chemical composition of synthetic HA resembles that of the mineral component found in natural bone. Synthetic HA is generally mechanically stronger than synthetic TCP, however it does not possess the bioactivity of its counterpart. TCP may be formed due to phase transitions on sintering of synthetic HA, provided the Ca:P ratio is non-stoichiometric i.e. does not equal 10:6. Vacancies present in the structure allow Ca^{2+} and PO_4^{3-} ions to form apatite precipitations within the ceramic substrate. This stimulates bone growth and enhances the integration of the implant material with natural bone [4].

Factors such as porosity, biocompatibility and structural integrity are of critical importance in the development of bioactive calcium phosphates [5, 6]. The macroporosity of such bioceramics plays an important role in osteoconduction. Osteoconductive bioceramics provide a scaffold for the ingrowth of bone and are affected by the total pore volume of the material [7].

This study involves fabricating CaP ceramics that encapsulate both a porosity network appropriate for bone regeneration and mechanical properties that resemble those of natural bone.

Open porous scaffolds (OPS) were produced with specifically orientated porosity (spherical, longitudinal and transverse) in order to replicate the structural anisotropy found in trabecular bone. It was hypothesised that the different shaped pores would result in a range of strengths, as elliptical shaped pores would decrease the critical crack size for failure and hence be weaker than CaP scaffolds with spherical pores.

Materials and Methods

A ceramic slurry was prepared using two forms of hydroxyapatite Grades 118 and 130 powders, supplied by Stryker Howmedica Osteonics. Grade 130 is a stable, crystalline phase of HA that does not thermally transform to other apatitic structures. Grade 118 is less crystalline than Grade 130 and is calcium deficient, allowing the transformation at high temperatures to β- and α-TCP. Blending the powders in different proportions allows the fabrication of any composition of HA/TCP bioceramic. The powders were incorporated into distilled water with other constituents - binders, plasticisers and surfactants - in order to avoid agglomeration and to ensure that the slip was thixotropic. Once formed the slip was ball milled with zirconia milling media for 24hrs at 20rpm.

Polyurethane (PU) foams were used as a structural template for the manufacture of CaP OPS bioceramics. Figure 1 shows the PU foam structure and illustrates the open interconnected porosity of the foam in the as-received condition. The PU foams were graded as 30 or 45 ppi (pore per inch). The untreated foams possessed spherical pores ranging in size from 850-1500μm. In order to achieve the elongated structure resembling cancellous bone, a technique was developed to elongate the cells of PU reticulated foam. Sheets of foam were stretched and thermally transformed to produce elliptical shaped pores. Following this procedure, 120 foam samples were cut from the sheets to dimensions of 40mm x 25mm x 10mm in both longitudinal and transverse directions. This produced PU scaffolds with pore structures classed as normal i.e. untreated foam (N), longitudinal (L) or transverse (T).

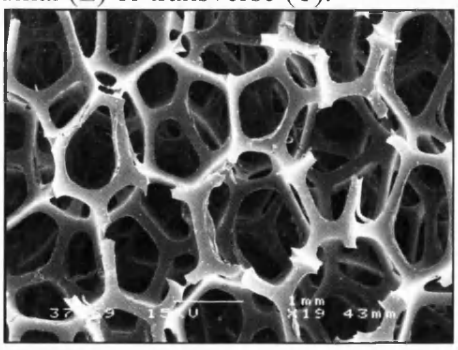

Figure 1: The structure of a 45ppi PU foam used for impregnation of slip. Note the open, interconnected porosity of the foam that resembles cancellous bone.

The thixotropic slurry was incorporated into the PU foam samples with the aid of a mechanical plunging device that ensured the slip coated the walls of the foam; the thixotropic nature of the slip assists this process. The sample was held above the slip bath to allow the slip to flow and coat the struts of the foam. The samples were simultaneously dried on tissue paper and treated with high velocity compressed air to ensure the interconnectivity of the porosity network. Drying of the final samples was carried out at 120°C for 15 hours followed by sintering at either 1150°C or 1280°C in order to produce HA/TCP bioceramics with both α- and β-TCP phases, such as 80:20 HA/TCP. Scanning electron microscopy and image analysis were used to assess the porosity distribution and 3-point bending was used to evaluate the mechanical properties.

Results and Discussion

One hundred and twenty OPS samples with an interconnected macroporosity network were produced. Figure 2 shows the broad distribution of pore sizes in the samples analysed; it can be seen that the majority of pores fall in the 150-300μm size range appropriate for bone ingrowth. Figure 3 gives a summary of the mechanical properties for the OPS produced. The results are given at 95% confidence levels and indicate consistent low strength and a low apparent density. Those samples sintered at 1280°C possess slightly greater strengths than those sintered at 1150°C due to the allotropic transformation to α-TCP at high temperatures. The consistently low strengths reported indicate a different failure mechanism than that originally hypothesised i.e. due to the elongation of PU foam.

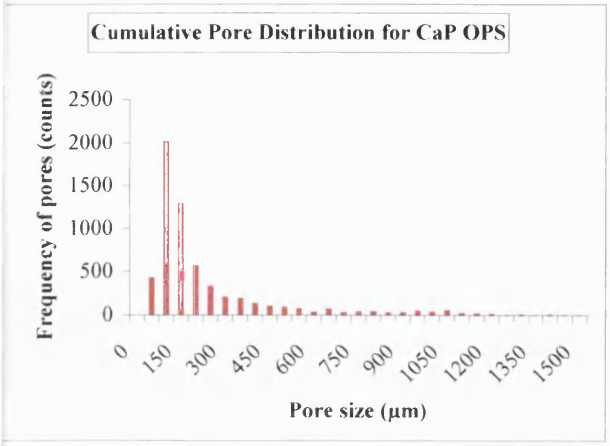

Figure 2: Macropore distribution of CaP OPS

	CaP Open Porous Scaffolds
Bending Strength (MPa)	0.30 ± 0.01
Apparent Density (g/cm^3)	0.35 ± 0.05
Porosity (%)	40 – 70
Sample size	120
Samples sintered at 1280°C (MPa)	0.35 ± 0.05
Samples sintered at 1150°C (MPa)	0.28 ± 0.02

Figure 3: Mechanical data summary for CaP OPS

Figure 4 shows scanning electron micrographs (SEM) of the CaP OPS samples produced using foams with the different orientations and pore sizes (30 or 45ppi) – normal (a), longitudinal (b) and transverse (c). It was hypothesised in the initial stages of this work, that the elliptical shaped pores would create higher stress concentration factors at their tips than the spherical pores of the untreated foams, hence decreasing their resistance to mechanical stress.

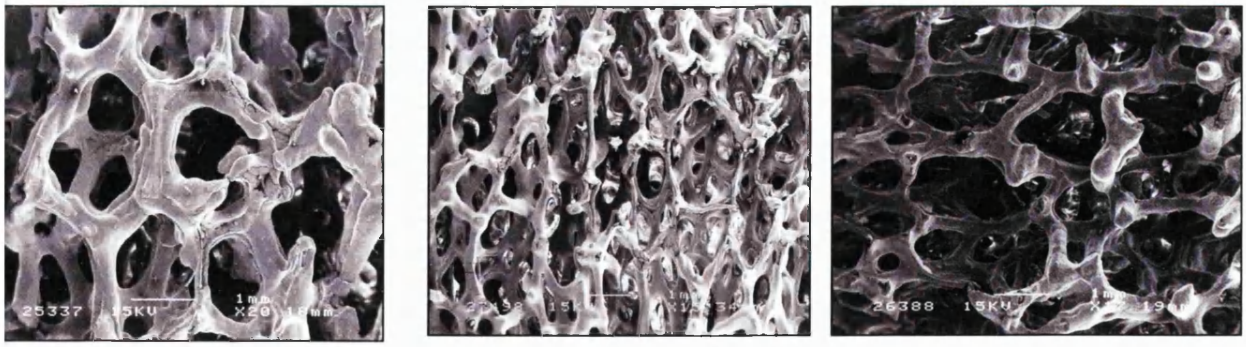

(a) *(b)* *(c)*

Figure 4: CaP OPS from left to right: (a) 30N 1280°C, (b) 45L 1280°C, (c) 30T 1280°C.

However, SEM studies revealed the low strengths reported were due to the formation of microcracks during thermal shrinkage on cooling. Figure 5 shows examples of the thermal shrinkage due to sintering and the resulting weakness in the scaffold structure thus created. On stressing, these microcracks severely limit the strength of the bioceramic. Therefore, the mechanical properties of the OPS were not controlled by the different shaped pore structures as

hypothesised, but by the microcracks formed due to thermal shrinkage. This explains the consistently low strengths measured.

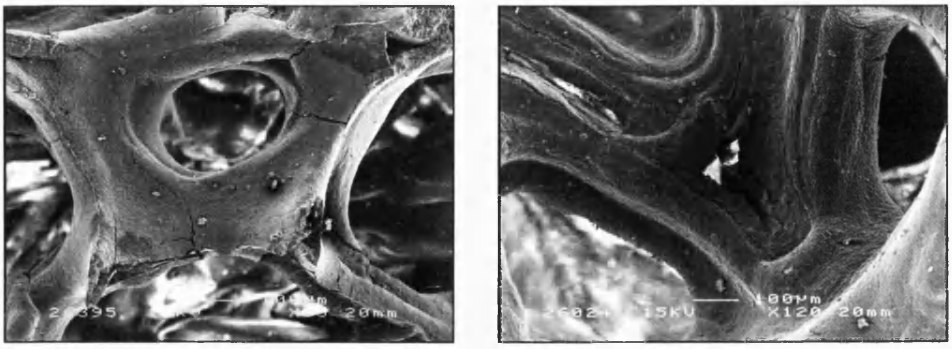

Figure 5: Formation of microcracks lowering the strength of the bioceramic

Conclusions

A technique has been successfully developed for the production of CaP open porous scaffold (OPS) bioceramics with completely interconnected porosity. The samples produced have a superior network of interconnected porosity compared to previously produced forms of porous bioceramics. OPS have pores typically in the size range 150 – 300μm and 40 – 70% porosity by volume. The majority of pores were in the appropriate size range for bone ingrowth. The mechanical properties of the samples produced were found to be low. SEM revealed the cause to be microcrack formation on sintering. Elongating the pore structure in transverse and longitudinal directions did not affect the total porosity of the bioceramics or their mechanical properties. Further work will focus on the elimination of the microcracks in order to optimise the properties of the materials produced.

Acknowledgments

The authors wish to thank the University of Bath and Stryker Howmedica Osteonics for their financial support and the Centre of Electron Optics at the University of Bath for use of their facilities.

References

[1] M. Jarcho: Clinical Orthopaedics and Related Research. Vol. 157 (1981), p.259.
[2] A. Ravaglioli, A. Krajewski: Materials Science Forum. Vol. 250 (1997), p.221.
[3] R. Z. LeGeros: Clinical Orthopaedics and Related Research. Vol. 395 (2002), p.81.
[4] A. Royer, J. C. Vigiue, M. Heughebaert, J. C. Heughebaert: Journal of Mat. Sci.: Mat. in Med. Vol. 4 (1993), p.76.
[5] D. M. Liu: Materials Science Forum. Vol. 250 (1997), p.183.
[6] O. Richart, M. Descamps, A. Liebetrau: Bioceramics 14: Key Engineering Materials. No. 218-2 (2002), p. 9.
[7] J. Wang, W. Chen, Y. Li, S. Fan, J. Weng, X. Zhang: Biomaterials. Vol. 19 (1998), p. 1387.